Pentadecyl Phenol Functionalized Perylenebisimide Building Blocks for Optoelectronic Applications

Thesis Submitted to AcSIR for the Award of the Degree of
DOCTOR OF PHILOSOPHY
In Chemical Science

By
Prajitha. K. P.
Registration Number: 10CC11J26030

Under the guidance of
Dr. S. K. Asha

CSIR-National Chemical Laboratory

राष्ट्रीय रासायनिक प्रयोगशाला
(वैज्ञानिक तथा औद्योगिक अनुसंधान परिषद)
डॉ. होमी भाभा रोड, पुणे - 411 008. भारत
NATIONAL CHEMICAL LABORATORY
(Council of Scientific & Industrial Research)
Dr. Homi Bhabha Road, Pune - 411008. India

Certificate

This is to certify that the work incorporated in this Ph.D. thesis entitled **"Pentadecyl Phenol Functionalized Perylenebisimide Building Blocks for Optoelectronic Applications"** submitted by **Ms. Prajitha.K.P.** to **Academy of Scientific and Innovative Research (AcSIR)** in fulfillment of the requirements for the award of the Degree of Doctor of Philosophy, embodies original research work under my supervision. I further certify that this work has not been submitted to any other University or Institution in part or full for the award of any degree or diploma. Research material obtained from other sources has been duly acknowledged in the thesis. Any text, illustration, table etc., used in the thesis from other sources, have been duly cited and acknowledged.

Prajitha K. P.
(Student)

Dr. S. K. Asha
(Supervisor)

Communications Channels ☎ +91 20 25902000
+91 20 25893300
+91 20 25893400
Fax +91 20 25902601 (Director)
+91 20 25902660 (Admin.)
+91 20 25902639 (Business Development)
URL : www.ncl-india.org

DECLARATION

I hereby declare that the research work embodied in the thesis entitled **"Pentadecyl Phenol Functionalized Perylenebisimide Building Blocks for Optoelectronic Applications"** has been carried out by me at Polymer Science and Engineering Division of CSIR-National Chemical Laboratory, Pune under the supervision of Dr. S. K. Asha. I also affirm that this work is original and has not been submitted in part or full, for any other degree or diploma to this or any other University or Institution.

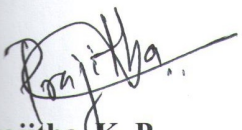

Prajitha. K. P

Polymer Science and Engineering Division

CSIR-National Chemical Laboratory,

Pune-411 008, India.

April 2017

Dedicated to.....

My Madam,Teachers and Parents

ACKNOWLEDGEMENTS

Firstly, I would like to express my sincere gratitude and thanks to my research supervisor Dr. Asha S. K. for the continuous support that she provided to my Ph.D study for her patience, motivation, and immense knowledge. Her guidance helped me throughout the period of research and writing of manuscripts. She was always with me during the tough phase of my research and personal life. Working with her was really a great pleasure and fetched me a lot of learning experience. I could not have imagined having a better advisor and mentor for my Ph.D. study.

I owe my most sincere gratitude to Professor. M. Jayakannan (Department of Chemistry IISER, Pune) for his valuable suggestions that have been very helpful for this study.

I would like to thank the rest of my DAC committee: Dr. P. P. Wadgaonkar, Dr.D.Srinivas Reddy, Dr. C.P.Vinod, , for their insightful comments and encouragement, but also for the hard question which incented me to widen my research from various perspectives.

My sincere thanks to Dr. S. Sivaram and Dr. S. Sourav Pal (former director CSIR – NCL) and Prof. Ashwini Kumar Nangia (director CSIR – NCL) for providing me such a fantastic infrastructure to do better research.

My sincere thanks to Dr. Prof .V. A. Ragunathan and Mrs. K.N.Vasudha (RRI Bangalore) for carrying out XRD measurements. I also thank to Dr. K. Krishnamoorthy (NCL, Pune) Prof. M.Thelakkat (University Bayreuth) for SCLC measurements. I would like to thank Dr.R.Nandini Devi for valuable suggestion for XRD analysis. My sincere thanks to Mr. Chithiravel who helped for the SCLC measurements.

I would like to thank all the instrumental faculties of NCL and J wing who helped me to carry out the analysis. I extend my thanks to Mr. Shamal K. Menon for helping me in GPC measurements. I would also like to thank Mrs. B. Santhakumari, Mr. Pankaj Sankapalli, Mr. Venkatesh Thogiti and Mr. Pankaj Raj for helping me lot in various characterization of my samples. I extend my thanks to Mrs. Deepa Dhoble, Mrs. Anuya Nisal, Mr. Saroj Kumar Jha and Mrs. Poorvi Purohit for their kind help in giving training for the divisional instrumental facility. I would like to thank all the members of

NMR divisions, especially Kavya, Anjali, Sanoop for the fast analysis of my samples. I also thanks to all the members of glass blowing sections.

My sincere thanks to Dr. Chinmay G. Nardele and Dr. Mahima, my senior lab mates who taught me the basic instruments for this reserch. My sincere thanks to Mr. Ghanashyam who guided me to put my first reaction of this thesis work. I extended my sincere thanks to all my seniors Dr. Nagesh B. Kolhe, Dr. Kaushlendra kumar, Dr. Rekha Narayan, Dr. T. Senthil kumar, Dr.Nisha, Dr. Balamurugan, Dr. Pramod, Dr. Smitha, Dr. Anadraj along with my batch mates Dr. Shekhar Dr.Saibal, Dr.Swapnil, Dr. Bapu for providing a good platform form my research work. My special thanks to Mr.Sandeep Kumar Sharama for helping me to transport solvents without any hesitations.

I owe my special thanks to all my labmates and friends from CSIR-NCL and IISER Pune; Dr.Suresh, Sandeep, Shrikant, Sarabjoth, Moumita Roy, Navanath, Akhil, Moumita Gupta, Bhagyashree, Narsimha, Rajendra, Nilesh, Sonashree, Maitri, Nitesh,Yogita and Mehak for their unstinted support, timely motivation and maintaining cheerful environment in lab.Ialso thank the past and present project tranies: Bavitha, Indra, Jeena, Vinay, Charu, Alok, Vikash, Akshata, Harish, Vidhya, Priyanka, Devendra, Shreya, Durga, Sharat, Sharanya, Anju, Suchitra, Agnus , Nithin,Indrajith for bringing cheerful environment to the lab.

I extended My Sincere thanks to Dr. Jancy Nixon and her family for her care and support. She is a good friend and sister of mine who cared me during this period.

My sincere mention to Meenu, Shyam, Shreeansh, Appu, Raichel, Jennice, Kittu , Shreya along with Swathichechi for making my Pune life more beautiful.

I would like to thank Meenukutty and Momu for making my hostel life comfortable. Along with them I thank my roommates Dr. Mandakini, Sharamila, Dr.Soumya, Richa, Rubbena. I also thank my other hostel mates Dr.Shubha, Dr. Thanaya, Dr. Munmun, Dr.Jumur, Vineetha, Neetha, Sumen, Debopriya, Vaiashnavi. My sincere thanks to my classmate Dr. Jaya for making my pune life more comfortable. I also thank Dr. Dhanya and Anjali.

My sincere thanks to my sister Leenachechi. She is with me for all the up and down of my life during this research period. My sincere thanks to my brother Mathewsettan for his valuable guidance and support. I would like to thank Pappa and Mummy and Kunjumol for their prayer and support.

I don't have words to express for you my best friends Nishamol and Bessy, who is there for me always. I thank to my Pappa who cares me like his daughter, Mummy, Noble and Mable chechi,Binu, Ammu, Akku, Annu and Nichu.

I also like to thank my brother Vidyanand who has helped me a lot during this research. A special thanksto my brothers Sharath and Thameez for their care. I would like to thank Manjunath and Dr. Rajesh who helped me for Variable temperature XRD measurements. I also thanks Arunettan for helping me XRD measurements along with Minu Arun. Special thanks to kuttettan for his valuable guidance. I also thank to Manoj Sharma for valuable discussions and Dev Raj and Ashok for helping me for processing documents. I also thanks my best buddies Vinayan, Hari, Rajeesh,Vineesh, Sujesh, Sruthi, Soumya, Shreethi, Jaya, Roshni, Sandeep. I would like to address my special thanks to all the present and past members of D-wing for keeping me always alert. I also thank all my NCL friends and NCL Keralites. I would like to express my sincere thanks to Eldho chettan, Anumon chettan, Jijil, , Anurag, Dr. Remya, Anu priya, Karthika, Pranav, Shibin, Sanoop, Tony, Rejith, , Renjeesh, Shebib, Sandeep, Abdul Kayum, Munnavir, Fayis, Vipin, Sarath, for their lovely care and support. Special thanks to Chinnu mol for helping me in final correction.

My sincere thanks to my Teachers who is the back bone of my life. I deeply acknowledged the Chemistry department of Payyannur college and BK college. My sincere Thanks to Sister Rose Valiyaparambil and all the members of Sanjo hostel.

Words cannot express the feelings I have for my parents P.K. Thampan Poduval and K.P.Shailaja for their constant unconditional love and support. My special thanks to my Achamma, Ammuma and Achachan who encouraged me a lot in my studies during my child hood. I would like to thank my Cute sisters Chinnu, Devu and Drishya all my relatives for having showered so much love on me since my childhood.

Above all, praises and thanks to the God, the Almighty, for His showers of blessings throughout my research task to complete the research successfully.

Prajitha

TABLE OF CONTENTS

List of Abbreviations

Abbreviations	Expansion
CH_3CN	Acetonitrile
Al	Aluminum
Å	Angstrom
ATR	Attenuated total reflectance
AFM	Atomic force microscopy
cm	Centimeter
$CHCl_3$	Chloroform
T_c	Crystallization temperature
Jsc	Current density
dL	Deciliter
T_D	Decomposition temperature
DFT	Density functional theory
$CDCl_3$	Deuterated chloroform
ODCB	1,2 –Dichlorobenzene
DCM	Dichloromethane
DSC	Differential scanning calorimetry
DMAc	N,N-Dimethylacetamide
DMF	N,N-Dimethylformamide
Eg (ele)	Electronic band gap
eV	Electron volt
EtOAc	Ethyl acetate
F.F.	Fill factor
FL	Fluorescence
FT-IR	Fourier transform infrared
GPC	Gel permeation chromatography
T_g	Glass transition temperature
Au	Gold
gm	Gram
HMDS	Hexamethylenedisilazane
HOMO	Highest occupied molecular orbital
HCl	Hydrochloric acid
ITO	Indium tin oxide
η_{inh}	Inherent viscosity
KJ	Kilojoule
LC	Liquid crystal
LCPs	Liquid crystalline polymers
LUMO	Lowest occupied molecular orbital
MALDI-TOF	Matrix-assisted laser desorption ionization-time of flight
MHz	Megahertz
T_m	Melting temperature
µL	Micro liter
mg	Milligram
mL	Milliliter
mol	Mole
nm	Nanometer
N_2	Nitrogen

NMR	Nuclear magnetic resonance
Voc	Open circuit voltage
Eg (opt)	Optical band gap
OD	Optical density
OFET	Organic field effect transistor
OLED	Organic light emitting diode
ppm	Part per million
PLM	Polarized light microscope
K_2CO_3	Potassium carbonate
KI	Potassium iodide
PCE	Power conversion efficiency
η_{red}	Reduced Viscosity
RI	Refractive index
SEM	Scanning electron microscope
s	Second
SiO_2	Silicon dioxide
Ag	Silver
SEC	Size exclusion chromatography
SAXS	Small angle X-ray scattering
SCLC	Space charge limited current
H_2SO_4	Sulfuric acid
TGA	Thermo gravimetric Analysis
TEM	Transmission electron microscopy
TFA	Trifluoroacetic acid
UV	Ultraviolet
V	Volt
λ	Wavelength
Mw	Weight average molecular weight
WXRD	Wide angle X-ray diffraction

PREFACE

Organic optoelectronics has emerged as an interesting area of research due to its enormous applications in today's life. Organic semiconductors play a key role in the charge transporting mechanism of these devices. A variety of p-type (electron rich) semiconducting small molecules and polymers are available with good charge carrier mobility. However the n type (electron poor) semiconducting materials are comparatively less available. Fullerene and its derivatives are the most extensively studied n-type semiconductors. But they are poor in terms of solubility, processability, air stability etc. So there is a huge demand for an alternative n type semiconducting material which can overcome these issues. Perylenebisimide is one of the members in rylene family with excellent photostability and thermal stability. Both the bay and core positions can be easily substituted with different functional groups. They have excellent self assembling abilities and they are known to organize into liquid crystals, gels, nano wires, nano roads etc.

The self assembly of organic semiconductors play a crucial role in improving the charge transport and overall device efficiency. To induce self assembly, we have adopted two approaches 1) Liquid Crystalline Self-assembly and 2) Hydrogen Bond Assisted Self-assembly. Both the symmetrically and the unsymmetrically pentadecyl phenol substituted perylenebisimides and their derivatives are designed and synthesized to study the self assembling behaviour. The second and third chapters briefly describe the structure-property relationship in the liquid crystalline behavior of perylenebisimide, where both the terminal and middle spacers are varied. The last two chapters of this thesis work explore the hydrogen bonding induce self assembly of unsymmetrical perylenebisimides with poly 4 vinyl pyridine (P4VP) and poly styrene block poly 4 vinyl pyridine (PS-b-P4VP) respectively . The charge transporting properties of these systems were studied by SCLC (Space Charge Limited Current) method which clearly indicated the importance of self assembly in charge transport. Both the small molecules and supramolecular complexes were prepared and characterized well. The liquid crystalline properties were well studied with DSC, PLM and WXRD. The charge transporting properties were studied by SCLC method with device configuration of Glass/ Al / PBI / Al.

Chapter 1 gives a brief introduction about organic optoelectronics. This section includes organic electronics and their use, charge transport mechanism, challenges and opportunities, effect of self-assembly in device performances, types of organic semiconductor devices, techniques to measure the mobility in organic semiconductors are discussed. A brief description about n type semiconducting perylenebisimides and its self assembly ,Synthetic approaches, optical, and semiconducting properties are discussed in detail with latest literature examples including small molecules and polymers.

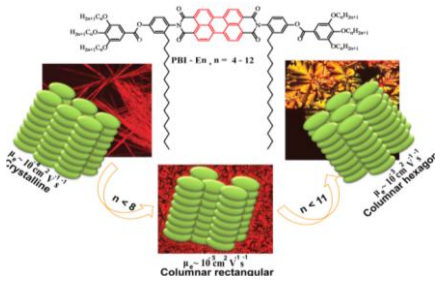

Chapter 2 explains the terminal spacer effect on a homologous series of pentadecyl phenol functionalized perylenebisimide (PBI) terminated with trialkoxy gallate esters were synthesized, where the terminal alkyl chain length was varied from n = 4 to 12 (**PBI-En**). A clear odd-even oscillation was observed in the melting as well as isotropization enthalpies as a function of alkyl spacer length in the terminal gallate unit with the even spacers exhibiting higher values. The higher members of the series with n > 8 exhibited thermotropic liquid crystalline textures in the PLM which remained stable until room temperature. The nature of the LC phase was identified to be columnar rectangular and columnar hexagonal based on detailed analysis of the WXRD pattern recorded in the LC phases. The SCLC mobility values columnar hexagonal phase exhibited a mobility value one order (10^{-3} $cm^2V^{-1}s^{-1}$) higher than that of crystalline (10^{-4} $cm^2V^{-1}s^{-1}$) and two orders higher than that of columnar rectangular phase (10^{-5} cm^2 V^{-1} s^{-1}) indicating a strong dependence of packing on bulk mobility.

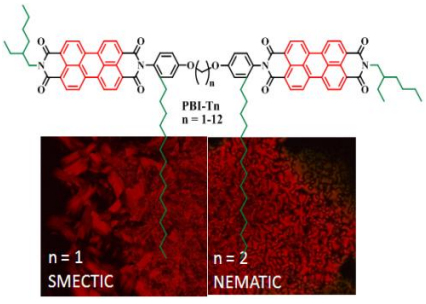

Chapter 3 explains the effect of middle alkyl spacer on a series of twin Perylene bisimide (**PBI-Tn**) molecules having the structure PBI-(methylene spacer)n-PBI where the length of the central poly methylene spacer segment was varied from n = 1 to 12. The PBI unit was imidized with ethyl hexyl branched alkyl segment at the terminal and pentadecyl phenol at the other end which was linked up through the poly methylene spacer to form the twin molecules. The differential packing afforded by the odd and even spaced central methylene segments resulted in an odd-even oscillation of the clearing transitions as well as their enthalpies

with higher values observed for the even twins. The odd-even oscillation was quite prominent for the spacers till n<7 after which it tapered off. **PBI-T1** and **PBI-T3** exhibited tendencies to form smectic liquid crystalline (LC) phases while the rest of the twin molecules exhibited tendencies for high temperature nematic phases.

Chapter 4 explains the supramolecular comb copolymer formation of unsymmetrical **PBI** with **P4VP**. Unsymmetrical perylenebisimide with different alkyl substitution was developed with free –OH group at the termini (**UPBI**). These UPBIs exhibited thermotropic columnar liquid crystalline phase. Supramolecular nano organization of **UPBI** with the polymer template P4VP was achieved with the help of non covalent interaction like H-bonding and π-π stacking. FT-IR and ^{1}H NMR spectroscopy were used for confirmation of complex formation. Small angle X-ray scattering (SAXS) and wide angle X-ray diffraction (WXRD) were used to understand the solid state supramolecular structure. Thin film morphology of the acceptor complexes with **P4VP** showed nice lamellar arrangement in the range of < 10 nm. Effect of self-organization on bulk mobility was measured via SCLC method and improvement in mobility was observed after complex formation.

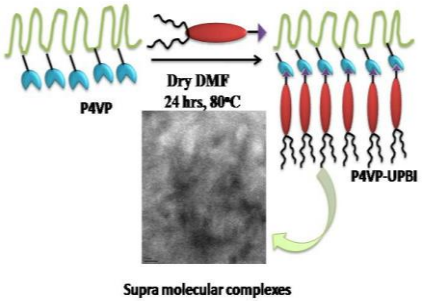

Chapter 5 explains the Supra molecular comb coil copolymer of **PS-b-P4VP** block copolymers with an unsymmetrical perylenebisimide (**UPBIHH**) were synthesized through the hydrogen bond interaction between the pyridine unit and the phenolic –OH on the perylenebisimides. The self assembled nano structures are well studied with help of TEM, SAXS and WXRD. The supra molecular complexes has shown worm like morphology in the TEM at 100 nm scale. In addition, lamellar morphology at length scale of 5 nm could also be observed in TEM. This confirms the assembly-within-assembly of comb copolymer formation inside the larger block co polymer organization.

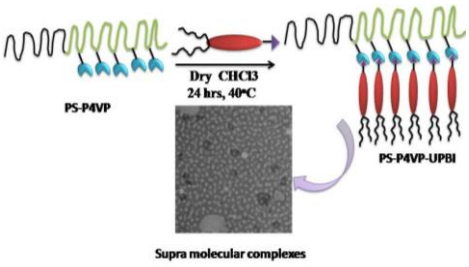

Chapter 6 summarizes the outcome of research work carried out in thesis.

Chapter 1

Introduction

1 .1 Organic Opto electronics:

Conduction of electricity by plastics is the break through invention of last era which made a revolution in opto electronics afterwards. The Nobel prize for Chemistry in the year 2000 was awarded for those brilliant minds behind this break through invention; Heeger, Shirakawa, Macdiarmid.[1,2] Prior to this, plastic was considered as an insulating material without any electronic applications. Today organic electronics is the largest and fastest growing research area because of its advantages like low cost, large area, flexible and light weight devices. What makes an organic material (small molecules or a polymer) conductive? According to their electrical properties materials are classified as 1) conductor 2) semiconductor 3) insulator. Conductors have a good overlap between the HOMO (valance band) and the LUMO (conduction band) so that they are electrically active, where as insulating materials have a huge energy gap between the HOMO and LUMO which make them electrically inactive. Consider the case of semiconducting materials where the energy gap between the HOMO and LUMO is very less. In the case of inorganic semiconductors, applying external forces like heat or doping with some metals from different group can render them either n type (electron transport) or p type conductivity (hole transport).

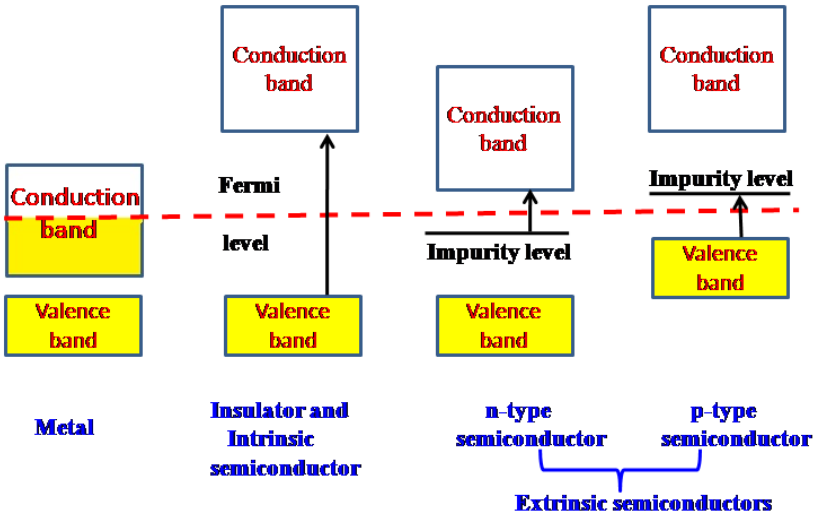

Figure 1.1: Energy band diagram of conductors, insulators and semiconductors.

In the case of organic semiconductors the extended pi conjugation helps to bring down the energy gap between HOMO and LUMO.[3] Upon photo excitation, the electron from the HOMO can get excited to the LUMO leaving a hole in the HOMO. While applying voltage the electron can move to the cathode and the hole can move to the anode and

produce electricity. This is the basic principle of organic electronics where the active materials can be pi conjugated small molecules or polymers.

Organic semiconducting materials have several advantages as compared to the inorganic ones, even if they lag in the conducting properties. Processing of silicon based semiconductors require harsh temperature conditions like 1000^{o}C whereas organic materials mostly require room temperature. The manufacturing procedure is simple; the organic material is deposited over a transparent electrode followed by the cathode deposition. Small molecule based devices are usually made by thermal evaporation method whereas polymeric devices are made by solution processing like spin coating, ink injecting etc. Thus the resulting device is thin and low in weight.[4-9] The devices made from organic materials are flexible, stretchable and soft which can never be afforded by silicon based electronics. Organic opto electronics have novel properties which cannot be replicated by silicon, thereby expanding the world of smart materials into unimaginable dimensions. Organic electronics is still a developing area of technology including devices such as Organic Field Effect transistors (OFET), Organic photovoltaics (OPV), Organic Light Emitting Diodes (OLED) etc.[10-14] However the field of organic electronics is still in its infancy and many challenges are yet to be overcome in this field. A material chemist can design and develop new molecules where the optical and electronic properties can be tuned, thereby a better performance from organic optoelectronic devices can be expected.

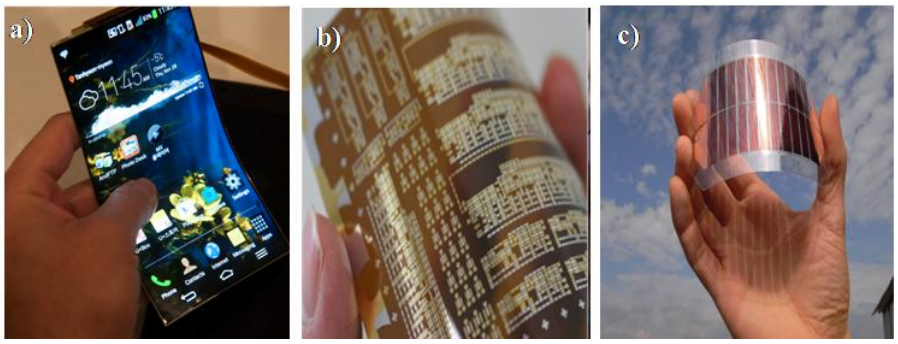

Figure 1.2: Examples of Flexible a) OLED b) OFET (c) OPV [adapted from *http://www.aps.org/publications/capitolhillquarterly/201302/whatsnewininnov.cfm*].

1.2. Organic Semiconductors:

Organic semiconductors provide the electronic advantages of semiconductors like conductivity along with unique photophysical properties. They are either organic small molecules or polymers which mainly consist of carbon and hydrogen along with some

hetro atoms like oxygen, sulphur, nitrogen etc.[15,16] Traditional semiconductors like silicon, germanium have low band gap 0.67 eV (Ge), 1.1eV (Si) and 1.4 ev (GaAs). Free charges can be created at room temperature by the thermal excitation from the HOMO to the LUMO. In contrast, the conductivity of organic molecules is extrinsic, which resulted from the injection of charges at electrodes, from intentional or unintentional doping and from the dissociation of photo generated electron hole pair that is bound by their mutual Coulomb interaction. Organic semiconductors are classified mainly in to two types a) n type b) p type according to their charge carrying nature. The electron rich p type materials are hole transporters in nature whereas the electron deficient n type semiconductors are electron transporters. Some examples of well studied p type and n type semiconducting materials are given below in chart 1.1 and chart 1.2. There is a library of small molecules and polymers which are p type semiconducting in nature. Fused acenes are possibly the most important family of p type organic semiconductors; especially pentacene is well known to exhibit extremely high hole mobility up to 3 $cm^2 V^{-1} s^{-1}$in thin films while single crystal mobilities reached up to 35 $cm^2 V^{-1} s^{-1}$.[17-20] Thiophenes (oligo and poly) form a separate class of p-type semiconductors that are widely studied due to their high charge carrier mobility and facile synthesis.[21] For example the sexithiophene (hexamer) shows good p-type properties but has solubility issues, whereas regioregular n-hexyl substituted polythiophene (P3HT) showed better solubility and self-organization behaviour with improved mobilities up to 0.1$cm^2 V^{-1} s^{-1}$.[22,23]

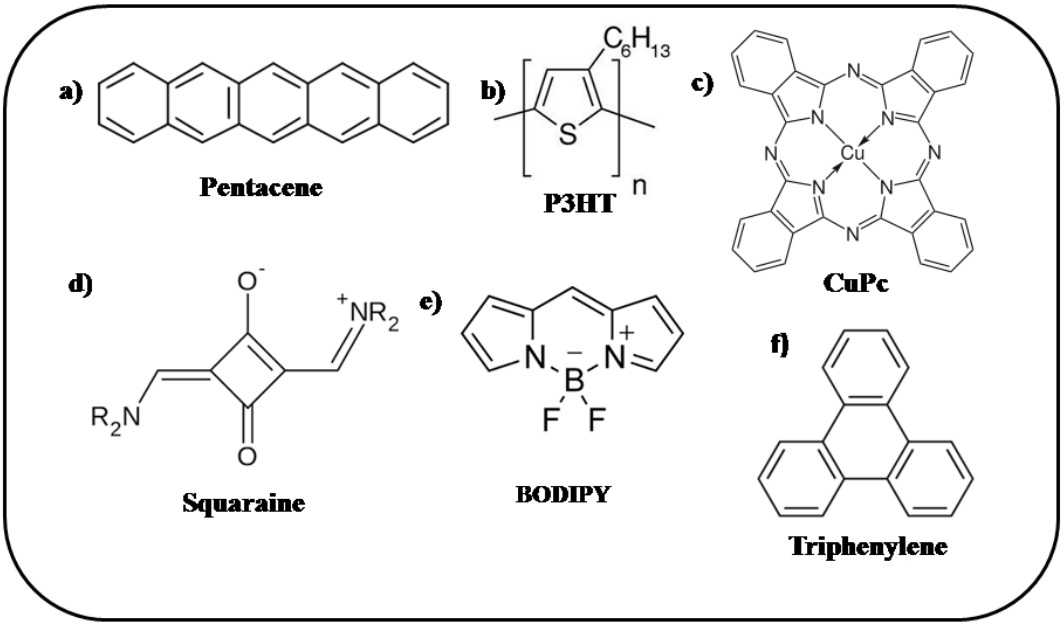

Chart-1.1: A selection of p-type organic semiconductor materials.

Other important p type materials are phthalocyanines (Pc) and its derivatives like Cu-phthalocyanine, merocyanine etc. Squaraine (SQ), borondipyrromethene (BODIPY), diketopyrrolopyrroles (DPP) etc are the new generation p type semiconductors which shows promising hole mobility.[24] Apart from these, hexabenzocoronene and triphenylene derivatives are the well studied p-type semiconductors which form discotic liquid crystalline phase.[25-28]

n type semiconductors are comparatively less available in literature since they have high electron affinity and less air stability. Fullerene and its derivatives (especially Phenyl-C61-butyric acid-methyl ester -$PC_{61}BM$) are the most extensively studied n-type semiconductors.[29] But they are poor in terms of solubility, processability, air stability etc. So there is a huge demand for non fullerene n-type semiconducting materials which can overcome these issues. Among the non-fullerene acceptors, Perylenebisimides (PBI) and Naphthalenebisimides (NBI) are the most promising candidates due to their excellent thermal and photostability, large absorption coefficients, tunable HOMO-LUMO band gap upon various substitutions at the bay positions.[30,31] Perylene based n-type small molecule and polymeric semiconductors will be discussed in detail in the following sections. Introducing electron withdrawing groups like fluorine or cyano groups to the aromatic core of the p type semiconductors make them n type in nature. For example perfluoropentacene (PFP), hexadecafluorinated copper phthalocyanine have exhibited electron mobilities up to $5x10^{-3}cm^2V^{-1}s^{-1}$.[32] Similarly, oligothiophenes with perfluorinated substituents also exhibited high electron mobility of 0.5 $cm^2 V^{-1} s^{-1}$.[33]

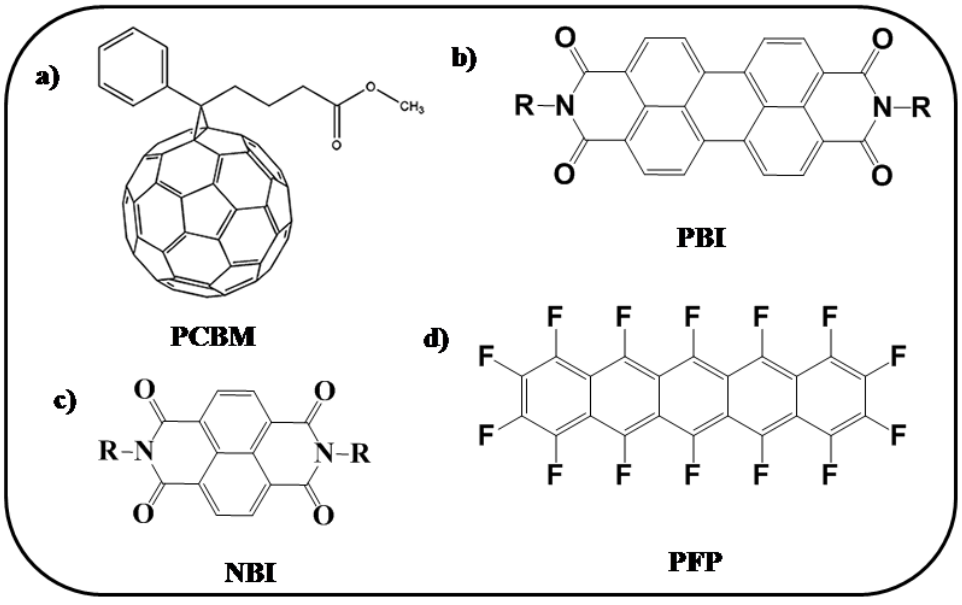

Chart-1.2: A selection of n-type organic semiconductor materials.

1.3 Experimental Techniques to Measure the Charge Carrier Mobility (μ)

1.3.1 Space-Charge Limited Current-Voltage Characteristics (SCLC) measurements

The experimental set up for this method consists of the organic layer sandwiched between two electrodes and uses a steady state voltage source. After applying a voltage through the sample, the current produced is measured. The current-voltage characteristics are then fitted to particular models based on two assumptions: (i) the charge transport is due to a single type of carrier only and (ii) the contacts are ohmic. From the acquired current-voltage behaviour at high electric fields, the mobility is calculated. However at lower injection levels, the presence of traps due to disordered nature of organic materials causes a reduction in current. Figure 1.3 shows the predicted crossover from the Ohmic region to the space-charge-limited current at higher electric fields.

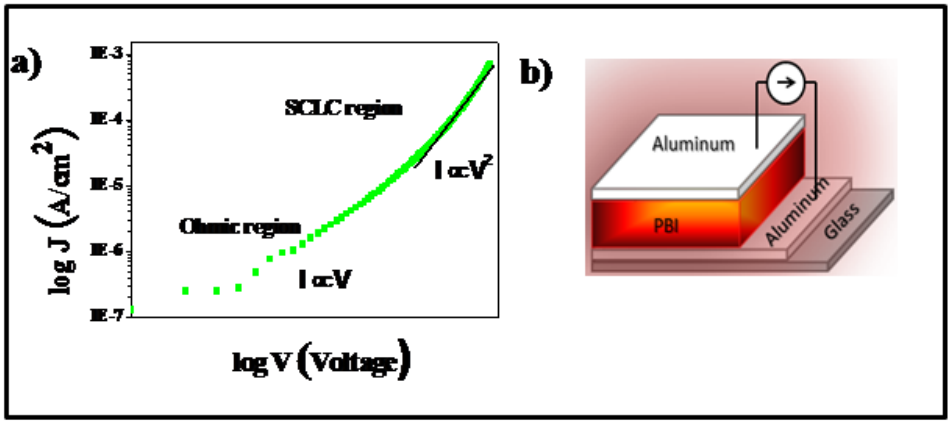

Figure 1.3: (a) log J – log V characteristic of SCLC measurements b) device structure

The first part of the graph corresponds to ohmic region (I α V), the second part corresponds to shallow trapping and when electric field is further increased all traps are filled at once. Finally the third part, trap-free SCLC region is reached where I α V^2 and the mobility can be most accurately determined from this region. Even if the trap-free regime is not available by experiments, the lower limits for intrinsic mobilities can be obtained by Child's law (Mott-Gurney equation):[34-36]

$$J_{SCLC} = \frac{9}{8}\varepsilon_0\varepsilon_r\mu\frac{V^2}{L^3}$$

Where J_{SCLC} is the current density, V the applied bias voltage, ε_0 the permittivity of free space, ε_0 the relative dielectric constant of the medium and L is the thickness of the device.

1.3.2. Time of Flight Method (TOF)

For TOF measurements an organic layer is embedded between two electrodes and irradiated by a short laser pulse near to one of the electrodes and this generates a thin layer of electron-hole pairs close to the contact. Depending on the polarity of the applied electric field the photo generated charges move across the layer towards the other electrode where the time dependent current is monitored. All the carriers simultaneously reach the electrode in case of highly ordered crystalline materials, whereas for amorphous systems the signal is broadened. Mobility is then calculated according to the equation:

$$\mu = \frac{d}{Ft} = \frac{d^2}{Vt}$$

Where d is the distance between the electrodes, F is the electric field, t is the averaged transient time and V is the applied voltage.[37]

1.4 Perylenebisimide as n type semiconductor

Perylene dye is a higher member of rylene family which is known for more than 100 years. The soluble derivative of perylene-3, 4, 9, 10-tetracarboxylic acid bisimide (PBI) was first prepared by Kardos in 1913 from the parent compound perylene-3,4,9,10-tetracarboxylic acid dianhydride (PTCDA).[17] Initially PBIs were extensively used as industrial dyes (soluble) and pigments (insoluble), due to light and weather fastness, high thermal stability, chemical inertness and most importantly due to high tinctorial strength with colors ranging from red to maroon to violet and even shades of black.[38,39] Later on perylenebisimides were explored as n type semiconductors (acceptor molecule) in the field of organic electronics. They have unique properties like high electron affinity, high photochemical stability, large molar absorption coefficients, high fluorescence quantum yield, easy substitution at the bay and the core positions by different functional groups etc.[40] PBIs have excellent self assembling properties and they are used to form liquid crystals, gels, nano wires, nano rods, nano plates, etc.[40]

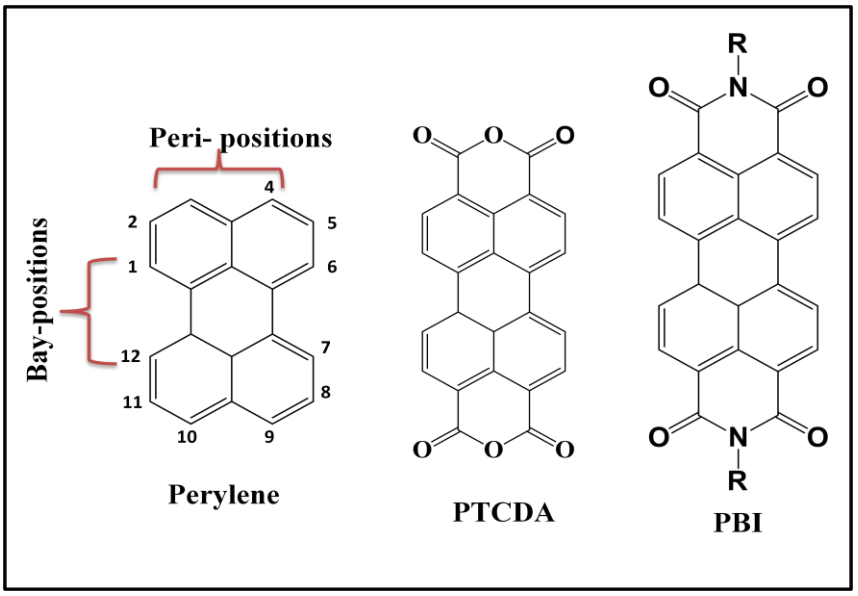

Figure 1.4: Chemical structures of perylene, PTCDA and PBI.

1.4.1 Synthesis of PBI:

The symmetrically substituted PBIs (SPBI) can be synthesised from PTCDA by the imidization reaction of aliphatic or aromatic amines at moderately high temperature in the presence of catalytic amount of Zinc acetate.[41] Dimethyl formamide (DMF), dimethyl acetamide (DMAc), quinoline, isoquinoline, acetic acid etc are the common solvents used for aliphatic amines where as for aromatic amines imidazole is used as solvent. The exact role of zinc acetate in this reaction is not yet understood properly but zinc salts might be acting as solubilizers on the basis of complexation with the anhydride. In literature SPBI molecules are reported with different substitutions like linear, cyclic, branched alkyl chains, oligo ethylene derivatives, aromatic group etc. Varying the imide substitution does not affect the optical properties and HOMO-LUMO energies of PBIs because the presence of nodes at the imide nitrogen atom prevents the conjugation between perylene core and the imide substituents.

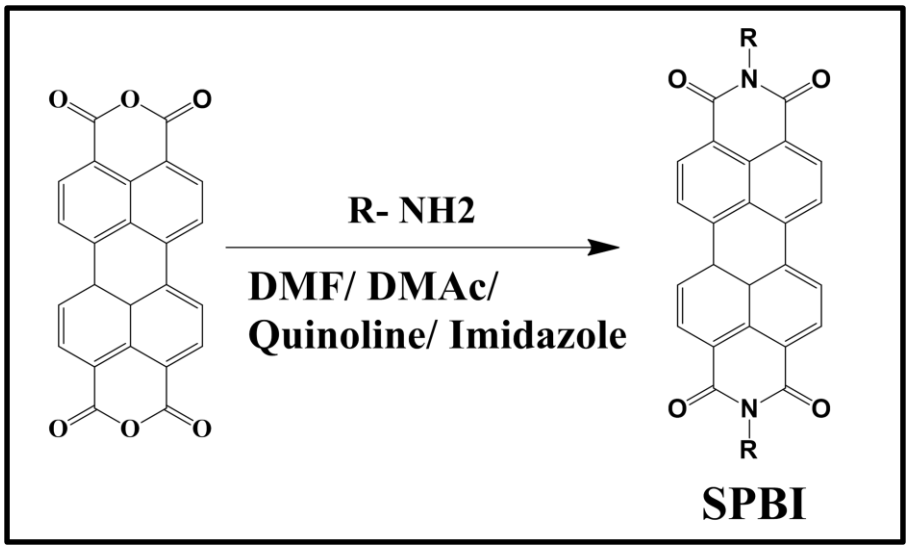

Figure 1.5: Synthesis of Symmetrical PBIs.

The synthesis of unsymmetrical substituted PBIs (UPBI) with different substituent on each imide position is achieved by multistep synthesis. The most frequently used method for the synthesis of unsymmetrical PBIs was developed by Langhals and co-workers, which involves the partial alkaline saponification of the symmetrically substituted PBIs to perylene mono-imide-mono-anhydride compounds. The symmetrical bisimides are readily hydrolyzed by a concentrated solution of KOH in *tert*-butyl alcohol and this reaction gives mixtures of PTCDA, SPBI, mono-imide mono- anhydride.[42-45]

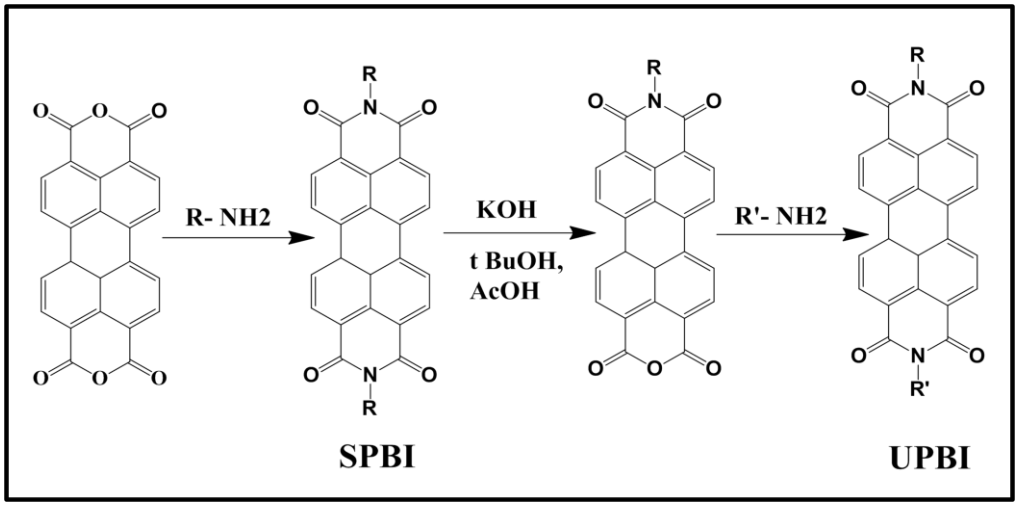

Figure 1.6: Synthesis of unsymmetrical PBI derivatives by Langhals's method.

Separation of the mono-imide-mono-anhydride from the starting bisimide and the completely saponified product can be easily done because only the PTCDA is soluble in concentrated alkali while the bisimide is insoluble and the mono-imide-mono-anhydride can be isolated by treatment of the residue with hot distilled water followed by acidification with dilute HCl. Further coupling of this mono imide with different amine will give the UPBI.

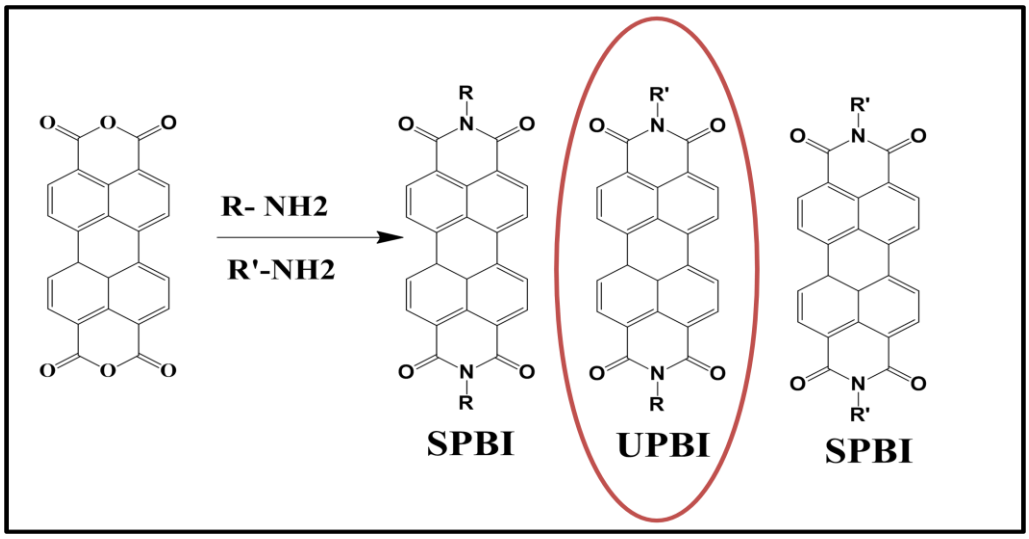

Figure 1.7: Synthesis of unsymmetrical PBI (UPBI) derivatives by simultaneous addition of two different amines (one pot synthesis).

Recently simultaneous condensation of PTCDA with a mixture of two different primary amines (one pot synthesis) was reported for the synthesis of unsymmetrical PBI. It is observed that if the reactivity of the amines are equal the yield of UPBIs is quite high and the desired unsymmetrical PBI can be separated (see figure 1.7) from this mixture by simple column chromatography technique.

1.4.2 Photophysical properties of perylenebisimides:

The absorption spectrum of PBIs in solution shows three predominant peaks in the range 450 nm to 540 nm corresponding to the 0-2, 0-1, 0-0 transitions. The molar absorption coefficients of isolated PBIs are typically in the range of 10^{-5} M^{-1} cm^{-1}, and have a quantum yield near to unity in the absence of any aggregation effects.[46] The emission spectrum used resembles the mirror images of the absorption spectrum with the singlet excited state lifetime being approximately 4 ns. Figure 1.8 shows the absorption and emission spectrum of PBI in chloroform solution. The lowest electronic transition

between the ground state (S0) and the first excited state (S1) as shown in the Jablonski daigram.

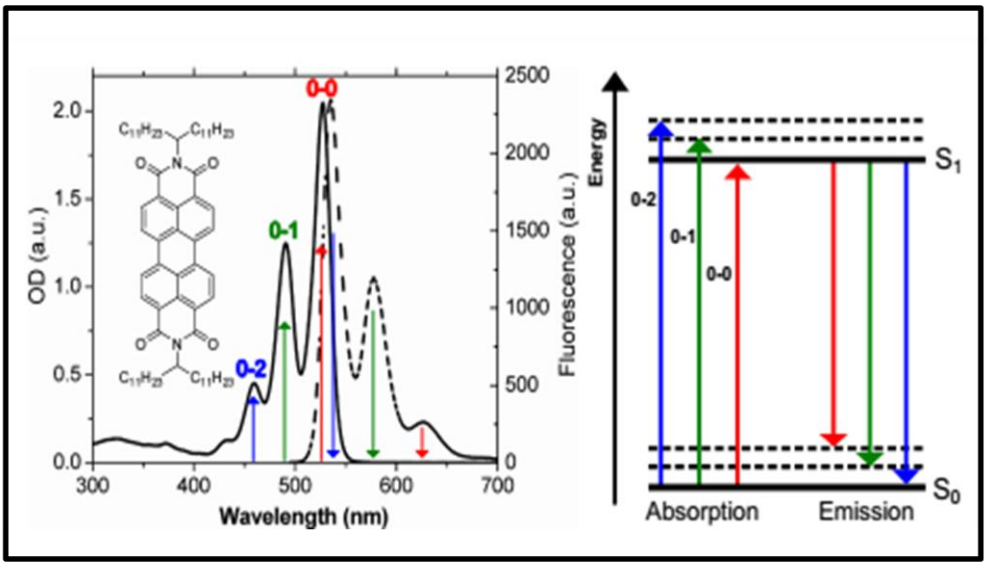

Figure 1.8: The Absorption and Emission Spectrum of PBI in chloroform (*adapted from ref.46*)

Most of the PBI derivatives exhibited solubility in polar solvents like chloroform, DCM, toluene, DMF, DMSO, acetonitrile etc. The strong π-π interaction between aromatic cores of PBI allowed them to stack in solid sate as well as solution. The solubility and aggregation properties of PBIs essentially depends upon the nature of substituents on the imide and the core. The nature of aggregation or supramolecular assemblies in solution exhibit distinct changes in the absorption and emission bands compared to monomeric species. The nature of aggregation in different solvent media can be divided in to two major types '*J*-type' and '*H*-type' depending upon spectral shift observed in absorption spectrum. Usually, *J*-type aggregates leads to a shift in the absorption spectrum to relatively longer wavelength (red or bathochromic shift) compared to monomer band, whereas *H*-type aggregation often shifts the absorption spectrum towards shorter wavelength (blue or hypsochromic shift). This phenomenon can be well explained by molecular exciton coupling theory i,e coupling between transition moments of the constituent molecules developed by Kasha *et al*. The difference in the spectral properties of the two types of aggregates is caused by distinct arrangements of molecules in stacks. Molecules can stack in parallel fashion (face-to-face or plane-to-plane stacking) to form sandwich type arrangement (*H*-dimer) or head-to-tail arrangement (end-to-end stacking) to form a *J*-dimer **(**Figure 1.9**)**. Actually, this difference in the stacking is due to the

different slip angle between stacked molecules. The angle between long axes of one of the parallel molecules in stack with respect to the line of centre of column within stack is called as 'slippage angle'. [47-53]

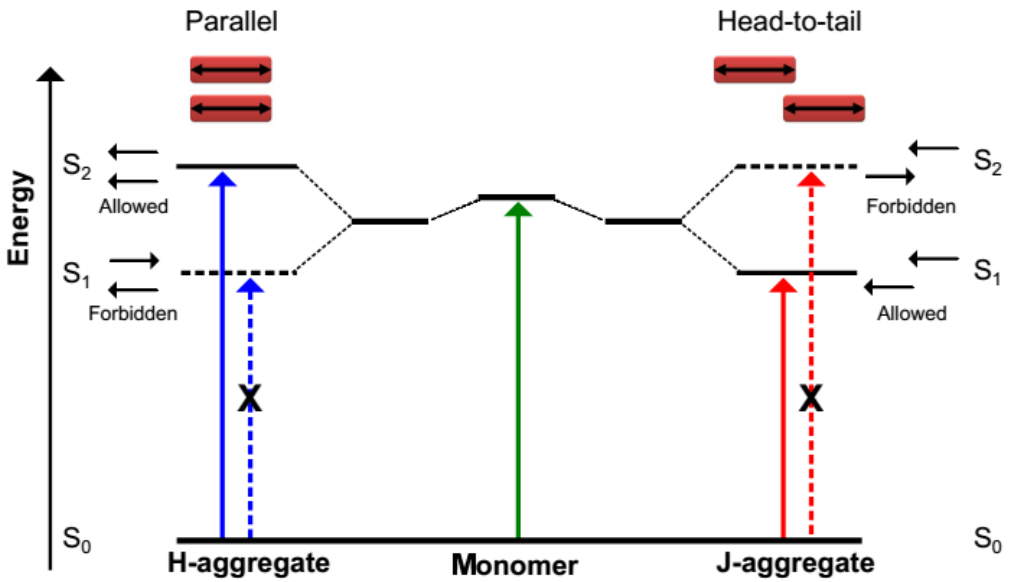

Figure 1.9: Schematic representation of relation between stacking (*J*-type or *H*-type) and spectral shift based on exciton theory.

According to exciton theory, each molecule in stack is considered as point dipole and the interaction between transition dipole in excited sate of aggregate leads to splitting of energy levels; one with higher energy level and the other with lower energy level than monomer energy level (Figure 1.9). For *J*-aggregates with large molecular slippage, only lower energy excited state transition is allowed. As a result, they show red shifted absorption band with high fluorescence quantum yield. On the other hand, only higher energy transition is allowed for *H*-aggregates (small molecular slippage) which results in blue shifted absorption band. The *H*-type aggregates exhibit strong quenching in fluorescence due to rapid energy relaxation to lower energy excited states.

1.5 Supramolecular Self assembly of Perylenebisimides:

The term 'Supramolecular Chemistry' was introduced by Jean Marie Lehn, which implies 'chemistry beyond the molecule' or the chemistry of molecular assemblies using non covalent bonds.[54]Supramolecular chemistry is a powerful tool for building larger

structures out of small building blocks by secondary interactions. The molecules in supra molecular architectures are non covalently self-assembled; they are held together reversibly by weak secondary intra and intermolecular attractive and repulsive forces.[55] Supramolecular architectures are formed by using weak intermolecular interactions such as hydrogen bonding, π-stacking, dipolar and van der Waals forces.[56] Construction of self-assemblies of π-conjugated molecules with controlled size, shape and overall morphologies is a topic of current interest as the bottom-up approach towards organic optoelectronic devices. Two important secondary interactions in the design of supra molecular materials are π-π and hydrogen bonding interactions. The π-π interactions often exist in π-conjugated materials; they are weak electrostatic interactions between aromatic rings. Hydrogen bonds are highly selective and directional and hence they are ideal secondary interactions to construct supra molecular architectures. Hydrogen bonds are formed when a donor with an available acidic hydrogen atom interacts with an acceptor carrying available nonbonding lone pairs of electron. The strength depends largely on the solvent as well as the number and sequence of hydrogen bonds. Thus, the packing of π-conjugated materials can be directed by means of supra molecular chemistry. The combinations of hydrogen bonding and π-π stacking interactions influence the orientation and spacing of these materials. In the coming section the two major supra molecular assembly formed by these interactions in PBIs will be discussed.

1.5.1 Liquid crystalline self assembly:

Liquid crystal (LC) is a state of matter that has properties between those of conventional liquid and solid crystal. Liquid crystals are fluidic in nature, like a liquid, but also exhibit a degree of molecular order like crystalline solids as shown in the figure 1. 10. Such an intermediate state of matter is called a "mesophase". Broadly, liquid crystals can be divided into two categories: thermotropic or lyotropic. Thermotropic LCs exhibits a phase transition into the LC phase as a function of temperature.[57-61] Lyotropic LCs exhibit phase transitions as a function of both temperature and concentration of the LC molecules in a solvent.Thus lyotropic phases are mainly found in biological systems. Depending on the type of ordering in mesogens, liquid crystals are mainly classified in to four different phases known as nematic, smectic, cholesteric and columnar phases. With respect to the shape of the LC molecules liquid crystalline materials are further classified in to calamitic and discotic liquid crystalline phase. Calamitic phase is formed by rod shaped molecules;

nematic and Smectic phase LC come under this classification. Discotic phase is formed by disk like molecules; columnar mesophase comes in this category.[62,63]

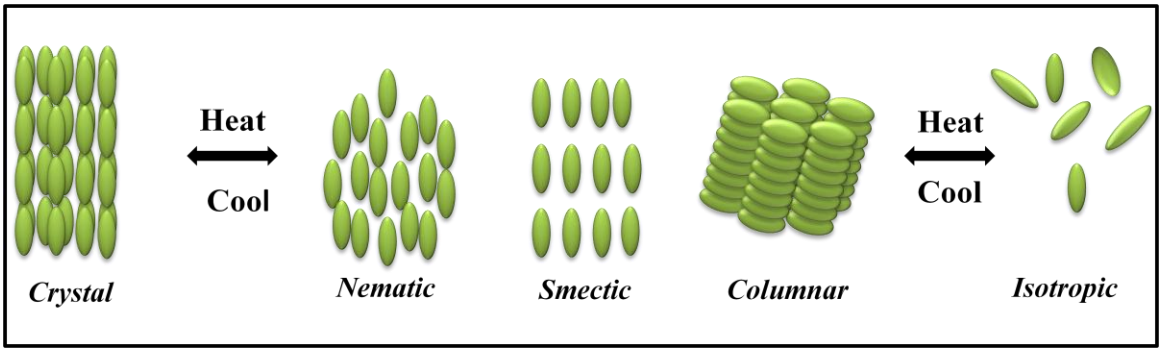

Figure 1.10: Schematic diagrams depicting orientation of molecules in crystalline, nematic, smectic, columnar and isotropic phases.

a) **Nematic phase:** The least ordered liquid crystalline phase having no positional order, but self-aligns to have long range directional order with their long axes roughly parallel to each other. Thus, the molecules are free to flow and their centres of mass positions are randomly distributed like a liquid, but the long-range directional order is preserved. Nematic phases are generally observed at higher temperatures with thread like textures.

b) **Smectic phase:** This is a higher ordered liquid crystalline phase as compared with the nematic phase. In addition to orientational order, the molecules in smectic phases are arranged in layers. The molecules in each smectic layer are randomly distributed, but, oriented in same direction. Depending on the orientation of the molecules with respect to smectic layer normal, this phase can be mainly classified in to smectic A, smectic C, smectic G and smectic F. In smectic A, the long molecular axis of the mesogens is parallel to the layer normal; however, in smectic C mesophases, the molecules are tilted with respect to layer normal by a tilt angle θ. The layer thickness of the smectic C phase is related to tilt angle as $d = l \cos\theta$.

c) **Cholesteric (or chiral nematic) phase:** The cholesteric N* phase can be understood as a chiral version of the nematic phase possessing only orientational order of the long molecular axis. This phase consists of local nematic layers, which are continuously twisted with respect to each other giving rise to helical superstructure with a twist axis perpendicular to local director.

d) **Columnar (discotic) phase:** A majority of discotic mesogens form columnar mesophases probably due to intense pi–pi interactions of poly aromatic cores. The core–core separation in a columnar mesophase is usually of the order of 3.5 A˚ so that there is considerable overlap of p-orbitals. As flexible long aliphatic chains surround the core, the intercolumnar distance is usually 20–40 A˚, depending on the lateral chain length. Therefore, interactions between neighbouring molecules within the same column would be much stronger than interactions between neighbouring columns. Consequently, charge migration in these materials is expected to be quasi one-dimensional.[64]

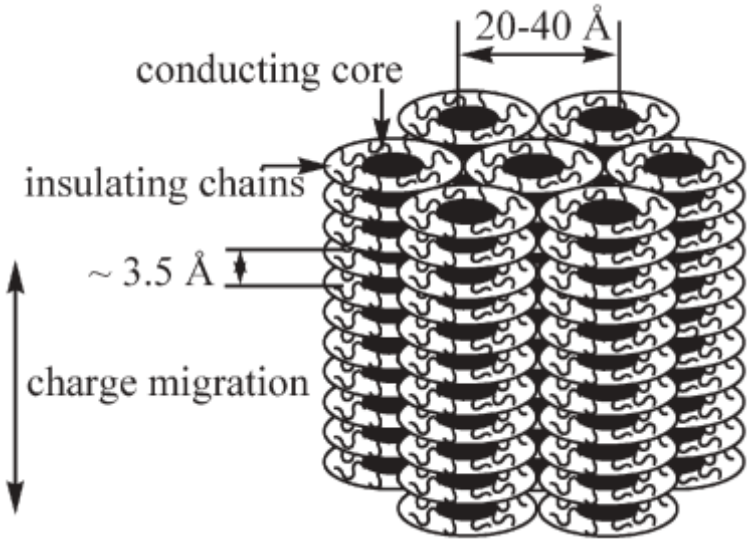

Figure 1.11: Schematic representation of mesogen arrangement in columnar phase.

Among the various new materials for organic electronics, π-conjugated liquid crystals (LCs) are currently viewed as new generation of organic semiconductors. These materials offer the advantages of controlling the order in the bulk at all length scales from molecular to macroscopic distances. Upon thermal annealing these molecules can form single large domain with less number of grain boundaries. This is because of their inherent self healing property due to the partial liquid like behaviour. π-conjugated calamitic (rod-like) LCs differ from discotic (disc-like) mesogens in terms of molecular shape, phase symmetry, the dimensionality of their charge transport, exciton migration and in the extent of their orbital overlap (figure 1.12). Therefore columnar liquid crystalline materials have several advantages over organic single crystalline materials like easy processing, ability to form thin films, long range self assembly, less number of grain boundaries etc which are the key factors for efficient charge transporting. But the main

challenges in this area are the attainment of mesogenicity in a temperature range that is adaptable on a device substrate; the clearing temperatures should be low and ideally the liquid crystalline phase should be retained at room temperature and the formation of single metastable mesophase since the charge mobility will vary from one mesophase to another.

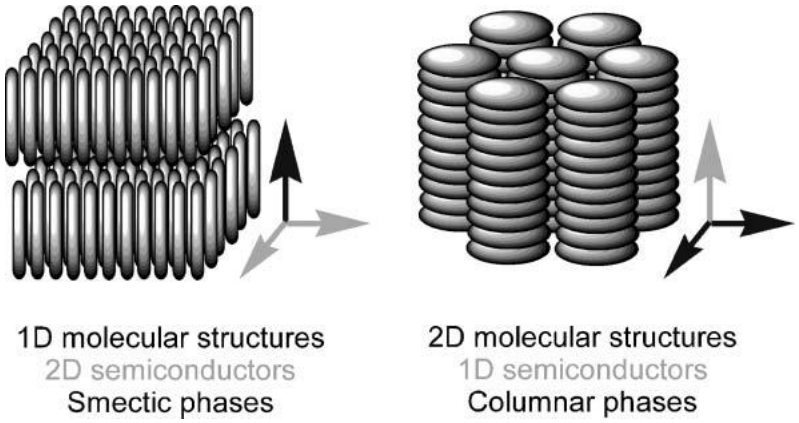

Figure 1.12: Mesogen arrangement in calamitic and discotic liquid crystals

The history of discotic liquid crystals dates back to the year 1977 when Chandrasekhar et al. reported that not only rod-like molecules, but also compounds with disc-like molecular shapes formed liquid crystalline mesophases. Discotic LCs consists of a large planar conjugated rigid aromatic core and flexible peripheral chains.[64]These molecules self-organized to form stacks and high electron wave function overlap along the stacks in the columnar phases resulted in high charge carrier mobilities. The chemical

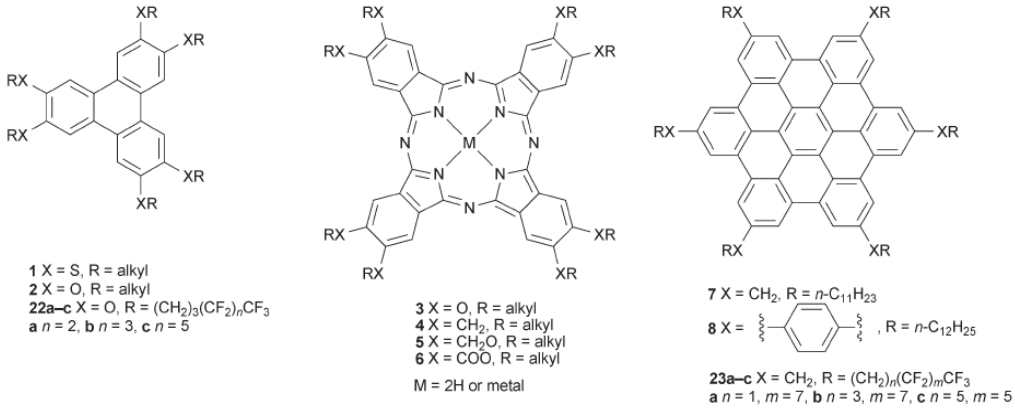

Figure 1.13**:** Chemical structures of commonly used π- conjugated discotic LCs.

structures of some of the extensively studied π- conjugated discotic LC materials are shown in the figure 1.13.

1.5.2 Spacer effect on liquid crystalline behavior:

A liquid crystalline material consists of two parts 1) one rigid core called as mesogen and 2) the flexible part called spacer. A minimum balance between this rigidity and flexibility is required for getting liquid crystalline phase since the rigid core contributes to the crystalline nature where as the flexible part imparts the fluid like behavior. The flexible spacer can be either methyl chain, oligo ethylene chain or silicoxy chain.[65] The nature and packing of these spacer units play a crucial role in the entire packing and liquid crystalline behavior of these materials. In the case of liquid crystalline dimer, where the mesogenic units are connected by middle flexible alkyl spacer, an even spaced molecule will have a zig zag confirmation in which the mesogenic units are anti parallel where as the odd spacered molecule will have a bent conformation (see figure 1.14) where the mesogenic units are inclined with respect to each other. This results in a better packing in even spacered twin molecule as compared with their odd one which can reflect in their high values in melting transitions and enthalpy of transitions. Similar are the observations with the terminal methyl spacers. The dramatic dependence of the translational properties on the length and parity of flexible spacers linking the mesogenic unit is called as odd-even effect. This is observed in the properties like melting point, clearing enthalpies in most of the liquid crystalline systems.[65] This concept will be further discussed in detail in the coming sections.

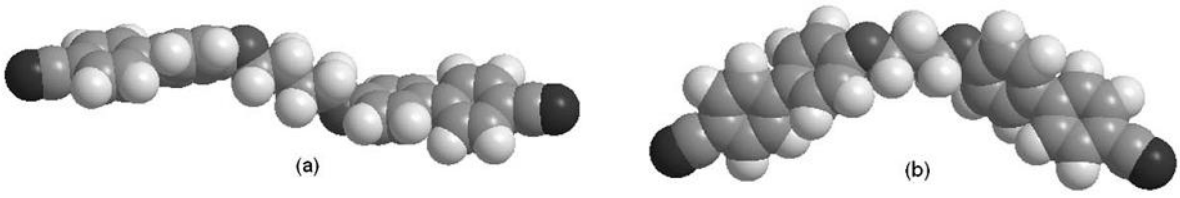

.

Figure 1.14: The molecular shape of (a) an even (b) an odd membered liquid crystalline dimer. (*Adapted from ref. 65*)

1.5.3 Liquid Crystalline Perylenebisimides:

The first liquid crystalline perylenebisimide was reported by Cornier et al in 1997, where symmetrically substituted perylenebisimide with linear alkyl or poly (oxy ethylene) chains were reported. This was the first report on an n type semiconducting liquid crystalline material even though p type LC materials were reported and the charge carrier mobilities were studied.[66,67] Later, Strujik et al reported a series of symmetrical perylenebisimide with different alkyl substitution (n = 7, 12 and 18) as given in figure

1.15. The isotropisation temperature was found to decrease with decreasing the alkyl chain length. Both the smectic and columnar phases were observed in these systems. The charge carrier mobilities of liquid crystalline derivatives (0.1 cm^2 V^{-1} s^{-1}) were comparable with that of crystalline derivatives (0.2 cm^2 V^{-1} s^{-1}).[68]

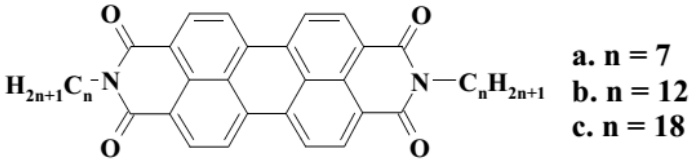

Figure 1.15: The structure and spacer length of PBI reported by Strujik et.al.

The research group of Professor Frank Wrutner has contributed enormously to the understanding of the effect of substitution on liquid crystalline and photophysical behavior of perylenebisimide by varying the substituents (figure 1.16) at the core as well as the bay position. Even though the bay substitution disturbs the packing of the perylene core, liquid crystalline properties were observed in these systems. The tridodecyl phenyl substituent (gallate unit) has inherent self assembling behavior which upon substitution with perylene helps to enhance the fluorescence quantum yield along with liquid crystalline properties. Most of these systems formed columnar mesophase with wide liquid crystalline windows and some of them exhibited room temperature liquid crystallinity.[69,70]

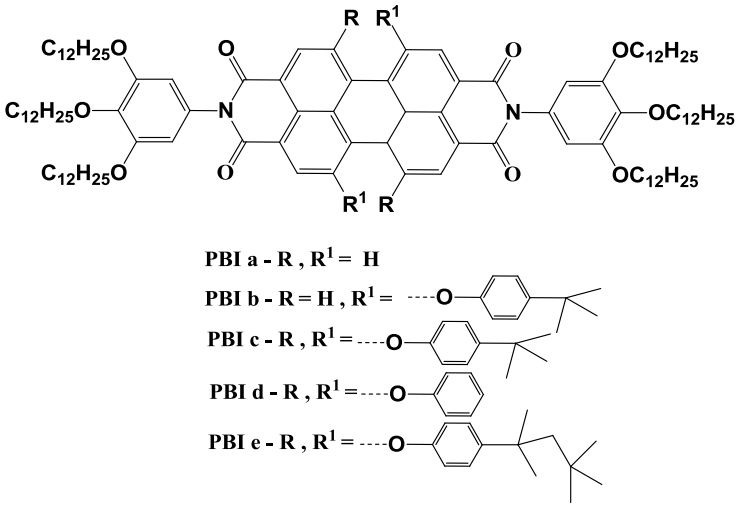

Figure 1.16: The structure of SPBI with different substituents (*adapted from ref.70*)

Except the last member in the series all of the others showed columnar mesophase. Later on Marder et al studied the SCLC mobility of room temperature columnar hexagonal perylenebisimide. He studied two PBIs 1) where the gallate units were directly connected to the imide linkage (PBI a) 2) gallate units were connected through a flexible methyl spacer (PBI b).[71] The structures are shown in figure 1.17. The melting point of PBIa was 373 ^{o}C where as the flexible spacer reduced the melting point of PDI 2 to 226 ^{o}C. The SCLC mobility of PBI b of 0.2 cm^2 V^{-1} s^{-1} is the highest mobility value reported for a liquid crystalline perylenebisimide till now with a device configuration of Glass / Al/ PBI / Al.

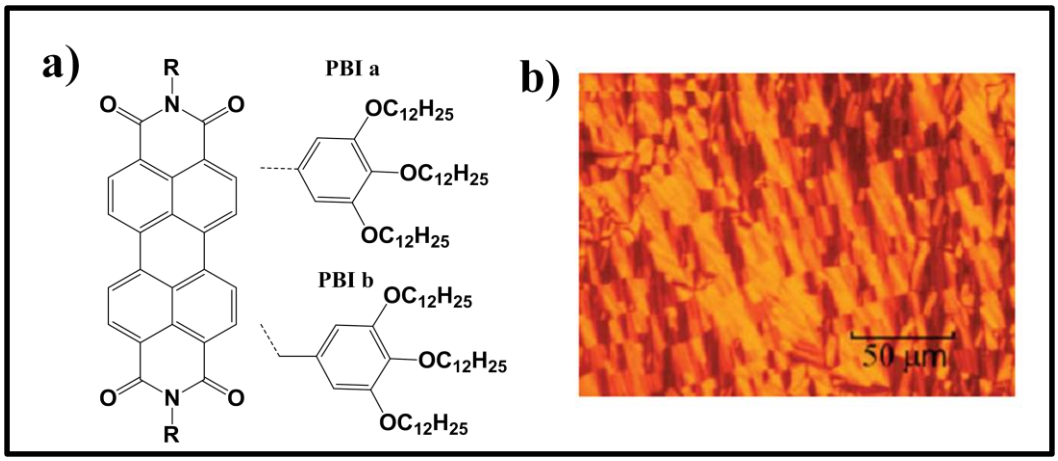

Figure1.17: a) The structures of PBI a and PBI b and b) the PLM image of PBI b (*adapted from ref.71*)

Jancy et al studied different factors such as 1) spacer length (C2, C6, C12), 2) spacer type (linear vs cyclic) 3) nature of linkage (ester vs amide) on symmetrical perylenebisimide. Among the linear and cyclic spacers, linear spacer was found to be best for inducing liquid crystallinity, among them the hexyl spacer was found to be the best.[72] Among the hexyl spacered system ester system was found to be more favorable for inducing liquid crystallinity as compared with the rigid amide system. They also synthesized a series of highly fluorescent liquid-crystalline perylenebisimide molecules having amide or ester linkage and end capped with phenyl, mono dodecyloxy phenyl or tri dodecyloxy phenyl units. The structure of PBI with ester linkage with mono dodecyloxy phenyl substitution showed figure 1.18.

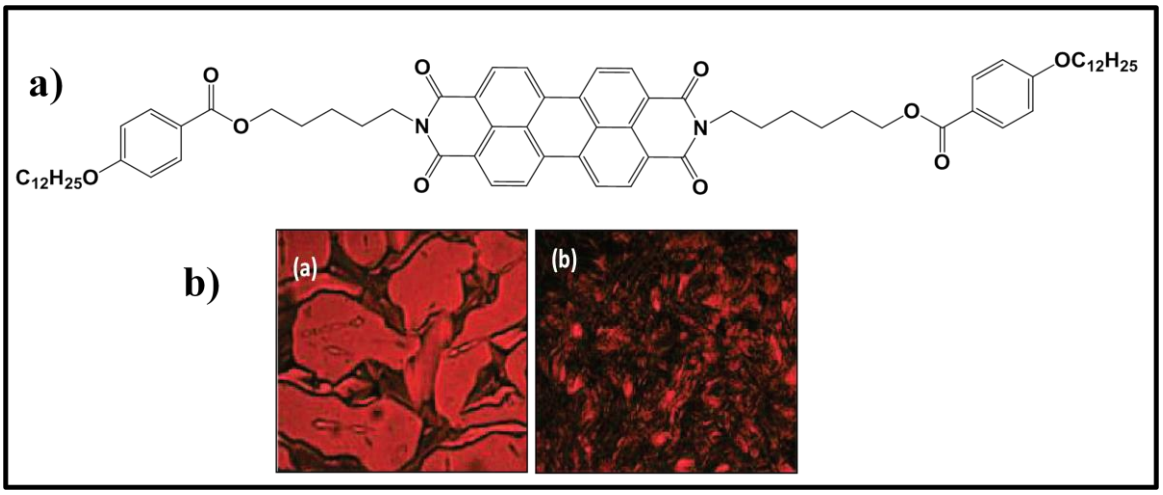

Figure 1.18: a) the structure and b) the PLM images of the PBIs (a*dapted from ref. 72*)

The study indicated that the presence of a single terminal dodecyloxy phenyl substituent had a very stabilizing effect on the overall properties like stability of liquid crystalline phases, stability of aggregates formed, etc., when compared to no terminal dodecyloxy benzyl substitution or tridodecyloxy benzyl substitution. This was true for both the ester as well as amide linkage having mono dodecyloxy benzene substitution.

Thelekkat et al reported for the first time the liquid crystalline behavior of unsymmetrically substituted perylenebisimides. The PBIs were both symmetrically and unsymmetrically substituted with either alkyl swallow tail or oligo ethylene glycoether (OEG) swallow tail chains. Symmetrically and unsymmetrically *N*-substituted perylenebisimides were synthesized by two different synthetic strategies. They used swallow-tail and linear alkyl or oligo oxy ethylene (OEG) substituents.[73] The introduction of oligoethylene chain facilitated liquid crystalline behavior and the unsymmetrical substitution helped to tune the mesophase window. The mesophases exhibited characteristic columnar hexagonal packing arising from π-π interactions between cofacially orientated perylene molecules.

Recently Thelekat et al carried out a comparative study of SCLC mobility with liquid crystalline PBI and its crystalline counterpart. The results are quite promising; the SCLC mobility of liquid crystalline PBI is increased by 2 orders of magnitude up to 7 x 10^{-3} cm^2 V^{-1} s^{-1} while the mobility of the crystalline one decreased by 4 order after annealing.[74] Cheng et al reported a similar result where the liquid crystalline PBI showed better power conversion efficiency as well as better SCLC mobility as compared to the crystalline one at the same conditions.[75] The fluid like behavior of the liquid crystalline material heals

the grain boundaries. This along with its ordered arrangement may help to improve the better charge transporting.

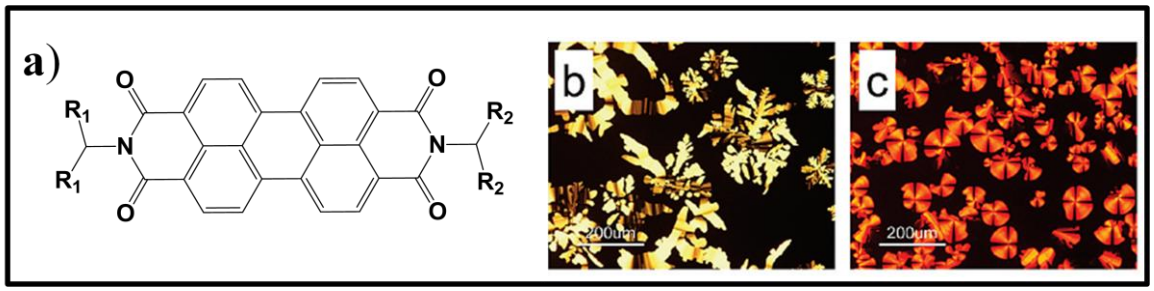

Figure 1.19: a) the structure and b) the PLM images of the PBIs (*adapted from ref.73*)

Further reports are coming in this direction, but the values are not too high. Various molecular designs and theories have been proposed for understanding structure property relationships, however, a clear understanding of these relationships is a missing link in the literature and there is still more to explore.

1.6 Hydrogen bond assisted self assemblies:

Hydrogen bonding interactions can be considered as a master key for molecular self-assembly due to its directionality and relatively predictable strength. A large number of functional units such as phenols, amines, trans-amides, sulphonamides, etc. dimerise through a single H-bond.[76-80] Similarly, carboxylic acids, cis and trans amides, oxalamides and urea groups have been incorporated in π-conjugated backbone for dimerization through two hydrogen bonds. Tridentate H-bonding units such as diaminotriazine exhibited significantly higher stabilities as compared to bidentate hydrogen bonding groups. Functional units that form four hydrogen bonds (quadruple hydrogen bonding units) have become extremely popular in π-conjugated materials because of high stability imparted to supramolecular assemblies. Supramolecular organization of these electronically active π-conjugated molecules through hydrogen bonding interactions has been extensively utilized for fine-tuning and optimizing their electronic properties.The hierarchical self-assembly of p-type oligo(*p*-phenylenevinylene) and n-type perylenebisimide into chiral fibers with a diamino triazine hydrogen bonding motif has been reported from Meijers group.[81] This is one of the most cited reports where a donor and an acceptor molecule were arranged in to nano fibers using non covalent hydrogen bonding. Perylenebisimide acceptor has two complementary binding sites for the diamino triazine hydrogen-bonded moiety of OPV molecule. Upon photo illumination of these fibers, electron transfer takes place leading to charge separation within the

aggregated dyes. These assemblies showed photo induced electron transfer that is useful for solar cell applications.

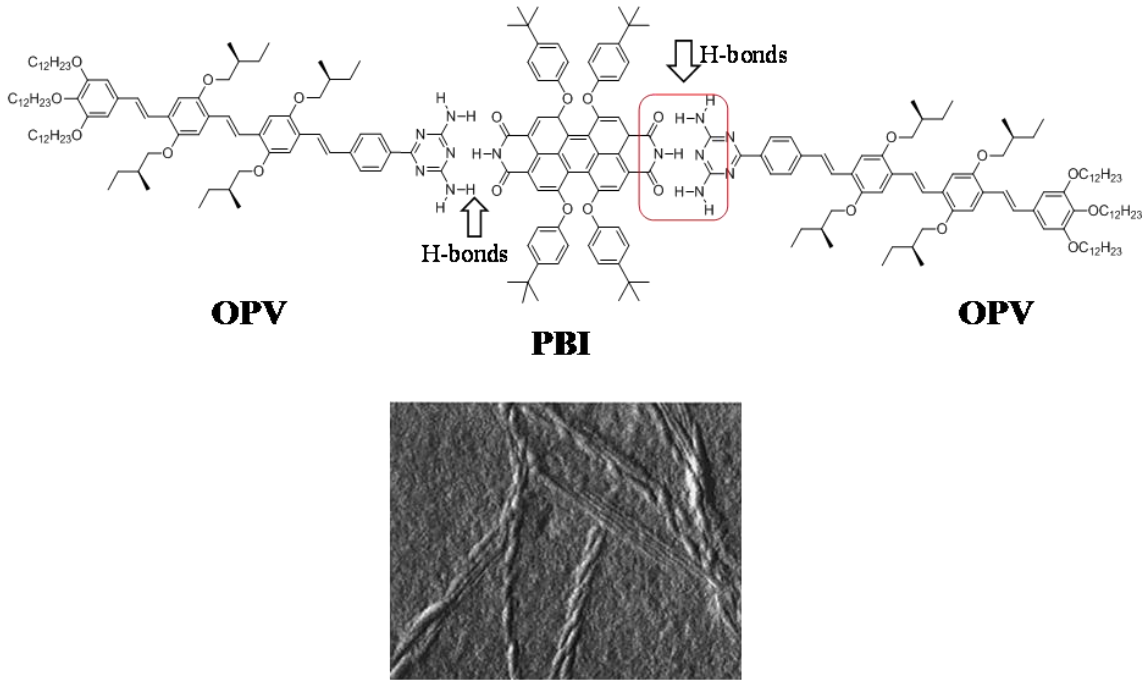

Figure 1.20: Hydrogen bond assisted self assembly of OPV and PBI and helical nano structures formed by this assembly. *(Adapted from ref. 81).*

Later on Meijer and co-workers reported the supra molecular copolymers of three different π-conjugated oligomers; a blue-emitting oligofluorene, a green-emitting oligo (phenylenevinylene) and a red-emitting perylenebisimide functionalized with self-complementary quadruple hydrogen bonding ureidopyrimidinone (UPy) units at both ends as shown in the figure 1.21.[82] The molecules were self-assembled in solution and in the bulk, forming supra molecular white emissive polymers. Light emitting diodes based on these supra molecular polymers were also prepared from all three types of pure materials, yielding blue, green, and red devices respectively. At suitable mixing ratios of these three compounds, white electroluminescence was observed.

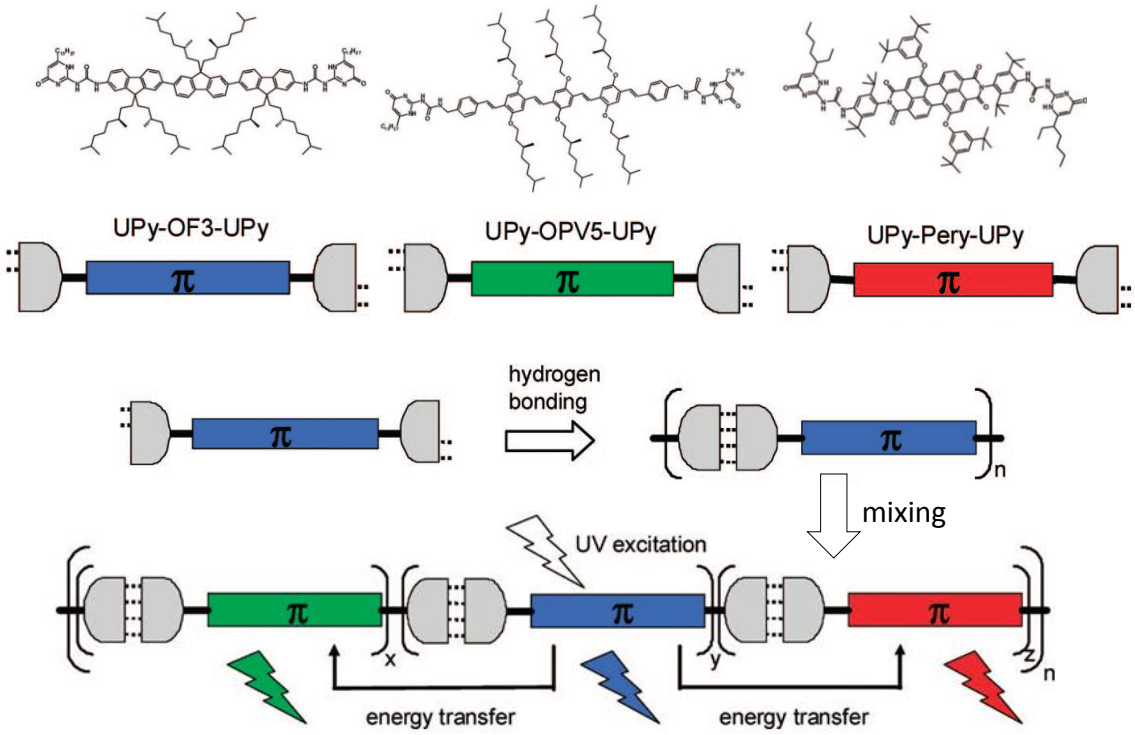

Figure 1.21: structures of di-UPy functionalized chromophores and a schematic illustration of white photoluminescence*(Adapted from ref. 82)*

Supramolecular comb polymers are formed by the hydrogen bonding interaction between donor polymers with acceptor small molecules. Several design principles have been developed to create different functional materials based on supramolecular polymeric architectures. In this regard, a novel strategy for side-chain hydrogen bonded supra molecular polymers was introduced by Ikkala and ten Brinke *et al*, where the bulk state properties of comb-shaped supra molecules obtained by hydrogen bonding of short, flexible, non-mesogenic amphiphiles with a readymade polymer poly(4-vinylpyridine) (P4VP) were studied.[83-90] The complexation of P4VP via hydrogen bonding to pentadecylphenol (PDP) and nonadecylphenol (NDP) showed that for a stoichiometric composition denoted as $P4VP(PDP)_{1.0}$ the system ordered into a lamellar morphology confirmed by transmission electron microscopy (TEM) and small angle X-ray scattering (SAXS) data.

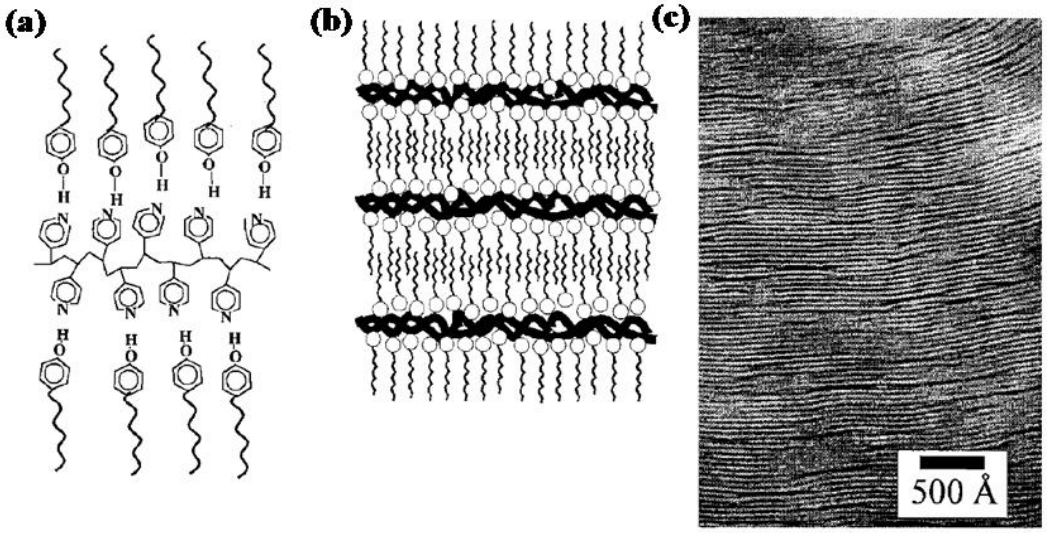

Figure 1.22: a) Comb-shaped supramolecule P4VP(PDP)$_{1.0}$ b) and c) Cartoon and TEM picture of self-organized lamellar structure respectively. [*Adapted from ref. 83]*

The same group further extended this concept to the formation of comb-coil supra molecular diblock copolymers where the comb was formed by hydrogen bonded P4VP-PDP and NDP (nonadecyl phenol) block whereas the coil was formed by polystyrene (PS) block; the resulting block copolymer supra molecule P4VP (PDP)$_{1.0}$-*b*-PS is shown figure 1.23.

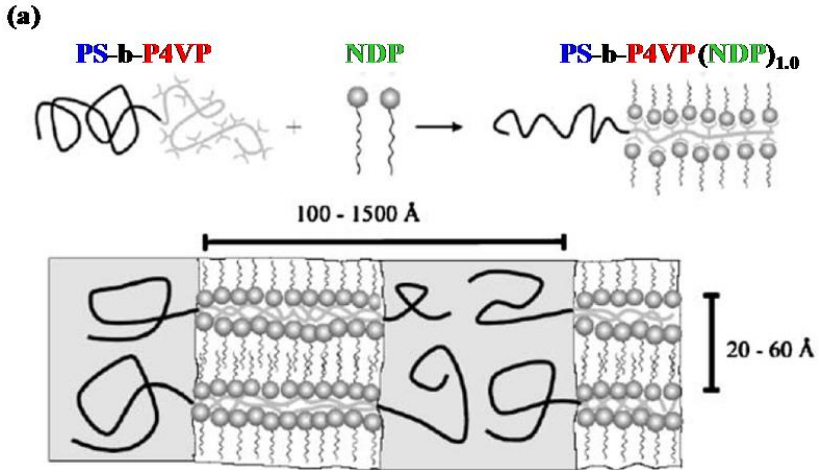

Figure 1.23: (a) Schematic representation of the PS-*b*-P4VP (NDP)$_{1.0}$ supra molecule showing the two length scale structures.

The overall self-assembly lead to hierarchical structures like lamellar-within-lamellar characterized by two length scales. The microphase separation between the comb-shaped supra molecular block P4VP (PDP)$_{1.0}$ and the linear coil PS block gave rise to a large

length scale structure while a small length scale structure was formed by microphase separation within P4VP(NDP)$_{1.0}$ domains. By varying the relative block lengths of the P4VP-*b*-PS selectively all the classical morphologies could be obtained with a series of structure-within-structure morphologies. Figure 1.24 shows the cartoon and TEM images of the different length scale structure-within-structure morphologies for supra molecular comb-coil diblock copolymer P4VP (NDP)$_{1.0}$-*b*-PS with slightly larger nonadecylphenol (NDP) side arms.[84]

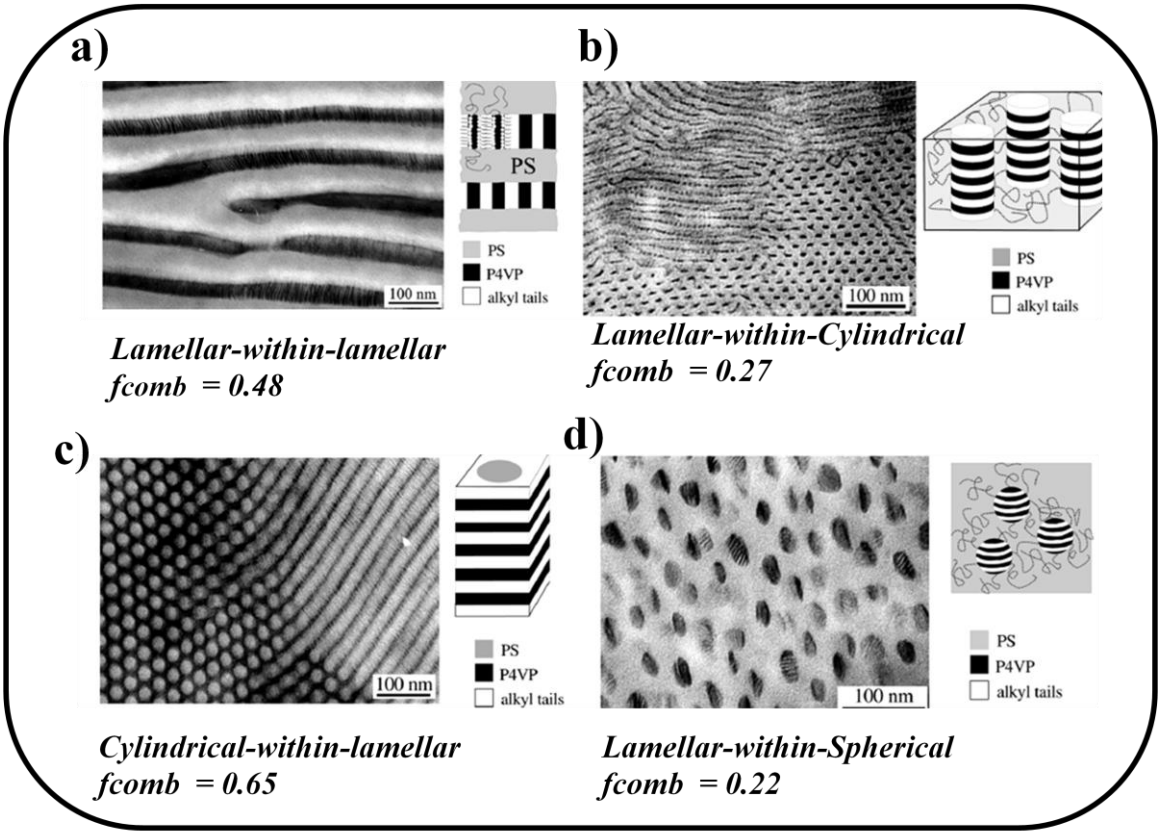

Figure 1.24 a) – d) shows the TEM images of different structure-within-structure morphologies obtained by varying the comb fraction of PS-*b*-P4VP (NDP)$_{1.0.}$ [*Adapted from ref.84*]

This concept of attaching small molecules to block copolymer based supra molecules was applied by the group of Ting Xu and Frèchet *et al.* to a p-type organic semiconductor like quaterthiophene named '4T' which was hydrogen bonded to PS-*b*-P4VP (figure 1.25) resulting in solution processable nanostructured semiconductor composites with charge carrier mobilities of order 10^{-4} $cm^2V^{-1}s^{-1}$ comparable to the existing semiconductors already used in OPV devices.[91]

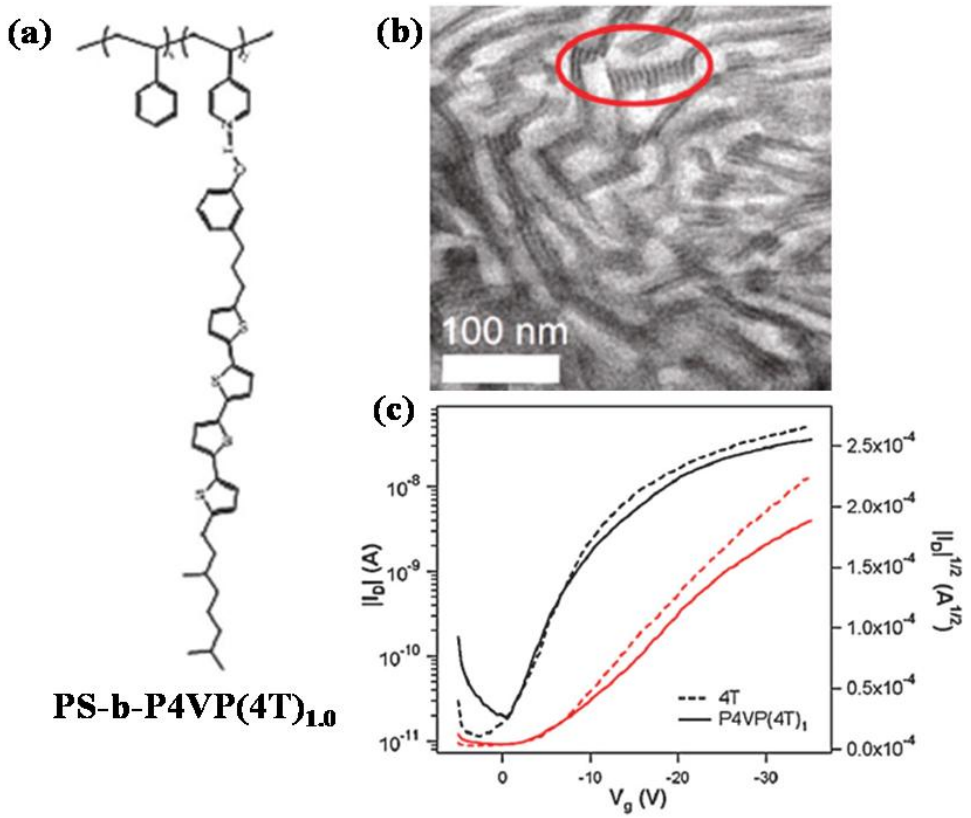

Figure 1.25: (a) Chemical structure of PS-*b*-P4VP(4T)$_{1.0}$ and its TEM image showing lamellar-within-lamellar morphology. (c) I-V curves of OFET devices from '4T' and P4VP(4T)$_{1.0}$ active layers. [*Adapted from ref. 91*]

Motivated by these successful accomplishments in the field of supra molecular assemblies, Rekha et al from our group initiated a novel approach of incorporating an n-type organic semiconductor molecule, perylenebisimide into polymer scaffold using secondary interactions.[92] This approach helped to improve the processability of perylenebisimides without looing its crystallinity. Pentadecylphenol (PDP) based unsymmetrical perylenebisimide (**PDP-UPBI**) was designed and synthesised which non covalently incorporated in to poly (4-vinyl pyridine) (P4VP) polymer via hydrogen bonding as shown in figure 1.26. Various stoichiometric complexes of **P4VP (PDP-UPBI)$_n$** where *n* was varied from 0.25 to 1.00 were prepared by simple solution mixing Nice lamellar morphology was observed in TEM for these complexes. A drastic improvement in charge carrier mobility was observed in the P4VP- UPBI complexes as

compared with the pristine UPBI. This study will be discussed in detail in the working chapters.

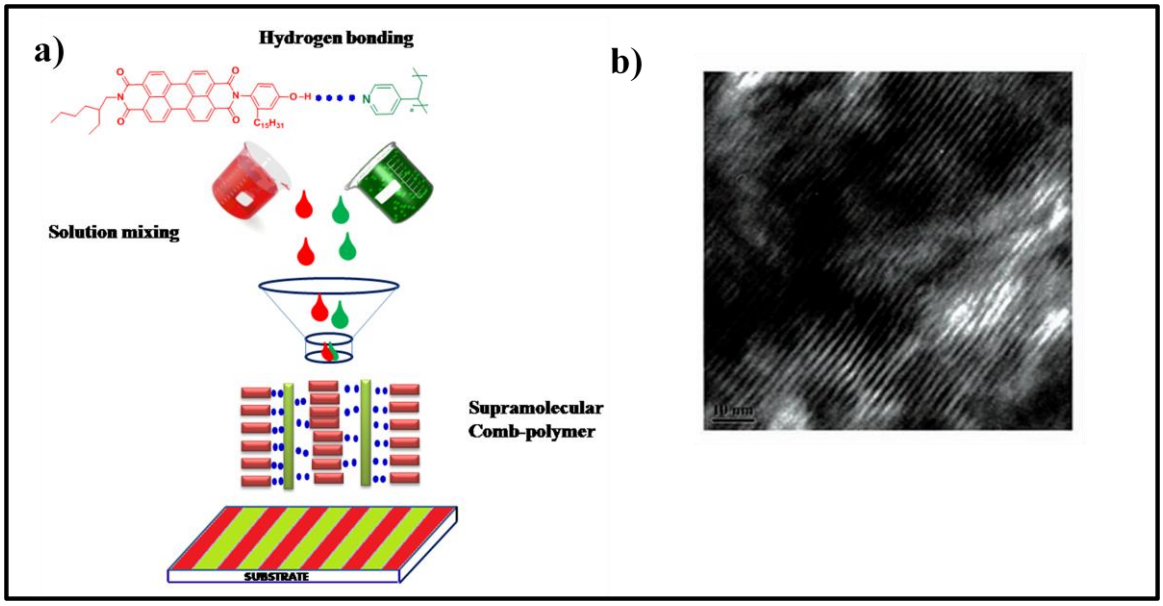

Figure 1.26: a) Schematic representation of hydrogen bonding between P4VP and UPBI b) TEM image of P4VP-UPBI complex in dry DMF showing nice lamellar morphology.(*Adapted from ref .92*)

1.7 Pentadecyl phenol (PDP): PDP is a natural amphiphilic molecule obtained from cashew nut shell liquid (CSNL), which is one of the rich renewable resources and industrial waste. The main constituents of CSNL are 1) Pentadecyl phenol (saturated C15- chain) and cardanol (unsaturated C_{15}-chains) as given in figure 1.27. The brown coloured mesocarp of the nut is processed to get the white coloured cashew nut along with cashew nut as waste by product.[93] The CSNL consist of 18-27% of total raw nut weight. They are amphiphilic in nature having a long 15 carbon alkyl chain meta to the phenolic group. This alkyl chain helps to improve the processability and solubility of pentadecyl phenol and cardanol derivatives.

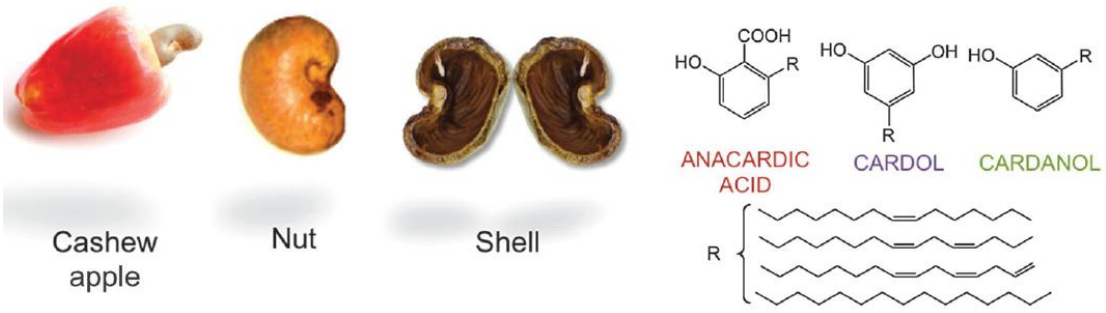

Figure 1.27: Cashew nut shell and its main constituents. (a*dapted from reference 94*)

These derivatives are not edible, and therefore, extensively used by various research groups including ours as renewable resource intermediates in material science for making polymers, nanomaterials, gels, etc. Prof. John et al studied the self assembly of glycolipid with pentadecyl phenol and its derivatives. The sugar moiety act as a non ionic polar head and bestows chirality to the molecules. This self assembly resulted in the formation of soft materials such as twisted fibers, helical coils, high aspect ratio nanotubes as given in the figure.[94]

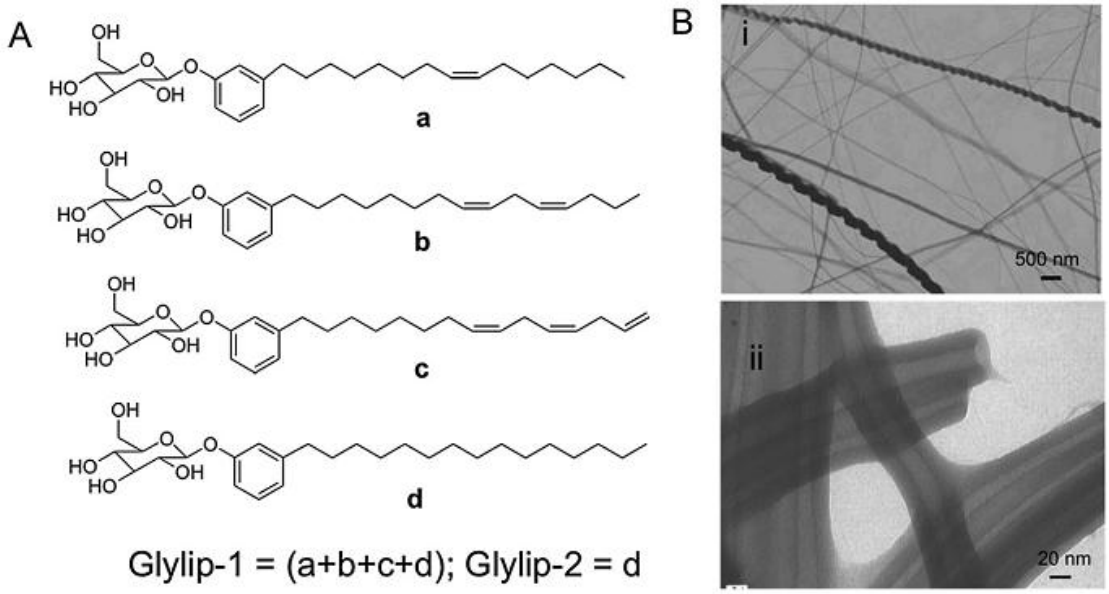

Figure 1.28: a) Chemical structure of glycolipids b) nanostructures formed by this assembly.

Prof Jayakannan *et al.* have reported benzene sulphonic acid derivative of cardanol and PDP as a dopant to produce polyaniline microspheres, dendritic and linear nanofibres, nanotubes, etc. (see figure 1.29). These molecule was also used to tune the size, shape and ordering of polymeric nanomaterials. The strategy was found to be very attractive for

new research activities in conducting polymer nano-materials more specifically for conducting polyaniline and related nano-materials.[97]

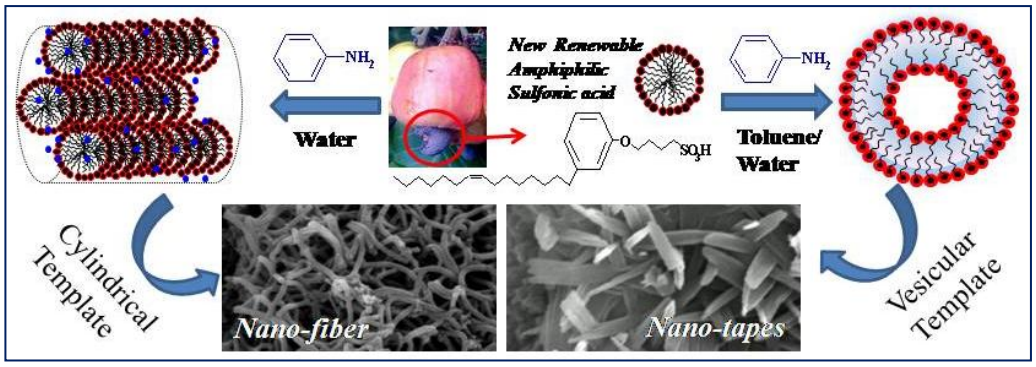

Figure 1.29: Polyaniline nanomaterials prepeared using benzene sulfonic acid derivative of cardanol.

1.7.1 Pentedecyl Phenol functionalied Perylenebisimides: The previous section emphasised the self assembly of pentadecyl phenol and its derivatives for different applications. Our group introduced a new building block where perylenebisimides (PBI) were substituted symmetrically and unsymmetrically with pentadecyl phenol as shown in figure 1.30

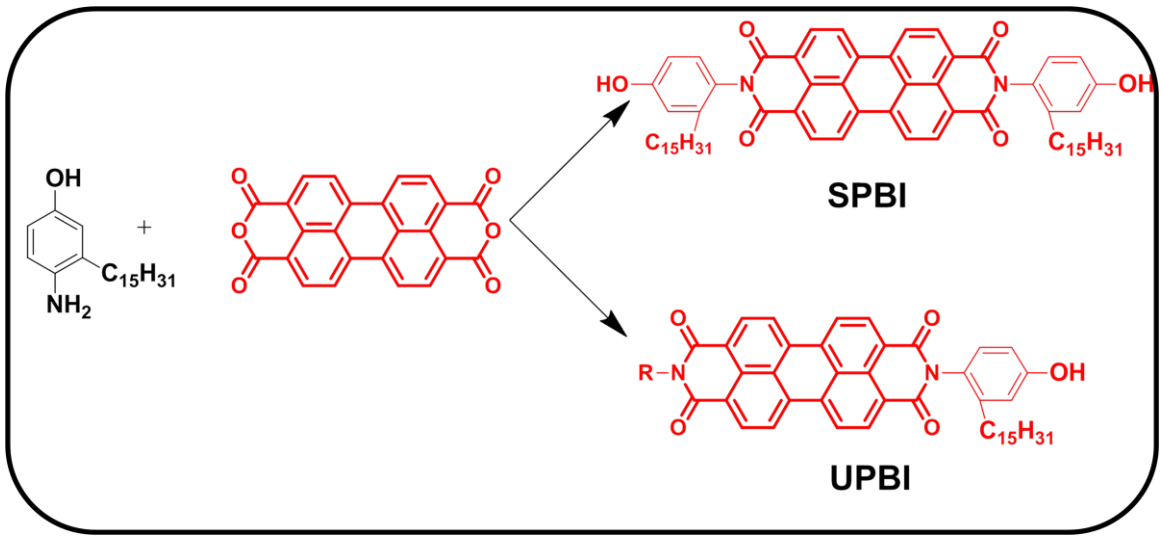

Figure 1.30: Novel symmetrical and unsymmetrical PBI with PDP substitution.

Ghanashyam et al first reported a PDP / Cardanol substituted SPBI, which upon esterification with 3,4,5-tridodecyloxy gallate resulted in highly emissive, room-temperature liquid-crystalline (LC) molecule (PBI-E12) as shown in Figure 1.31.[98]

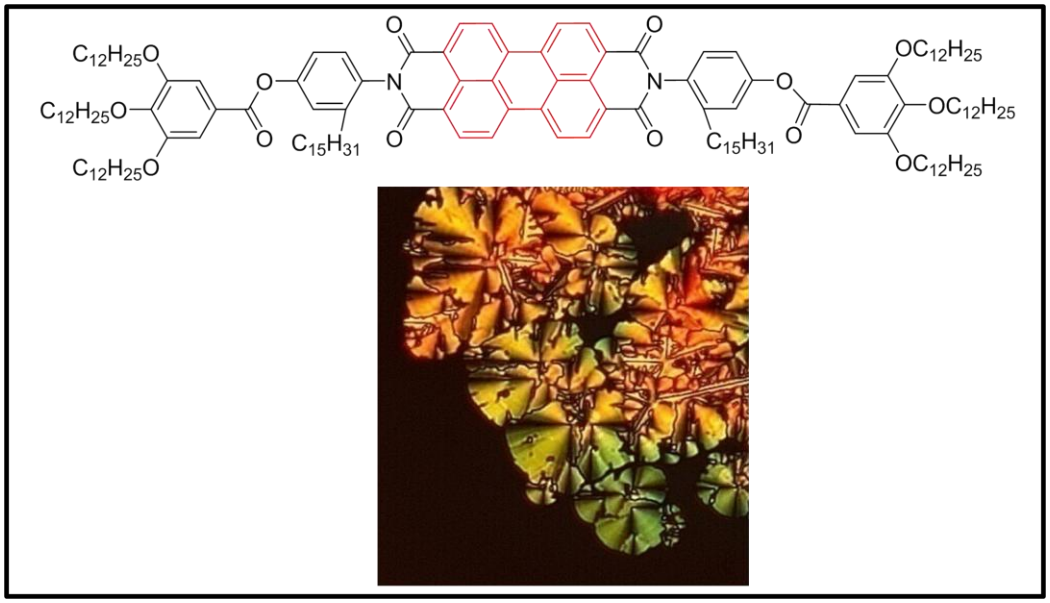

Figure 1.31: The structure and PLM images of PBI-E12.

Nisha et al developed an aliphatic diol functionalised derivative of PDP substituted SPBI which was covalently incorporated in to various molar ratios to an aliphatic polyester backbone via both solution blending and melt poly condensation methods.[99] The resulting polyesters had shown excellent photophysical properties along with film forming ability as given in figure 1.32. PDP functionalised perylene bisimide crosslinker was covalently incorporated to polystyrene back bone via two sage polydispersion polymerisation resulted in to highly emissive fluorescent microbeads[100] (figure 1.32).

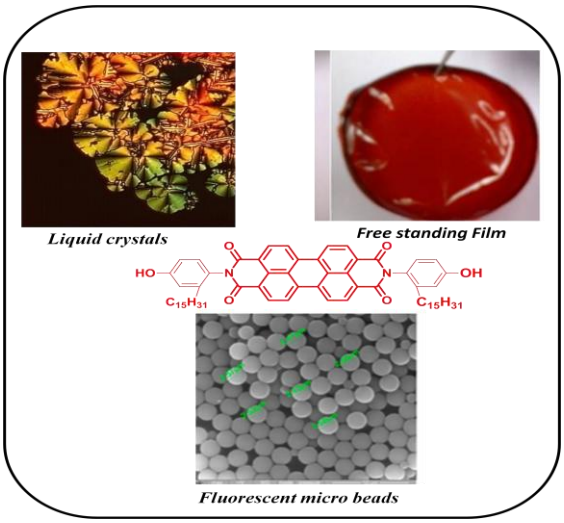

Figure 1.32: PDP functionalised PBI for different applications.

1.8 Aim of the Thesis

The detailed introduction clearly emphasised the potential application of Perylenebisimide as n type semiconducting material for optoelectronics applications owing to their unique combination of high electron mobility, large molar absorption coefficients, excellent self-assembling ability, versatile structural modification as well as good thermal and photochemical stabilities. The self assembly of PBI and its derivatives are very interesting and these self assembled structures can find many applications in different areas. Self assembly of organic semiconductors play a crucial role in improving the charge transport and overall device efficiency. So there is huge demand to focus on the self assembling behaviour of PBI based systems to improve the device performance. Both the bay and core positions of perylene can be easily substituted with different functional groups and they organize into liquid crystals, gels, nano wires, nano rods etc. Liquid crystals are mesophase between crystals and liquid and have the inherent self healing properties which can help to self heal the grain boundaries. This thesis attempts to study the liquid crystalline properties of novel perylenebisimides and its derivatives.

The ampiphilic pentadecyl phenol molecule is well known for its self assembling behaviour. This moiety was introduced both symmetrically and unsymmetrically to PBI core to enhance the solubility as well as the self assembling behaviour. The first two chapters of this thesis discuses the terminal and middle alkyl spacer effect on the liquid crystalline behaviour of small molecule based PBI system. This is the first time in the literature where a systematic study of spacer effect on the liquid crystalline properties of the small molecule based n type semiconducting PBI was presented. This study is very relevant since the spacer chain length plays a crucial role in the entire packing as well as mesogenic behaviour of the liquid crystalline materials. In the first chapter, PBI based ester system was studied where the terminal spacer length was varied from (n= 4-12). The second chapter detailed study on twin liquid crystalline perylenebisimide where the two PBI cores were linked through middle alkyl spacer (n = 1-12).

PBI based small molecules are highly crystalline in nature, therefore one can expect better charge transport among these systems. However, processing of small molecules requires harsh conditions and it is difficult to form uniform thin films. In this context polymer based perylenebisimides generated a lot of research interest since polymers could overcome these issues. One approach to this is blending of small molecule PBI with

other polymers to prepare smooth films, but it has the inherent problem of macrophase separation. Another option is covalently linking PBI in to a polymer backbone either in the main chain or as side groups of block copolymers. Although this approach may gain in terms of solution processability and microphase separation, it loses out in terms of the intrinsic crystallinity of the small molecule besides the low incorporation of PBI. Thus there is a need for an alternative approach which can promise the crystallinity of PBI molecules along with processability and thin film formation. Supramolecular comb copolymers are formed by the non covalent interactions such as hydrogen bonding, electrostatic interactions, metal-ion coordination, hydrophobic interactions etc. Several design principles have been developed to create different functional materials based on supramolecular polymeric architectures. The last two chapters of this thesis work explore the hydrogen bond induce supramolecular comb and comb-coil assembly of unsymmetrical perylenebisimides with poly 4 vinyl pyridine (P4VP) and poly styrene-block-poly 4 vinyl pyridine (PS-b-P4VP) respectively. The chapter 6 gives an overall summary and conclusion of the thesis work.

1.7. References:

1. H. Shirakawa, E. J. Louis, A. G. MacDiarmid, C. K. Chiang, A. J. Heeger, *Chem.Commun.* **1977**, 578.
2. C. K. Chiang, C. R Fincher, Y. W. Park, A. J. Heeger, H. Shirakawa, E. J. Louis, S. C. Gau, A. G. MacDiarmid, *Phys. Rev. Lett.***1977,** *39*, 1098.
3. V. Coropceanu, J. Cornil, D. A. S. Filho, Y. Olivier, R. Silbey, J.-L. Brédas, *Chem. Rev.***2007,** *107*, 926.
4. R. Farchioni, G.Grosso, Eds.;*"Organic electronic materials: conjugated polymers and low molecular weight organic solids."*Berlin, Germany:Springer, **2001**.
5. G. Malliaras, Ed.;*"Organic semiconductors and devices."* Hoboken, NJ: Wiley, **2003.**
6. A. Facchetti, M.-H. Yoon, T. J. Marks, *Adv. Mater.***2005,** *17*, 1705.
7. M. Muccini, *Nat. Mater.***2006,** *5*, 605.
8. C. D. Dimitrakopoulos, P. R. L. Malenfant, *Adv. Mater.***2002,** *14*, 99.
9. A. C. Arias, J. D. MacKenzie, I. McCulloch, J. Rivnay, A. Salleo, *Chem. Rev.* **2010,** *110*, 3.
10. Wise, D. L. *Electrical and Optical Polymer Systems: Fundamentals: Methods and Applications* CRC Press, **1998**.
11. Skotheim, T. A. *Handbook of Conducting Polymers*, Marcel Dekker, New York, **1986**.
12. Salamone, J. C. *Polymeric Materials Encyclopedia* CRC Press, **1996**.
13. Nalwa, H. S. *Handbook of Advanced Electronic and Photonic Materials and Devices*, Academic Press, **2000**.
14. Bredas, J. L. *Conjugated Oligomers, Polymers and Dendrimers: From Polyacetylene to DNA*, Proceedings of the Fourth Francqui Colloquium, Brussels, **1998**.
15. Shirakawa, H. *Angew. Chem. Int. Ed.***2001**, *40*, 2574.
16. Sun, S. S.; Sariciftci, N. S. *Organic Photovoltaics: Mechanism, Materials and Devices* CRC Press, **2005**.
17. W.P.Wu,Y. Q. Liu, D. B.Zhu, *Chem. Soc. Rev.***2010,***39*, 1489.
18. J. E. Anthony, *Chem. Rev.***2006,** *106*, 5028.Wu, W.; Liu, Y.; Zhu, D. *Chem. Soc. Rev.* **2010**, *39*, 1489-1502.

19. H. Klauk, M. Halik, U. Zschieschang, G. Schmidt, W. Radlik, W. Weber, *J. Appl. Phys.* **2002**, *92*, 5259.
20. O. D. Jurchescu, J. Baas, T. T. M. Palstra, *Appl. Phys. Lett*. **2004**, *84*, 3061
21. C. Wang, H. Dong, W. Hu, Y. Liu, D. Zhu, *Chem. Rev.* **2012,** *112*, 2208.
22. F. Garnier, R. Hjlaoui, A. Yassar, P. Srivastava, *Science* **1994**, *265*, 1684.
23. H. Sirringhaus, N. Tessler, R. H. Friend, *Science* **1998**, *280*, 1741.
24. Kunitake, A. *Supramolecular Chemistry- Fundamentals and Applications.* Springer-Verlag, Berlin, **2006**.
25. A. M. van de Craats, J. M. Warman, A. Fechtenkötter, J. D. Brand, M. A. Harbison,K. Müllen, *Adv. Mater.* **1999**, *11*, 1469.
26. D. Adam, P. Schuhmacher, J. Simmerer, L. Häussling, K. Siemensmeyer, K.H. Etzbachi, H. Ringsdorf, D. Haarer, *Nature*, **2004**, *371*, 141.
27. A. M. vande Craats, J. M. Warman, *Synth. Met.***2001**, *121*, 1287.
28. I. Parschiv, M.Giesbers, B. van Lagen, F. C. Grozema, R. D. Abellon, L. D. A. Siebbeles, A. T.M. Marcelis, H. Zuilhof, E. J. R. Sudhölter, *Chem.Mater.*, **2006**, *18*, 968.
29. C. Wang, H. Dong, W. Hu, Y. Liu, D. Zhu, *Chem. Rev.* **2012,** *112*, 2208.
30. Y. Lin, Y. Lia, X. Zhan, *Chem. Soc. Rev.***2012,** *41*, 4245.
31. C. Li, H. Wonneberger, *Adv. Mater*.**2012,** *24*, 613.
32. S. P. Singh, A. Sellinger, A. Dodabalapur, *J. Appl. Phys.***2010,** *107*, 44509.
33. Stillinger, F. H.; Wasserman, Z. *J. Phys. Chem*. **1978**, *82*, 929-940.
34. M. Lampert, P. Mark, "*Current injection in solids*"Academic Press, New York, **1970**.
35. A. Campbell,D. Bradley, H. Antoniadis,*J. Appl. Phys.***2001,** *89*, 3343.
36. A. M. Goodman, A. Rose, *J. Appl. Phys.***1971,** *41*, 2823.
37. W.-Y. Hung, T.-H. Ke, Y.-T. Lin, C.-C. Wu, T.-H. Hung, T.-C. Chao, K.-T.Wong, C.-I Wu, Appl.Phys. Lett. **2006,** *88*, 64102.
38. M. Kardos, *Ber.***1913,** *46*, 2068.
39. C. Liebermann, M. Kardos, *Ber.***1914,** *44*, 202.
40. F. Würthner, *Chem. Commun.***2004,** 1564.
41. H. Langhals, *Heterocycles* **1995,** *40*, 477.
42. M. Sommer, S. M.Lindner, M. Thelakkat,*Adv. Funct. Mater.***2007,** *17*, 1493.
43. M. Sommer, A. S. Lang, M.Thelakkat, *Angew. Chem. Int. Ed.***2008,** *47*, 7901.

44. Jonkheijm, P.; Zdanowska, A. M. M.; Hoeben, F. J. M.; Feyter, S. D.; Schenning, A. P. H. J.; Schryver, F. C. D.; Meijer, E. W. *Angew. Chem. Int. Ed.* **2004**, *43*, 78.
45. S. M. Lindner, S. Hüttner, A. Chiche, M. Thelakkat, G.Krausch, *Angew. Chem. Int. Ed.* **2006,** *45*, 3364.
46. a) S. Hüttner, M. Sommer,M. Thelakkat, *Appl. Phys. Lett.***2008,** *92*, 93302.b) G. Horowitz, F.Kouki, P.Spearman,D.Fichou,C. Nogues, X.Pan,F. Garnier, *Adv. Mater.* **1996,** *8*, 242.
47. A.H. Herz, *Adv. Colloid Interface Sci.***1977,** *8*, 237.
48. M. Kasha, H. R. Rawls, M.A. El-Bayoumi, *Pure Appl. Chem.***1965,** *11*,371.
49. V. Czikklely, H. D. Försterling, H.Kuhn,*Chem. Phys. Lett.***1970,***6*, 207.
50. G.Scheibe, *Z. Elektrochem.***1948,** *52*,283
51. D.Möbius, *Adv.Mater.***1995,** *7*, 437
52. E.Rabinowitch, L.Epstein, *J. Am. Chem. Soc.***1941,** 63, 69.
53. H.-M. Zhao, J. Pfister, V. Settels, M. Renz, M. Kaupp, V. C. Dehm, F. Würthner, R. F. Fink, B. Engels, *J. Am. Chem. Soc.***2009,***131*, 15660Park, S. M.; Herndon, W. C. *Tetrahedron lett.* **1978**, *19*, 2363-2366.
54. Lehn, J. M. PNAS, 2002, 99, 4763.
55. Nguyen, S. T.; Gin, D. L.; Hupp, J. T.; Zhang, Xi. *PNAS*, **2001**, 98, 11849.
56. Hoeben, F. J. M.; Jonkheijm, P.; Meijer, E. W.; Schenning, A. P. H. J. *Chem. Rev*. **2005**, 1491..
57. Wilson, M. R. *Chem. Soc. Rev*.**2007**, *36*, 1881-1888.
58. Tschierske, C. *Chem. Soc. Rev*.**2007**, *36*, 1930–1970
59. Goodby, J. W.; Cowling, V. S. J.; Mackenzie, G.; Martin, P.; Plusquellec, D.; Benvegnu, T.; Boullanger, P.; Lafont, D.; Queneau, Y.; Chamberte, S.; Fitremannf, J. *Chem. Soc. Rev.* **2007**, *36*, 1971-2032.
60. Kato, T.; Hirai, Y.; Nakaso, S.; Moriyama, M. *Chem. Soc. Rev.* **2007**, *36*, 1857-1867
61. Goodby, J. W. *Chem. Soc. Rev.* **2007**, *36*, 1855-1856.
62. Dierking, I. *Textures of Liquid Crystals*, 2nd ed.; Wiley-VCH VerlagGmBH: Berlin, **2003**.
63. Wang, X. J.; Zhou, Q. F. *Liquid crystalline Polymers*, World Scientific Publishing Co. Pte. Ltd. **2004.**
64. Sergeyev, S.; Pisula.W.; Geerts.Y.H.; *Chem. Soc. Rev.* **2007**, 36, 1902.

65. C. T. Imrie and P. A. Henderson, *Chem. Soc. Rev*., 2007, **36**, 2096.
66. Cörmier, R. A.; Gregg, B. A. J. Phys. Chem. B. 1997, 101, 11004.
67. Cörmier, R. A.; Gregg, B. A. Chem. Mater. 1998, 10, 1309.
68. Struijk, C. W.; Sieval, A. B.; Dakhorst, J. E. J.; van Dijk, M.; Kimkes, P.; Koehorst, R. B. M.; Donker, H.; Schaafsma, T. J.; Picken, S. J.; van de Craats, A. M.; Warman, J. M.; Zuilhof, H.; Sudhölter, E. J. R. *J. Am. Chem. Soc.* **2000**, 122, 11057.
69. Sautter, A.; Thalacker, C.; Würthner, F. *Angew. Chem*. **2001**, 113, 4557.
70. Chen, Z.; Stepanenko, V.; Dehm, V.; Prins, P.; Siebbeles, L. D. A.; Seibt, J.; Marquetand, P.; Engel, V.; Würthner, F. *Chem. Eur. J.* **2007**, 13, 436.
71. Z. An, J. Yu, S. C. Jones, S. Barlow, S. Yoo, B. Domercq,P. Prins, L. D. A. Siebbeles, B. Kippelen and S. R. Marder, *Adv. Mater.*, **2005**, 17, 2580.
72. Jancy, B.; Asha, S. K. *Chem. Mater.* **2008**, *20*, 169-181
73. Wicklein, A.; Lang, A.; Muth, M.; Thelakkat, M. *J. Am. Chem. Soc.***2009**, *131*, 14442-14453.
74. M.-A. Muth, G. Gupta, A. Wicklein, M. Carrasco-Orozco,T. Thurn-Albrecht and M. Thelakkat, *J. Phys. Chem. C*, **2014**,118, 92.
75. Y. Zhang, H. Wang, Y. Xiao, L. Wang, D. Shi and C. Cheng, *ACS Appl. Mater. Interfaces*, **2014**, 5, 11093.
76. Tazawa, T.; Yagai, S.; Kikkawa, Y.; Karatsu, T.; Kitamuraa, A.; Ajayaghosh, A. *Chem. Commun.***2010**, *46*, 1076.
77. Wilson, A. J. *Nature Chem.***2011**,*3*, 193-194.
78. Babu, S. S.; Praveen, V. K.; Prasanthkumar, S.; Ajayaghosh, A. *Chem. Eur. J.* **2008**, *14*, 9577.
79. Tazawa, T.; Yagai, S.; Kikkawa, Y.; Karatsu, T.; Kitamuraa, A.; Ajayaghosh, A. *Chem. Commun.***2010**, *46*, 1076-1078.
80. Pisula, W.; Tomovic, Z.; Wegner, M.; R.; Pouderoijen, M. J.; Meijer, E. W.; Schenning, A. P. H. J. *J. Mater. Chem.***2008**, *18*, 2968.
81. Schenning, A. P. H. J.; Herrikhuyzen, J.; Jonkheijm, P.; Chen, Z.; Wu¨ rthner, F.; Meijer, E. W. *J. Am. Chem. Soc.***2002**, *124*, 10252**.**
82. Sijbesma, R.P.;Beijer, F.H.;Brunsveld, L.;Folmer, B.J.B.; Hirschberg, J.H.K.K.; Lange, R.F.M.; Lowe, J.K.L.; Meijer, E.W. *Science* **1997**, *278*, 1601. (b) Hirschberg, J.H.K.K.; Brunsveld, L.;Ramzi, A.;Vekemans, J.A.J.M.; Sijbesma,

R.P.; Meijer, E.W. *Nature* **2000**, *407*, 167. (c) Abbel, R.; Grenier, C.; Pouderoijen, M. J.; Stouwdam, J. W.; Lecle` re, P. E. L. G.; Sijbesma, R. P.; Meijer, E. W.; Schenning, A. P. H. J. *J. Am. Chem. Soc.* **2009**, *131*, 833-843Funahashi, M.; Hanna, J. *Adv. Mater.* **2005**, *17*, 594-598.

83. J. Ruokolainen, R. Mäkinen, M. Torkkeli, R. Serimaa, T. Mäkelä, G. Ten Brinke, O. Ikkala, *Science* **1998,** *280*, 557.
84. J. Ruokolainen, G. Ten Brinke, O. Ikkala, *Adv. Mater.* **1999,** *11*, 777.
85. K. de Moel, A. G. O.R. van Ekenstein, H. Nijland, E. Polushkin, G. Ten Brinke, *Chem. Mater.* **2001,** *13*, 4580.
86. O. Ikkala, G. Ten Brinke, *Science* **2002,** *295*, 2407.
87. O. Ikkala, G. Ten Brinke, *Chem. Commun.* **2004,** 2131.
88. W. Van Zoelen, T. Asumaa, J. Ruokolainen, O. Ikkala, G. Ten Brinke, *Macromolecules* **2008,** *41*, 3199.
89. J. Ruokolainen, G. Ten Brinke, O. Ikkala, *Macromolecules* **1996,** *29,* 3409.
90. G. Ten Brinke, O. Ikkala, *Macromol. Symp.* **2003,** *203,* 103.
91. Rancatore, B. J.; Mauldin, C. E.; Tung, S-H.; Wang, C.; Hexemer, A.; Strzalka, J.; Fréchet, J. M. J.; Xu, T. *ACS Nano*, **2010**, 4, 2721.
92. Narayan, R.; Kumar, P.; Narayan, K. S.; Asha, S. K. *Adv. Funct. Mater.* **2013**, 23, 2033.
93. John, G.; Vemula, P. K. *Soft Matter* **2006**, *2*, 909-914
94. Balachandran , V.S.; Jadhav, S.R.; Vemula. P.K.; John, G.; *Chem.Soc. Rev.*; 2013, 42, 427.
95. Anillkumar, P.; Jayakannan, M. *Macromolecules,* **2007**, *40*, 7311-7319
96. Anilkumar, P.; Jayakannan, M. *J. Phys. Chem. B* **2009**, *113*, 11614
97. Anillkumar, P.; Jayakannan, M. *Macromolecules* **2008**, *41*, 7706.
98. G. A. Bhavsar and S. K. Asha, *Chem.Eur. J.*, **2011**, 17, 12646.
99. Nisha, S. K.; Asha, S. K. *J. Polym. Sci. A Polym. Chem.* **2013**, 51, 509–524
100. Sonawane, S.L.; S. K. Asha Asha, *ACS Appl. Mater. Interfaces*, **2013**, 5, 12205−12214

Chapter 2

Structure-Property Relationship in Charge Transporting Behaviour of Room Temperature Liquid Crystalline Perylenebisimides

2.1 Abstract:

A homologous series of pentadecyl phenol functionalized perylenebisimide (PBI) terminated with trialkoxy gallate esters were synthesized, where the terminal alkyl chain length was varied from n = 4 to 12 (**PBI-En**). The thermotropic liquid crystalline (LC) characteristics of the molecules were analyzed using differential scanning calorimetry (DSC), polarized light microscopy (PLM) combined with variable temperature wide angle X-ray diffraction (WXRD) techniques. A clear odd-even oscillation was observed in the melting as well as isotropization enthalpies as a function of alkyl spacer length in the terminal gallate unit with the even spacers exhibiting higher values. The higher members of the series with n > 8 exhibited thermotropic liquid crystalline textures in the PLM which remained stable until room temperature. The nature of the LC phase was identified to be columnar rectangular and columnar hexagonal based on detailed analysis of the WXRD pattern recorded in the LC phases. The WXRD pattern of the room temperature LC frozen samples indicated a nearly constant intra columnar stack distance of ~3.7 Å for all the members. The space charge limited current (SCLC) values of the LC frozen sample films were analyzed for dependence of bulk mobility estimate on the nature of the LC phase. The columnar hexagonal phase exhibited a mobility value one order (10^{-3} $cm^2V^{-1}s^{-1}$) higher than that of crystalline (10^{-4} $cm^2V^{-1}s^{-1}$) and two orders higher than that of columnar rectangular phase (10^{-5} $cm^2V^{-1}s^{-1}$) indicating a strong dependence of packing on bulk mobility.

2.2 Introduction:

Columnar liquid crystalline materials have several advantages over organic single crystalline materials including easy processing, ability to form thin films, long range self assembly, less number of grain boundaries etc which are the key factors for efficient charge transporting. Therefore, they find applications in optoelectronic materials such as organic field effect transistors (OFET), organic light emitting diodes (OLED), organic photovoltaic cells (OPV) etc.[1-4] In the columnar liquid crystals, the disc like mesogens are stacked one on top of another surrounded by the flexible alkyl chain resulting in mesophase formation. The disc like molecules can form stable columns (typical intra columnar distance of 3.5-3.9 Å) due to the strong π-π stacking between the poly aromatic core with significant overlap of p-orbital, which results in effective charge transport. [5-8] Upon thermal annealing, these molecules can form single large domain with less number of grain boundaries as a result of their inherent self healing property due to their partial liquid-like behaviour.[9,10] But the main challenge in this area is the attainment of mesogenicity in a temperature range that is adaptable on a device substrate.[11]The clearing temperatures should be low and ideally the liquid crystalline phase should be retained at room temperature. However, the design of a suitable LC material for a desired application requires a basic understanding of the structure-property relationship.

The liquid crystalline and charge transporting properties of p type semiconducting systems like triphenylenes, pthalocyanine, hexabenzocoronene are well studied in literature.[12-14] Since there are not many options available for n type semiconducting liquid crystalline materials,[15,16] research in this area have to go far ahead. As discussed earlier, Perylenebisimide is an inherent mesogen having high thermal and photo stability along with the high absorption coefficient in the solar spectrum.[17] Along with these the high electron affinity makes them an alternative for fullerene based n type semiconductors. [24,25]The easy synthetic approach for both the bay and core substitution of this moiety leads to a library of molecule where the optical and electronic properties can be easily tuned. The efficient π-π stacking in the PBI will help to enhance the exciton diffusion length there by slowing down the charge recombination.[18] Aromatic π-π stacking, van der waals force, hydrogen bonding, chirality etc are the major driving tools which help to self assemble PBI based systems in to desired architectures. Even though the bay

substitution can lead to a bathochromic shift in the absorption with a lowering in clearing transitions, the distorted packing leads to less self assembled structure there by only a few reports on bay substituted LC PBI have appeared in this area.

Previously we had reported the liquid crystalline ordering of 3,4,5-tri dodecyloxy substituted pentadecyl phenol based PBI ester which was shown to exhibit room temperature columnar mesophase.[19] Taking advantage of the unique self assembling characteristics afforded by the pentadecyl phenol imide substitution on PBI, we designed a series of PBI derivatives (**PBI-En**; n: 4-12) where the terminal spacer in the alkoxy chain was varied from 4 to 12 for understanding the effect of spacer length on the intrinsic properties. The molecules were structurally characterized and their mesophase characteristics were determined using differential scanning calorimetry (DSC), polarizing light microscope (PLM) and variable temperature wide angle X-ray diffraction (VT-WXRD) studies. The charge transport properties were explored using space charge limited current (SCLC) measurements. The present work highlights two important aspects which are listed below.

1) A detailed structure-property analysis relating the role of varying spacer length on the liquid crystalline ordering in the PBI-En series.
2) Correlation of the bulk mobility estimate among the different LC and crystalline phases.

2.3 Experimental section

Materials: Perylene-3,4,9,10-tetracarboxylic dianhydride (PTCDA), 3-pentadecyl phenol, zinc acetate, imidazole, methyl-3,4,5-trihydroxybenzoate, triethylamine, 1-bromobutane, 1-bromopentane, 1-bromohexane, 1-bromoheptane, 1-bromooctane, 1-bromononane, 1-bromo decane, 1-bromoundecane and 1-bromododecane were purchased from Sigma–Aldrich and used without further purification. Sodium nitrite and potassium carbonate were purchased from Merck Chemicals Ltd and used as such. Thionyl chloride, tri-ethyl amine, dimethyl formamide (DMF), dichloromethane (DCM), tetrahydrofuran (THF) and ethanol were purchased from Merck Chemicals Ltd and were purified using standard procedures.

2.3.1 Instrumentation:

^{1}H-NMR and ^{13}C-NMR spectra of **PBI-En** molecules were recorded on a Bruker-AVANCE 200 MHz spectrometer. Chemical shifts are reported in ppm at 25 ^{0}C using

$CDCl_3$ as solvent containing small amount of tetramethylsilane (TMS) as internal standard. The purity of samples was confirmed using elemental analysis, which was done using a Thermo Finnigan Flash EA 1112 series CHNS analyzer. Gel Permeation Chromatography (GPC) was carried out on Polymer Laboratories PL-GPC-220 using $CHCl_3$ as eluent. The flow rate of $CHCl_3$ was maintained as 1 µL/min throughout the experiments and the sample solutions at concentrations 2-3 mg/ml were filtered through syringe filter and injected for recording the chromatograms at 30 ^{0}C. The mass spectral analysis was carried out in reflecting mode with an accelerating voltage of 25 kV using a Voyager-De-STRMALDI-TOF (Applied Biosystems, Framingham, MA, USA) instrument equipped with 337 nm pulsed nitrogen laser used for desorption and ionization. The sample was made in $CHCl_3$ and premixed with dithranol matrix before spotting on 96-well stainless steel MALDI plate by dried droplet method. Infrared spectra were recorded using Bruker FT-IR (ATR mode) spectrophotometer in the range of 4000-600 cm^{-1}. The thermal stability of the **PBI-En** were analyzed using PerkinElmer STA-6000 thermogravimetric analyser (TGA) under nitrogen atmosphere from 40-800 ^{0}C at 10 ^{0}C/min. Differential Scanning Calorimetry (DSC) was performed using a TA Q10 model. About 2–3 mg of the samples were taken in aluminium pan, sealed and scanned at 10 ^{0}C/min under nitrogen atmosphere. The instrument was calibrated with indium standards before measurements. The phase behaviour of the molecules was analyzed using LIECA DM2500P polarized optical microscope equipped with Linkam TMS 94 heating and cooling stage connected to a Linkam TMS 600 temperature programmer. The Transition from isotropic to liquid crystalline phase was monitored by the evolution of characteristic textures. X-ray diffraction of all the annealed samples were recorded by a DY 1042-Empyrean XRD with Programmable Divergence Slit (PDS) and PIXcel 3D detector using Cu Kα (1.54 Å) emission. The spectra were recorded in the range of (2θ) 2–50° and analyzed using X'pert software. Variable temperature in situ XRD experiments were carried out in an Anton-Paar XRK900 reactor.

2.3.2 Device Fabrication: SCLC electron-only devices were fabricated using the following structure: glass/Al/active layer/Al. The glass substrates were cleaned using the following sequence in an ultrasonic bath: water, acetone, and 2-propanol.[20] The bottom aluminum electrode was deposited by thermal evaporation technique with a thickness of 100 nm under vacuum in a glove box. 20 mg/ml of **PBI-En** samples were dissolved in dry chloroform and 70 micro liters was drop cast on top of the aluminum electrode. The

drop cast films were annealed above their clearing temperature for 20 minutes and cooled to room temperature. Aluminum counter electrodes were evaporated through a shadow mask on top of the active layer to a thickness of ~100 nm in a thermal evaporation chamber. The active device area was found to be in the range of 0.08 - 0.12 cm^2. The mobility measurements were carried out by measuring the current–voltage characteristics with a Keithley 2400 source meter.

2.3.3 Synthesis of Ester derivatives:

Synthesis of symmetrical perylenebisimide (1):

PTCDA (5 g, 0.013 mol, 1 equivalent) was heated with 4- amino-3-pentadecylphenol (8.9 g, 0.028 mol, 2.2 equivalent) and Zn $(OAc)_2$ (0.5 g) in imidazole (40 g) at 160 ^oC for 4 h. The reaction mixture was then cooled to room temperature and precipitated by adding 2N HCl and washed with deionized water (1 L). The crude product was purified by dissolving in a minimum amount of THF and precipitating into methanol. The methanol washing was continued until the washings were clear and finally washed with hexane. The purified dark red solid was dried in a vacuum oven at 80 ^oC for 12 h. Yield: 11.0 g (74%); m.p.>400 ^0C; ^1H NMR ($CDCl_3$+TFA): δ =8.91 (s, 8**H**; perylene), 6.89–7.16 (m, 6**H**; Ar**H**-PDP), 2.39 (t, 4H; Ar-C$\mathbf{H}_2$), 1.53 (t, 4H; Ar-C$\mathbf{H}_2$-C$\mathbf{H}_2$), 1.0–1.4 (br, 48**H**; aliphatic C$\mathbf{H}_2$), 0.84 ppm (t, 6**H**; terminal C$\mathbf{H}_3$); ^{13}C NMR: d= 166.27, 163.21, 162.65, 160.62, 155.86, 143.08, 136.66, 134.16, 130.32, 127.00, 126.14, 124.92, 123.12, 122.59, 115.03, 111.82, 106.19, 32.17, 31.28, 29.92, 29.60, 22.85, 13.81 ppm; FTIR:(ν) =3359 (ν(-OH stretch)), 2922, 2853, 1698 (ν(C=Oimide)), 1656, 1592, 1498, 1403, 1360, 1348, 1300, 1250, 1231, 1198, 1176, 967, 862, 813, 796, 750 cm^{-1}; MALDI-TOF (dithranol matrix): m/z calcd for $C_{66}H_{78}N_2O_6$: 995.34; found: 996.65 [M+1], 1018.58 [M + Na].

Synthesis of ester-functionalized perylene bisimides: 3,4,5-Tri (alkoxy) benzoic acid was synthesized using literature procedure [34] and converted to the acid chloride by heating to reflux in an excess amount of thionyl chloride. The conversion was monitored by IR spectroscopy.

Synthesis of PBI–E4:

Per-PDP-Diol (0.5 g, 0.5 mmol) was dissolved in dry THF (15 mL) and the solution was cooled to 0 °C. A small amount of triethylamine was added as catalyst. 3, 4, 5 Tri (butyloxy)benzoyl chloride (0.36 g, 1.1 mmol) dissolved in dry THF (5 mL) was added

drop wise over a period of 10 min while the temperature was maintained at 0 °C. The reaction mixture was left stirring under ice-cold conditions for 4 h. For workup, THF was distilled and removed. The crude product was purified by column chromatography in DCM/methanol. Yield: 0.67 g (58 %); m.p. 264 °C; ^{1}H NMR ($CDCl_3$): δ = 8.7–8.9 (m, 8**H**; perylene), 7.44 (s,4**H**; Ar-H), 7.25–7.40 (m, 6**H**; Ar**H** - PDP), 4.06 (t, 12**H**; Ar-O-C**H**$_2$), 2.48 (t, 4**H**; PDP Ar-C**H**$_2$), 1.0–1.9 (m, 72**H**; aliphatic C**H**$_2$), 0.87 ppm (m, 24**H**; terminal C**H**$_3$); ^{13}C NMR: 164.70, 163.42, 152.95, 151.46, 150.50, 146.75, 142.93, 142.13, 135.08, 132.04, 131.16, 129.96, 126.78, 123.86, 123.39, 122.00, 120.38, 108.50, 73.60, 69.24, 31.92, 31.13, 30.33, 29.37, 26.09, 22.69, 14.11; FTIR: (υ) 2962 ($CH_{stretch}$), 2923, 2853, 1730 ($C=O_{ester}$), 1702 ($C=O_{imide}$)), 1663, 1593, 1503, 1465, 1429, 1359, 1337, 1261, 1198, 1097, 1025, 970, 804, 751 cm^{-1}; MALDI-TOF (dithranol matrix): m/z calcd for $C_{104}H_{136}N_2O_{14}$: 1636.18; found: 1657.98 [M^+ Na]; elemental analysis calcd (%): C 76.34, H 8.25, N 1.71; found: C 75.62, H 8.66, N 1.64.

Synthesis of PBI–E5: A similar procedure to that of PBI-E4 was adopted by using Per-PDP-Diol 0.5 g (0.5 mmol) and 3,4,5 Tri (pentyloxy) benzoyl chloride (0.39 g, 1.1 mmol). Yield: 0.63 g (51 %); m.p. 244 °C; ^{1}H NMR ($CDCl_3$): δ = 8.7–8.9 (m, 8**H**; perylene), 7.44 (s, 4**H**; Ar-H),7.25–7.40 (m, 6**H**; Ar**H** - PDP), 4.06 (t, 12**H**; Ar-O-C**H**$_2$), 2.48 (t, 4**H**; PDP Ar-C**H**$_2$), 1.0–1.9 (m, 84**H**; aliphatic C**H**$_2$), 0.87 ppm (m, 24**H**; terminal C**H**$_3$); ^{13}C NMR: 164.70, 163.42, 152.95, 151.46, 150.50, 146.75, 142.93, 142.13, 135.08, 132.04, 131.16, 129.96, 126.78, 123.86, 123.39, 122.00, 120.38, 108.50, 73.60, 69.24, 31.92, 31.13, 30.33, 29.37, 26.09, 22.69, 14.11; FTIR: (υ) 2962 (-$CH_{stretch}$), 2923, 2853, 1730 ($C=O_{ester}$), 1702 ($C=O_{imide}$), 1663, 1593, 1503, 1465, 1429, 1359, 1337, 1261, 1199,1098, 1025, 971, 804, 752 cm $^{-1}$; MALDI-TOF (dithranol matrix): m/z calcd for $C_{110}H_{148}N_2O_{14}$: 1722.2; found: 1742.1 [M^+ Na]; elemental analysis calcd (%): C 76.80, H 8.55, N 1.63; found: C 75.98, H 8.94, N 1.62.

Synthesis of PBI–E6: A similar procedure to that of PBI-E4 was adopted by using Per-PDP-Diol 0.5 g (0.5 mmol) and 3,4,5 Tri (hexyloxy) benzoyl chloride (0.44 g, 1.1 mmol). Yield: 0.64 g (53 %); m.p. 239 °C; ^{1}H NMR ($CDCl_3$): δ = 8.7–8.9 (m, 8**H**; perylene), 7.44 (4**H**, s ; Ar-H),7.25–7.40 (m, 6**H**; Ar**H** - PDP), 4.06 (t, 12**H**; Ar-O-C**H**$_2$), 2.48 (t, 4**H**; PDP Ar-C**H**$_2$), 1.0–1.9 (m, 98**H**; aliphatic C**H**$_2$), 0.87 ppm (m, 24**H**; terminal C**H**$_3$); ^{13}C NMR: 164.70, 163.42, 152.95, 151.46, 150.50, 146.75, 142.93, 142.13, 135.08, 132.04, 131.16, 129.96, 126.78, 123.86, 123.39, 122.00, 120.38, 108.50, 73.60, 69.24, 31.92,

31.13, 30.33, 29.37, 26.09, 22.69, 14.11; FTIR: (υ) 2962 (-$CH_{stretch}$), 2923, 2853, 1730 (C=O_{ester}), 1702 (C=O_{imide}), 1663, 1593, 1503, 1465, 1429, 1359, 1337, 1260, 1199,1098, 1023, 969, 805, 750 cm^{-1}; MALDI-TOF (dithranol matrix): m/z calcd for $C_{116}H_{130}N_2O_{14}$: 1806.5; found: 1806.57 [M^+], 1826.51 [M^+ Na]; elemental analysis calcd (%): C 77.21, H 8.83, N 1.55; found: C 76.78, H 8.54, N 1.72.

Synthesis of PBI–E7: A similar procedure to that of PBI-E4 was adopted by using Per-PDP-Diol 0.5 g (0.5 mmol) and 3,4,5 Tri (heptyloxy) benzoyl chloride (0.48 g, 1.1 mmol). Yield: 0.59 g (49 %); m.p. 227 °C; ^{1}H NMR ($CDCl_3$): δ =8.7–8.9 (m, 8**H**; perylene), 7.44 (s, 4**H**; Ar-H),7.25–7.40 (m, 6**H**; Ar**H** - PDP), 4.06 (t, 12**H**; Ar-O-C$\mathbf{H}_2$), 2.48 (t, 4**H**; PDP Ar-C$\mathbf{H}_2$), 1.0–1.9 (m, 112**H**; aliphatic C$\mathbf{H}_2$), 0.87 ppm (m, 24**H**; terminal C$\mathbf{H}_3$); ^{13}C NMR: d=164.70, 163.42, 152.95, 151.46, 150.50, 146.75, 142.93, 142.13, 135.08, 132.04, 131.16, 129.96, 126.78, 123.86, 123.39, 122.00, 120.38, 108.50, 73.60, 69.24, 31.92, 31.13, 30.33, 29.37, 26.09, 22.69, 14.11; FTIR: (υ) 2962 ($CH_{stretch}$), 2923, 2853, 1730 (C=O_{ester}), 1702 (C=O_{imide}), 1663, 1593, 1503, 1465, 1429, 1359, 1337, 1260, 1199,1098, 1025, 970, 805, 751 cm^{-1}; MALDI-TOF (dithranol matrix): m/z calcd for $C_{122}H_{172}N_2O_{14}$: 1888.66; found: 1910.32 [M^+ Na]; elemental analysis calcd (%): C 77.58, H 9.07, N 1.48; found: C 76.84, H 9.63, N 1.60.

Synthesis of PBI–E8: A similar procedure to that of PBI-E4 was adopted by using Per-PDP-Diol 0.5 g (0.5 mmol) and 3,4,5 Tri (octyloxy) benzoyl chloride (0.52 g, 1.1 mmol). Yield: 0.62 g (52 %); m.p. 221 °C; ^{1}H NMR ($CDCl_3$): δ =8.7–8.9 (m, 8**H**; perylene), 7.44 (s, 4**H**; Ar-H),7.25–7.40 (m, 6**H**; Ar**H** - PDP), 4.06 (t, 12**H**; Ar-O-C$\mathbf{H}_2$), 2.48 (t, 4**H**; PDP Ar-C$\mathbf{H}_2$), 1.0–1.9 (m, 134**H**; aliphatic C$\mathbf{H}_2$), 0.87 ppm (m, 24**H**; terminal C$\mathbf{H}_3$); ^{13}C NMR: d=164.70, 163.42, 152.95, 151.46, 150.50, 146.75, 142.93, 142.13, 135.08, 132.04, 131.16, 129.96, 126.78, 123.86, 123.39, 122.00, 120.38, 108.50, 73.60, 69.24, 31.92, 31.13, 30.33, 29.37, 26.09, 22.69, 14.11; FTIR: (υ) 2962 ($CH_{stretch}$), 2923, 2853, 1730 (C=O_{ester}), 1702 (C=O_{imide}), 1663, 1593, 1503, 1465, 1429, 1359, 1337, 1260, 1199,1098, 1025, 972, 804, 751 cm^{-1}; MALDI-TOF (dithranol matrix): m/z calcd for $C_{128}H_{184}N_2O_{14}$: 1972.2 found: 1994.4 [M^+ Na]; elemental analysis calcd (%): C 77.93, H 9.30, N 1.42 found: C 77.49, H 9.62, N 1.43.

Synthesis of PBI–E9: A similar procedure to that of PBI-E4 was adopted by using Per-PDP-Diol 0.5 g (0.5 mmol) and 3,4,5 Tri (nonyloxy) benzoyl chloride (0.57 g, 1.1 mmol). Yield: 0.61g (51%); m.p. 202°C; ^{1}H NMR ($CDCl_3$): δ =8.7–8.9 (m, 8**H**; perylene), 7.44 (4**H** , s; Ar-H),7.25–7.40 (m, 6**H**; Ar**H** - PDP), 4.06 (t, 12**H**; Ar-O-C**H**$_2$), 2.48 (t, 4**H**; PDP Ar-C**H**$_2$), 1.0–1.9 (m, 148**H**; aliphatic C**H**$_2$), 0.87 ppm (m, 24**H**; terminal C**H**$_3$); ^{13}C NMR: d=164.70, 163.42, 152.95, 151.46, 150.50, 146.75, 142.93, 142.13, 135.08, 132.04, 131.16, 129.96, 126.78, 123.86, 123.39, 122.00, 120.38, 108.50, 73.60, 69.24, 31.92, 31.13, 30.33, 29.37, 26.09, 22.69, 14.11; FTIR: (υ) 2962 ($CH_{stretch}$), 2923, 2853, 1730 ($C=O_{ester}$), 1702 ($C=O_{imide}$), 1663, 1593, 1503, 1465, 1429, 1359, 1337, 1260, 1199,1098, 1025, 970, 806, 752 cm^{-1}; MALDI-TOF (dithranol matrix): m/z calcd for $C_{134}H_{196}N_2O_{14}$: 2056.99; found: 2078.39 [M^+Na]; elemental analysis calcd (%): C 78.24, H 9.5, N 1.36; found: C 77.54, H 10.05, N 1.37.

Synthesis of PBI–E10: A similar procedure to that of PBI-E4 was adopted by using Per-PDP-Diol 0.5 g (0.5 mmol) and 3,4,5 Tri (decyloxy) benzoyl chloride (0.67 g, 1.1 mmol). Yield: 0.68 g (55 %); m.p. 213 °C; ^{1}H NMR ($CDCl_3$): δ =8.7–8.9 (m, 8**H**; perylene), 7.44 (s, 4**H**; Ar-H),7.25–7.40 (m, 6**H**; Ar**H** - PDP), 4.06 (t, 12**H**; Ar-O-C**H**$_2$), 2.48 (t, 4**H**; PDP Ar-C**H**$_2$), 1.0–1.9 (m, 160**H**; aliphatic C**H**$_2$), 0.87 ppm (m, 24**H**; terminal C**H**$_3$); ^{13}C NMR: d=164.70, 163.42, 152.95, 151.46, 150.50, 146.75, 142.93, 142.13, 135.08, 132.04, 131.16, 129.96, 126.78, 123.86, 123.39, 122.00, 120.38, 108.50, 73.60, 69.24, 31.92, 31.13, 30.33, 29.37, 26.09, 22.69, 14.11; FTIR: (υ) 2962 ($CH_{stretch}$), 2923, 2853, 1730 ($C=O_{ester}$), 1702 ($C=O_{imide}$), 1663, 1593, 1503, 1465, 1429, 1359, 1337, 1260, 1199,1098, 1023, 971, 806, 751 cm^{-1}; MALDI-TOF (dithranol matrix): m/z calcd for $C_{140}H_{208}N_2O_{14}$: 2141.56; found: 2142.56 [M^+ 1], 2176.39 [M^+ Na]; elemental analysis calcd (%): C 78.53, H 9.7, N 1.31; found: C 77.83, H 9.6, N 1.26.

Synthesis of PBI–E11: A similar procedure to that of PBI-E4 was adopted by using Per-PDP-Diol 0.5 g (0.5 mmol) and 3,4,5 Tri (undecyloxy) benzoyl chloride (0.77 g, 1.1 mmol). Yield: 0.60 g (52%); m.p. 200 °C; ^{1}H NMR ($CDCl_3$): d=8.7–8.9 (m, 8**H**; perylene), 7.44 (s, 4**H**; Ar-H),7.25–7.40 (m, 6**H**; Ar**H** - PDP), 4.06 (t, 12**H**; Ar-O-C**H**$_2$), 2.48 (t, 4**H**; PDP Ar-C**H**$_2$), 1.0–1.9 (m, 172**H**; aliphatic C**H**$_2$), 0.87 ppm (m, 24**H**; terminal C**H**$_3$); ^{13}C NMR: d=164.70, 163.42, 152.95, 151.46, 150.50, 146.75, 142.93, 142.13, 135.08, 132.04, 131.16, 129.96, 126.78, 123.86, 123.39, 122.00, 120.38, 108.50,

73.60, 69.24, 31.92, 31.13, 30.33, 29.37, 26.09, 22.69, 14.11; FTIR: (υ) 2962 ($-CH_{stretch}$), 2923, 2853, 1730 ($C=O_{ester}$), 1702 ($C=O_{imide}$), 1663, 1593, 1503, 1465, 1429, 1359, 1337, 1260, 1199,1098, 1025, 970, 805, 751 cm^{-1}; MALDI-TOF (dithranol matrix): m/z calcd for $C_{146}H_{220}N_2O_{14}$: 2225.3; found: 2246.95 [M^+ Na]; elemental analysis calcd (%): C 78.80, H 9.87, N 1.26; found: C 77.9, H 9.37, N 0.92.

Synthesis of PBI–E12: A similar procedure to that of PBI-E4 was adopted by using Per-PDP-Diol 0.5 g (0.5 mmol) and 3,4,5 Tri (undecyloxy) benzoyl chloride (0.77 g, 1.1 mmol). Yield: 0.60 g (52%); m.p. 200 °C; ^{1}H NMR ($CDCl_3$): δ =8.7–8.9 (m, 8**H**; perylene), 7.44 (s, 4**H**; Ar-H),7.25–7.40 (m, 6**H**; Ar**H** - PDP), 4.06 (t, 12**H**; Ar-O-C**H**$_2$), 2.48 (t, 4**H**; PDP Ar-C**H**$_2$), 1.0–1.9 (m, 184**H**; aliphatic C**H**$_2$), 0.87 ppm (m, 24**H**; terminal C**H**$_3$); ^{13}C NMR: d=164.70, 163.42, 152.95, 151.46, 150.50, 146.75, 142.93, 142.13, 135.08, 132.04, 131.16, 129.96, 126.78, 123.86, 123.39, 122.00, 120.38, 108.50, 73.60, 69.24, 31.92, 31.13, 30.33, 29.37, 26.09, 22.69, 14.11; FTIR: (υ) 2962 ($-CH_{stretch}$), 2923, 2853, 1730 ($C=O_{ester}$), 1702 ($C=O_{imide}$), 1663, 1593, 1503, 1465, 1429, 1359, 1337, 1260, 1199,1098, 1025, 970, 805, 751 cm^{-1}; MALDI-TOF (dithranol matrix): m/z calcd for $C_{146}H_{220}N_2O_{14}$: 2309.46; found: 2309.95 [M^+]; elemental analysis calcd (%): C 79.05, H 10.04, N 1.21; found: C 79.67, H 9.57, N 0.97.

2.4 Results and Discussions:

A series of trialkoxy ester terminated derivatives of perylenebisimide (**PBI-En**; n = 4-12) was designed and developed by esterification reaction between pentadecyl phenol substituted perylenebisimide and 3,4,5-trialkoxy benzoyl chloride. The alkoxy spacer length was varied from 4 to 12 and the synthetic route is shown in scheme-1. The peripheral 3,4,5-trialkoxyphenyl substitution is known to be helpful in inducing mesogenicity in perylenebisimides, however the long C15 alkyl chain in the ortho position to the imide linkage proved crucial in widening the liquid crystalline window as well as to retain the liquid crystalline order until room temperature. The resulting highly fluorescent **PBI-En** molecules were structurally characterized using proton NMR spectroscopy, mass analysis using MALDI-TOF and purity confirmed by single peak in Gel Permeation Chromatography (GPC) as well as elemental analysis. The proton NMR spectra as well as the other structural characterization data are given below.

The structures of PBI-En were confirmed by ^{1}H NMR spectra (figure 1). The peaks at 8.76 ppm corresponded to the 8 protons of perylene while the peaks at 7.4-7.25 pm

C

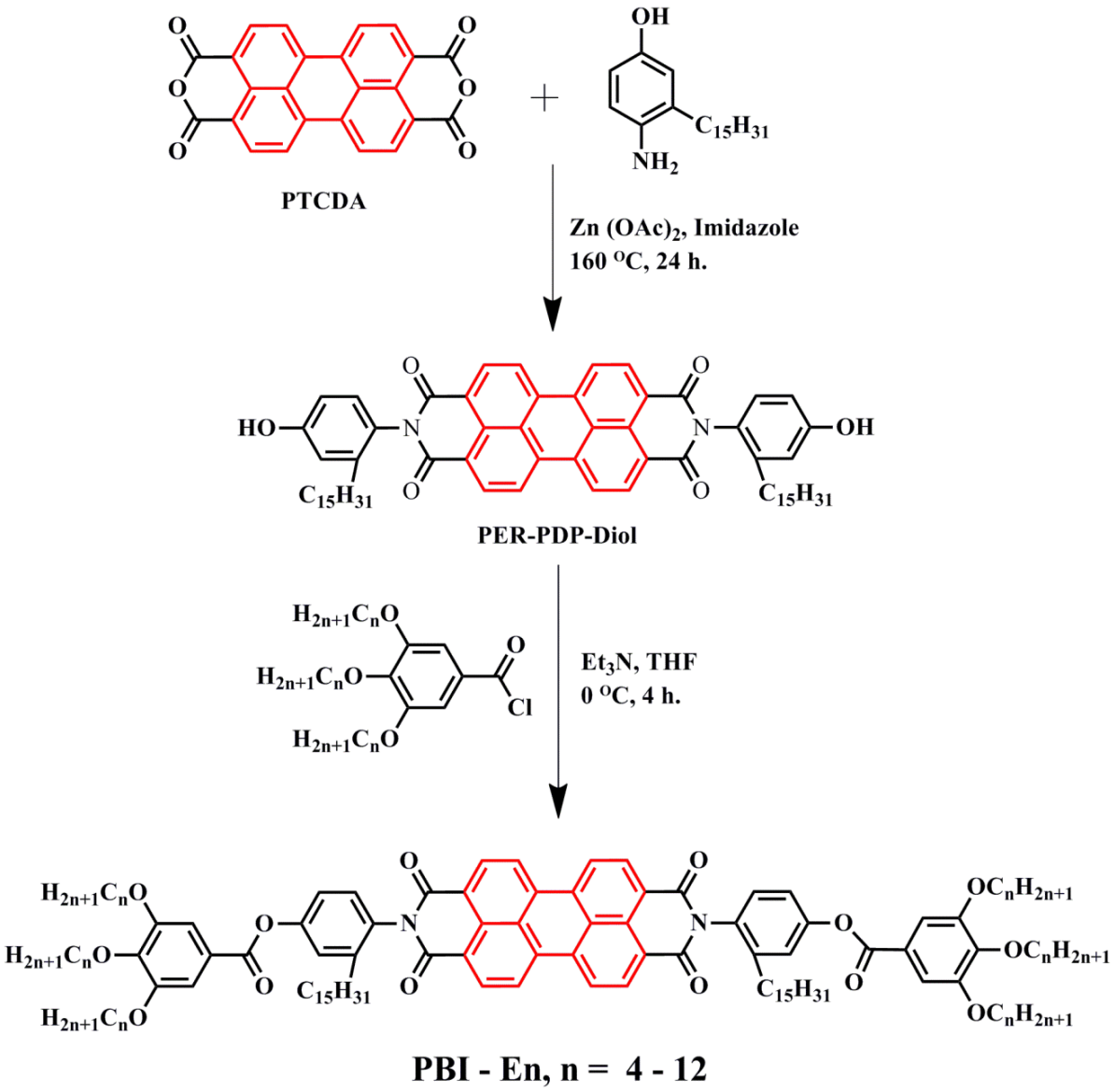

Scheme 1: Synthesis and Chemical structures of PBI esters (**PBI-En**)

corresponded to the PDP protons (6 H) and the aromatic protons (2H) from the gallate units. The $–OCH_2$ protons (12H) appeared at 4 ppm as triplet and the four benzylic hydrogen appeared at 2.5 ppm. Further confirmation of the structure was done with the help of Maldi TOF analysis as given in figure 2. Most of the PBI-En showed molecular ion peak but in some of the cases the M+ Na peak was also observed. The purity of the PBI En was further confirmed with CHN analysis.

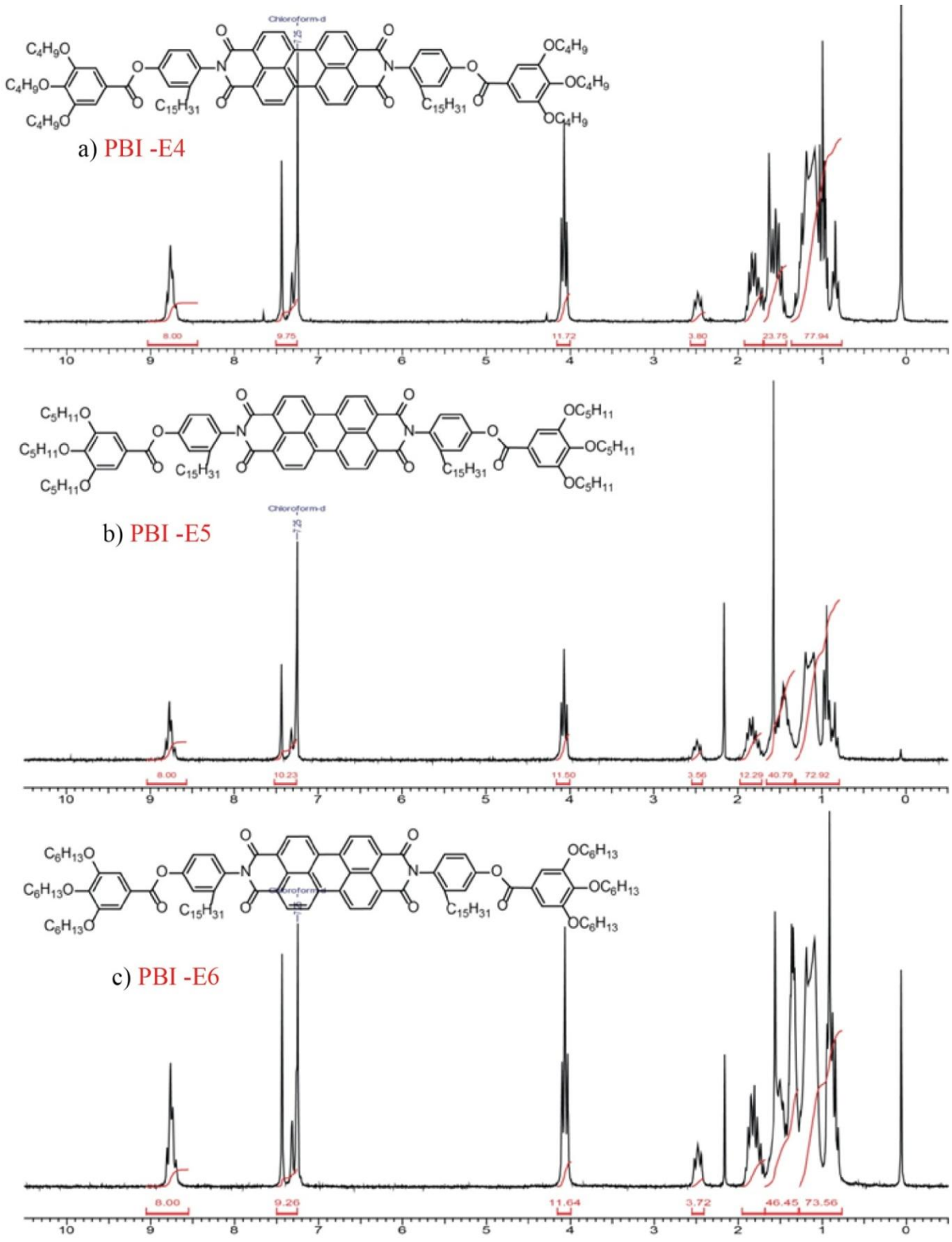
a) PBI -E4
b) PBI -E5
c) PBI -E6

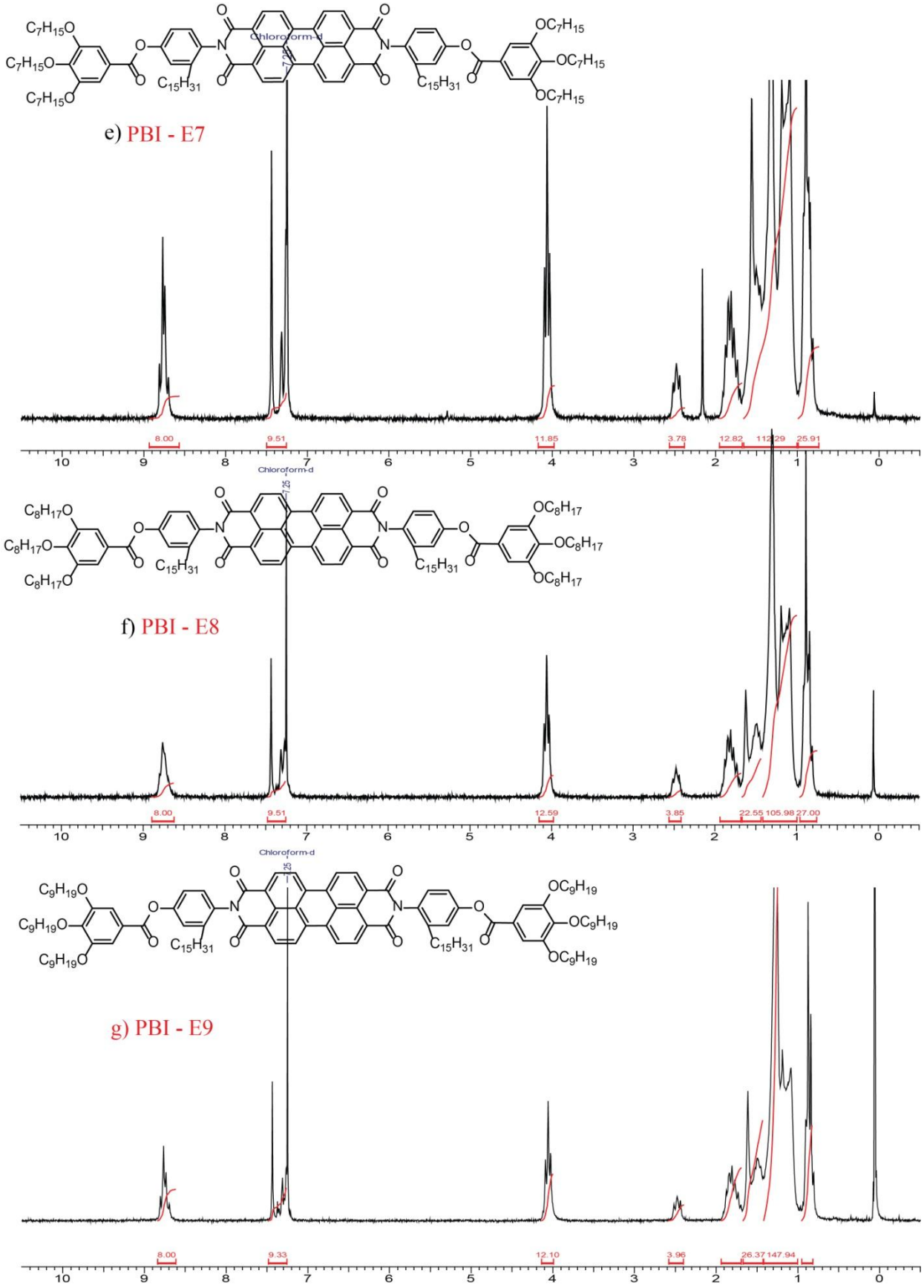
e) PBI - E7
Chloroform-d
8.00
9.51
11.85
3.78
12.82
11.29
25.91
f) PBI - E8
Chloroform-d
8.00
9.51
12.59
3.85
22.55
105.98
27.00
g) PBI - E9
Chloroform-d
8.00
9.33
12.10
3.96
26.37
147.94

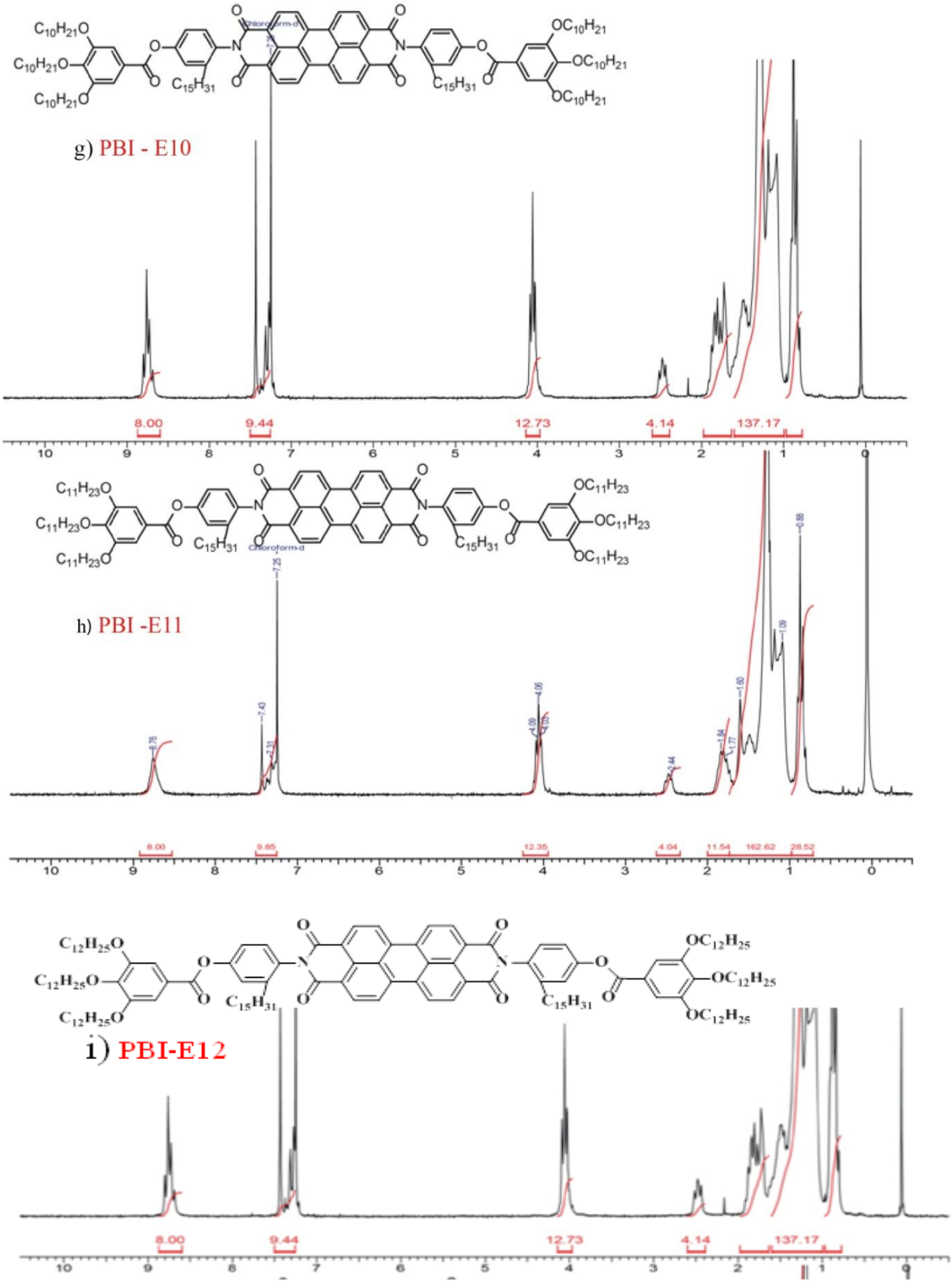

Figure 1: ^{1}H NMR spectrum of **PBI-En** in chloroform.

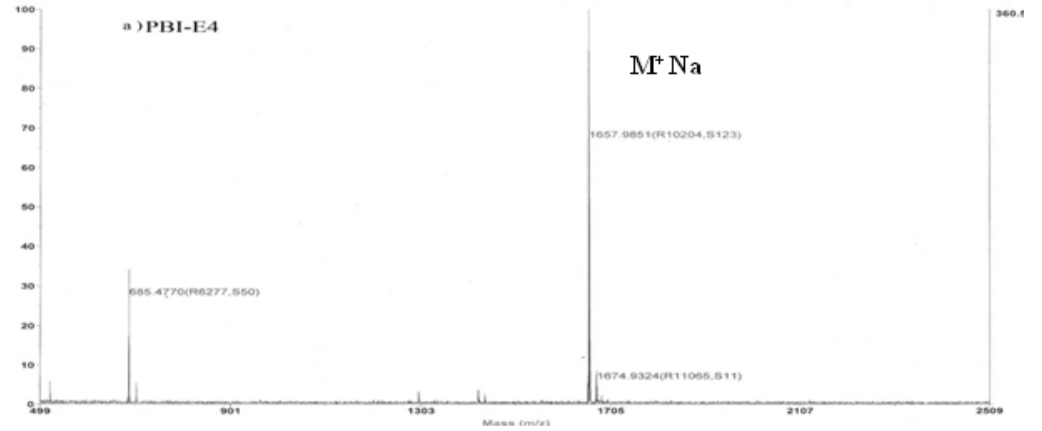
a) PBI-E4
M⁺Na
1657.9851(R10204,S123)
685.4770(R6277,S50)
1674.9324(R11065,S11)
Mass (m/z)

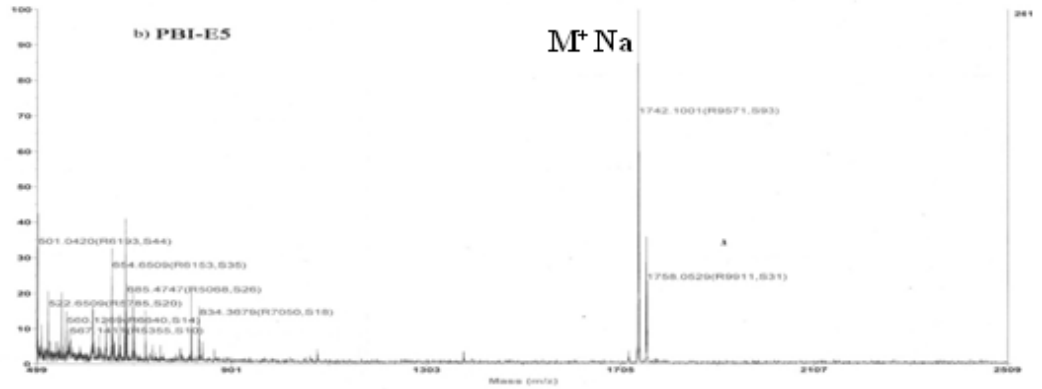
b) PBI-E5
M⁺Na
1742.1001(R9571,S93)
1758.0529(R9911,S31)
Mass (m/z)

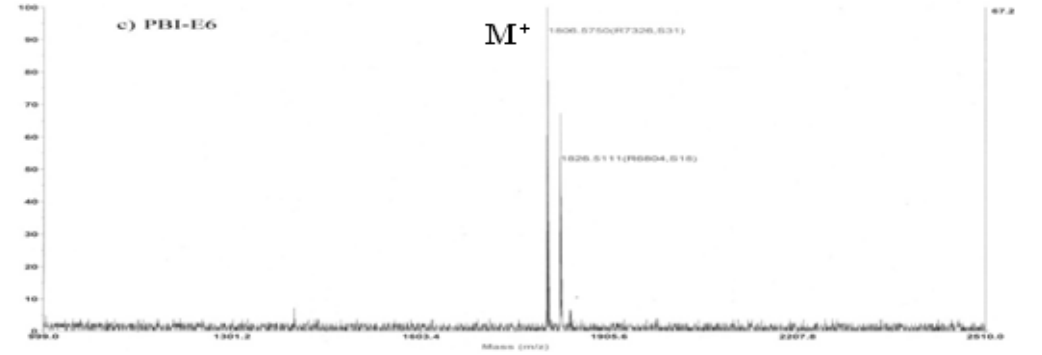
c) PBI-E6
M⁺
1826.5111(R6804,S18)
Mass (m/z)

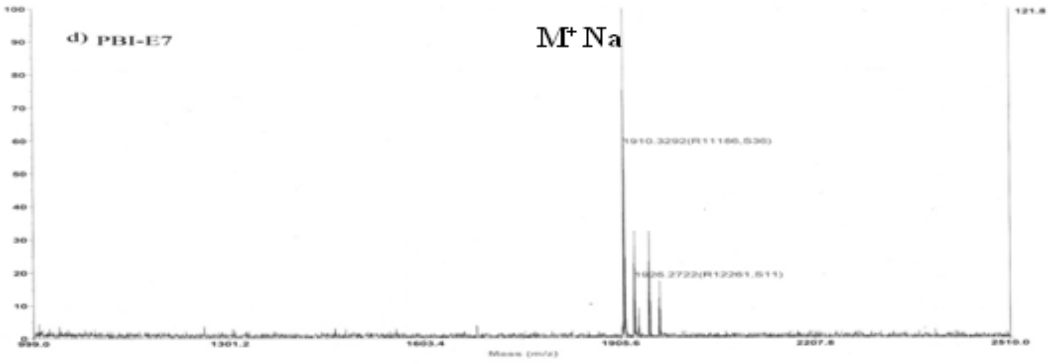
d) PBI-E7
M⁺Na
1910.3292(R11186,S36)
Mass (m/z)

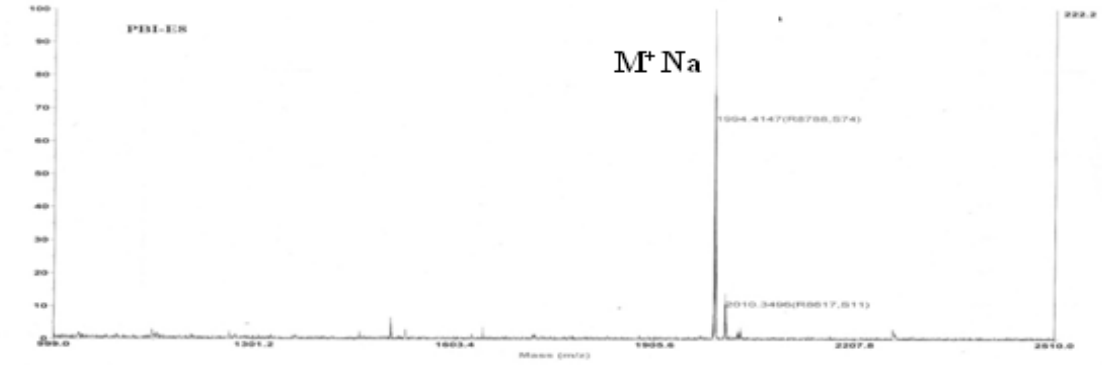
PBI-E8
M+ Na

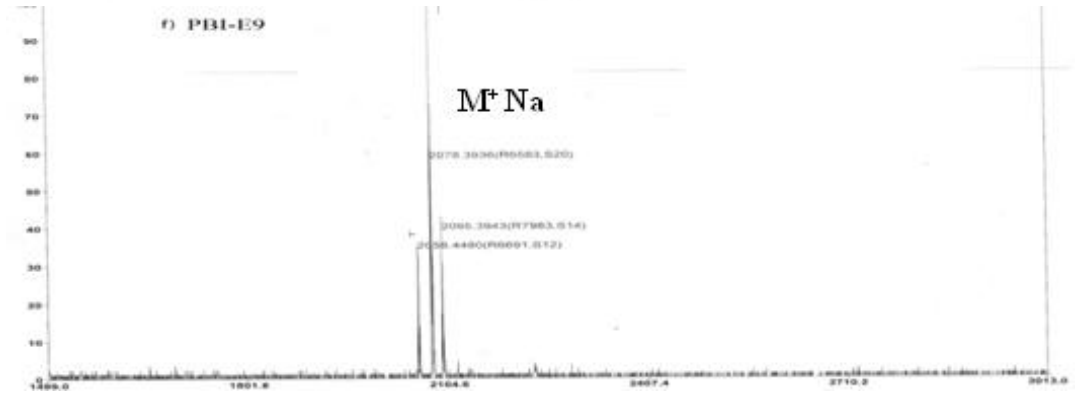
f) PBI-E9
M+ Na

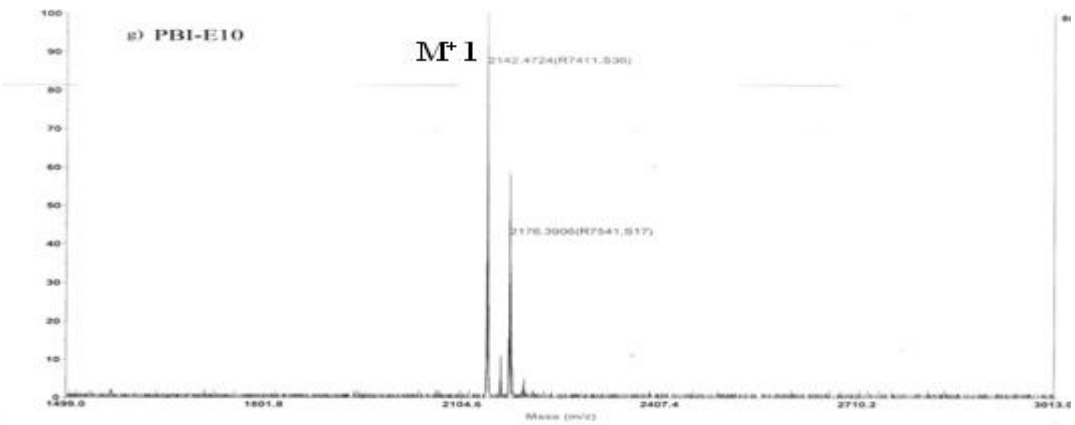
g) PBI-E10
M+ 1


PBI-E11
M+ Na

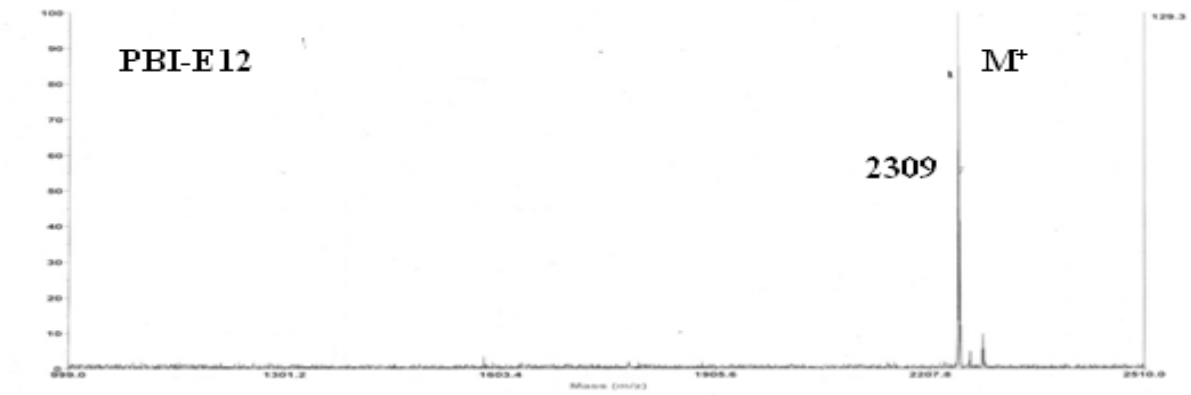

Figure 2. Maldi- TOF spectra of **PBI-En** molecules in dithranol matrix.

2.4.1 Thermal Analysis of PBI-En

The thermal stability of the PBI-En series of molecules was determined by TGA under N_2 atmosphere. Figure 3 shows the TGA curves of the series recorded at a heating rate of 10 $^{\circ}$C/min from 40-800 $^{\circ}$C. All molecules were observed to be thermally stable up to 370 $^{\circ}$C. Table-1 shows the 10 wt % decomposition temperature of the molecules.

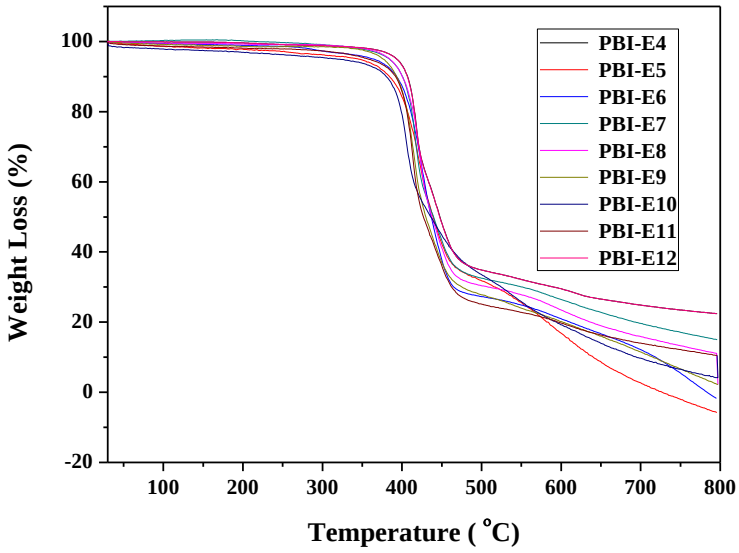

Figure 3: Thermogravimetric analysis of **PBI-En** molecules under N_2 atmosphere.

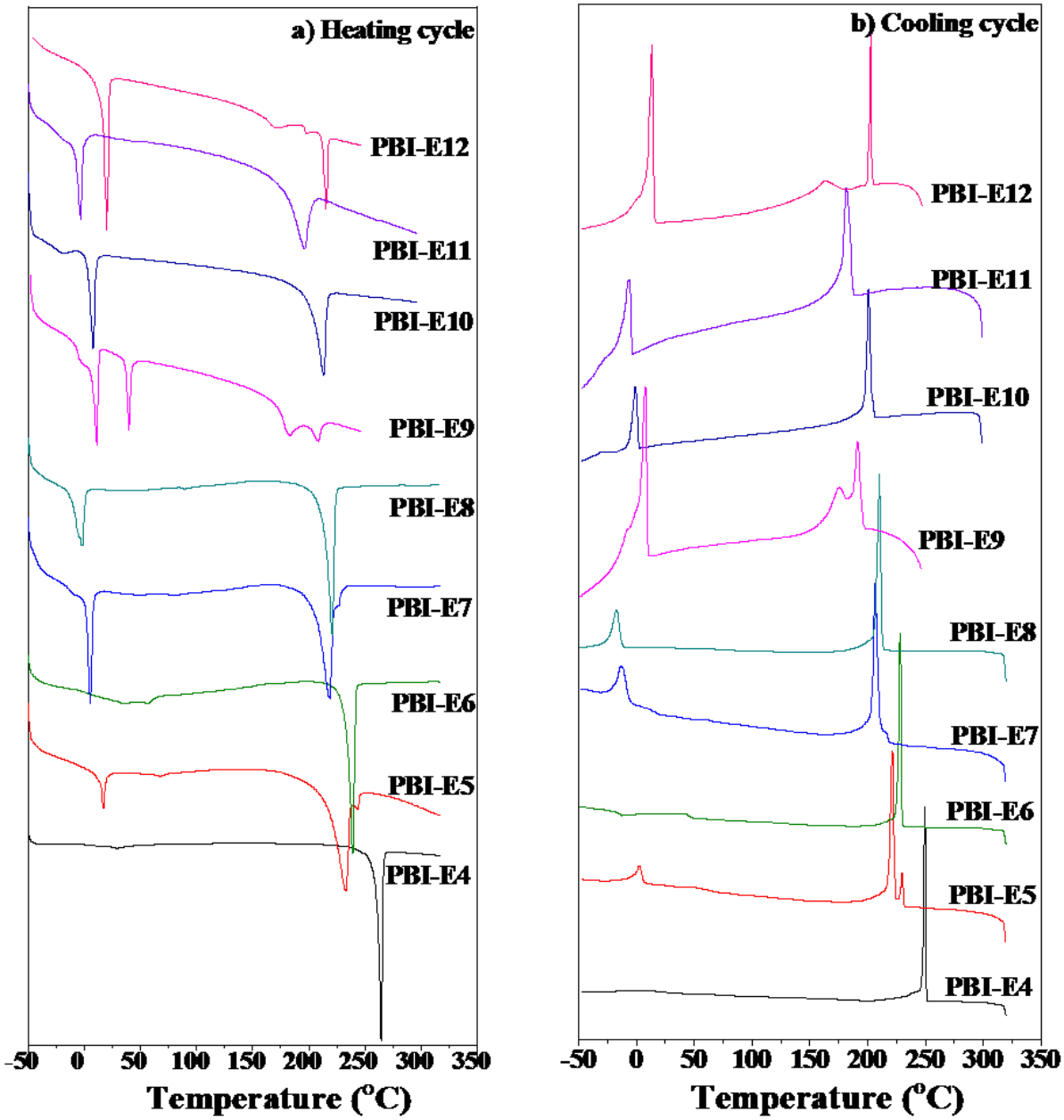

Figure 4: DSC thermogram of **PBI-En** under N2 atmosphere.

The thermotropic liquid crystalline characteristics of the PBI-En series were studied using differential scanning calorimetry (DSC) analysis coupled with polarized light microscope (PLM) as well as temperature dependant X-ray diffraction (VTXRD). Most of the molecules exhibited multiple transitions both in the heating and cooling cycles. Figure 4 shows the DSC second heating and cooling scans of the entire series and the transition temperatures and corresponding enthalpies in the cooling cycle are summarized and given in table-1. **PBI-E4** exhibited two transitions both in the heating (22 °C, 1.99 kJ/mol ;

264.4 °C, 71.86 kJ/mol) as well as cooling cycle (21.05 °C, 2.06 kJ/mol; 250.5 °C, 71.43 kJ/mol). Multiple transitions (more than two) were observed in the case of almost all other molecules in the series. Figure 5a shows the plot of the transition enthalpies for the clearing (while heating) and the crystallization (while cooling) transitions as a function of the number of carbon atoms in the terminal alkoxy spacer length. An interesting odd-even oscillation could be observed in the change in enthalpy (ΔH), with the even members exhibiting higher values as a function of the number of carbon atom in the terminal alkoxy spacer segment.

Name	T_{cl} [a] (°C) (Lc/C-I)	ΔH_{cl} [a] (KJ/mol)	T_c [b] (°C) I-Lc/C	ΔH_c [b] (KJ/mol)	T_c [b] (°C) (Lc-C) /(C-C)	ΔH_c [b] (KJ/mol)	T_D [c] (°C)
PBI-E4	264	72.83	251	53.17	10	3.81	379
PBI-E5	244	37.46	231	35.10	6	6.28	375
PBI-E6	239	48.23	230	48.68	47	1.23	372
PBI-E7	227	39.8	215	38.64	-6	13.65	376
PBI-E8	221	44.82	212	46.16	-12.7	17.76	376
PBI-E9	202	33.22	191	31.08	10	34.91	370
PBI-E10	212	43.58	205	42	-2.64	23	373
PBI-E11	200	29.17	192	28.17	-8	16.65	372
PBI-E12	215	16.72	202	15.31	13	52.55	370

[a] clearing transition and corresponding enthalpy values during heating cycle, [b] phase transitions and corresponding enthalpy values during cooling cycles, [c] 10 % weight loss under N_2 atmosphere during TGA.

Table 1. Transition temperature and corresponding enthalpies of **PBI-En** molecules during the second heating and cooling cycles.

The clearing and the crystallization temperature were also plotted as a function of the number of carbon atom in the terminal alkoxy spacer segment (figure 5b). A weak odd-even oscillation with a steady decrease in the transition temperature was observed as the spacer length increased from 4 to 9; thereafter a strong odd-even oscillation was observed

for members 9 to 12. It is a well studied and understood concept that the even spacer can pack more efficiently compared to the odd one. The highly packed structure requires more energy for melting (endothermic) and similarly releases more energy (exothermic) while crystallizing as compared to the weakly packed molecules.

This is reflected in the clearing transitions as well as entropies and enthalpy values. The enthalpy of clearing transitions was almost equal to the first transition from isotropic to crystalline / liquid crystalline phase, which indicated a thermodynamically stable phase rather than a kinetically driven one.[21] Although odd-even oscillation in transition temperature has been reported for a variety of mesogens like azobenzene, biphenyl, and oligo(phenylenevinylenes), there has so far been no reports on similar observation in the perylenebisimide chromophores.[22-25]

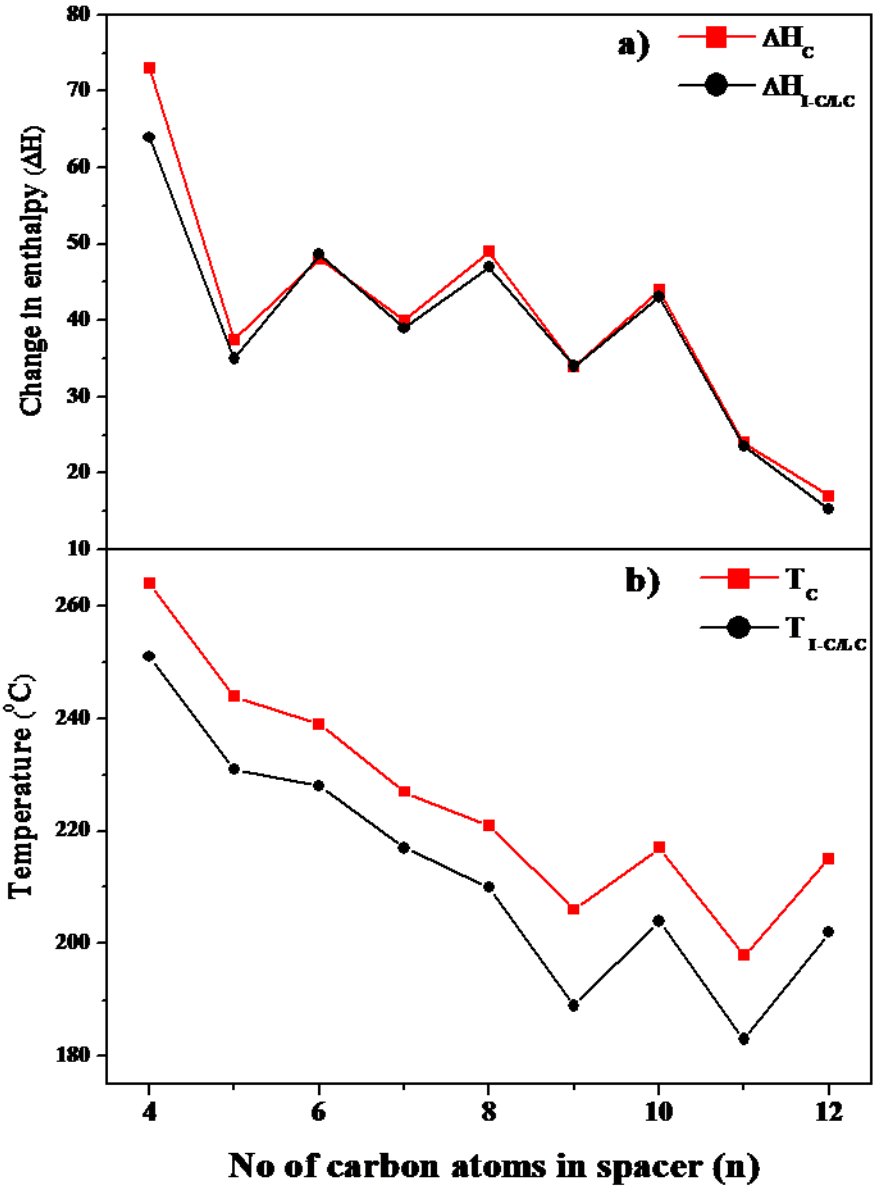

Figure 5: Odd–Even oscillations in the (a) clearing and the crystallization enthalpies and (b) clearing and the crystallization temperatures of **PBI-En** molecules as a function of number of carbon atoms in the terminal tri alkoxy spacer unit.

2.4.2 Polarised Light Microscope (PLM) analysis of PBI-En:

The phase identification of the various transitions observed in the DSC thermogram was carried out using Polarized Light Microscopic (PLM) analysis enabled with a programmable hot stage. The experimental procedure involved placing a trace amount of the sample on a cover glass plate, heating to melt at 10 °C /min, holding at isotropic state (10 °C higher than the clearing temperature) for 10 minutes followed by slow cooling of 5 °C / min. Figure 6 shows the texture retained at room temperature for all the samples.

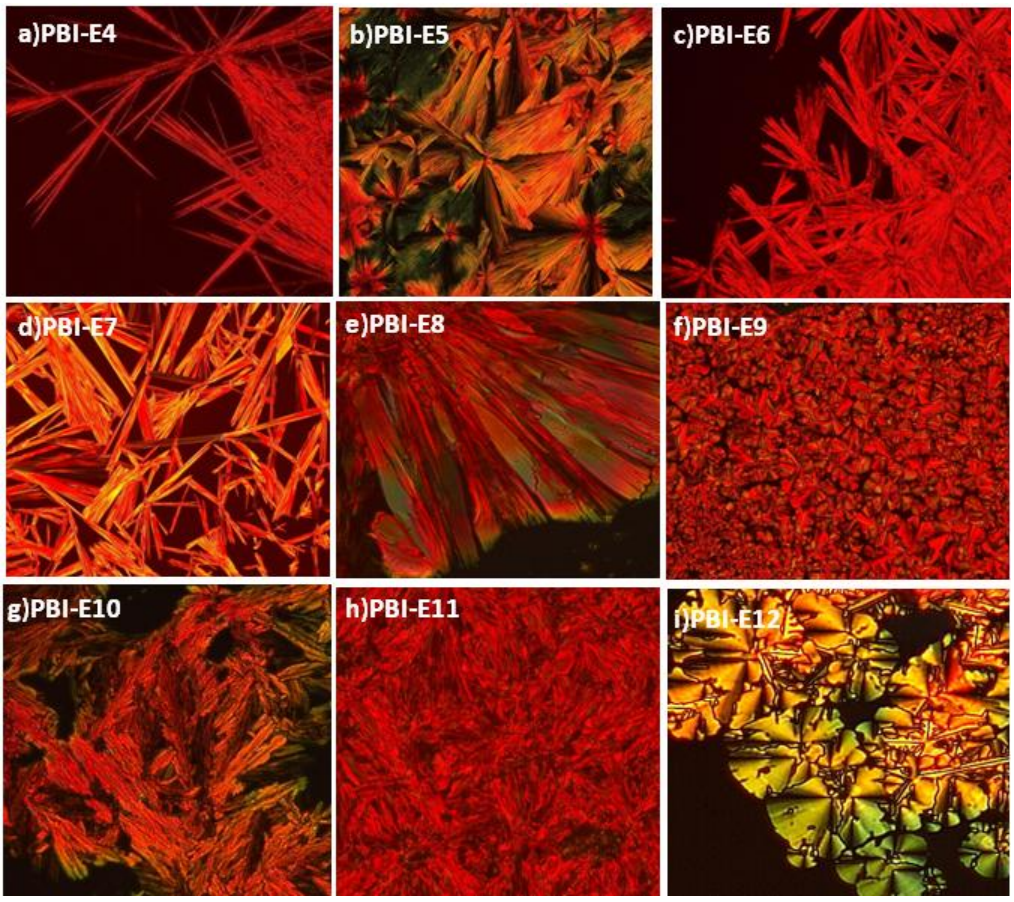

Figure 6: Polarized Light microscopic images of **PBI-En** molecules (under crossed polarizer) at room temperature. a) **PBI-E4** b) **PBI –E5** c) **PBI –E6** d) **PBI –E7** e) **PBI –E8** f) **PBI-E9** g) **PBI –E10** h) **PBI – E11** and i) **PBI – E12**.

Although two transitions were observed both in heating and cooling cycle for **PBI-E4**, the transition at 250.5 °C while cooling corresponded to crystallization and that at 264 °C

while heating was the clearing transition. A fast crystallization with growth of sharp needle like textures which remained until room temperature, confirmed the crystalline nature for **PBI-E4**. Similarly, PBI-E5, PBI-E6 and PBI-E7 also exhibited fast crystallization upon cooling from the isotropic melt which confirmed the absence of liquid crystallinity in these samples. PBI-E8 formed lancet-like textures upon cooling from isotropic state to 212 °C. These were characteristic columnar textures and it remained unchanged until room temperature. PBI-E9 exhibited clearing transition at 202 °C; upon cooling from the isotropic melt it exhibited a characteristic snow-flake like texture identified as columnar mesophase at 190 °C. Upon slow cooling to 180 °C the domain size seemed to increase. In the DSC cooling cycle also a clearly distinguishable transition was observed around this temperature, indicating a phase transition. The columnar mesophase texture remained stable until room temperature (25 °C). The transitions observed during cooling could be attributed to a columnar disordered to a columnar ordered one. In all cases, the transition observed below room temperature in the DSC (which could not be traced under PLM), could be the reorganization of the alkyl segments. PBI-E10 exhibited beautiful leaf- like textures at 213 °C upon cooling from the isotropic melt which remained stable until room temperature. Similarly PBI-E11 also had a clearing point at 200 °C during heating which on cooling formed the leaf-like textures at 192 °C. The mesophase characterization of PBI-E12 was reported previously.. In short, it had a clearing point at 215 °C and upon cooling snow flake like textures appeared at 200 °C corresponding to columnar hexagonal disordered phase. Further cooling resulted in a large dendritic growth corresponding to formation of columnar ordered phase.Thus, based on the observation under the PLM it could be concluded that the PBI-En molecules with shorter terminal spacer exhibited a tendency to crystallize while those with longer spacer length exhibited typical columnar mesophases upon cooling from the isotropic melt.

2.4.3 Wide angle X-ray diffraction (WXRD) analysis of the liquid crystalline phase

The phase identification of the **PBI-En** series was undertaken with the help of wide angle X-ray diffraction (WXRD) studies from 2θ = 2-35°. Variable temperature wide angle X-ray diffraction (VT-WXRD) studies were undertaken for the samples **PBI-E8**, **PBI-E9**, **PBI-E10, PBI-E11**. The WXRD pattern of PBI-E12, which we had reported previously is provided in figure 7 for comparison purpose. A sharp reflection at $2\theta = 2.09°$ having a d spacing of 42.19 Å was indexed as the d_{100} reflection. The other peaks which followed the characteristic ratios of $1:1/\sqrt{4}:1/\sqrt{7}:1/\sqrt{12}$ were indexed as the (100), (200), (210), (220) reflections of the hexagonal lattice.

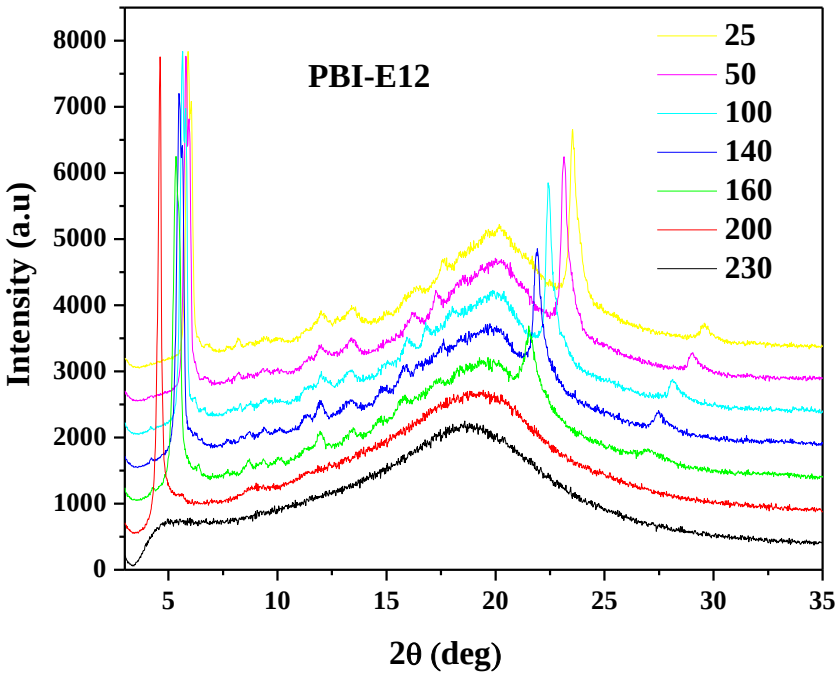

Figure 7: Variable temperature XRD of **PBI-E12**.

Figure 8a-d compares the WXRD of PBI-E8 to E11. Figure 8a shows that no reflections were observed for **PBI-E8** in the isotropic state at 235 °C. Around 212 °C, sharp reflections appeared at 2θ values of 2.45°, 5.28° and 5.63° followed by small intense reflections in the 2θ range from 5°-22°. The DSC thermogram had also indicated a transition at 212.6 °C, which was supported by the observation of lancet like patterns under PLM around 212 ^{0}C. Further cooling of the sample resulted in more sharp reflections and shift in peak positions, especially for reflections at 5.28°, and 5.63° and at 2θ = 21.24°. The sharp reflection at 2θ = 2.45° having a d spacing of 35.12 Å was indexed as the d_{100} reflection.[36] The peak corresponding to the (200) plane of the **PBI-E12** at 2θ =5.35^o (figure 7) split into two equal intense reflections at 5.28°, and 5.63° in PBI-E8, which is a characteristic feature of the columnar rectangular phase. [20] A similar split was observed for the reflection around 2θ =5.5^o for PBI-E9, PBI-E10 and PBI-E11 also, which indicated that all of them belonged to the same columnar rectangular phase. Table-2 shows the temperature and the corresponding d spacing of peaks which followed the characteristic pattern of a columnar rectangular organization (a ratio of ≅ 1: 4/2 : 5/2 for the d spacing) which is in almost good agreement with the reported ratio.[20]

Depending on the core-core interaction columnar rectangular lattice can form different symmetry and the d spacing values do not following a fixed ratio as in the case of

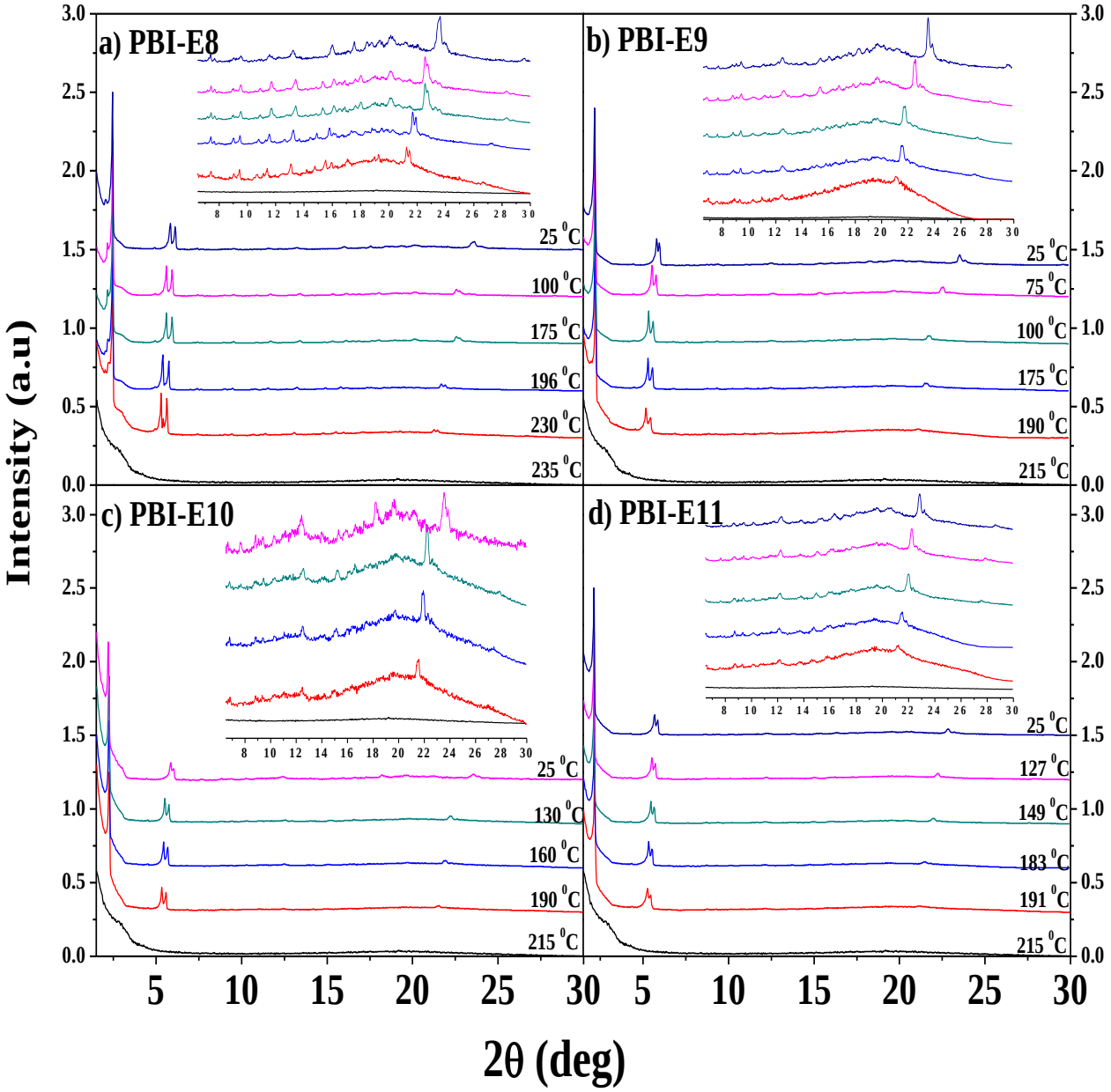

Figure 8: Variable Temperature XRD of **PBI-E8** to **PBI-E11**.

columnar hexagonal systems therefore the indexing of these systems are quite difficult. The reflection at 2θ = 21.24° (4.18 Å) and 2θ = 21.46° (4.14 Å) corresponded to the π-π stacking of the perylene core .Upon cooling a gradual shift was observed in the π stacking peaks to higher theta region. At room temperature (25 °C) the π-π stack distance reduced to 3.7 Å (from 4.1 Å at 230 °C), indicating strong overlapping of the aromatic core.

A split was observed in these transitions which was a characteristic signature of the columnar plastic phase. Plastic phase is characterized by higher crystallinity along with fluidity. The split in the π stacking reflection around 3.7 Å indicated better ordering in these systems and these two diffraction are from the two different planes Similar VTWXRD studies conducted for the other higher member samples also revealed some common trends. No shift was observed in the d_{100} reflection as a function of temperature, however regular shifts to higher 2θ values were observed for the double reflections around 5.28° and 5.63° as well as for the reflection around 2θ = 21.24° corresponding to the π-π stacking of the perylene aromatic core (inset expanded plot 2θ = 6.5° - 30° in figure 8a-d).

In contrast to the appearance of the plastic phase at higher temperature observed in the case of **PBI-E8**, the higher spacer samples like **PBI-E9**, **PBI-E10**, and **PBI-E11** exhibited a split of the π-π stacking reflection around 2θ = 21.46° (4.14 Å) only upon cooling to room temperature. Another striking difference in behavior exhibited by the odd membered samples like **PBI-E9** and **PBI-E11** in comparison with their even membered analogues was the formation of an initial disordered phase at high temperature characterized by absence of the columnar π-π stacking. This was clearly observed in the DSC thermogram also during the cooling cycle for **PBI-E9**. The cooling cycle in the DSC thermogram of **PBI-E9** (figure 8b) had two exothermic transitions at 191.38 ^{o}C (9.37 kJ/mol) and 181.4 ^{o}C (3.76 kJ/mol) – the first one corresponding to the isotropic-disordered columnar rectangular phase and the second transition at 181 ^{o}C corresponding to the transition of the disordered phase to a more ordered columnar one. The reflection for the π-π stacking interaction became prominent in the WXRD pattern only below 180 ^{0}C. **PBI-E11** also exhibited a similar trend, although the disordered to ordered transition was observed only as a shoulder in the DSC thermogram. The lower homologues **PBI-E4**, **PBI-E5**, **PBI-E6** and **PBI-E7** did not exhibit any liquid crystalline textures as explained earlier. Thus the entire series from spacer 4 to spacer 12 could be classified into 3 groups – a lower member group **PBI-E4** to **PBI-E7** which did not exhibit mesophase, a middle spacer series from **PBI-E8** to **PBI-E11** ordered columnar plastic phases and the highest member **PBI-E12** which formed hexagonal ordered columnar phase.

Sample	Temperature and d-spacing (Å)					
	230 (°C)	**211** (°C)	**196** (°C)	**175** (°C)	**100** (°C)	**25** (°C)
PBI – E8	35.92 16.17 15.72 4.17 4.13 **Col_{rp}**	35.94 16.45 15.49 4.12 4.07 **Col_{rp}**	35.97 16.21 15.27 4.10 4.05 **Col_{rp}**	35.99 15. 98 15.64 4.05 4.01 **Col_{rp}**	36.00 15.52 14.77 3.93 3.90 **Col_{rp}**	36.12 15.43 14.57 3.81 3.72 **Col_{rp}**
PBI – E9	**190** (°C) 38.49 16.8 15.88 **Col_{rd}**	**175** (°C) 38.52 16.45 15.73 4.15 **Col_{ro}**	**100** (°C) 38.54 16.20 15.57 4.09 4.05 **Col_{rp}**	**75** (°C) 38.56 15.64 14.98 4.05 3.9 **Col_{rp}**	**25** (°C) 38.58 14.89 14.53 3.82 3.75 **Col_{rp}**	
PBI- E10	**190** (°C) 39.98 17.54 16.80 4.3 **Col_{ro}**	**160** (°C) 40.01 17.44 16.75 4.13 4.11 **Col_{rp}**	**130** (°C) 40.03 17.12 16.48 4.05 4.03 **Col_{rp}**	**25** (°C) 40.07 15.27 15.14 3.81 3.72 **Col_{rp}**		
PBI- E11	**191** (°C) 40.97 16.71 16.20 **Col_{rd}**	**183** (°C) 41.03 16.54 15.96 4.12 **Col_{ro}**	**127** (°C) 41.06 16.04 15.27 4.03 4.01 **Col_{rp}**	**149** (°C) 41.1 16 15.47 4.01 3.9 **Col_{rp}**	**25** (°C) 41.13 15.41 15.12 3.8 3.7 **Col_{rp}**	

Note: **Col_{rp}** - columnar rectangular plastic phase, **Col_{rd}** - columnar rectangular disordered phase and **Col_{ro}** - columnar rectangular ordered phase.

Table 2. d-spacing values and phase behavior of the Liquid crystalline **PBI-En** molecules at various temperatures.

2.4.4 SCLC mobility measurements:

SCLC measurement is preferred over the FET measurement due to the stacking of the molecule parallel to the substrate. Therefore, the charge transport is expected to be perpendicular to the substrate. The electron transport characteristics of all members of the **PBI-En** series were investigated by space-charge-limited current (SCLC) method.

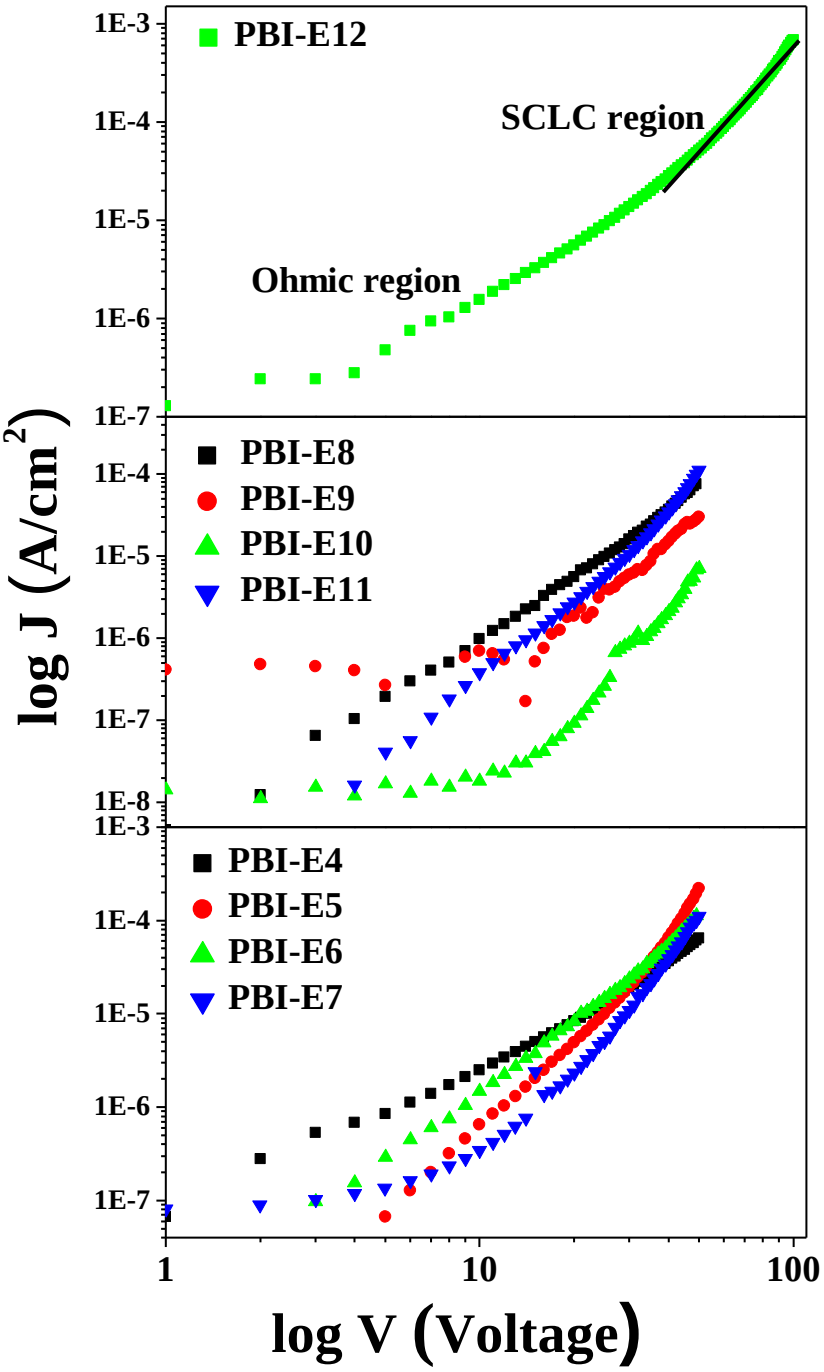

Figure 9: Double logarithmic plot of the current density (J) versus applied voltage (V) measured for the **PBI-En** molecules at room temperature (25 ^{0}C) in devices with area around 0.08 – 0.12 cm^2 and thickness 0f 10 μm. The drop cast sample films were annealed above their clearing temperature for 20 minutes and cooled to room temperature before the measurement.

This method allows for determination of the macroscopic bulk mobility of a material in thin film. The semiconducting PBIs were sandwiched between an electron injecting Aluminum electrode as top and bottom contact with a configuration of glass/Al/**PBI-En**/Al. Aluminum electrodes were chosen for the electron only devices due to the work function (4.3 eV) match with the LUMO of perylenebisimdes.[26] The samples were heated to isotropic and then cooled to room temperature (25 °C), following which the top Al electrode was deposited. The charge carrier mobilities were evaluated by the current – voltage (I-V) measurement under inert gas atmosphere.The J-V curves present two regimes i) at low voltages; ohmic region where the current measured is potentially limited by the charge traps and a linear relation between J and V exists; ii) at high voltages; SCLC region where the charge transport is through bulk with less number of traps and J α V^2. The slope of the region was determined from the log-log J-V plot. The charge carrier mobility was calculated from the slope 2 region, which was determined from the logarithmic plot. The charge carrier mobility in this SCLC region can be calculated from the J-V curve by using Mott-Gurney equation: [44]

$$J = \frac{9}{8}\,\varepsilon_r\,\varepsilon_0\,\mu\,\frac{V^2}{L^3}$$

Where J is the current density, ε_r is the dielectric constant of the organic semiconductor (assumed to be 3 in our calculations),[45] ε_0 is the permittivity of free space, μ is the charge carrier mobility, L is the thickness of the active layer, and V is the applied voltage across the device. The SCLC mobility was measured for 5 devices each, the active layer thickness ranged from 5-14 μm (determined using optical profilometer), and covered an area of ~ 0.08 – 0.12 cm^2. J−V characteristics of annealed films of **PBI-En** together with the respective fits according to the Mott−Gurney equation[27] are shown in Figure 6. The short spaced (n < 8) crystalline molecules exhibited a mobility in the order of 10^{-4} $cm^2\,V^{-1}\,s^{-1}$, where as the middle spaced (n = 8 to 11) columnar rectangular phase showed mobility in the range of 10^{-5} $cm^2\,V^{-1}\,s^{-1}$. The electron mobility value for the columnar hexagonal phase of **PBI-E12** (n= 12) was obtained as 1.6 x10^{-3} $cm^2\,V^{-1}\,s^{-1}$, which was two orders of magnitude higher compared to the other liquid crystalline analogues. This was the highest value observed among the series. The WXRD and PLM studies had indicated that **PBI-E12** assembled in the plastic columnar hexagonal phase upon cooling from the isotropic phase. The higher order with flexibility which is a characteristic of the plastic LC phase

supported better electron mobility in **PBI-E12** compared to the samples assembled in the columnar rectangular phase.

Sample	Maximum mobility μ_e max (cm^2/Vs)	Average mobility μ_e Avg (cm^2/Vs)	Mean deviation
PBI-E4	3.35×10^{-4}	2×10^{-4}	$\pm 0.85 \times 10^{-4}$
PBI-E5	8.9×10^{-4}	8.5×10^{-4}	$\pm 2.65 \times 10^{-4}$
PBI-E6	1.7×10^{-4}	1.2×10^{-4}	$\pm 0.40\times 10^{-4}$
PBI-E7	3.01×10^{-4}	1.81×10^{-4}	$\pm 0.67\times 10^{-4}$
PBI-E8	3.65×10^{-5}	1.85×10^{-5}	$\pm 1.82\times 10^{-5}$
PBI-E9	5.65×10^{-5}	2.05×10^{-5}	$\pm 2.05\times 10^{-5}$
PBI-E10	3.35×10^{-5}	1.81×10^{-5}	$\pm 1.81\times 10^{-5}$
PBI-E11	4.45×10^{-5}	3.6×10^{-5}	$\pm 1.24\times 10^{-5}$
PBI-E12	3.67×10^{-3}	2.02×10^{-3}	$\pm 0.67\times 10^{-3}$

Table 3. Maximum and average SCLC mobilities of the annealed **PBI-En** series of molecules.

2.5 Conclusion

A systematic study of the effect of molecular packing on the n-type charge transport characteristics in a novel series of highly soluble pentadecyl phenol substituted perylenebisimide ester derivatives was presented. The homologous PBI-En series constituted a 3, 4, 5-tri alkoxy ester derivative of a symmetrical petadecyl phenol substituted perylenebisimide, where the terminal alkyl spacer length was varied from n = 4 to 12. Detailed characterization using DSC, PLM and variable temperature WXRD established that the members of the homologous series with n > 8 exhibited columnar liquid crystalline phases at higher temperature and froze into a columnar plastic phase at room temperature as evidenced by the split appearance of the π-π stacking reflection

around 2θ = 22°. The lower members of the series with n < 8 were crystalline in nature. The PBI derivative with the longest spacer length n = 12 (PBI-E12) formed columnar hexagonal phase characterized by beautiful dendritic textures under the PLM. The enthalpy of the clearing and crystallization transitions exhibited a strong odd-even oscillation as a function of the number of carbon atoms in the terminal alkoxy unit. The even members exhibited higher enthalpy values due to the more efficient packing of the even membered alkyl spacers in the solid state compared to the odd ones. The bulk mobility of the molecules of the series annealed from the isotropic melt was estimated by the SCLC method using the device configuration of glass/Al/PBI-En/Al. The crystalline members with n < 8 gave a bulk mobility estimate in the order of 10^{-4} cm^2 V^{-1} s^{-1} while the intermediate spacers with n = 8 to 11 showed mobility in the range of 10^{-5} cm^2 V^{-1} s^{-1} only. A high mobility estimate of 1.6 x 10^{-3} cm^2 V^{-1} s^{-1} was observed for PBI-E12, which indicated the direct relation between charge transport and appropriate molecular ordering with better core packing. The liquid-like flexibility combined with the better core packing of the columnar hexagonal plastic phase facilitated slightly better charge transport compared to the three dimensional crystalline packing. The present study thus highlighted (a) the important role played by the flexible alkyl chains in fine tuning the mesophases in a homologous series of PBI derivatives functionalized with pentadecyl phenol and the importance of molecular structural factors that are to be taken into consideration while designing materials for better charge transport.

1.7. References:

1. H. Sirringhaus,*Adv. Mater*., **2005**, 17, 2411.
2. S.Gunes, H. Neugebauer and N. S. Sariciuici, *Chem. Rev*., **2007**, 107, 1324.
3 C. Wang, H. Dong, W. Hu, Y. Liu and D. Zhu, *Chem. Rev*., **2012**, 112, 2208.
4 Z. Jiang, Z. Zhong, S. Xue, Y. Zhou, Y. Meng, Z. Hu, N. Ai, J. Wang, L. Wang, J Peng, Y. Ma, J. Pei, J. Wang andY. Cao, *ACS Appl. Mater. Interfaces*, **2014,** 6, 8345**.**
5 L. Schmidt-Mende, A. Fechtenk¨otter, K. M¨ ullen, E. Moons, R. H. Friend and J. D. MacKenzie,*Science*, **2001**, 293, 1119
6 M. Yoshio, T. Mukai, H. Ohno and T. Kato, *J. Am. Chem. Soc*., **2004**,126, 994.
7 N. Boden, R. J. Bushby, J. Clements and B. Movaghar, *J.Mater. Chem*., **1999**, 9, 2081
8 S. Sergeyev, W. Pisula and Y. H. Geerts, *Chem. Soc. Rev*., **2007**,36, 1902–1929.
9 S. Kumar, *Chem. Soc. Rev*., **2006**, 35, 83.
10 A. J. J. M. van Breemen, P. T. Herwig, C. H. T. Chlon, J. Sweelssen, H. F. M. Schoo, S. Setayesh, W. M. Hardeman, C. A. Martin, D. M. de Leeuw, J. J. P. Valeton, C. W. M. Bastiaansen, D. J. Broer,A. R. Popa-Merticaru and S. C. J. Meskers, *J. Am. Chem. Soc*., **2006**, 128, 2336.
11 M. Funahashi and A. Sonoda, *J. Mater. Chem*., **2012**, 22, 25190.
12 M. O 'Neill and S. M. Kelly, *Adv. Mater*., **2003**, 15, 1135.
13 W. Pisula, M. Kastler, D. Wasserfallen, T. Pakula, K. M¨ ullen, *J. Am. Chem. Soc*., **2004**, 126, 8074.
14 S. Sergeyev, E. Pouzet, O. Debever, J. Levin, J. Gierschner, J. Cornil, R. G´omez Aspe and Y. H. Geerts, *J. Mater. Chem*., **2007**,17, 1777.
15 Y. Dienes, M. Eggenstein, T. K´arp´ati, T. C. Sutherland, L. Nyul´aszi and T. Baumgartner, *Chem.Eur. J*., **2008**, 14, 9878
16 B. A. Jones, A. Facchetti, M. R. Wasielewski and T. J. Marks, *J.Am. Chem. Soc*., **2007**, 129, 15259.
17 F. Wurthner, *Chem. Commun*., **2004**, 14, 1564.
18 A. Wicklein, A. Lang, M. Muth and M. Thelakkat, *J. Am. Chem. Soc*., **2009**, 131, 14442.
19 G. A. Bhavsar and S. K. Asha, *Chem-Eur. J*., **2011**, 17, 12646.
20 A. Arulkashmir, B. Jain, J. C. John, K. Roy, K. Krishnamoorthy, *Chem. Commun*., **2014**, 50, 326.

21 V. Percec, S. D. Hudson, M. Peterca, P. Leowanawat, E. Aqad, R. Graf, H. W. Spiess, X. Zeng, G. Ungar and P. A. Heiney, *J.Am. Chem. Soc*., **2011**, 133, 18479.

22 T. Kobayashi and T. Seki, *Langmuir*, **2003**, 19, 9297.

23 E. Białecka-Florjanczyk, I.Sledzinska, E. G´oreck , J. Przedmojski, *Liq. Cryst*., **2008**, 35, 401.

24 S. Kurihara, T. Ikeda and S. Tazuke, *Macromolecules*, **1993**, 26, 1590.

25 M. Goel and M. Jayakannan, *J. Phys. Chem. B*, **2010**, 114, 12508.

26 R. Narayan, P. Kumar, K. S. Narayan and S. K. Asha, *J. Mater. Chem. C*, **2014**, 2, 6511.

27 L. Bozano, S. A. Carter, J. C. Scott, G. G. Malliaras andP. J. Brock, *Appl. Phys. Lett*., 1999, 74, 1132.

Chapter 3

Twin Liquid crystalline Perylenebisimides: Synthesis and Structural Characterizations

3.1 Abstract:

A series of twin Perylenebisimide (PBI) molecules were synthesized and characterized having the structure PBI-(methylene spacer)n-PBI where the length of the central poly methylene spacer segment was varied from n = 1 to 12. The PBI unit was imidized with ethyl hexyl branched alkyl segment at the terminal and pentadecyl phenol at the other end which was linked up through the poly methylene spacer to form the twin molecules. The differential packing afforded by the odd and even spaced central methylene segments resulted in an odd-even oscillation of the clearing transitions as well as their enthalpies with higher values observed for the even twins. The odd-even oscillation was quite prominent for the spacers till n<7 after which it tapered off. PBI-T1 and PBI-T3 exhibited tendencies to form columnar phases while the rest of the twin molecules exhibited tendencies for high temperature nematic phases. The ability to control the crystalline or mesogenic nature of the PBI molecules, which constitute an important member of the n type rylenebisimide family that finds application as electron transporters in Field Effect Transistors (FET) and Organic Solar Cells, is promising as it provides a handle to design systems whose bulk packing is predefined to suit the requirements of the application.

3.2 Introduction

In the previous chapter we have discussed the effect of terminal spacer on the liquid crystalline behavior of PBI esters. This chapter is mainly focused on the effect of middle alkyl spacer on mesophase characteristics of twin liquid crystalline perylenebisismides (PBI-Tn). Linking of two chromophores in the manner chromophore-spacer-chromophore, also known as twin liquid crystals,[1] has been a well-studied approach to modify the liquid crystalline phases without making structural changes in the chromophore itself. The variation of the central spacer segment length (alkyl or ethyleneoxy) results in a change in the rigid versus flexible balance of the molecule, which has a direct influence on the nature of the LC phase.[2] In addition to the overall length of the spacer segment, the odd-even parity has a strong influence on the packing of the molecule with the even segmented twins having a collinear arrangement of the chromophores. The odd spacered twins usually have a bilaxial organization of the mesogens resulting in lower melting and transition temperatures for the odd twins compared to the even twins. This is reflected as an odd-even effect in the melting or LC transitions as well as the enthalpy and entropies of transition[3,4]. Although a multitude of twin LC designs have been reported using different mesogens like azobenzene, triphenylene,[5-8] etc there has only been one report as far as we are aware on twin molecules based on Perylenebisimides.[9-14] Xu Lin et. al reported twin PBI molecules having branched swallow tail terminus and central poly methylene spacer of varying segment length 5 to 10 units.[15] They could observe a surprising influence of the odd-even packing on the gelation abilities with the odd members clearly demonstrating gelation in toluene, which was not observed in the even members. This was due to the differences in their packing unraveled by powder Xray diffraction studies, which showed that the odd members organized into hexagonal lattices that lacked crystalline organization, while the even members self organized directly into crystalline structures. It is surprising that there have not been many other reports exploiting the benefits of the wide structural variation afforded by small changes in the central spacer length in the twin molecular design motif, based on the perylenebisimides.

In the current work we report dimeric or twin perylenebisimide molecules, where two pentadecyl phenol functionalized perylenebisimide moieties were linked with each other through central polymethylene spacer of length varying from one CH_2 unit to 12 CH_2 units. The pentadecyl phenol moiety is a wonderful molecular building block with a phenolic functionality and a long C15 alkyl chain on the aromatic ring. The unsymmetrical PBI having pentadecyl phenol in one termini and solubilizing branched ethyl hexyl units in other termini.

The etherification of this UPBI with different dialkyl bromide resulted the PBI-Tn molecules where the central methylene spacer is varried from 1 to 12. The molecules were characterized using differential scanning calorimetry (DSC), polarizing light microscope (PLM) and variable temperature wide angle X-ray diffraction (VT-WXRD) studies.

3.3 Experimental Section

Materials: Perylene-3,4,9,10-tetracarboxylic dianhydride (PTCDA), 3-pentadecyl phenol, zinc acetate, 1,1-Dibromo methane, 1,2-Dibromoethane, 1,3-Dibromopropane, 1,4-Dibromobutane, 1,5-Dibromopentane, 1,6-Dibromohexane, 1,7-Dibromoheptane, 1,8-Dibromooctane, 1,9-Dibromononane, 1,10-Dibromodecane, 1,11-Dibromoundecane and 1,12-Dibromododecane were purchased from Sigma–Aldrich and used without further purification. Sodium nitrite, imidazole, potassium hydroxide and potassium carbonate were purchased from Merck Chemicals Ltd and used as such. Dimethyl formamide (DMF), Acetic acid (AcOH), tertiary butanol (tBuOH) and ethanol were purchased from Merck Chemicals Ltd and were purified using standard procedures.

3.3.1 Instrumentation

^{1}H-NMR and ^{13}C-NMR spectra of PBI-Tn molecules were recorded on a Bruker-AVANCE 400 MHz spectrometer. Chemical shifts are reported in ppm at 25 $^{\circ}$C using $CDCl_3$ as solvent containing small amount of tetramethylsilane(TMS) as internal standard. The purity of samples was confirmed using elemental analysis, which was done using a ThermoFinnigan Flash EA 1112 series CHNS analyzer.Gel Permeation Chromatography (GPC) was carried out on Polymer Laboratories PL-GPC-220 using $CHCl_3$ as eluent. The flow rate of $CHCl_3$ was maintained as 1 µL/min throughout the experiments and the sample solutions at concentrations 2-3 mg/ml were filtered through syringe filter and injected for recording the chromatograms at 30 $^{\circ}$C. The mass spectral analysis was carried out in reflecting mode with an accelerating voltage of 25 kV using a Voyager-De-STRMALDI-TOF (Applied Biosystems, Framingham, MA, USA) instrument equipped with 337 nm pulsed nitrogen laser used for desorption and ionization. The sample was made in $CHCl_3$ and premixed with dithranol matrix before spotting on 96-well stainless steel MALDI plate by dried droplet method. Infrared spectra were recorded using Bruker FT-IR (ATR mode) spectrophotometer in the range of 4000-600 cm^{-1}.The thermal stability of the PBI-En were analyzed using PerkinElmer STA-6000 thermogravimetric analyser (TGA) under nitrogen atmosphere from 40-800 $^{\circ}$C at 10 $^{\circ}$C/min. Differential Scanning Calorimetry (DSC) was performed using a TA Q10 model. About 2–3 mg of the samples were taken in aluminium pan, sealed and scanned

at 10 °C/min under nitrogen atmosphere. The instrument was calibrated with indium standards before measurements. The phase behaviour of the PBI-Tn was analyzed using LIECA DM2500P polarized optical microscope equipped with Linkam TMS 94 heating and cooling stage connected to a Linkam TMS 600 temperature programmer. The Transition from isotropic to liquid crystalline phase was monitored by the evolution of characteristic textures. The geometry optimization was carried out with Guassian09 program[1] using B3PW91[2] functional and 6-31G basis sets[2] for H, C, and O atoms. Dispersion corrections have been included in the geometry optimization using an empirical dispersion correction (DFT-D3) proposed by Grimme.[16]

3.3.2 Synthesis and Characterization:

Unsymmetrical PBI (A): synthesized by the selective ring opening of ethyl hexyl amine substituted symmetrical PBI followed by the condensation with pentadecyl phenol as given in scheme 1.Yield: 600 mg (40 %); m.p. = 320 °C; ^{1}H NMR ($CDCl_3$+TFA): d = 8.91 (m, 8H; perylene), 6.89–7.16 (m, 3H; ArH-PDP), 4.01 (t, 2H; CH_2), 2.39 (t, 4H; Ar-CH_2), 1.53 (t, 4H; Ar-CH_2-CH_2), 1.0–1.4 (br, 48H; aliphatic CH_2), 0.84 ppm (t, 6H; terminal CH_3); ^{13}C NMR: 166.27, 163.21, 162.65, 160.62, 155.86,143.08, 136.66, 134.16, 130.32, 127.00, 126.14, 124.92, 123.12, 122.59, 115.03, 111.82, 106.19, 32.17, 31.28, 29.92, 29.60, 22.85, 13.81 ppm; FTIR: (υ) 3359 (OH stretch), 2922, 2853, 1698 (C=O imide), 1656, 1592, 1498, 1403, 1360, 1348, 1300, 1250, 1231, 1198, 1176, 967, 862, 813, 796, 750 cm^{-1}; MALDI-TOF (dihydroxy benzene matrix): m/z calcd for $C_{66}H_{78}N_2O_6$: 804; found: 805.35 [M+1], 827[M + Na].elemental analysis calcd (%): C 79.07, H 7.51, N 3.48; found: C 79.56, H 7.22, N 3.95.

Synthesis of **PBI–T1**:

The unsymmetrical PBI (A) (0.1g, 0.124 mmol) in dry DMF was taken in a two neck round bottom flask along with potassium carbonate (5 equivalent) and potassium iodide (catalytic amount) and stirred well for half hour at 50 °C. This was followed by the addition of dibromo methane (0.0042 ml, 0.0624 mmol) at 0 °C and the reaction was continued for 48 hrs at 80°C. The DMF was distilled off and the product was precipitated into water and purified by column chromatography in DCM/methanol. Yield: 20 mg (25 %); m.p. 236°C; ^{1}H NMR ($CDCl_3$): d= 8.7–8.9 (m, 16H; perylene), 7.23 – 7.17 (dd,6H; Ar-H), 5.85 (s,2H; Ar-O-CH_2-O-Ar), 4.15 (t, 4H; N-CH_2), 2.48 (t, 4H; PDP Ar-CH_2), 1.9–0.87 (m, 82H; aliphatic CH_2); ^{13}C NMR: 164.70, 163.42, 152.95, 151.46, 150.50, 146.75, 142.93, 142.13, 135.08, 132.04, 131.16, 129.96, 126.78, 123.86, 123.39, 122.00, 120.38, 93.50, 73.60, 69.24, 31.92, 31.13,

30.33, 29.37, 26.09, 22.69, 14.11; FTIR: (υ) 2962 ($CH_{stretch}$), 2923, 2853,1702 ($C=O_{imide}$), 1663, 1593, 1503, 1465, 1429, 1359, 1337, 1261, 1157 ($C-O_{ether}$), 1198, 1097, 1025, 970, 804, 751 cm^{-1}; MALDI-TOF (Dihydroxy benzene matrix): m/z calcd for $C_{107}H_{120}N_4O_{10}$: 1623.91; found: 1645.91[M^+Na], 1661.93 [M^+ K]; Elemental analysis calcd (%): C 79.23, H 7.46, N 3.45; found: C 79.56, H 7.82, N 3.05

Synthesis of **PBI–T2**:

The same procedure as above was repeated for unsymmetrical PBI (A) (0.1 g, 0.124 mmol) but dibromo ethane (0.0054ml, 0.0624 mmol) was used for the spacer segment. Yield: 26 mg (24 %); m.p. 278 °C;^{1}H NMR ($CDCl_3$): d= 8.7–8.9 (m, 16H; perylene), 7.23- 6.97 (dd ,6H; Ar-H), 4.43 (t, 4H; Ar-O-CH2), 4.15 (t, 4H; N-CH_2), 2.48 (t, 4H; PDP Ar-CH_2), 1.9-0.87 ppm (m, 72H; aliphatic CH_2),: ^{13}C NMR: 164.70, 163.42, 152.95, 151.46, 150.50, 146.75, 142.93, 142.13, 135.08, 132.04, 131.16, 129.96, 126.78, 123.86, 123.39, 122.00, 120.38, 108.50, 73.60, 69.24, 31.92, 31.13, 30.33, 29.37, 26.09, 22.69, 14.11; FTIR: (υ) 2962 ($CH_{stretch}$), 2923, 2853, 1702 ($C=O_{imide}$)), 1663, 1593, 1503, 1465, 1429, 1359, 1337, 1261, 1198, 1157 ($C-O_{ether}$),1097, 1025, 970, 804, 751 cm^{-1}; MALDI-TOF (Dihydroxy benzene matrix): m/z calcd for $C_{108}H_{122}N_4O_{10}$: 1637.91; found: 1661.98 [M^+ Na]; Elemental analysis calcd (%): C 79.28, H 7.52, N 3.42.71; found: C 79.62, H 7.66, N 3.46.

Synthesis of **PBI–T3**:

The same procedure as above was repeated for unsymmetrical PBI (A) (0.1 g, 0.124 mmol) but dibromo propane (0.0063 ml, 0.0624 mmol) was used for the spacer segment. Yield: 24 mg (23%); m.p. 266 °C; ^{1}H NMR ($CDCl_3$): d= 8.7–8.9 (m, 16H; perylene), 7.23- 6.98 (dd, 6H; ArH - PDP), 4.15 (t, 4H; N-CH_2), 2.48 (t, 4H; PDP Ar-CH_2), 1.9 – 0.87 (m, 84H; aliphatic CH_2),; ^{13}C NMR: 164.70, 163.42, 152.95, 151.46, 150.50, 146.75, 142.93, 142.13, 135.08, 132.04, 131.16, 129.96, 126.78, 123.86, 123.39, 122.00, 120.38, 108.50, 73.60, 69.24, 31.92, 31.13, 30.33, 29.37, 26.09, 22.69, 14.11; FTIR: (υ) 2962 ($CH_{stretch}$), 2923, 2853, , 1702 ($C=O_{imide}$), 1663, 1593, 1503, 1465, 1429, 1359, 1337, 1261, 1198, 1097,1157 ($C-O_{ether}$), 1025, 970, 804, 751 cm^{-1}; MALDI-TOF (Dihydroxy benzene matrix): m/z calcd for $C_{109}H_{124}N_4O_{10}$: 1650.91; found: 1657.98 [M^+], 1674.93 [M^+ Na]; Elemental analysis calcd (%): C 79.34, H 7.57, N 3.4; found: C 78.82, H 8.66, N 3.67.

Synthesis of **PBI–T4**:

The same procedure as above was repeated for unsymmetrical PBI (A) (0.1 g, 0.124 mmol) but dibromo butane (0.0074 ml , 0.0624 mmol) was used for the spacer segment. Yield: 30 mg (32 %); m.p. 288 °C; ^{1}H NMR ($CDCl_3$): d= 8.7–8.9 (m, 16H; perylene), 7.23–6.8 (m,

6H; ArH - PDP), 4.15 (t, 4H; N-CH_2), 2.48 (t, 4H; PDP Ar-CH_2), 1.9 -0.87 (m, 86H; aliphatic CH_2), ^{13}C NMR: 164.70, 163.42, 152.95, 151.46, 150.50, 146.75, 142.93, 142.13, 135.08, 132.04, 131.16, 129.96, 126.78, 123.86, 123.39, 122.00, 120.38, 108.50, 73.60, 69.24, 31.92, 31.13, 30.33, 29.37, 26.09, 22.69, 14.11; FTIR: (υ) 2962 ($CH_{stretch}$), 2923, 2853, 1702 (C=O_{imide})), 1663, 1593, 1503, 1465, 1429, 1359, 1337, 1261, 1198, 1157 (C-O_{ether}) 1025, 970, 804, 751 cm^{-1}; MALDI-TOF (Dihydroxy benzene matrix): m/z calcd for $C_{110}H_{126}N_4O_{10}$: 1664.91; found: 1657.98 [M^+], 1674.93 [M^+ Na]; Elemental analysis calcd (%): C 79.39, H 7.63, N 3.37; found: C 79.62, H 7.66, N 3.65

Synthesis of **PBI–T5**:

The same procedure as above was repeated for unsymmetrical PBI (A) (0.1g, 0.124 mmol) but dibromo pentane (0.0084 ml ,0.0624 mmol) was used for the spacer segment. Yield: 32 mg (36 %); m.p. 171°C; ^{1}H NMR ($CDCl_3$): d= 8.7–8.9 (m, 16H; perylene), 7.23–6.9 (dd, 6H; ArH - PDP), 4.15 (t, 4H; N-CH_2), 2.48 (t, 4H; PDP Ar-CH_2), 1.9 – 0.87 (m, 88H; aliphatic CH_2), ^{13}C NMR: 164.70, 163.42, 152.95, 151.46, 150.50, 146.75, 142.93, 142.13, 135.08, 132.04, 131.16, 129.96, 126.78, 123.86, 123.39, 122.00, 120.38, 108.50, 73.60, 69.24, 31.92, 31.13, 30.33, 29.37, 26.09, 22.69, 14.11; FTIR: (υ) 2962 ($CH_{stretch}$), 2923, 2853, 1702 (C=O_{imide})), 1663, 1593, 1503, 1465, 1429, 1359, 1337, 1261, 1198,1157 (C-O_{ether}) 1097, 1025, 970, 804, 751 cm^{-1}; MALDI-TOF (Dihydroxy benzene matrix): m/z calcd for $C_{111}H_{128}N_4O_{10}$: 1678.91; found: 1677.81 [M^+], 1715.77 [M^+ K]; Elemental analysis calcd (%): C 79.44, H 7.69, N 3.34; found: C 79.62, H 7.26, N 3.64.

Synthesis of **PBI–T6**:

The same procedure as above was repeated for unsymmetrical PBI (A) (0.1 g, 0.124 mmol) but dibromo hexane (0.0095 ml, 0.062 mmol) was used for the spacer segment. Yield: 30 mg (35 %); m.p. 282°C; ^{1}H NMR ($CDCl_3$): d= 8.7–8.9 (m, 16H; perylene), 7.23–6.8 (dd, 6H; ArH - PDP), 4.15 (t, 4H; N-CH_2), 2.48 (t, 4H; PDP Ar-CH_2), 1.9 – 0.87 (m, 88H; aliphatic CH_2); ^{13}C NMR: 164.70, 163.42, 152.95, 151.46, 150.50, 146.75, 142.93, 142.13, 135.08, 132.04, 131.16, 129.96, 126.78, 123.86, 123.39, 122.00, 120.38, 108.50, 73.60, 69.24, 31.92, 31.13, 30.33, 29.37, 26.09, 22.69, 14.11; FTIR: (υ) 2962 ($CH_{stretch}$), 2923, 2853, 1702 (C=O_{imide}), 1663, 1593, 1503, 1465, 1429, 1359, 1337, 1261, 1198,1157 (C-O_{ether}), 1097, 1025, 970, 804, 751 cm^{-1}; MALDI-TOF (Dihydroxy benzene matrix): m/z calcd for $C_{112}H_{130}N_4O_{10}$: 1692.91; found: 1713.81 [M^+ Na]; Elemental analysis calcd (%): C 79.49, H 7.74, N 3.31; found: C 79.62, H 7.66, N 3.34.

Synthesis of **PBI–T7**:

The same procedure as above for unsymmetrical PBI (A) (0.1 g, 0.124 mmol) was repeated but dibromoheptane (0.0106 ml, 0.0624 mmol) was used for the spacer segment. Yield: 30 mg (35 %); m.p. 171°C; ^{1}H NMR ($CDCl_3$): d= 8.7–8.9 (m, 16H; perylene), 7.23– 6.9 (dd, 6H; ArH - PDP), 4.13 (t, 4H; N-CH_2), 2.48 (t, 4H; PDP Ar-CH_2), 1.9-0.87 (m, 90H; aliphatic CH_2); ^{13}C NMR: 164.70, 163.42, 152.95, 151.46, 150.50, 146.75, 142.93, 142.13, 135.08, 132.04, 131.16, 129.96, 126.78, 123.86, 123.39, 122.00, 120.38, 108.50, 73.60, 69.24, 31.92, 31.13, 30.33, 29.37, 26.09, 22.69, 14.11; FTIR: (υ) 2962 ($CH_{stretch}$), 2923, 2853, 1702 ($C=O_{imide}$)), 1663, 1593, 1503, 1465, 1429, 1359, 1337, 1261, 1157 ($C-O_{ether}$), 1198, 1097, 1025, 970, 804, 751 cm^{-1}; MALDI-TOF (Dihydroxy benzene matrix): m/z calcd for $C_{113}H_{132}N_4O_{10}$: 1706.91; found: 1729.9 [M^+Na]; Elemental analysis calcd (%):C 79.54, H 7.80, N 3.28; found: C 79.99, H 8.56, N 3.74.

Synthesis of **PBI–T8**:

The same procedure as above was repeated for unsymmetrical PBI (A) (0.1g, 0.124 mmol) but dibromo octane (0.0114 ml, 0.0624 mmol) was used for the spacer segment. Yield: 30 mg (35 %); m.p. 202°C; ^{1}H NMR ($CDCl_3$): d= 8.7–8.9 (m, 16H; perylene), 7.23– 6.9 (dd, 6H; ArH - PDP), 4.15 (t, 4H; N-CH_2), 2.48 (t, 4H; PDP Ar-CH_2), 1.9-0.87 (m, 92H; aliphatic CH_2); ^{13}C NMR: 164.70, 163.42, 152.95, 151.46, 150.50, 146.75, 142.93, 142.13, 135.08, 132.04, 131.16, 129.96, 126.78, 123.86, 123.39, 122.00, 120.38, 108.50, 73.60, 69.24, 31.92, 31.13, 30.33, 29.37, 26.09, 22.69, 14.11; FTIR: (υ) 2962 ($CH_{stretch}$), 2923, 2853, 1730, 1702 ($C=O_{imide}$)), 1663, 1593, 1503, 1465, 1429, 1359, 1337, 1261, 1198,1157 ($C-O_{ether}$), 1097, 1025, 970, 804, 751 cm^{-1}; MALDI-TOF (Dihydroxy benzene matrix): m/z calcd for $C_{114}H_{134}N_4O_{10}$: 1720.91; found:1744.01 [M^+ Na]; Elemental analysis calcd (%): C 79.59, H 7.85, N 3.26; found: C 79.12, H 7.61, N 3.45.

Synthesis of **PBI–T9**:

The same procedure as above was repeated for unsymmetrical PBI (A) (0.1g, 0.124 mmol) but dibromononane (0.0126ml, 0.0624 mmol) was used for the spacer segment. Yield: 32 mg (36 %); m.p. 203°C; ^{1}H NMR ($CDCl_3$): d= 8.7–8.9 (m, 16H; perylene), 7.23–6.9 (dd, 6H; ArH - PDP), 4.15 (t, 4H; N-CH_2), 2.48 (t, 4H; PDP Ar-CH_2), 1.9 -0.87 (m, 98H; aliphatic CH_2); ^{13}C NMR: 164.70, 163.42, 152.95, 151.46, 150.50, 146.75, 142.93, 142.13, 135.08, 132.04, 131.16, 129.96, 126.78, 123.86, 123.39, 122.00, 120.38, 108.50, 73.60, 69.24, 31.92, 31.13, 30.33, 29.37, 26.09, 22.69, 14.11; FTIR: (υ) 2962 ($CH_{stretch}$), 2923, 2853, 1702 ($C=O_{imide}$), 1663, 1593, 1503, 1465, 1429, 1359, 1337, 1261, 1198,1157 ($C-O_{ether}$), 1097, 1025, 970, 804, 751 cm^{-1}; MALDI-TOF (Dihydroxy benzene matrix): m/z calcd for

$C_{115}H_{136}N_4O_{10}$: 1734.91; found: 1757.98 [M^+ Na]; Elemental analysis calcd (%): C 79.64, H 7.90, N 3.23; found: C 78.52, H 7.66, N 3.26

Synthesis of **PBI–T10**:

The same procedure as above was repeated for unsymmetrical PBI (A) (0.1g, 0.124 mmol) but dibromodecane (0.013 ml, 0.0624 mmol) was used for the spacer segment. Yield: 30 mg (35 %); m.p. 218°C; ^{1}H NMR ($CDCl_3$): d= 8.7–8.9 (m, 16H; perylene), 7.23–6.9 (dd, 6H; ArH - PDP), 4.13 (t, 4H; N-CH_2), 2.48 (t, 4H; PDP Ar-CH_2), 1.9 -0.87 (m, 98H; aliphatic CH_2); ^{13}C NMR: 164.70, 163.42, 152.95, 151.46, 150.50, 146.75, 142.93, 142.13, 135.08, 132.04, 131.16, 129.96, 126.78, 123.86, 123.39, 122.00, 120.38, 108.50, 73.60, 69.24, 31.92, 31.13, 30.33, 29.37, 26.09, 22.69, 14.11; FTIR: (υ) 2962 ($CH_{stretch}$), 2923, 2853, 1702 ($C=O_{imide}$), 1663, 1593, 1503, 1465, 1429, 1359, 1337, 1261, 1198, 1157 ($C\text{-}O_{ether}$), 1025, 970, 804, 751 cm^{-1}; MALDI-TOF (Dihydroxy benzene matrix): m/z calcd for $C_{116}H_{138}N_4O_{10}$: 1748.91; found: 1771.80 [M^+ Na]; Elemental analysis calcd (%): C 79.69, H 7.96 , N 3.2 found: C 80.12 H 7.66, N 3.64.

Synthesis of **PBI–T11**:

The same procedure as above was repeated for unsymmetrical PBI (A) (0.1g, 0.124 mmol) but dibromoundecane(0.0146 ml, 0.0624 mmol) was used for the spacer segment. Yield: 30 mg (35 %); m.p. 216°C; ^{1}H NMR ($CDCl_3$): d= 8.7–8.9 (m, 16H; perylene), 7.23–6.9 (t, 6H; ArH - PDP), 4.13 (t, 4H; N-CH_2), 2.48 (t, 4H; PDP Ar-CH_2), 1.9-0.87 (m, 100 H; aliphatic CH_2); ^{13}C NMR: 164.70, 163.42, 152.95, 151.46, 150.50, 146.75, 142.93, 142.13, 135.08, 132.04, 131.16, 129.96, 126.78, 123.86, 123.39, 122.00, 120.38, 108.50, 73.60, 69.24, 31.92, 31.13, 30.33, 29.37, 26.09, 22.69, 14.11; FTIR: (υ) 2962 ($CH_{stretch}$), 2923, 2853, 1702 ($C=O_{imide}$), 1663, 1593, 1503, 1465, 1429, 1359, 1337, 1261, 1198,1157 ($C\text{-}O_{ether}$),1097, 1025, 970, 804, 751 cm^{-1}; MALDI-TOF (Dihydroxy benzene matrix): m/z calcd for $C_{117}H_{140}N_4O_{10}$: 1762.91; found: 1786.91 [M^+ Na]; elemental analysis calcd (%): C 79.74, H 8.01, N 3.18; found: C 79.12, H 8.66, N 3.64.

Synthesis of **PBI–T12**:

The same procedure as above was repeated for unsymmetrical PBI (A) (0.1g, 0.124 mmol) but dibromododecane (0.023 mg, 0.0624 mmol) was used for the spacer segment. Yield: 40 mg (39 %); m.p. 202°C; ^{1}H NMR ($CDCl_3$): d= 8.7–8.9 (m, 16H; perylene), 7.23–6.8 (m, 6H; ArH - PDP), 4.13 (t, 4H; N-CH_2), 2.48 (t, 4H; PDP Ar-CH_2), 1.9-0.87 (m, 102H; aliphatic CH_2); ^{13}C NMR: 164.70, 163.42, 152.95, 151.46, 150.50, 146.75, 142.93, 142.13, 135.08, 132.04, 131.16, 129.96, 126.78, 123.86, 123.39, 122.00, 120.38, 108.50, 73.60, 69.24, 31.92,

31.13, 30.33, 29.37, 26.09, 22.69, 14.11; FTIR: (υ) 2962 ($CH_{stretch}$), 2923, 2853, 1702 ($C=O_{imide}$)), 1663, 1593, 1503, 1465, 1429, 1359, 1337, 1261, 1198,1157 ($C\text{-}O_{ether}$), 1097, 1025, 970, 804, 751 cm^{-1}; MALDI-TOF (Dihydroxy benzene matrix): m/z calcd for $C_{118}H_{142}N_4O_{10}$: 1776.91; found: 1800.01 [M^+ Na], 1816.38 [M^+ K]; elemental analysis calcd (%): C 79.78, H 8.06, N 3.15; found: C 80.14, H 8.26, N 3.29.

3.3 Results and Discussion

The synthetic scheme of the pentadecyl phenol functionalized perylenebisimide twin molecules is given in scheme-1. In short, symmetric ethyl hexyl functionalized perylenebisimide was ring opened followed by coupling with 4-amino pentadecyl phenol to obtain the unsymmetric perylenebisimide building block. This was dimerized by coupling with α, ω dibromo alkanes of varying alkyl chain length in dry DMF in presence of K_2CO_3 to obtain the twin series PBI-Tn (n = 1, 12). The twin molecules were purified by repeated column chromatography and their purity was confirmed by elemental analysis along with single peak in Gel Permeation Chromatography (GPC). They were structurally characterized using proton NMR spectroscopy and mass analysis was done using matrix-assisted laser desorption ionization–time of flight (MALDI-TOF) spectroscopy.

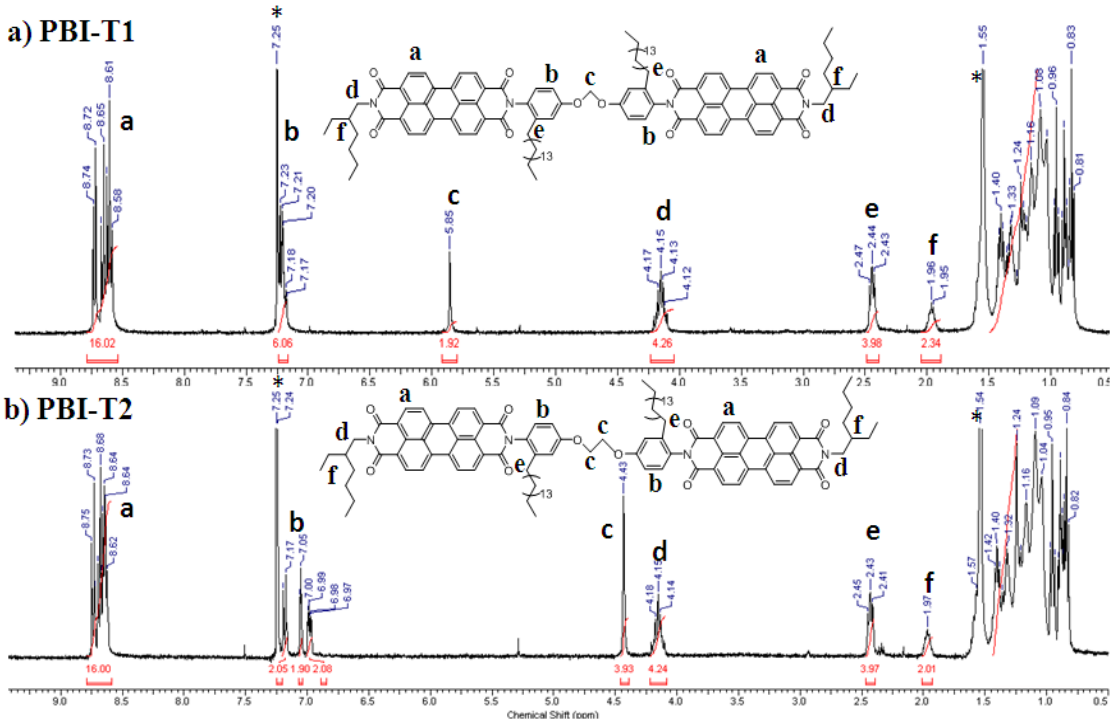

Figure 1. Labeled ^1H NMR spectra of a) **PBI-T1** and b) **PBI-T2**

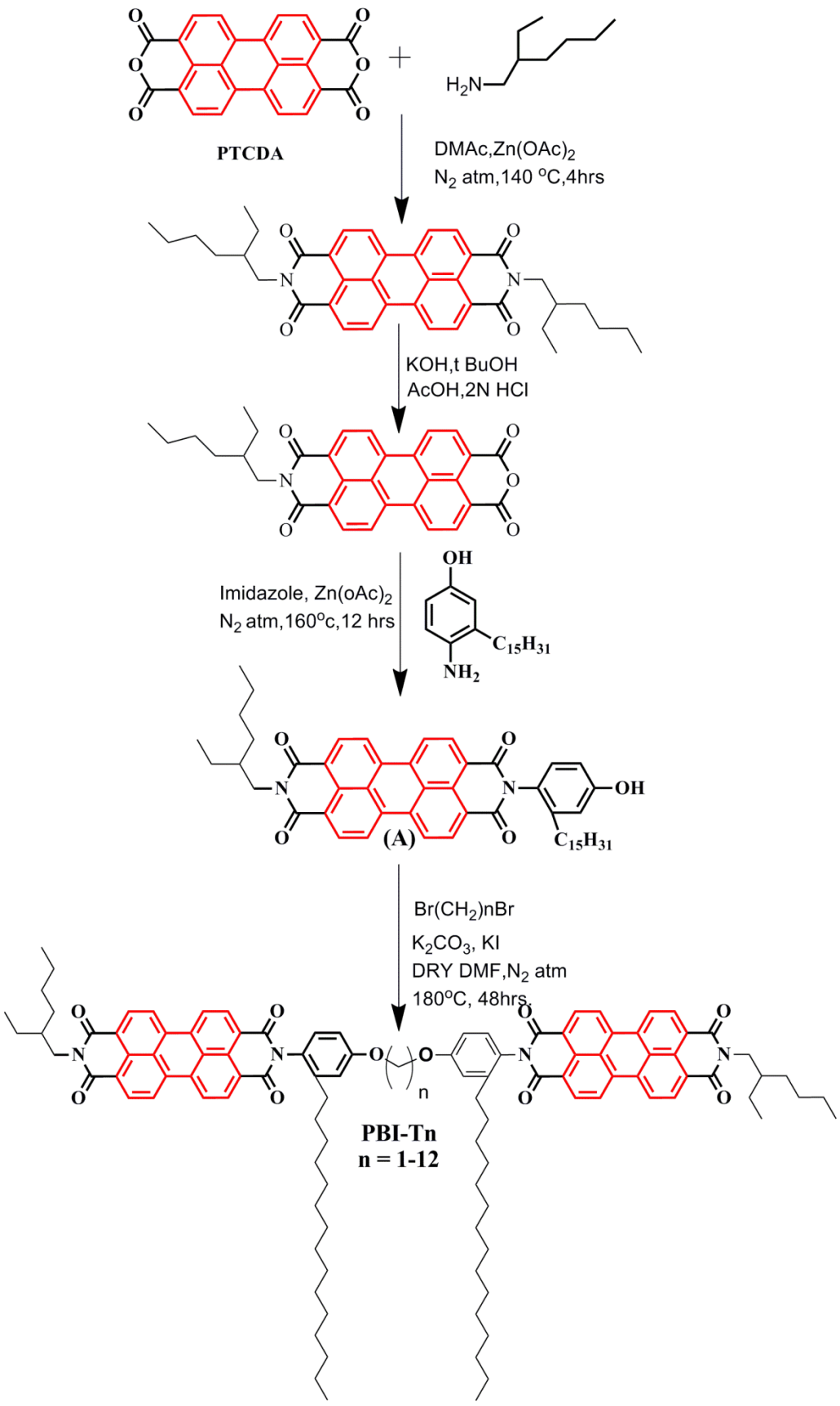
PTCDA
DMAc,Zn(OAc)2
N2 atm,140 °C,4hrs
KOH,t BuOH
AcOH,2N HCl
Imidazole, Zn(oAc)2
N2 atm,160°c,12 hrs
(A)
Br(CH2)nBr
K2CO3, KI
DRY DMF,N2 atm
180°C, 48hrs
PBI-Tn
n = 1-12

Scheme 1:Synthesis and chemical structures of **PBI-Tn** molecules

The ^{1}H NMR Spectra of the **PBI-T1** and **PBI-T2** are given in figure 1. The constraint introduced by the shortest spacer segment of n =1 was evident in **PBI-T1** with slightlydifferent proton signals for the cental methylene spacer segment (labeled 'c') as well as the aromatic protons of the pentadecyl phenol unit (labeled 'b') linked to the imide position of perylenebisimide. The constraint introduced by the short central spacer segment resulted in the perylene core within each twin molecule to be at right angles to each other. The proton splitting pattern for the rest of the **PBI-Tn** twin molecules were similar to that of **PBI-T2**. The ^{1}H NMR spectrum of **PBI-T3** to **PBI-T12** is given in figure 3 and figure 4 respectively.

Molecular modeling using Density Functional Theory (DFT) was carried out to understand the constraints in the central alkyl chain packing in the shorter spacer twin molecules. Figure 2 compares the energy minimized structures of the PBI-T1 and PBI-T2 obtained using DFT. The large number of atoms in the twin molecules made it difficult to carry out the energy minimization for systems with central spacer length larger than 2 carbon atoms. The energy minimized structures revealed that the phenyl ring was perpendicular to the perylene plane.

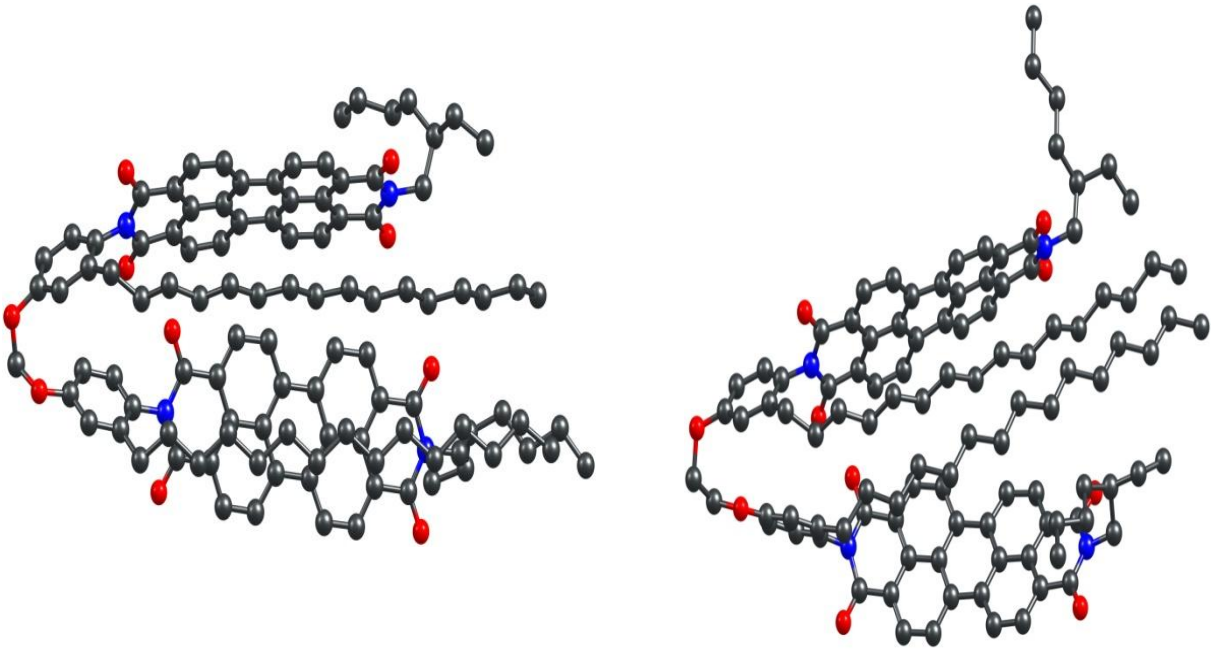

a) PBI-T1 **b) PBI-T2**

Figure 2: Energy minimized structures (using density functional theory) of **a) PBI-T1, b) PBI-T2.**

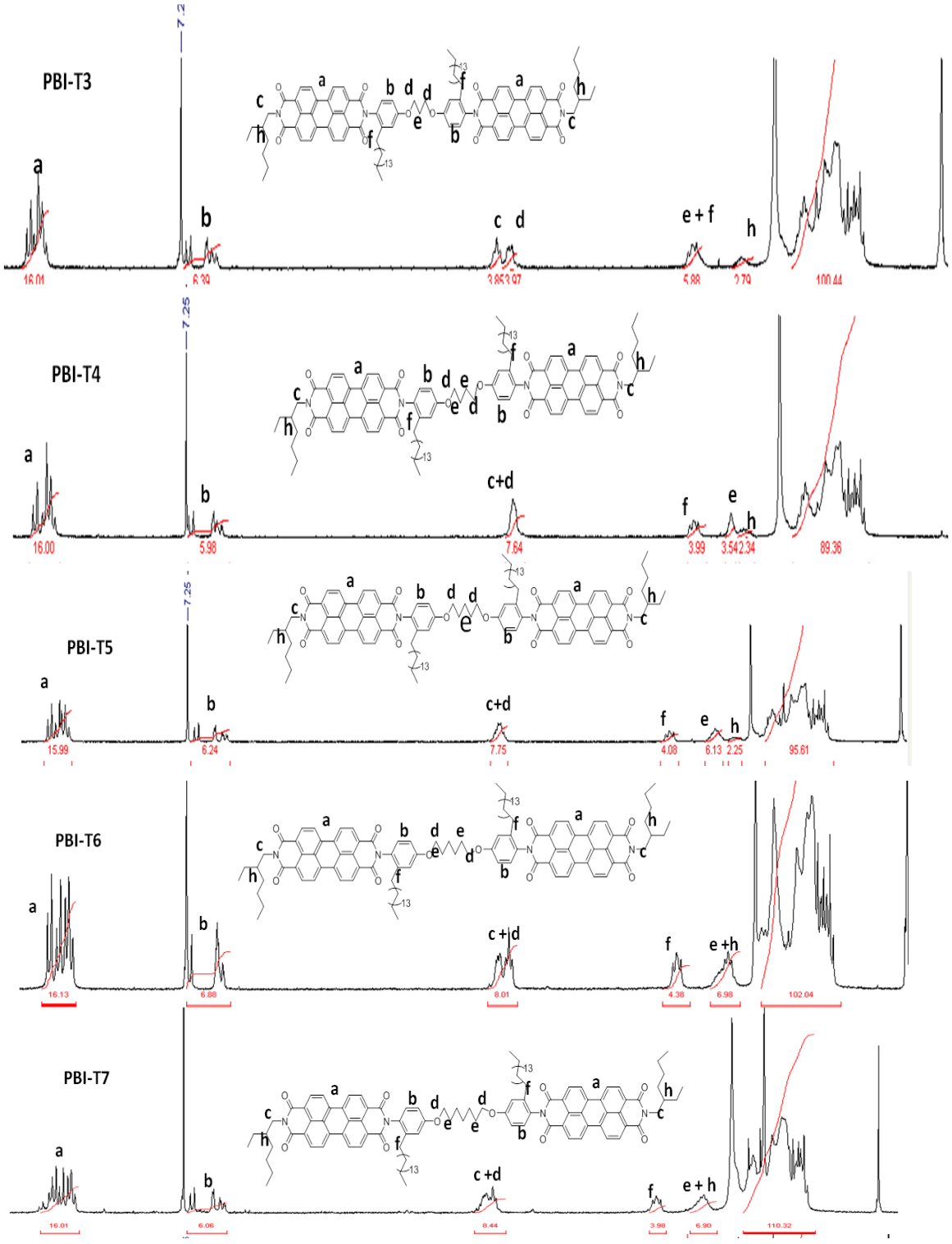

Figure 2: ^{1}HNMR stack plot of **PBI-T3** to **PBI-T7** in $CDCl_3$.

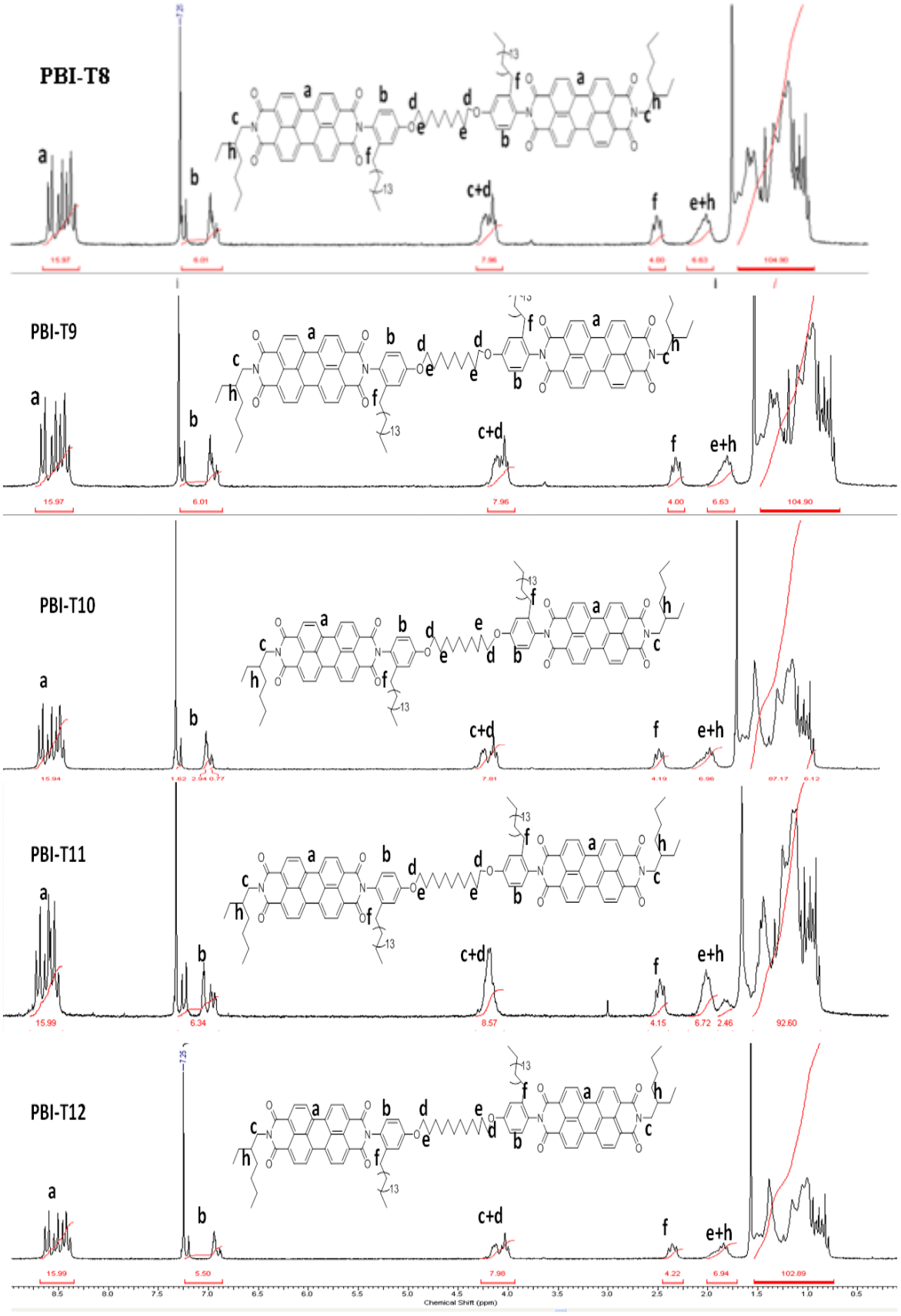
PBI-T8
PBI-T9
PBI-T10
PBI-T11
PBI-T12
a
b
c+d
e+h
f
Chemical Shift (ppm)

Figure 4: ^{1}HNMR stack plot of **PBI-T9** to **PBI-T12** in $CDCl_3$.

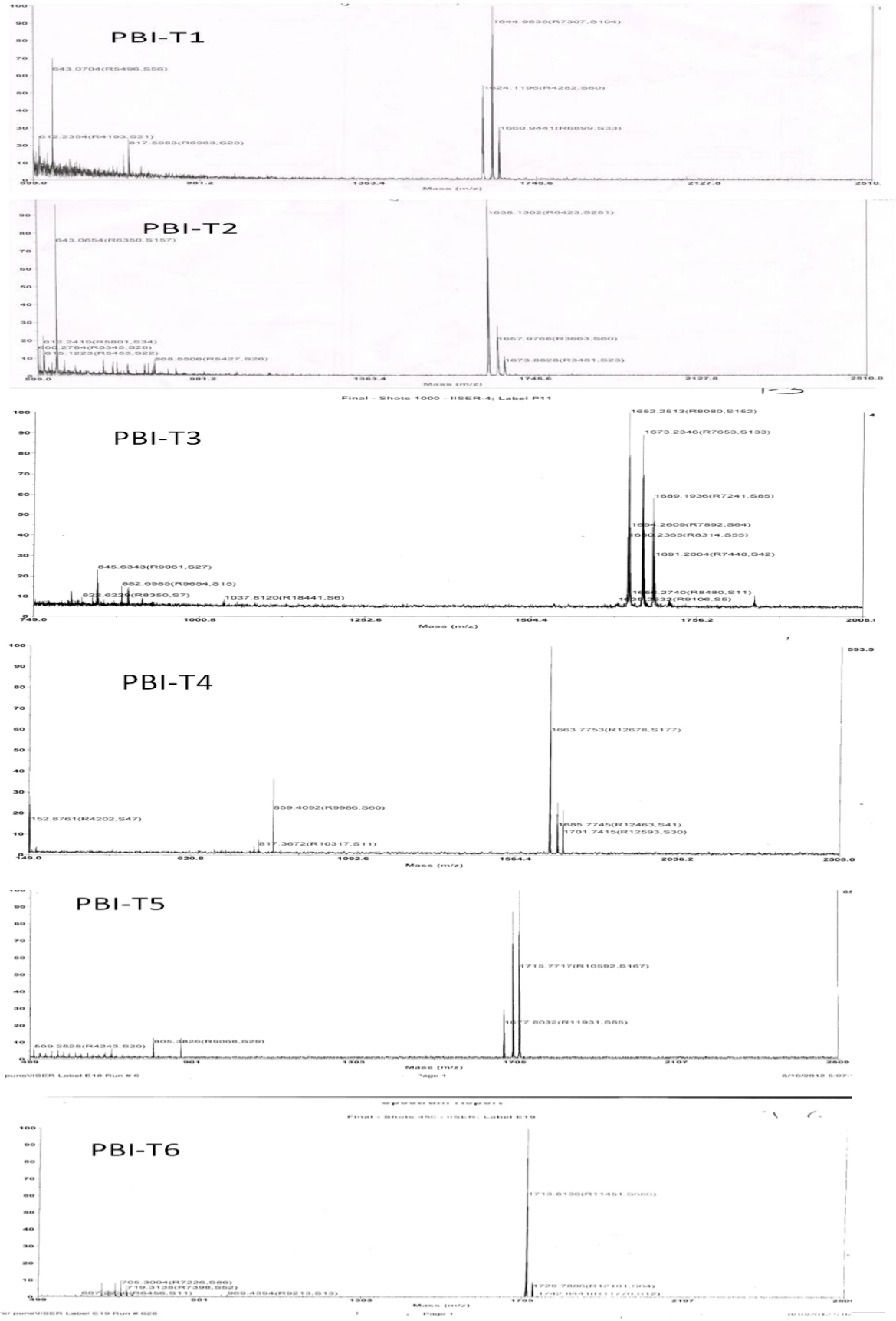

Figure 5 : Maldi-TOF spectra of PBI-Tn molecules in DHB matrix

.

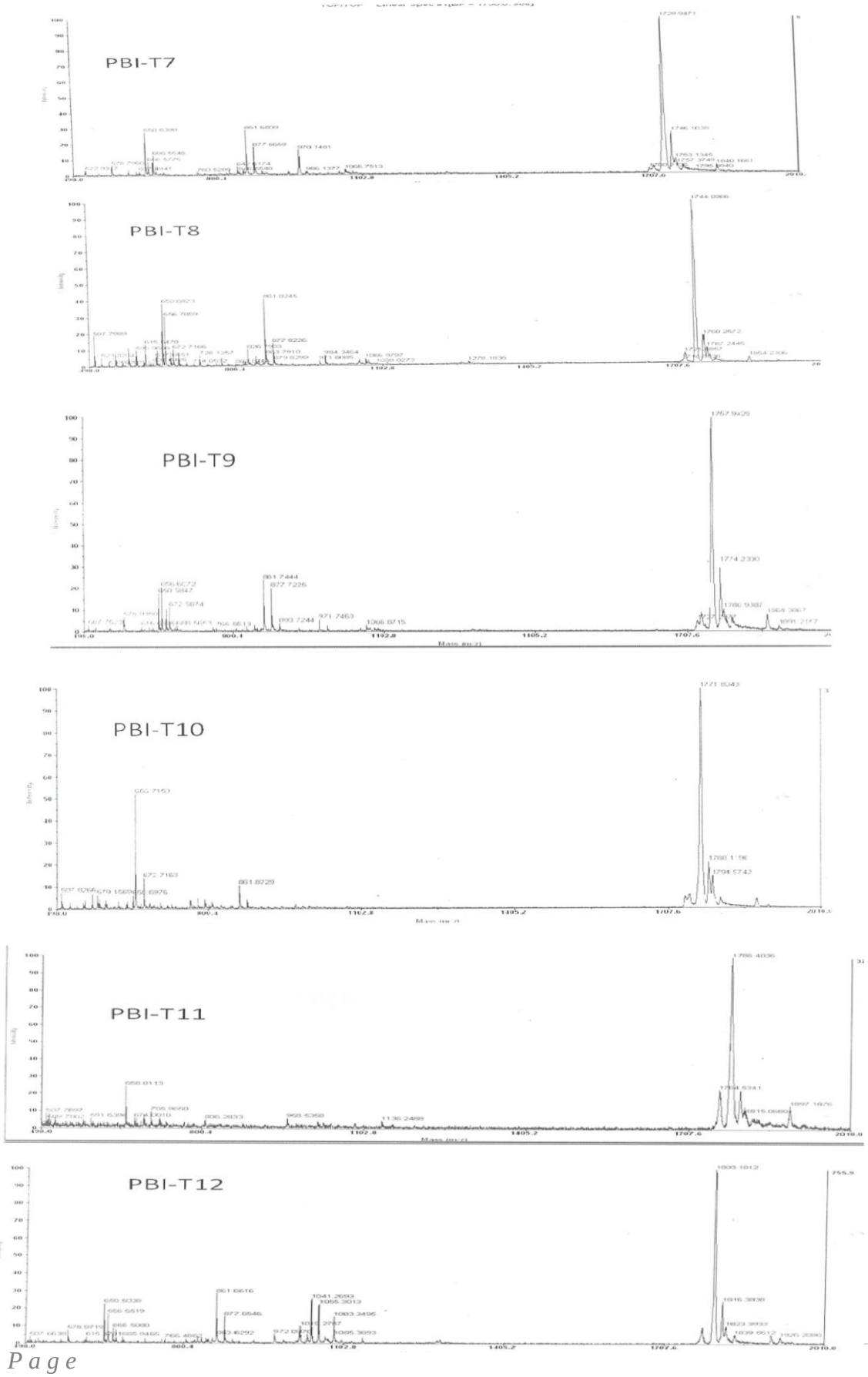

Figure 6: Maldi- TOF spectra of **PBI-Tn** molecules in DHB matrix.

3.3.1 Liquid Crystalline characteristics of PBI-Tn

Thermogravimetric analysis conducted at a heating rate of 10 °C /min from 40-800 °C under nitrogen atmosphere showed that the twin molecules were thermally stable until 370 °C. The TGA curves are given in figure 7 and the 10 wt % decomposition temperature is included in table-1.

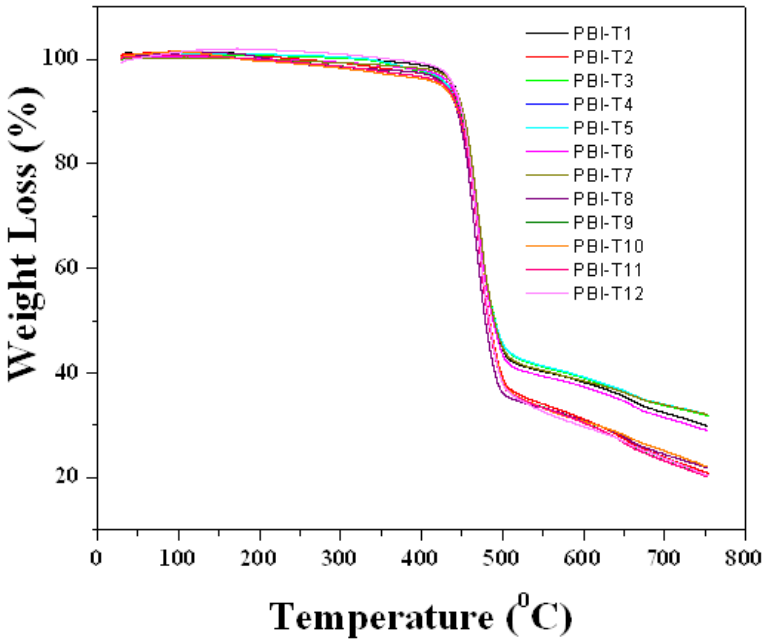

Figure 7: Thermogravimetric analysis (TGA) of **PBI-Tn** molecules under N_2 atmosphere.

After the TGA analysis the DSC thermograms of the twin molecules were collected at 10 °C /min heating rate. The DSC thermograms of the second heating cycle and second cooling cycles (Figure 8) were compiled for the 12 molecules .Figure 9 shows the plot of the clearing transition Tm (from the second heating cycle) as well as the corresponding transition enthalpies ΔHm as a function of the number of carbon atoms in the middle alkyl spacer length. An odd-even oscillation could be observed in both these values, with the even members exhibiting higher values compared to the odd counterparts. This clearly reflected better packing in the even spacer twins as compared with the odd ones.[18,22] The odd even oscillation was quite sharp for the middle members with n = 4 to 7 while it tapered off beyond n = 8. After n = 8 a predominant spacer effect was not observed for the enthalpy also.

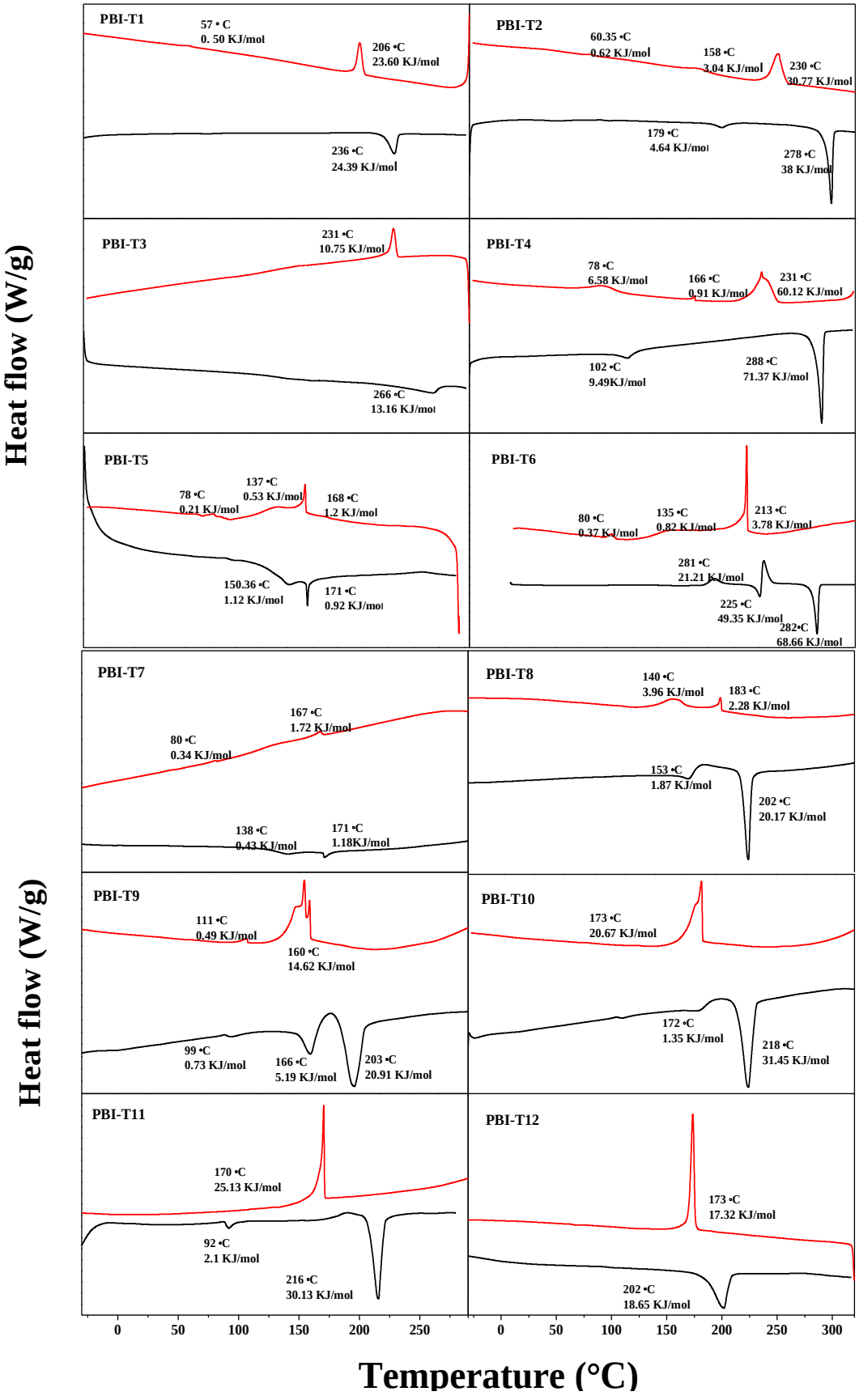
PBI-T1
57 °C
0. 50 KJ/mol
206 °C
23.60 KJ/mol
236 °C
24.39 KJ/mol
PBI-T2
60.35 °C
0.62 KJ/mol
158 °C
3.04 KJ/mol
230 °C
30.77 KJ/mol
179 °C
4.64 KJ/mol
278 °C
38 KJ/mol
PBI-T3
231 °C
10.75 KJ/mol
266 °C
13.16 KJ/mol
PBI-T4
78 °C
6.58 KJ/mol
166 °C
0.91 KJ/mol
231 °C
60.12 KJ/mol
102 °C
9.49KJ/mol
288 °C
71.37 KJ/mol
PBI-T5
78 °C
0.21 KJ/mol
137 °C
0.53 KJ/mol
168 °C
1.2 KJ/mol
150.36 °C
1.12 KJ/mol
171 °C
0.92 KJ/mol
PBI-T6
80 °C
0.37 KJ/mol
135 °C
0.82 KJ/mol
213 °C
3.78 KJ/mol
281 °C
21.21 KJ/mol
225 °C
49.35 KJ/mol
282°C
68.66 KJ/mol
PBI-T7
80 °C
0.34 KJ/mol
167 °C
1.72 KJ/mol
138 °C
0.43 KJ/mol
171 °C
1.18KJ/mol
PBI-T8
140 °C
3.96 KJ/mol
183 °C
2.28 KJ/mol
153 °C
1.87 KJ/mol
202 °C
20.17 KJ/mol
PBI-T9
111 °C
0.49 KJ/mol
160 °C
14.62 KJ/mol
99 °C
0.73 KJ/mol
166 °C
5.19 KJ/mol
203 °C
20.91 KJ/mol
PBI-T10
173 °C
20.67 KJ/mol
172 °C
1.35 KJ/mol
218 °C
31.45 KJ/mol
PBI-T11
170 °C
25.13 KJ/mol
92 °C
2.1 KJ/mol
216 °C
30.13 KJ/mol
PBI-T12
173 °C
17.32 KJ/mol
202 °C
18.65 KJ/mol
Heat flow (W/g)
Heat flow (W/g)
0 50 100 150 200 250
0 50 100 150 200 250 300
Temperature (°C)

Figure 8: DSC thermograms of the **PBI-Tn** molecules in the a) second heating and b) cooling cycle at 10 ^{0}C /min.

Name	T_{cl}^{a} (^{0}C) (Lc/C-I)	ΔH_{cl}^{a} (KJ/mol)	T_{c}^{b} (^{0}C) I-Lc/C	ΔH_{c}^{b} (KJ/mol)	T_{c}^{b} (^{0}C) (Lc-C) /(C-C)	ΔH_{c}^{b} (KJ/mol)	T_{D}^{c} (^{0}C)
PBI-T1	236	24.39	210	23.6	64	0.81	379
PBI-T2	278	37.97	230	30.77	169	3.04	375
PBI-T3	266	13.16	231	10.75	144	1.78	375
PBI-T4	288	71.37	230	60.12	78	12.7	376
PBI-T5	171	0.92	168	1.2	132	0.53	379
PBI-T6	282	68.66	213	3.78	80	0.34	380
PBI-T7	171	1.18	167	1.22	80	0.25	380
PBI-T8	202	20.17	183	2.28	140	3.96	380
PBI-T9	203	20.91	160	14.62	111	0.49	376
PBI-T10	218	31.45	173	20.67	159	1.32	380
PBI-T11	216	30.13	170	25.13	65	1.54	380
PBI-T12	202	18.65	173	17.32			380

[a] clearing transition and corresponding enthalpy values during heating cycle, [b] phase transitions and corresponding enthalpy values during cooling cycles, [c] 10 % weight loss under N_2 atmosphere during TGA.

Table 1.Transition temperature and corresponding enthalpies of **PBI-Tn** molecules during the second heating and cooling cycles.

It is a well studied and understood concept that the even spacer can pack more efficiently compared to the odd one. The highly packed structure requires more energy for melting (endothermic) and similarly releases more energy (exothermic) while crystallizing as compared to the weakly packed molecules. This is reflected in the clearing transitions as well as enthalpy values. Although odd-even oscillation in transition temperature has been reported for a variety of mesogens like biphenyl, azobenzene, and oligophenylene vinylenes,[8,9] there has so far been no reports on similar observation in the perylenebisimide family. Since the perylenebisimides are a highly explored family of chromophores for potential optoelectronic

application, this information regarding the influence of spacer length on the packing could prove beneficial in designing systems with appropriate odd or even numbered spacers.

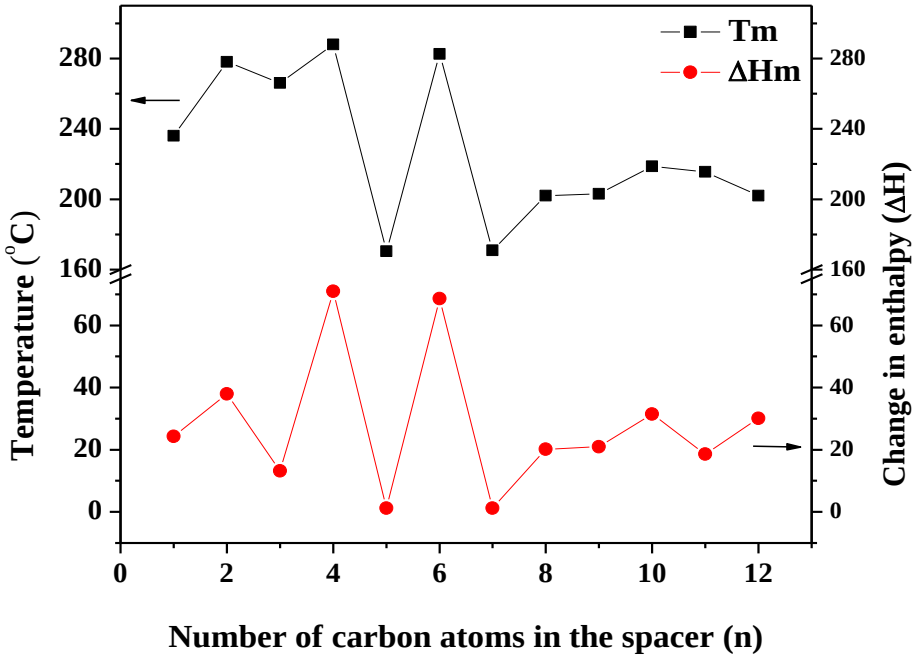

Figure 9: Odd–Even oscillations in the (a) clearing transition and the corresponding enthalpies of **PBI-Tn** molecules as a function of number of carbon atoms in the middle alkyl spacer unit (n).

Multiple transitions were observed in the heating as well as cooling cycles for most of the **PBI-Tn** molecules, which indicated the probable existence of mesogenic phases. The presence or absence of mesogenic phases could be further confirmed using the polarized Light Microscopic (PLM) analysis. **PBI-T1** exhibited a single melting transition at 236 °C (24.39 kJ/mol) in the heating cycle. In the second cooling cycle in DSC, birefringent patterns typical of smectic phases were observed for **PBI-T1** around 210 °C (figure 10), which remained stable until room temperature (25 °C). PBI-T2 exhibited two transitions during the heating cycles (278 °C, 23.21 kJ/mol; 179 °C, 4.64 kJ/mol). While cooling, a broad transition was observed around 230 °C (18.80 kJ/mol), followed by two weak transitions at 169 °C (1.86mol) and 65 °C (0.624 kJ/mol).

Figure 10 shows the PLM images collected for the samples at different temperature intervals. Corresponding to the transition observed the second cooling cycle in DSC, birefringent patterns typical of smetic phases were observed for **PBI-T1** around 210 °C, which remained

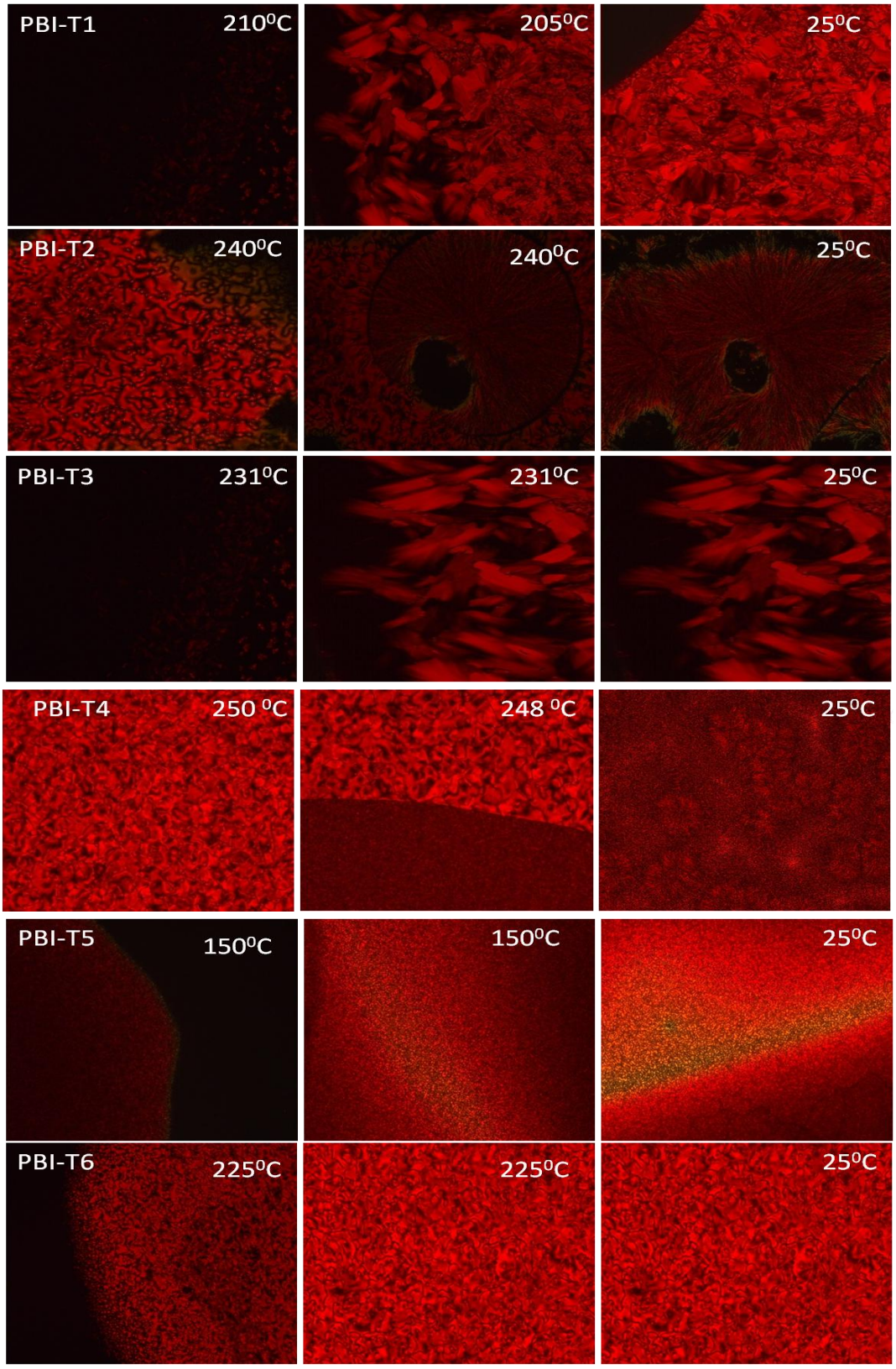

Figure 10: Polarized Light microscopic images of **PBI-Tn (n < 7)** molecules (under crossed polarizer) at room temperature with magnification of 1.5x2.

stable until room temperature (25 °C). PBI-T2 exhibited two transitions during the heating cycles (278 °C, 23.21 kJ/mol; 179 °C, 4.64 kJ/mol). While cooling, a broad transition was observed around 230 °C (18.80 kJ/mol), followed by two weak transitions at 169 °C (1.86 kJ/mol) and 65 °C (0.624 kJ/mol). During the observation under the PLM, thread-like nematic textures were observed at 240 °C, which crystallized almost immediately. Figure 10 shows the images of the transient nematic phase as well as the crystallization occurring at the same temperature. No further visible changes were observed under the PLM till 25 °C, although DSC recorded two more weak transitions. **PBI-T3** exhibited clearing at 266 °C upon heating with an enthalpy of 13.16 kJ/mol. Upon cooling, transition was observed around 230 °C (10.75 kJ/mol) in the DSC thermogram, which matched with the observation of birefringent pattern under the PLM. The birefringent patterns of **PBI-T1** and **PBI-T3** were somewhat similar as can be observed from figure 10 and was retained until room temperature as was the case with **PBI-T1**. The next member in the series – **PBI-T4**, exhibited a sharp melting at 288 °C with an enthalpy of 71.37 kJ/mol. The first transition in the cooling cycle around 250 °C was rather broad (250 – 200 °C) with a sharp shoulder at 230 °C. The enthalpy of this broad transition was 60.12 kJ/mol. The PLM showed emergence of thread-like birefringent patterns at 250 °C upon cooling, but almost immediately ~ 248 °C, crystallization also occurred. Although transitions were observed in the DSC thermogram at 166 °C and 78 °C, no visible changes were observed under the PLM until room temperature (25 °C). Thus, **PBI-T4** behaved similar to **PBI-T2** exhibiting a very short window for the nematic liquid crystalline phase before crystallizing. The other higher spacer PBI-Tn molecules also exhibited a similar tendency of high temperature nematic phase. Unlike the **PBI-T2** and **PBI-T4**, crystallization was not observed during the cooling cycle under the PLM; the initially observed thread like features seemed to be retained until room temperature. However, WXRD studies clearly showed crystalline pattern for the annealed sample at room temperature.

The DSC thermogram also showed multiple transitions in the cooling cycle whose total enthalpy values did not match that of the clearing transition. For the molecules **PBI-T6**, **PBI-T8**, **PBI-T9** and **PBI-T10** cold crystallization peaks were observed during the cooling cycles, which accounted for the mismatch in enthalpy. The PLM images of the cold crystallization of PBI-T6 captured during the second heating cycle has given in figure 12. The nematic texture formed during the first cooling of **PBI-T6** remain unchanged upto room temperature which

upon heating get Crystallized at 180 ^{o}C. Upon further heating this crystalline phases got melted at 226 ^{o}C followed by the second cold crystallization at 231 ^{o}C. This crystallized phase finally got melted to isotropic phase at 285 ^{o}C (figure 12)

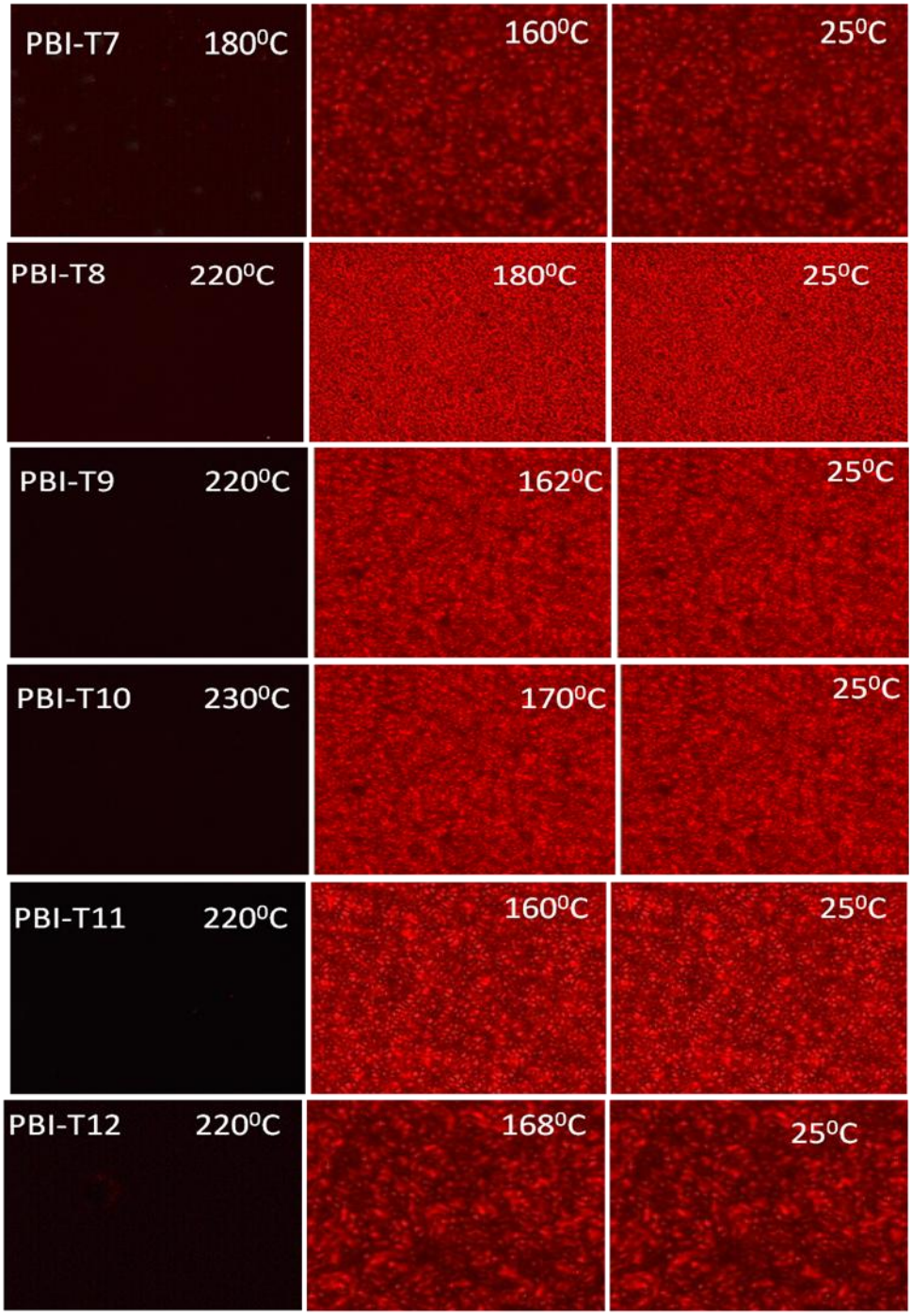

Figure 11: Polarized Light microscopic images of **PBI-Tn (n > 6)** molecules (under crossed polarizer) at room temperature with magnification of 1.5x2.

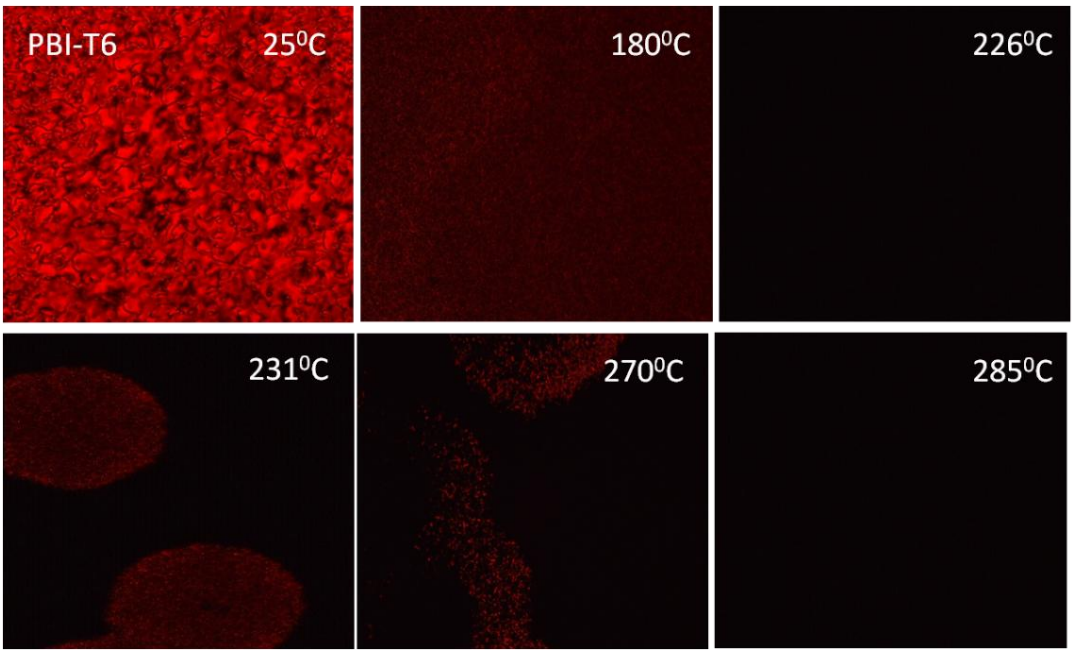

Figure 12: Polarized Light microscopic images of cold crystallization observed in **PBI-T6** during the second heating cycle.

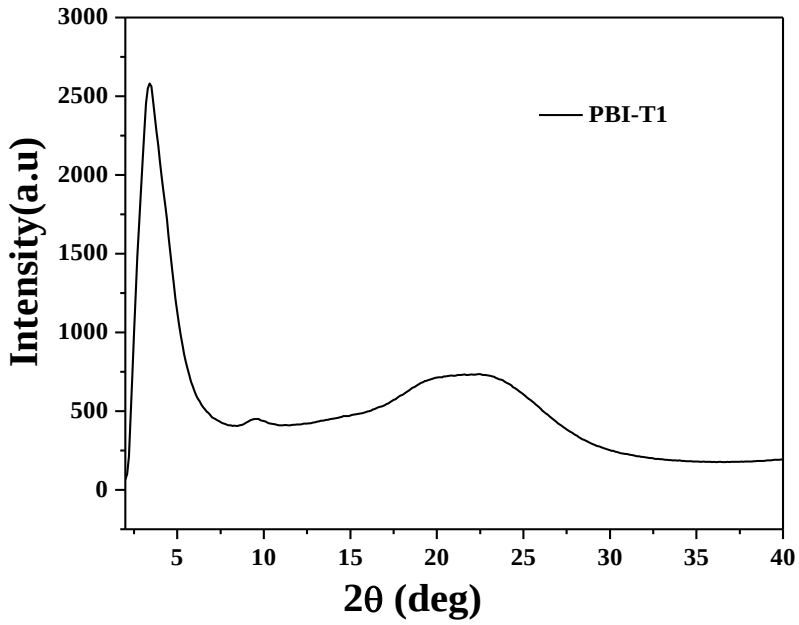

Figure 13: Room temperature XRD pattern of annealed **PBI-T1** recorded from 2θ = 2-40°.

Variable temperature WXRD data for the molecules **PBI-T1** to **PBI-T6** is given figure 14. Unfortunately the WXRD facility was sensitive only beyond 2θ> 3°, due to which the long period length of the molecules could not be obtained.

.

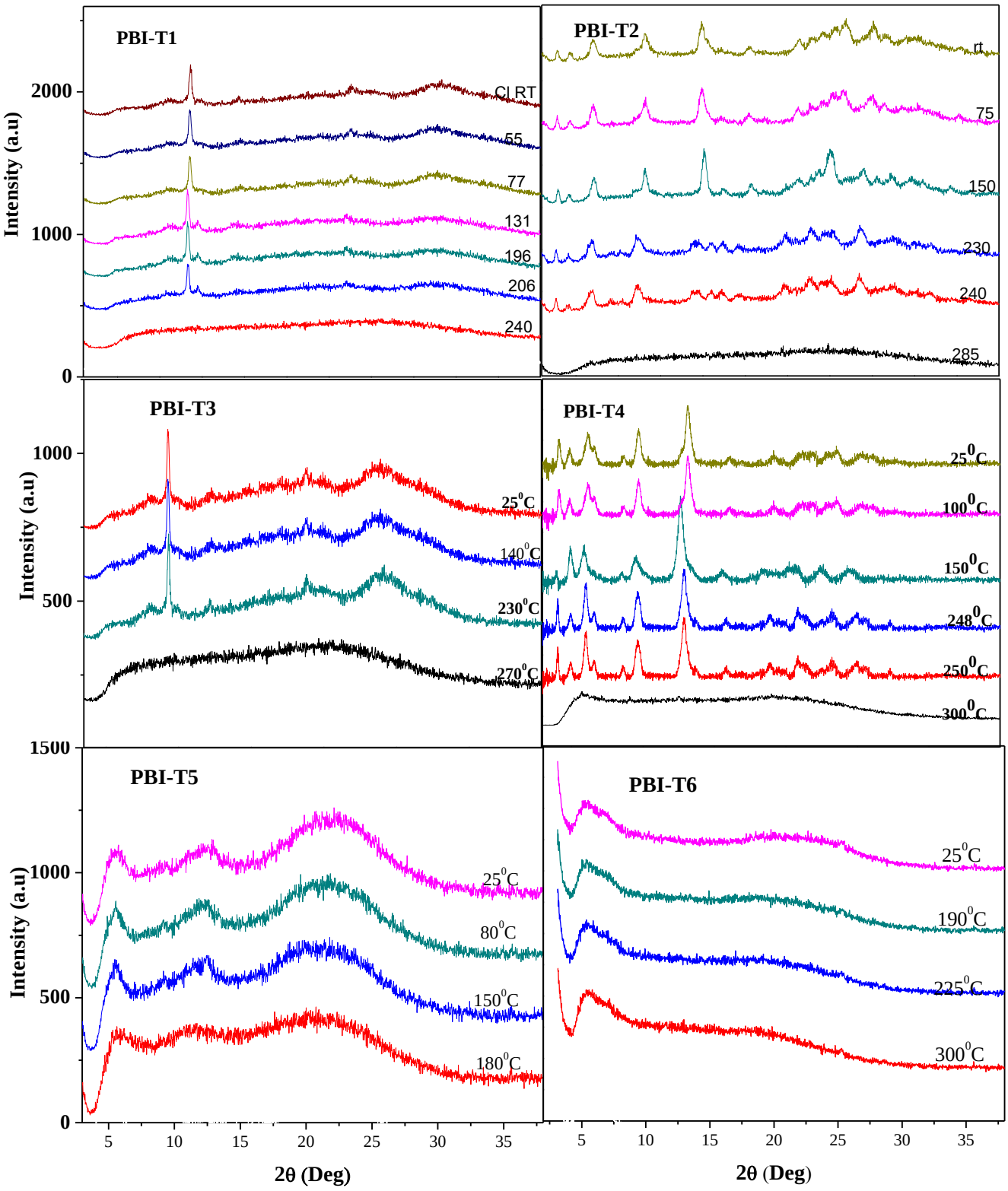

Figure 14.Variable temperature XRD patterns for **PBI-Tn** (n = 1-6).

However, the obtained variable temperature WXRD data collected from 2θ = 3-30° reflected the observation from PLM. For instance, the WXRD pattern for **PBI-T1** and **PBI-T3** were quite similar. The wide angle XRD data of annealed sample of PBI-T1 was collected at room temperature in a diffractometer (figure 13), where the data could be collected from 2θ = 3°. It clearly showed a peak at 2θ = 3.42 ° corresponding to a length of 13.21 Å, which exhibited a d spacing ratio of ~1:3 with the peak observed at 2θ = 9.57 ° (4.59 Å). Multiplicity of peaks in the low angle region along with a diffuse halo in the wide angle region is typical of smectic A mesophase. PBI-T3 had also shown similar LC textures and XRD pattern as that of **PBI-T1,** which indicated its tendency to form smectic LC phase. WXRD pattern for **PBI-T2** and **PBI-T4** exhibited sharp peaks characteristic of crystalline sample. The high temperature nematic phase was too short lived to be captured by the variable temperature WXRD measurement. The high temperature nematic phase observed in **PBI-T2** and **PBI-T4** was difficult to observe. **PBI-T3** had also shown similar LC textures and XRD pattern as that of **PBI-T1**, which indicated its tendency to form smectic LC phase. WXRD pattern for **PBI-T2** and **PBI-T4** phase was too short lived to be captured by the variable temperature WXRD measurement. The **PBI-T5** and PBI-**T6** showed characterstic nematic pattern in the XRD confirming the room temparaturenematic phases formed by this system.The higher spacered twin (n> 6), exhibited characteristic crystalline features as was confirmed by the presence of several sharp peaks in the XRD as given in figure 15.

Summing up, the LC phases exhibited by these **PBI-Tn** molecules, **PBI-T1** and **PBI-T3** exhibited smectic LC phases, while the rest of the molecules showed nematic characteristics. It is interesting to analyze the reason for only the shorter twins and that too only the odd ones exhibiting tendency for forming smectic LC phase. The monomeric building unit i.e the unsymmetrical perylenebisimide (**A**) substituted with ethyl hexyl at one end and pentadecyl phenol at the other termini had quite high melting transition at 320 °C and also did not exhibit thermotropic liquid crystalline behavior.[16] However, its powder XRD data clearly established its layered structure with Bragg reflections in the ratio 1: 1/2: 1/3.[21] Upon tethering two of these unsymmetrical perylenebisimides using the short connecting spacer segment –OCH_2O- as in **PBI-T1**, the melting transition was observed at much lower temperature (236 °C) and the molecule exhibited smectic LC phase which is characterized by its layered structure. **PBI-T3** with a –$O(CH_2)_3O$- spacer also showed similar tendencies for smectic liquid crystalline

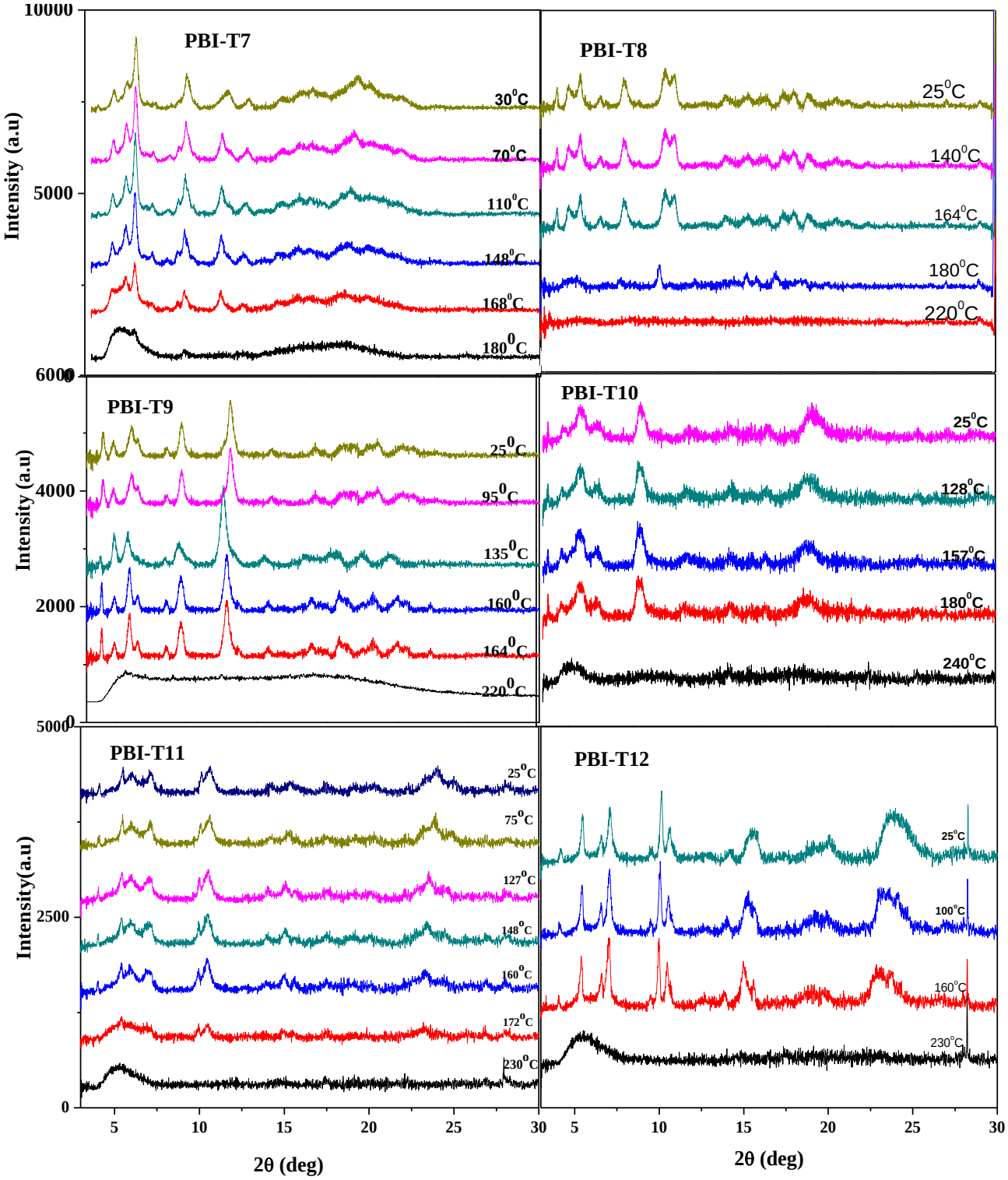
PBI-T7
30°C
70°C
110°C
148°C
168°C
180°C
PBI-T8
25°C
140°C
164°C
180°C
220°C
PBI-T9
25°C
95°C
135°C
160°C
164°C
220°C
PBI-T10
25°C
128°C
157°C
180°C
240°C
PBI-T11
25°C
75°C
127°C
148°C
160°C
172°C
230°C
PBI-T12
25°C
100°C
160°C
230°C
Intensity (a.u)
Intensity(a.u)
2θ (deg)
2θ (deg)

Figure 15: Variable temperature XRD patterns for **PBI-Tn** (n = 7-12).

phases which was retained till room temperature. However the **PBI-T2**, which was the shortest even spaced twin, had a higher melting temperature at 278 °C due to its collinear chromophore arrangement which resulted in better packing. The tendency to crystallize out was prominent among the even membered twins with the observation of high temperature nematic LC phase. The disappearance of the smectic LC phase and the appearance of nematic phase with increase in the length of the central alkyl spacer segment in twin molecules has been observed and well studied in literature. Elaborate studies conducted on dimeric liquid crystalline molecules has established that the smectic phases are observed when the length of the terminal alkyl spacer exceeds more than half the length of the central alkyl spacer length. Thus, as the central alkyl spacer length increases the general tendency observed is for the nematic phase to appear and the smectic phase to disappear. The smectic phases again reappear at much longer spacer length due to phase segregation of the aliphatic and aromatic moieties. In the **PBI-Tn** series though, the reappearance of the smectic liquid crystalline phase was not observed until n = 12.

The observation of higher intensity for the odd-even oscillation in the transition temperature as well as the corresponding enthalpies for the middle series of members from n = 4-7 also could be understood as an interplay of the smectic versus nematic LC phases observed. The nematic phase prefers a linear conformation, which is more easily attained by the even spacered twins compared to the odd counterparts, which are more bent. Therefore, the odd – even oscillation of the nematic to isotropic transition is expected to be quite large, especially in the lower homologues. From figure 9 it was quite obvious that this was so, especially for the spacers 2 to 7. However, the two lower odd twin molecules - **PBI-T1** and **PBI-T3** preferred to pack in a layered smectic phase. Therefore, the intensity of the odd-even oscillation in their transition temperature as well as transition enthalpy was not so pronounced compared to that of the **PBI-T2**, and **PBI-T4 - PBI-T6**, which all formed the nematic phases upon cooling from the isotropic state. Beyond n = 7, the considerable flexibility of the alkyl component increases the number of conformations possible, leading to a dampening of the difference between odd and even homologues.

3.3.2 Photophysical Properties

The absorption and emission characteristics of the twin molecules were explored in chloroform as well as methyl cyclohexane (MCH) as solvents. In chloroform, the twin molecules exhibited typical absorption features of isolated perylenebisimides with peaks in the range of 400 -530 nm. The emission spectra was a mirror image of the absorption with peaks at 534, 576, 626 nm. Figure 16 (top) shows the normalized absorption and emission spectra of PBI-T1 as a typical example. But in MCH, the absorption and emission exhibited features of aggregation.[17,18]

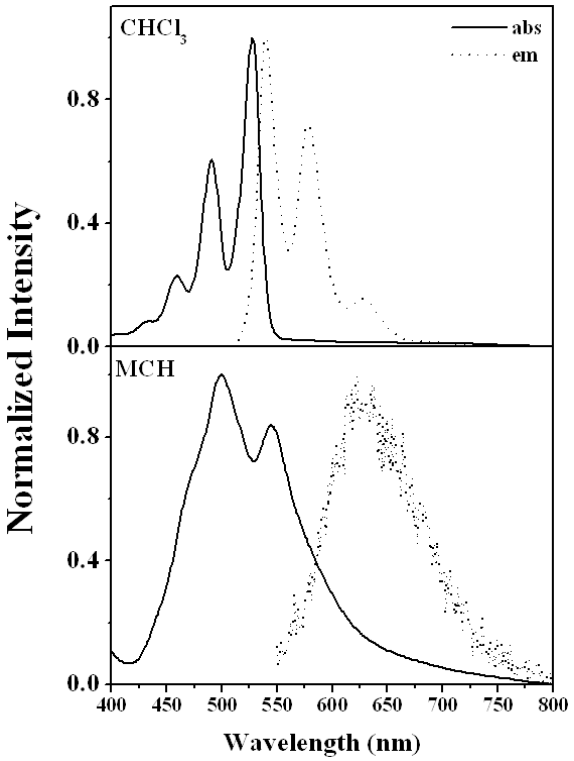

Figure 16: Normalized absorption and emission spectra of **PBI-T1** in chloroform ($CHCl_3$) and methylcyclohexane (MCH).

Figure 16 bottom shows the normalized absorption and emission spectra of PBI-T1 in MCH. From the figure it can be seen that the absorption spectra had lost much of its vibrational fine structure and was broad with hypsochromically shifted peak maxima (498 nm) and presence of an additional red shifted peak.The emission was highly quenched and also red shifted in comparison with that in chloroform. Figure 17 shows a stack plot of variable temperature absorption spectra for PBI-T2 in MCH upon heating from 20 to 100 °C. As temperature increased, the aggregated peak at 540 nm reduced in intensity, while the hypsochromically shifted peak maxima at 498 nm shifted to 513 nm. The existence of an isobestic point indicated the presence of only two species – the molecularly dissolved one and the

aggregated ones, being present in the solution. Even at the highest recorded temperature of 100 °C, the peak due to aggregation had not fully disappeared. Almost all the lower members of the series which were soluble in MCH (n < 7) exhibited similar behavior. The higher members of the twin series had very poor solubility in MCH.

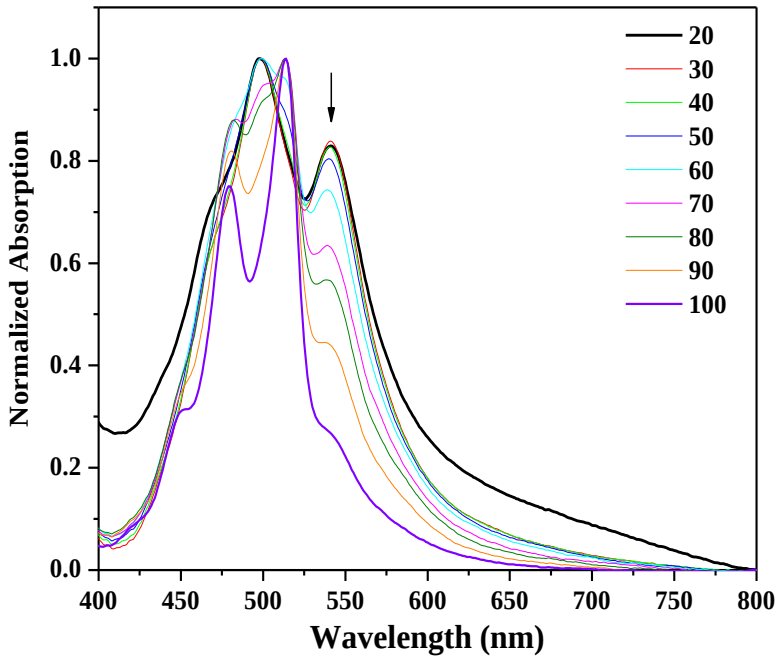

Figure 17: Normalized variable temperature absorption spectra of **PBI –T2** in methyl cyclohexane.

3.3.3 Conclusions

In summary, a series of twin liquid crystalline perylenebisimide molecules having the structure PBI-methylene spacer- PBI and having a pentadecyl phenol substitution at one of the imide positions were designed and synthesized. The central poly methylene spacer length was varied from n = 1 to 12. Except for the two odd lower members PBI-T1 and PBI-T3, all other samples exhibited nematic liquid crystalline phases. PBI-T1 and PBI-T3 exhibited smetic phase which was retained till room temperature upon cooling. PBI-T2 and PBI-T4 showed a higher temperature nematic LC phase which was short lived and crystallized out immediately while cooling, whereas PBI-T5 and PBI-T6 formed room temperature nematic phase. The higher spacered twins n > 7 also showed nematic LC phase. As expected, an odd-even oscillation was observed in the clearing transition temperature as well as the corresponding enthalpy values with the even membered molecules exhibiting higher values.

1.7. References:

1. C. T. Imrie and P. A. Henderson, *Chem.Soc.Rev*., **2007**,36, 2096.
2. J. W. Emsley, G. R. Luckhurst, G. N. Shilstone and I. Sage, *Mol. Cryst. Liq. Cryst*., **1984,** 102, 223.
3. G. R. Luckhurst ,*Liq. Cryst*., **2005**, 32, 1335.
4. S. Umadevi, B. K. Sadashiva, H. N. Shreenivasa Murthy,V. A. Raghunathan,*Soft Matter*, **2006**, 2, 2010
5. T. Kobayashi and T. Seki, *Langmuir*, **2003**, 19, 9297**.**
6. E. Białecka-Florja´ nczyk, I. ´Sledzi´ nska, E. G´orecka ,J. Przedmojski, *Liq. Cryst.,* **2008**, 35, 401.
7. S. Kurihara, T. Ikeda and S. Tazuke, *Macromolecules*, **1993**, 26, 1590.
8. M. Goel and M. Jayakannan,*J. Phys. Chem. B*, **2010**, 114, 12508.
9. Y. Dienes, M. Eggenstein, T. K´arp´ati, T. C. Sutherland, L. Nyul´aszi,T. Baumgartner, *Chem.Eur. J.*, **2008**, 14,
10. B. A. Jones, A. Facchetti, M. R. Wasielewski and T. J. Marks, *J.Am. Chem. Soc*., **2007**, 129, 15259
11. F. Wurthner,*Chem. Commun*., **2004**, 14, 1564.
12. A. Wicklein, A. Lang, M. Muth and M. Thelakkat, *J. Am .Chem. Soc*., **2009**, 131, 14442.
13. C. W. Struijk, A. B. Sieval, J. E. J. Dakhorst, M. van Dijk,P. Kimkes, R. B. M. Koehorst, H. Donker, T. J. Schaafsma,S. J. Picken, A. M. van de Craats, J. M. Warman, H. Zuilhof ,E. J. R. Sudh¨olter, *J. Am. Chem. Soc*., **2000**, 122, 11057.
14. Z. An, J. Yu, S. C. Jones, S. Barlow, S. Yoo, B. Domercq,P. Prins, L. D. A. Siebbeles, B. Kippelen and S. R. Marder, *Adv. Mater*., **2005**, 17, 2580
15. X. Lin, M. Hirono, T. Seki, H. Kurata, T. Karatsu, A. Kitamura, D. Kuzuhara, H. Yamada, T. Ohba, A. Saeki,S. Seki , S. Yagai, *Chem. Eur. J*., **2013**, 19, 6561.
16. a) Ditchfield, R.; Hehre, W. J.; Pople, J. A. *J. Chem. Phys.* 1971, *54*, 724. b) Hehre, W. J.; Ditchfield, R.; Pople, J. A. *J. Chem. Phys.* 1972, *56*, 2257. c) Hariharan, P. C.; Pople, J. A. *Theor. Chem. Acc.* 1973, *28*, 213. d) Francl, M. M.; Pietro, W. J.; Hehre, W. J.; Binkley, J. S.; De Frees, D. J.; Pople, J. A.; Gordon, M. S. *J. Chem. Phys.* 1982, *77*, 3654. e) Grimme, S.; Ehrlich, S.; Goerigk, L. *J. Comput. Chem.*, 2011, *32*, 1456.
17. Narayan, R.; Kumar, P.; Narayan, K. S.; Asha, S. K. *Adv. Funct. Mater*. **2013**, 23, 2033–2043.
18. M. Kasha, H. R. Rawls, M. A. El-Bayoumi, *Pure Appl. Chem.,* **1965,** *11*, 371.

19. G. A. Bhavsar, S. K. Asha, *Chem. Eur. J.* **2011,** *17*, 12646.

Chapter 4

Hydrogen Bond Assisted Nano Self Assembly of Unsymmetrical Perylenebisimides with Poly(4-vinyl pyridine) for Better Charge Transport

4.1Abstract:

The self assembly of unsymmetrical perylenebisimides (UPBIs) having pentadecyl phenol at one end and different alkyl groups like cyclo hexyl (UPBICH), octyl dodecyl (UPBIOD), hexyl heptyl (UPBIHH), dodecyl (UPBIDD) on the other termini were studied. All the UPBIs exhibited room temperature columnar liquid crystalline phases. UPBIOD organised in to columnar hexagonal phase, UPBICH formed columnar lamellar phase while both UPBIDD and UPBIHH exhibited columnar rectangular phase. The supramolecular comb copolymer of these UPBIs with P4VP homopolymers (P4VP-UPBI) were synthesised by dissolving 1:1 molar ratio of UPBI with P4VP in solvent followed by the removal of solvent. All the P4VP-UPBI comb copolymers showed lamellar morphology in TEM analysis. The SCLC mobility measurements of the P4VP–UPBI comb copolymers showed comparable mobility values with respect to the pristine UPBI molecules.

4.2. Introduction

In the last two chapters, the discussion was focussed mainly on the effect of spacer on the mesophase behaviour of perylenebisimide based small molecules. As discussed earlier perylenebisimides are one of the most widely studied n type semiconductors for optoelectronics applications owing to their unique combination of high electron mobility, large molar absorption coefficients, excellent self-assembling ability, versatile structural modification as well as good thermal and photochemical stabilities.[1-5] PBI based small molecules are highly crystalline in nature therefore one can expect good charge transport in these systems. However, processing of small molecules requires harsh conditions and it is difficult to form uniform thin films.[6] In this context polymer based perylenebisimides generated a lot of research interest since polymers could overcome these issues. One approach to this is blending of small molecule PBI with other polymers to prepare smooth films, but it has the inherent problem of macrophase separation.[7] Another option is covalently linking PBI in to a polymer backbone either in the main chain or as side groups of block copolymers. Although this approach may gain in terms of solution processability and microphase separation, it looses out in terms of the intrinsic crystallinity of the small molecule besides the low incorporation of PBI.[8] Thus there is a need for an alternative approach which can promise the crystallinity of PBI molecules along with processability and thin film formation.

Supramolecular comb copolymers are formed by the non covalent interactions such as hydrogen bonding, electrostatic interactions, metal-ion coordination, hydrophobic interactions etc. Several design principles have been developed to create different functional materials based on supramolecular polymeric architectures.[9] In this regard, a novel strategy for side-chain hydrogen bonded supramolecular polymers pioneered by Ikkala and ten Brinke *et al.* is very inspiring, where they studied the bulk state properties of comb-shaped supramolecules obtained by hydrogen bonding of short, flexible, non-mesogenic amphiphiles with poly (4-vinylpyridine) (P4VP). Motivated by this our group initiated a novel approach of incorporating an n-type organic semiconductor molecule, perylenebisimide into P4VP.[10-17] Supramolecular complexes of varying ratios of a 3-pentadecyl phenol based unsymmetrical perylenebisimide (**UPBIEH**) to (P4VP) polymer

via hydrogen bonding indicated that the polymeric complexes retained high crystallinity, which is very difficult to achieve in the case of polymer based covalent systems. TEM imaging also showed the presence of microphase separated lamellar structures. The space charge limited current (SCLC) measurements of these complexes were three orders of magnitude higher compared to pristine **UPBIEH** molecules.[18]

This concept was later extended to different systems like naphthalene bisimide (NBI), oligo(phenylenevinylene) (OPV) – perylenebisimide based donor acceptor systems, photo polymerisation of non covalently hydrogen bonded perylenebisimide etc.[19-21] The present study focusses on the effect of various terminal alkyl branching on the supramolecular self assembly of these comb copolymers. The unsymmetrical PBI was designed with different alkyl substitution 1) long chain dodecyl (**UPBIDD**) 2) symmetrically branched hexylheptyl (**UPBIHH**) 3) unsymmetrically branched octyl dodecyl (**UPBIOD**) 4) cyclo hexyl (**UPBICH**) (the structures are given in the scheme 1). The UPBIs were well characterised before complexing with the poly 4 vinyl pyridine. The supramolecular complex with P4VP were prepared in dry DMF and was confirmed with IR, NMR, XRD, TEM etc. The charge carrier mobilities of the comb polymer were studied using the electrode configuration of Al/PBI/Al. The main highlights of this work are given below

1) The effect of terminal alkyl chain substitution in the mesophase formation of Unsymmetrical Perylenebisimide (UPBI)
2) The effect of terminal alkyl chain substitution in the self assembly of supra molecular comb copolymer.

4.3. Experimental Section

4.3.1. Materials: Poly (4-vinylpyridine) (P4VP) (Mw =60,000) was purchased from Aldrich. It was dried in vacuum oven at 60 °C for 3 days prior to use. PTCDA, 3-amino pentadecyl phenol, cyclo hexane and amino dodecane were purchased from Sigma Aldrich and used without further purification. Hexyl heptyl amine and octyl dodecyl amine were synthesised as per procedure.[22] Sodium nitrite, imidazole, potassium hydroxide and potassium carbonate were purchased from Merck Chemicals Ltd and used as such. Dimethyl Acetamide (DMF), Acetic acid (AcOH), tertiary butanol (tBuOH) and

ethanol were purchased from Merck Chemicals Ltd and were purified using standard procedures.

4.3.2. Instrumentation techniques: Infrared spectra were obtained using Bruker α-T spectrophotometer in the range of 4000-400 cm^{-1}. ^{1}H and ^{13}C-NMR spectra were recorded in $CDCl_3$ using Bruker AVENS spectrophotometer. Chemical shifts (δ) are reported in ppm at 298 K, with trace amount of tetramethylsilane (TMS) as internal standard. MALDI-TOF analysis was carried out on a Voyager-De-STRMALDI-TOF (Applied Biosystems, Framingham, MA, USA) instrument equipped with 337 nm pulsed nitrogen laser used for desorption and ionization. The operation was in a reflector mode with an accelerating voltage of 25 kV. Micromolar solutions of the compounds in THF were mixed with Dithranol matrix and spotted on stainless steel MALDI plate and dried well. Thermogravimetric analysis (TGA) was performed using a PerkinElmer STA 6000 thermogravimetric analyser. Samples were run from 40 to 800 °C with a heating rate of 10 °C/min under nitrogen. DSC (differential scanning colorimeter) measurements were performed on TA Q10 differential scanning calorimeter at a heating rate of 10 °C/min under nitrogen atmosphere. Typically, 3-4 mg of samples was placed in an aluminium pan, sealed properly and scanned from -30 to 380 °C. The instrument was calibrated with indium standards before measurements. The first heating cycles were avoided to get rid of thermal history of the samples. Wide Angle X-ray Diffractogram (WXRD) were obtained using a Philips analytical diffractometer with CuKα emission. All the samples were recorded in the (2θ) range of 3–50 degrees using a PANalytical X'pert Pro dual goniometer diffractometer and analyzed using X'pert software. An X'celerator solid-state detector was employed in wide-angle experiments. The radiation used was CuKα (1.54 Å) with a Ni filter, and the data collection was carried out using a flat holder in Bragg–Brentano geometry.

4.3.3. Device Fabrication: SCLC electron-only devices were fabricated using the following structure: glass/Al/active layer/Al. The glass substrates were cleaned using the following sequence in an ultrasonic bath: water, acetone, and 2-propanol.[23] The bottom aluminum electrode was deposited by thermal evaporation technique with a thickness of 100 nm under vacuum in a glove box. 20 mg/ml of **UPBI and P4VP-UPBI** complexes were dissolved in dry DMF and 70 micro liters was drop cast on top of the aluminum

electrode. The drop cast films were annealed up to 100 ^{o}C for 10 minutes and cooled to room temperature. Aluminum counter electrodes were evaporated through a shadow mask on top of the active layer to a thickness of ~100 nm in a thermal evaporation chamber. The active device area was found to be in the range of 0.08 - 0.12 cm^2. The mobility measurements were carried out by measuring the current–voltage characteristics with a Keithley 2400 source meter.

4.3.4. Synthesis of Unsymmetrical Perylenebisimide (UPBI)

1) UPBIDD: The symmetrical PBI substituted with dodecyl amine at both side was synthesised as given in scheme 1. Selective ring opening with KOH followed by the addition of amino pentadecyl phenol resulted in the formation of UPBIDD, which was further purified using column chromatography in DCM / MeOH systems. Yield: 46%. M.P.: 290 °C. ^{1}H NMR (400 MHz, $CDCl_3$, δ ppm) : 8.55-8.36 (m, 8H, perylene), 6.86–7.09 (m, 3H; Ar**H**-PDP), 4.16 (m, 2H, imide-N-C**H**$_2$), 2.41 (t, (t, ^{3}J= 2.8 Hz, 4H; Ar-C**H**$_2$), 2.00 (m, 1H, imide-N-CH_2-C**H**), 0.98-0.86 (m, 6H, end CH_3 of dodecyl group + terminal C**H**$_3$ of C-15 alkyl chain). ^{13}C NMR (100 MHz, $CDCl_3$, δ ppm) : 166.3, 163.6, 161.9, 158.9, 155.8, 143.1, 136.7, 130.3, 129.8, 126.2, 124.9, 123.1, 122.6, 113.3, 106.2, 55.6, 32.7, 31.9, 29.9, 26.9, 22.8, 14.3.FT-IR (KBr, cm^{-1}): 3367, 2957, 2921, 2854, 1698, 1655, 1591, 1505, 1463, 1441, 1402, 1348, 1299, 1249, 1177, 1092, 967, 856, 806, 749, 632. MALDI-TOF (DHB matrix): m/z calculated for $C_{57}H_{68}N_2O_5$: 860.51; found 861.51[M^{+}1], Elemental analysis calculated (%): C 79.50, H 7.96, N 3.25; found: C 79.98, H 8.24, N 3.71.

2) UPBIHH: same procedure as given above was repeated for symmetrical PBI with hexyl heptyl amine. Yield: 68%. M.P.: 235 °C.^{1}H NMR (400 MHz, $CDCl_3$, δ ppm) : 8.74-8.51 (m, 8H, perylene), 6.86–7.09 (m, 3H; Ar**H**-PDP), 5.18 (m, 1H, imide-N-C**H**), 2.41 (t, ^{3}J= 2.8 Hz, 4H; Ar-C**H**$_2$), 2.00 (m, 1H, imide-N-CH_2-C**H**), 0.98-0.86 (m, 9H, end CH_3 of hexyl heptyl group + terminal C**H**$_3$ of C-15 alkyl chain). ^{13}C NMR (100 MHz, $CDCl_3$, δ ppm): 166.3, 163.6, 161.9, 158.9, 155.8, 143.1, 136.7, 130.3, 129.8, 126.2, 124.9, 123.1, 122.6, 113.3, 106.2, 55.6, 32.7, 31.9, 29.9, 26.9, 22.8, 14.3. FT-IR (KBr, cm^{-1}): 3367, 2957, 2921, 2854, 1698, 1655, 1591, 1505, 1463, 1441, 1402, 1348, 1299, 1249, 1177, 1092, 967, 856, 806, 749, 632. MALDI-TOF (DHB matrix): m/z calculated for

$C_{60}H_{74}N_2O_5$: 860.51; found 861.51$[M+1]^+$, 827.3 Elemental analysis calculated (%): C 79.78, H 8.26, N 3.10; found: C 79.29, H 8.32, N 3.81.

3) UPBIOD: same procedure as given above was repeated for symmetrical PBI with octyl decyl amine. Yield: 49%. M.P.: 270 °C. ^{1}H NMR (400 MHz, $CDCl_3$, δ ppm) : 8.68-8.46 (m, 8H, perylene), 6.86–7.09 (m, 3H; Ar**H**-PDP), 5.18 (m, 2H, imide-N-C**H**), 2.41 (t, ^{3}J= 2.8 Hz, 4H; Ar-C**H**$_2$), 2.00 (m, 1H, imide-N-CH_2-C**H**), 0.98-0.86 (m, 9H, end CH_3 of octyldecyl group + terminal C**H**$_3$ of C-15 alkyl chain). ^{13}C NMR (100 MHz, $CDCl_3$, δ ppm): 166.3, 163.6, 161.9, 158.9, 155.8, 143.1, 136.7, 130.3, 129.8, 126.2, 124.9, 123.1, 122.6, 113.3, 106.2, 55.6, 32.7, 31.9, 29.9, 26.9, 22.8, 14.3. FT-IR (KBr, cm^{-1}): 3367, 2957, 2921, 2854, 1698, 1655, 1591, 1505, 1463, 1441, 1402, 1348, 1299, 1249, 1177, 1092, 967, 856, 806, 749, 632. MALDI-TOF (DHB matrix): m/z calculated for $C_{65}H_{84}N_2O_5$: 972.64; found 973 [M^+1], Elemental analysis calculated (%): C 80.21, H 8.7, N 2.88; found: C80.56, H 8.32, N 3.21.

4) UPBICH: same procedure as given above was repeated for symmetrical PBI with cyclohexyl amine. Yield : 55%. M.P.: 326 °C.^{1}H NMR (400 MHz, $CDCl_3$, δ ppm) : 8.65-8.41 (m, 8H, perylene), 6.86–7.09 (m, 3H;Ar**H**-PDP), 5.03 (m, 1H, imide-N-C**H**), 2.41 (t, ^{3}J= 2.8 Hz, 4H; Ar-C**H**$_2$), 2.00 (m, 1H, imide-N-CH_2-C**H**), 0.98-0.86 (m, 3H, terminal C**H**$_3$ of C-15 alkyl chain). ^{13}C NMR (100 MHz, $CDCl_3$, δ ppm) : 166.3, 163.6, 161.9, 158.9, 155.8, 143.1, 136.7, 130.3, 129.8, 126.2, 124.9, 123.1, 122.6, 113.3, 106.2, 55.6, 32.7, 31.9, 29.9, 26.9, 22.8, 14.3. FT-IR (KBr, cm^{-1}): 3367, 2957, 2921, 2854, 1698, 1655, 1591, 1505, 1463, 1441, 1402, 1348, 1299, 1249, 1177, 1092, 967, 856, 806, 749, 632. MALDI-TOF (DHB matrix): m/z calculated for $C_{51}H_{54}N_2O_5$: 775.4; found: 776 [M^+1].Elemental analysis calculated (%): C 79.04, H 7.02, N 3.61; found: C 79.89, H 7.32, N 3.81.

4.3.6: Supramolecular complex preparation: Poly (4-vinylpyridine) (P4VP) as well as the unsymmetrical perylenebisimide (**UPBI**) was dried in vacuum oven at 60 °C for 3 days. **P4VP-UPBI** complexes were prepared from dry DMF solutions taking 1:1 molar ratio of P4VP with UPBI. In a typical procedure P4VP was first dissolved in DMF to which desired amount of **UPBI** was added and the solution was stirred for 24 hours. Concentration of the solutions were maintained at 1wt%. Subsequently the solvent was

evaporated slowly on a hot plate at 60 °C and further dried in vacuum oven at 65 °C for 3 days, slowly cooled to room temperature and stored in desiccator thereafter.

4.4. Results and Discussion

4.4.1. Synthesis and Characterization of Unsymmetrical PBI (UPBI)

The unsymmetrical perylenebisimide (UPBI) having a 3-pentadecylphenol moiety which could involve in hydrogen bonding interaction with the pyridine units of P4VP and other side with different alkyl group was synthesized by following the reported procedure as shown in Scheme-1.The synthesis of UPBI was started from the symmetrical PBI derivative obtained by condensation of the dianhydride PTCDA with excess respective amine along with a catalytic amount of Lewis acid $Zn(OAc)_2$. A partial saponification of this symmetric derivative under strong basic conditions with KOH in *tert*-BuOH as the reaction medium was done according to Langhals method, which gave the mono-imide-mono-anhydride derivative. Subsequent condensation of this one side alkyl mono-imide-mono-anhydride derivative with 4-amino-3-pentadecyl phenol gave the desired UPBI.

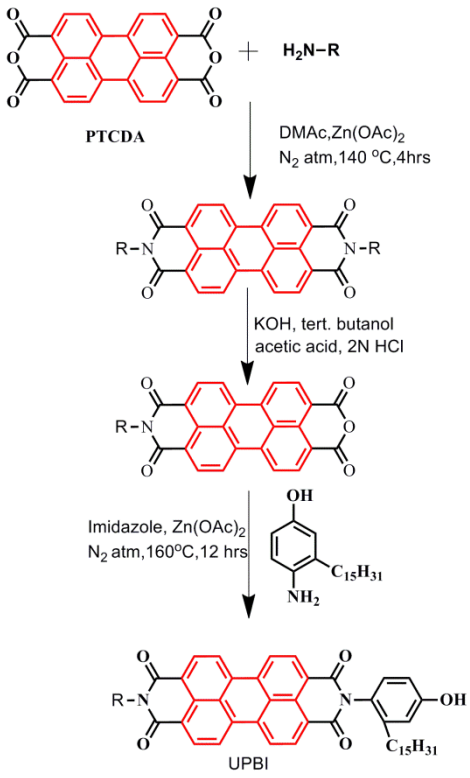

R – alkyl chain	UPBI
C_7H_{15} C_6H_{13}	UPBI HH
$-C_{12}H_{25}$	UPBIDD
	UPBICH
C_8H_{17} $C_{10}H_{21}$	UPBIOD

Scheme 1: Synthesis and Structures of UPBIs

a)UPBICH

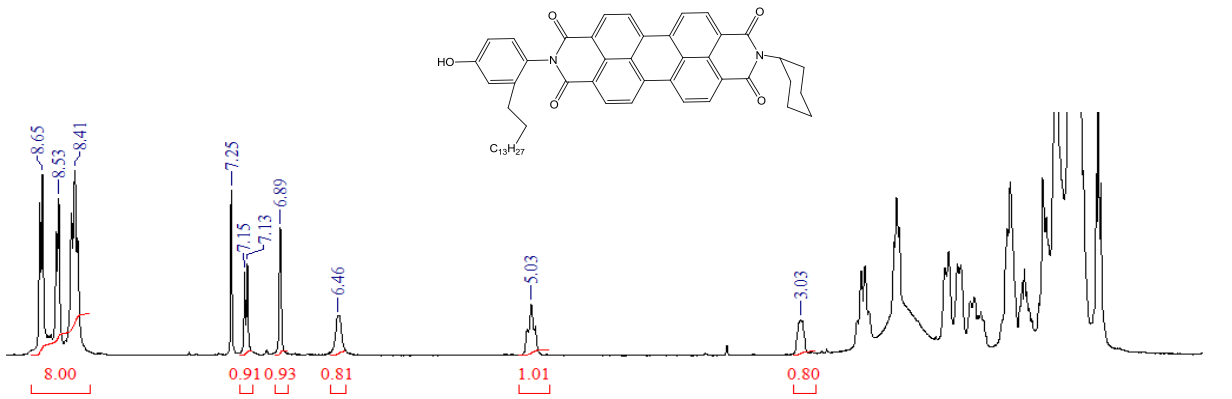

b) UPBIDD

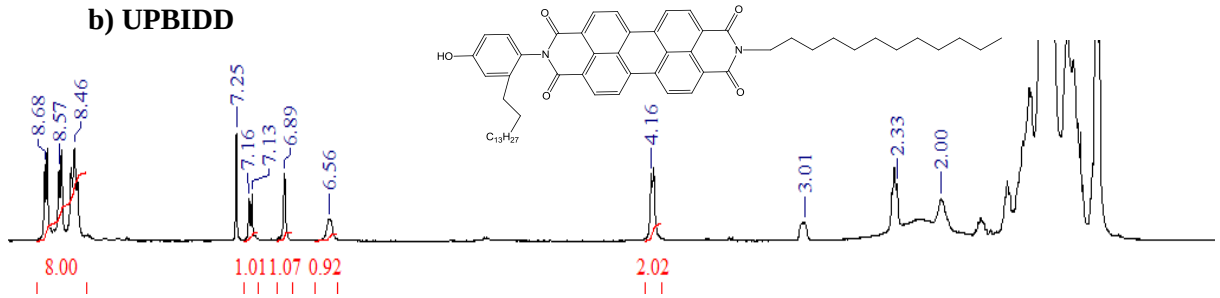

c) **UPBIHH**

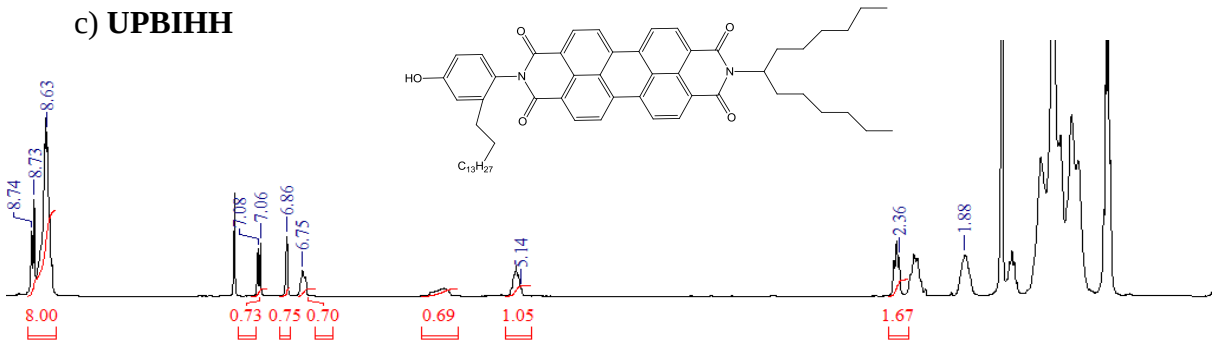

d) UPBIOD

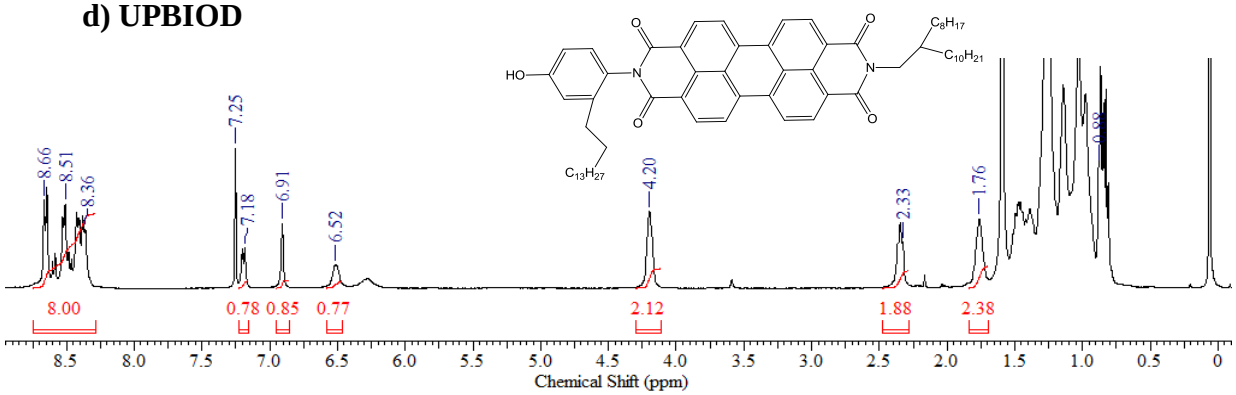

Figure 1: ^{1}H NMR spectrum of **UPBIs** in $CDCl_3$ (10 mg/ ml)

The structures of PDP-UPBI along with the intermediate products were fully characterized by ^{1}H-NMR, ^{13}C-NMR, FT-IR and MALDI-TOF spectroscopies with details given in experimental section. The ^{1}H NMR spectrum of UPBIs in $CDCl_3$ (10 mg/ ml) is given in figure 1. **UPBIOD,** had sharp signals corresponding to the 8 aromatic protons of perylene in the region 8.55-8.44 ppm (labelled as 'a' protons) and signals corresponding to the 3 aromatic protons of pentadecyl phenol (PDP) unit at 7.16 (d, 1H), 6.89 (s, 1H) and 6.56 (d, 1H) ppm respectively. **UPBICH**, also showed the 8 aromatic perylene protons in the region 8.55-8.39 ppm ('a' protons) and PDP protons at 7.19 (d, 1H), 6.89 (s, 1H) and 6.46 (d, 1H) ppm respectively. Similarly for **UPBIHH,** the perylene protons appeared at 8.69-8.51 ppm ('a' protons) and the 3 aromatic protons of PDP unit at 7.06 (d, 1H), 6.86 (s, 1H) and 6.74 (d, 1H) ppm respectively. For **UPBIDD**, the perylene aromatic protons appeared at 8.55-8.36 ppm ('a' protons) and the PDP protons at 7.2 (d, 1H), 6.91 (s, 1H) and 6.51 (d, 1H) ppm respectively.

Thermal properties of these newly synthesised UPBIs was studied by thermogravimetric (TGA) and differential scanning calorimetric (DSC) analysis. The UPBIs were found to exhibit high thermal stability up to the temperature range of 350-400 °C with no signs of decomposition as observed from the TGA curves in figure 2. The second heating and cooling cycles from the DSC thermogram of the UPBIs are given in figure 3.

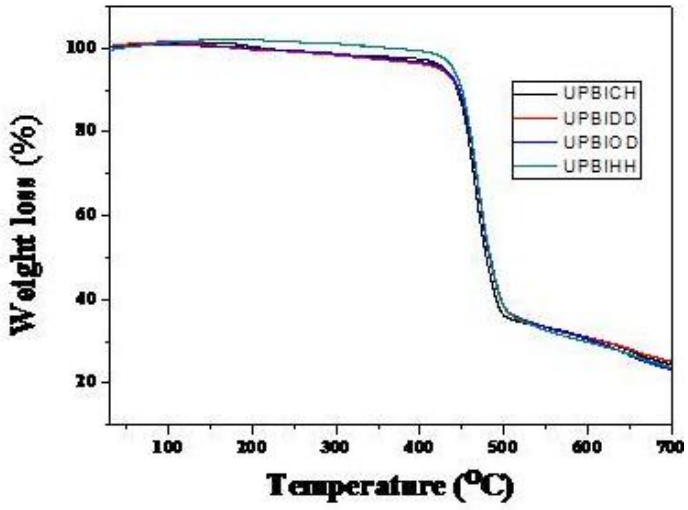

Figure 2: Thermo gravimetric analysis (TGA) of **UPBIs** under N_2 atmosphere

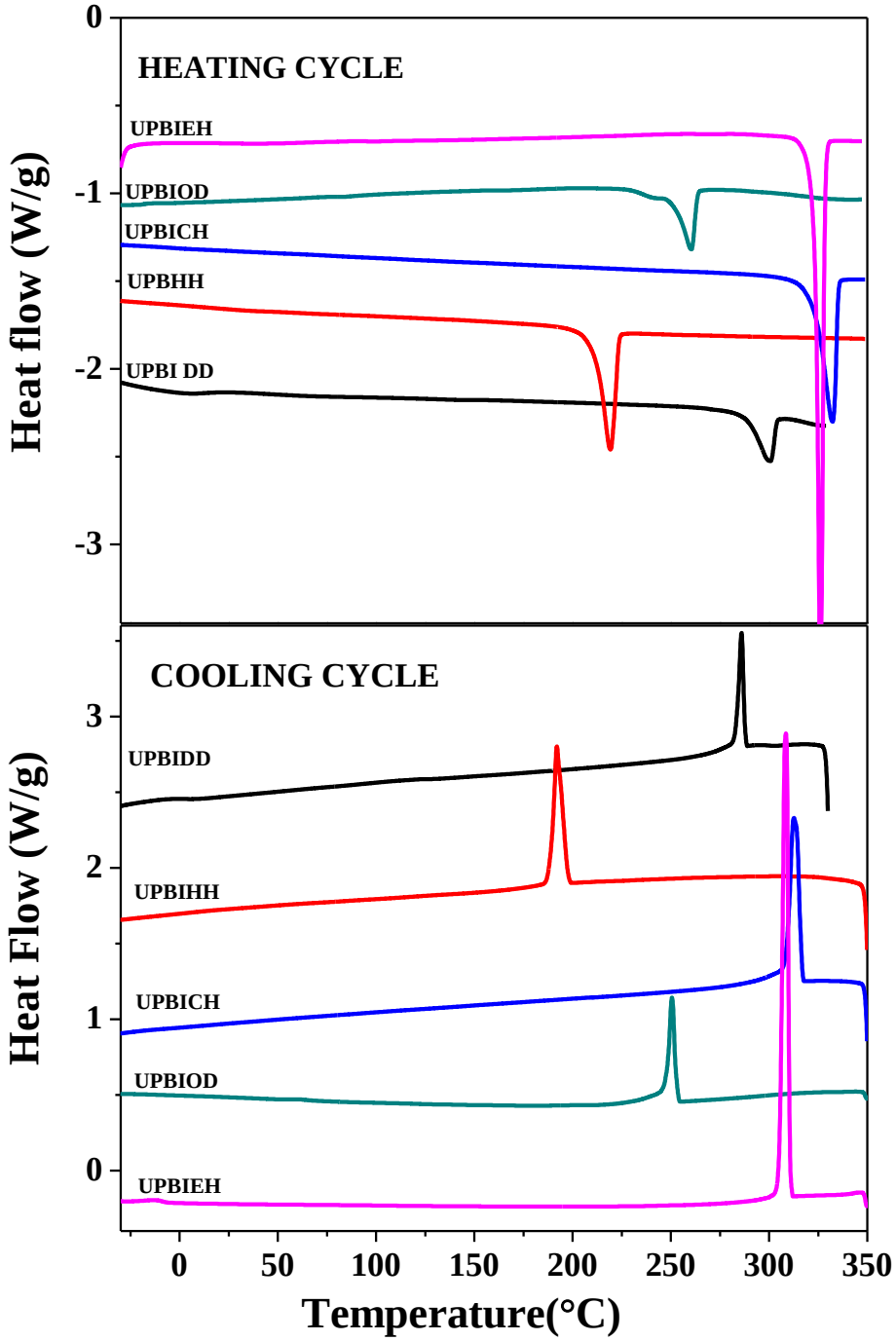

Figure 3: DSC thermogram of second heating and cooling cycles of **UPBIs** under N_2 atmosphere (10 ^{o}C / min).

For comparison the DSC thermogram of UPBIEH (discussed in chapter 3) also is included in the figure 3. It showed a melting transition at 320 ^{o}C with an enthalpy of 61 kJ/mol which crystallised at 318 ^{0}C (60.5kJ / mol). Except UPBIOD all other UPBIs are showed single transition in both the heating and cooling cycle. Among the UPBIs, the UPBICH showed the highest melting transition at 327 ^{o}C (32 kJ/ mol) which crystallised at 314 ^{o}C (30.5 kJ/mol). While UPBIHH showed lowest melting transition of 221 ^{o}C (28 kJ/ mol), (crystallisation at 196 ^{o}C with an enthalpy of 25KJ/ mol). Similarly UPBIDD showed a single transition during heating at 300.5 ^{o}C and while cooling at 286 ^{o}C (15.6 kJ/mol). UPBIOD showed multiple transitions, a small transition at 240 ^{o}C followed by melting transition at 263 ^{o}C (20 kJ/ mol). While cooling the crystallisation occurred at 250 ^{o}C (18 kJ/ mol), with a broad transition. The enthalpyof these transitions were low as compared with the enthalpy of UPBIEH which is highly crystalline in nature.

PBI molecules inherently have mesogenic tendancies and when the rigid and flexible parts match the requirements they can exhibit liquid crystallanity.[26] So the molecules were probed for their LC characteristics using PLM. The polarised light microscopic images of the UPBIs while cooling from the isotropic melt are given in figure 4. All the UPBIs exhibited characteristic liquid crystalline textures. While cooling from the isotropic state only single mesophase was observed in all of these sytems which remained unchanged until room temperature. All the UPBIs showed characteristic liquid crystalline pattern except UPBIEH which showed needle like textures confirming its crystalline behaviour. The UPBIOD showed clear dentrintic textures which indicated that it had the tendancy to form columnar hexagonal LC phase. Other UPBI also showed textures which were commonly observed for columnar LC phase. The PBIs are known for their tendencies to form columnar phases since the conjugated core can pack in to columns.

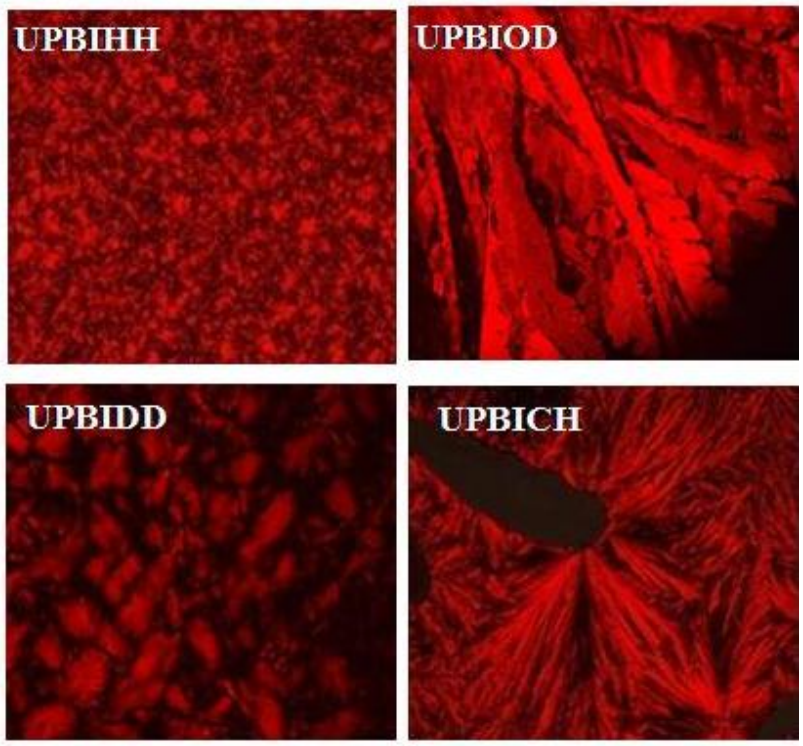

Figure 4: Polarised Light microscopic images of **UPBIs**

To confirm the liquid crystalline phases of UPBIs the annealed XRD measurements have done as given in figure 5.

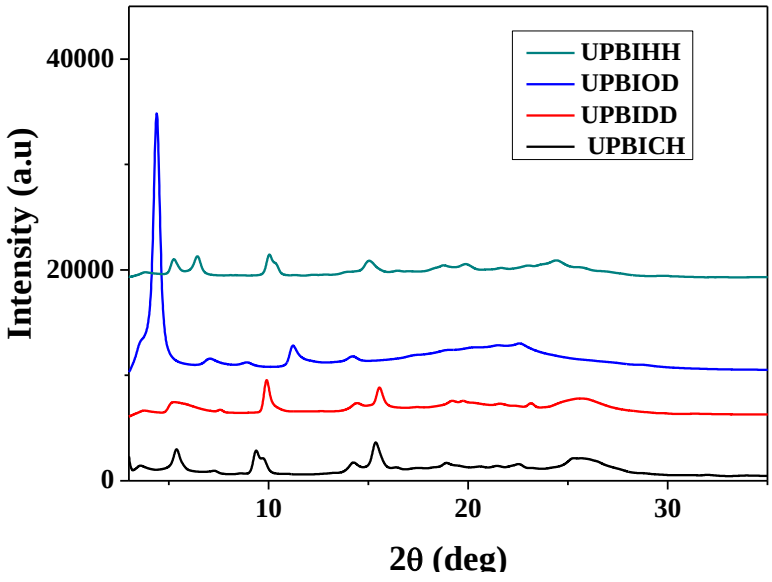

Figure 5: Annealed XRD pattern of annealed samples of **UPBI**s.

All the UPBIs were annealed up to isotropic state then cooled to room temperature and the XRD was done. For UPBIOD the first peak was observed at $2\theta = 4.04^{o}$ corresponding to a d spacing of 33.4 Å ollowed by the small peaks at 2θ = 7.07, 8.89, 11.01, 14.14 . These peaks were in a ratio of of 1: $1/\sqrt{3}$: 1/2 :1/5 which clearly confirmed the columnar hexagonal (Col h) liquid crystalline phase in UPBIOD.[24] For UPBIHH and UPBIDD the d spacing were in a ratio of 1: 1/ 2 : 1/ 4 which clearly indicated that they had tendancies to form columnar rectangular phase (Col r) and the d spacing ratio for UPBICH was in the ratio 1: 1/ 2: 1/ 3:1/4 which indicated that UPBICH is preferred the columnar lamellar phase (Col l). [25]The above analysis confirmed the influence of terminal alkyl chain in the packing in unsymmetrical perylenebisimides. All the UPBIs discussed here except UPBIEH had the tendancy to form mesophases. UPBICH which had the highest melting point formed columnar lamellar phase. UPBIOD with branched alkyl chain has form columnar hexagonal phase while UPBIDD and UPBIHH formed columnar rectangular phase. From this it is very clear that upon varying the alkyl chain substitution of UPBI it is possible to tune their mesophase. Additionally, these UPBIs showed room temperature liquid crystallinity which is a promising observation for device applications.

The liquid crystalline PBI molecules were incorporated in to a polymeric backbone. As discussed in the introduction section the supramolecular comb copolymer approach was adopted where one could load 100% PBI molecule on to a polymer back bone using non covalent interactions which was not possible by other approaches. The coming sections of these chapters will discuss in detail the supramolecular comb copolymer of P4VP with the different UPBIs.

4.4.2. Supramolecular comb polymer formation with P4VP

The hydrogen bonded complexes were prepared by dissolving 1:1 molar ratio of **UPBIs** with P4VP in dry DMF as solvent, stirring at 80^{o}C conditions for 24 hours, followed by removal of solvent by heating. The complexes were named **P4VP-UPBIDD, P4VP-**

UPBIHH, P4VP-UPBIOD, P4VP-UPBICH according to the unsymmetrical PBI used for complex formation. The schematic drawing along with the chemical structure of the hydrogen bonded polymeric **P4VP-UPBI** stoichiometric 1:1 complex is given in Scheme-2,

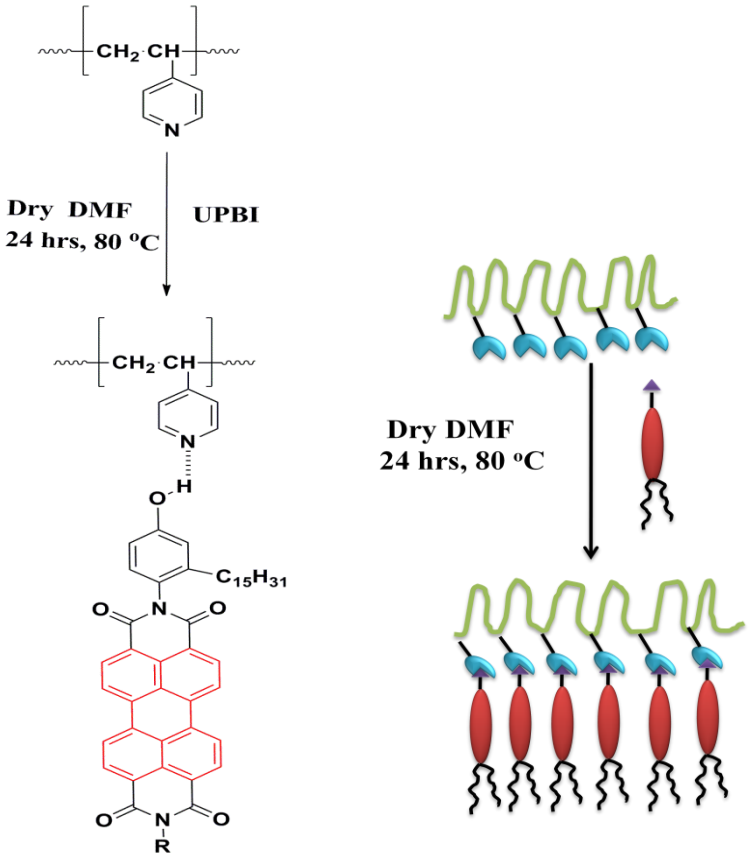

Scheme 2. Structure and Schematic diagram of the **P4VP-UPBI** polymeric supramolecular complex formed by 1:1 stoichiometric interaction of the unsymmetrical **UPBI** with P4VP polymer.

4.4.3. Confirmation of hydrogen bonding - FT-IR and ^{1}H-NMR studies

The formation of the complex formation was traced by FT-IR spectroscopy as given in literature for the complexes of P4VP with pentadecyl phenol. P4VP shows a symmetric ring stretching vibration mode at 993 cm^{-1} and a strong carbon-nitrogen stretching band at 1597 cm^{-1} for free pyridine groups, which shifts to higher wavenumbers upon hydrogen bonding interaction with the phenol unit of PDP. The shift corresponding to the 1597 cm^{-1} peak was difficult to trace in the **P4VP UPBI** complexes since pentadecyl phenol unit attached to the perylene core also had absorption band in the same region. Another characteristic absorption band of pure P4VP around 1413 cm^{-1} was devoid of any overlapping absorptions from pristine **UPBI**. Ikkala *et al.* had shown that for the nominally fully complexed P4VP(PDP)$_{1.0}$, the 1413 cm^{-1} band shifted to 1421 cm^{-1}, upon hydrogen bond formation.

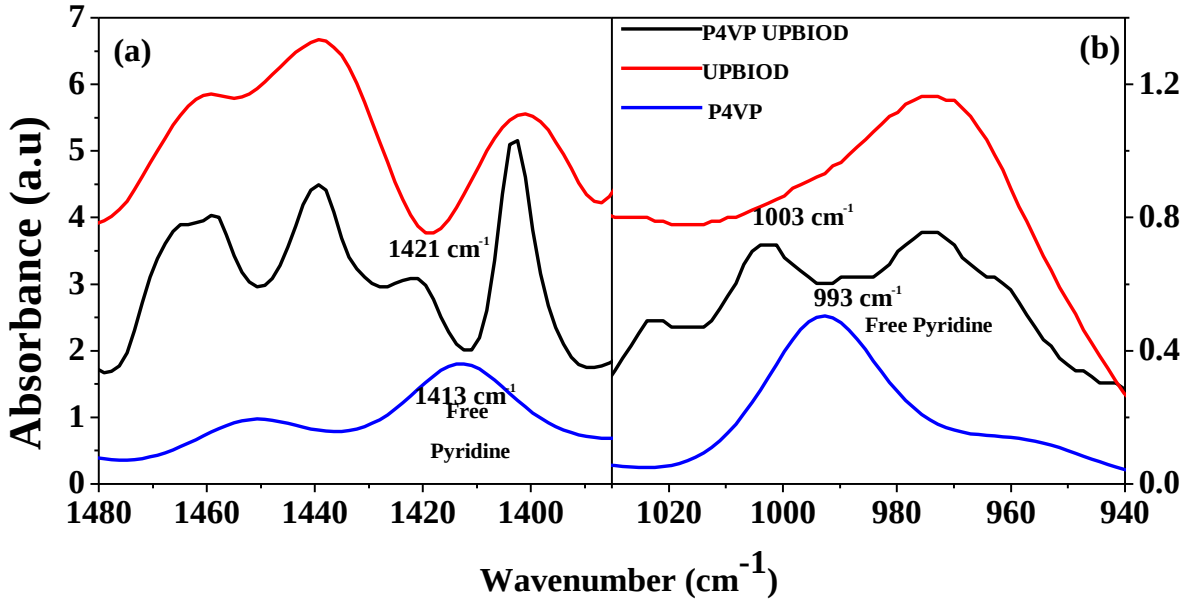

Figure 6: FTIR plots comparing the (a) 1413 cm^{-1} and (b) 993 cm^{-1} region of **P4VP-UPBIOD** complex with that of pure **P4VP** and **UPBIOD.**

Figure 6 shows the representative FT-IR spectra comparing the 993 cm^{-1} and 1413 cm^{-1} region of the 1:1 complex **P4VP-UPBIOD** (all the four P4VP-UPBI complexes showed similar spectrum in the same region) along with that of **P4VP** and **UPBIOD** . It could be seen from the figure that the hydrogen bonding of the pyridine ring of P4VP with the

phenol of **UPBIOD** was almost complete in the 1:1 complex which was indicated by the complete vanishing of 993 cm^{-1} band, with the simultaneous appearance of two new bands at 1003 and 1023 cm^{-1} corresponding to hydrogen bonded pyridine. Similarly, in the 1413 cm^{-1} region, a new peak appeared at 1421 cm^{-1} in **P4VP-UPBIOD** which also confirmed the supramolecular complex formation.[18]

The complexation between P4VP and UPBIOD could also be traced by ^{1}H NMR analysis. The expanded aromatic region of the ^{1}HNMR spectrum of **P4VP-UPBI** complex, **P4VP**, **UPBI** are given in figure 7a-d. Taking one typical example; **UPBIOD,** had sharp signals corresponding to the 8 aromatic perylene protons in the region 8.67-8.43 ppm and signals corresponding to the 3 aromatic protons of pentadecyl phenol (PDP) unit at 7.16 (d, 1H), 6.89 (s, 1H) and 6.56 (d, 1H) ppm respectively. On the other hand, P4VP had two sets of broad signals corresponding to four aromatic pyridine protons with intensity distribution corresponding to two protons each at 8.32 (d, 2H,) and 6.36 ppm (d, 2H,) respectively. Upon comparison, it could be clearly seen that in the 1:1 complex the perylene signals also had a broadened appearance. A down field shift was observed for the PDP protons in all the systems from upon complexation (Figure 7a-d). For P4VP-UPBICH complexes a down field shift of PDP protons from 6.45 ppm (in pristine) to 6.56 ppm was observed. Table 1. lists the shift in PDP protons upon complex formation with P4VP in all 4 UPBI systems. This shift could be justified with the proximity of the pentadecyl phenol aromatic protons to the hydroxyl unit, involved in the hydrogen bonding interaction with the pyridine 'N' on the P4VP units.[18] A complimentary downfield shift (6.37 ppm to 6.42 ppm) was observed for P4VP protons, although it was not so prominent as that of the PDP aromatic proton shift due to the broad nature of the P4VP protons.

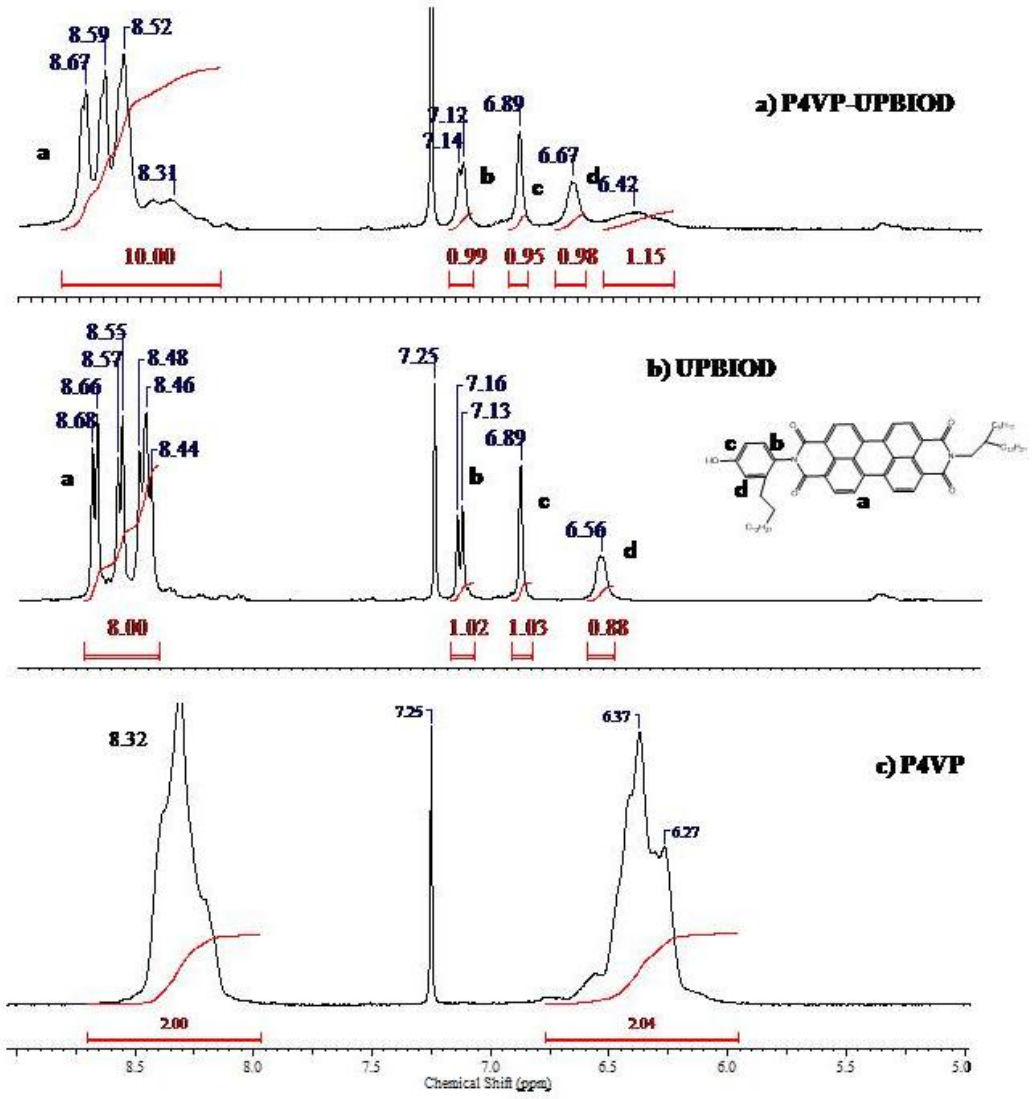

Figure 7a: ^{1}H NMR spectrum of a) **P4VP-UPBIOD** b) **UPBIOD** c) **P4VP** in $CDCl_3$.

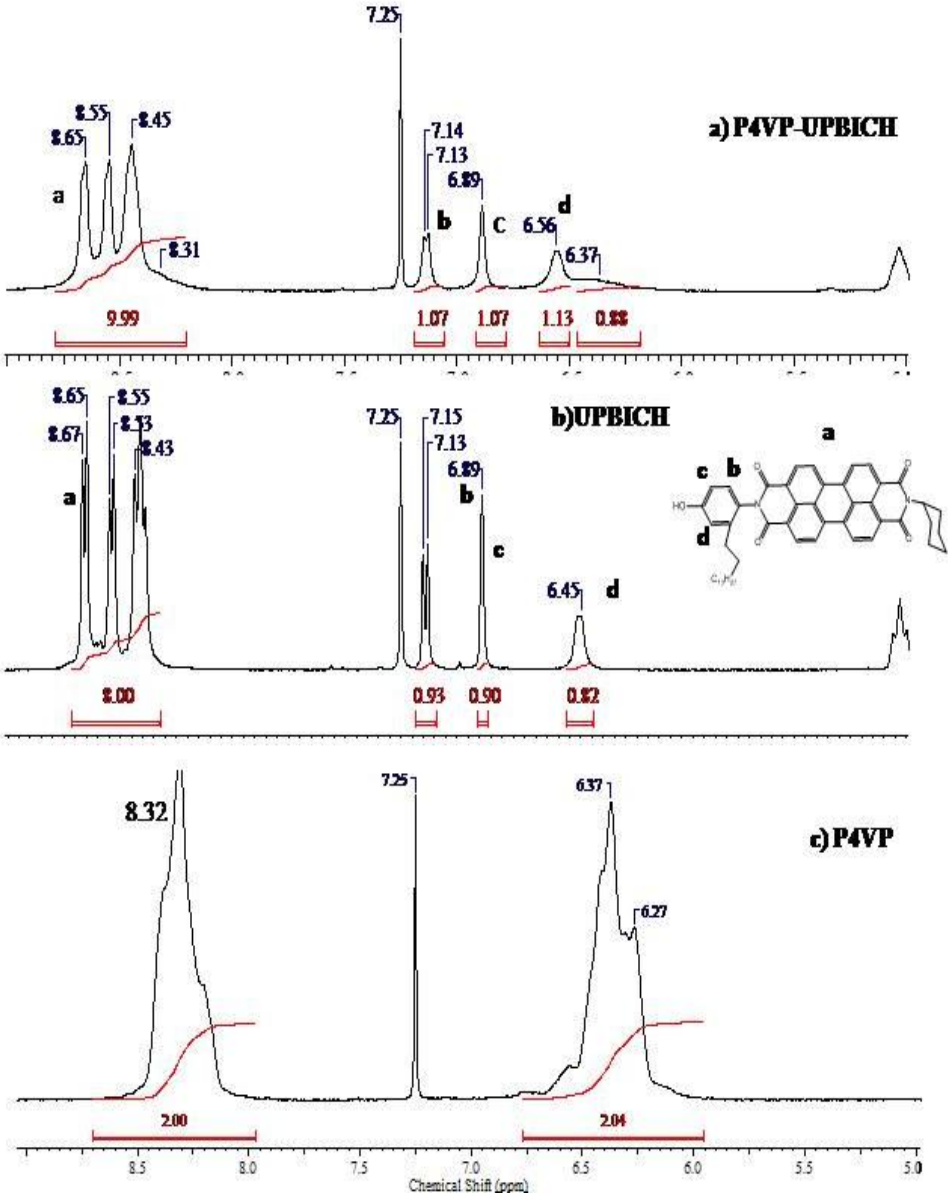

Figure 7b: ^{1}H NMR spectrum of a) **P4VP-UPBICH** b) **UPBICH** c) **P4VP** in $CDCl_3$.

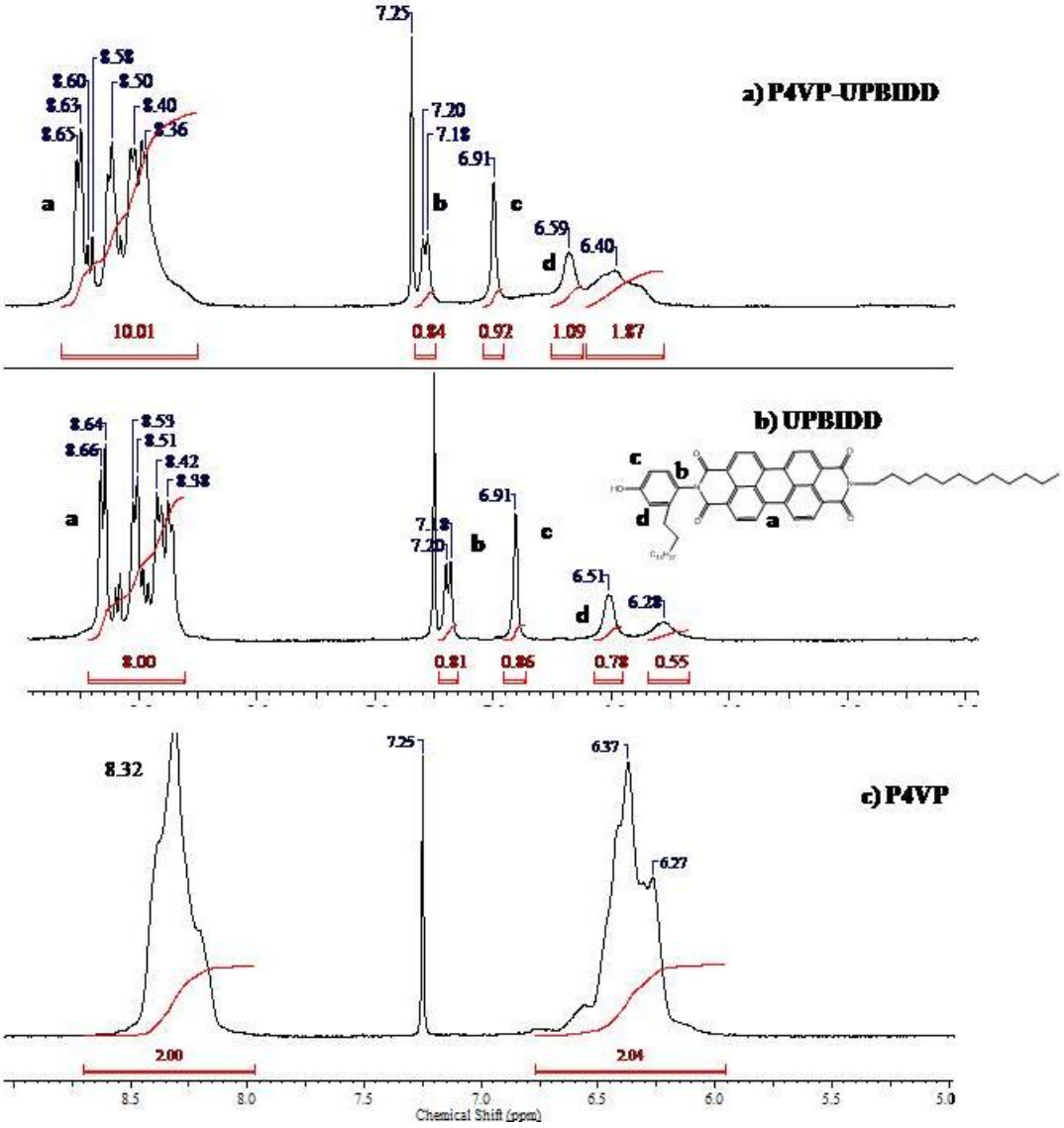

Figure 7c: ^{1}H NMR spectrum of a) **P4VP-UPBIDD** b) **UPBIDD** c) **P4VP** in $CDCl_3$.

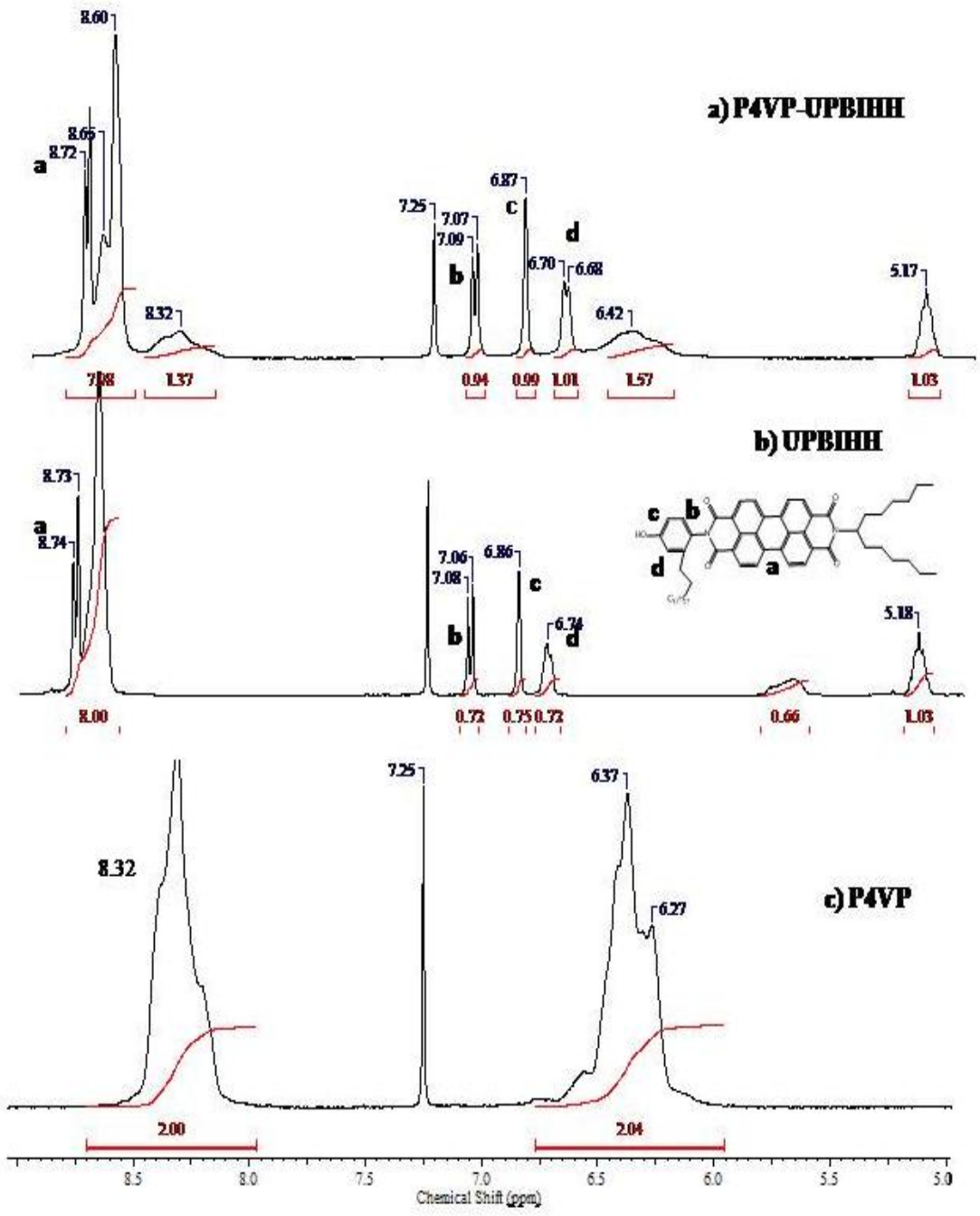

Figure 7d : ^{1}H NMR spectrum of a) **P4VP-UPBIHH** b) **UPBIHH** c) **P4VP** in $CDCl_3$.

UPBI	**Pristine UPBI (ppm)**	**P4VP-UPBI Complex (ppm)**
UPBIOD	**6.56**	**6.67 (0.12)**
UPBICH	**6.45**	**6.56 (0.11)**
UPBIDD	**6.51**	**6.59 (0.08)**
UPBIHH	**6. 74**	**6.70 (0.04)**

Table 1: Peak shift of PDP proton in prisine **UPBI** and **P4VP-UPBI** Complexes.

4.4.4. XRD and TEM analysis:

Wide angle X-ray diffraction (WXRD) can give confirmation regarding the bulk packing changes, if any, upon complexation. Therefore the room temperature XRD information was collected for all the supramolecular complexes and compared with the room temperature XRD of pristine UPBIs (figure 8).After complexation, the crystalline nature of the supramolecular complexes appeared to be enhanced as compared to the pristine UPBIs. This is because the P4VP acts as a template which helps to align the PBI molecules in a better way so that the packing between the PBI molecules increases. The **P4VP-UPBIOD** complexes showed columnar hexagonal phase even after complexation. From the XRD pattern of **P4VP-UPBIOD** complexes it is very clear that the peak ratio matched with columnar hexagonal phase. A slight shift was observed for the fundamental peak of **P4VP-UPBIOD** with respect to the **UPBIOD**. The peak shift to the higher angle region confirmed the better packing since the d spacing reduced. The other three

complexes **P4VP-UPBIDD**, **P4VP-UPBIHH**, **P4VP-UPBICH** has showed lamellar pattern in the XRD since their peak ratio followed the ratio of 1: 1 /2 : 1/ 3. In the pristine molecules the **UPBIDD** and **UPBIHH** exhibited columnar rectangular arrangement upon anealing. While after complexing with **P4VP** the arrangement changed to a lamella.

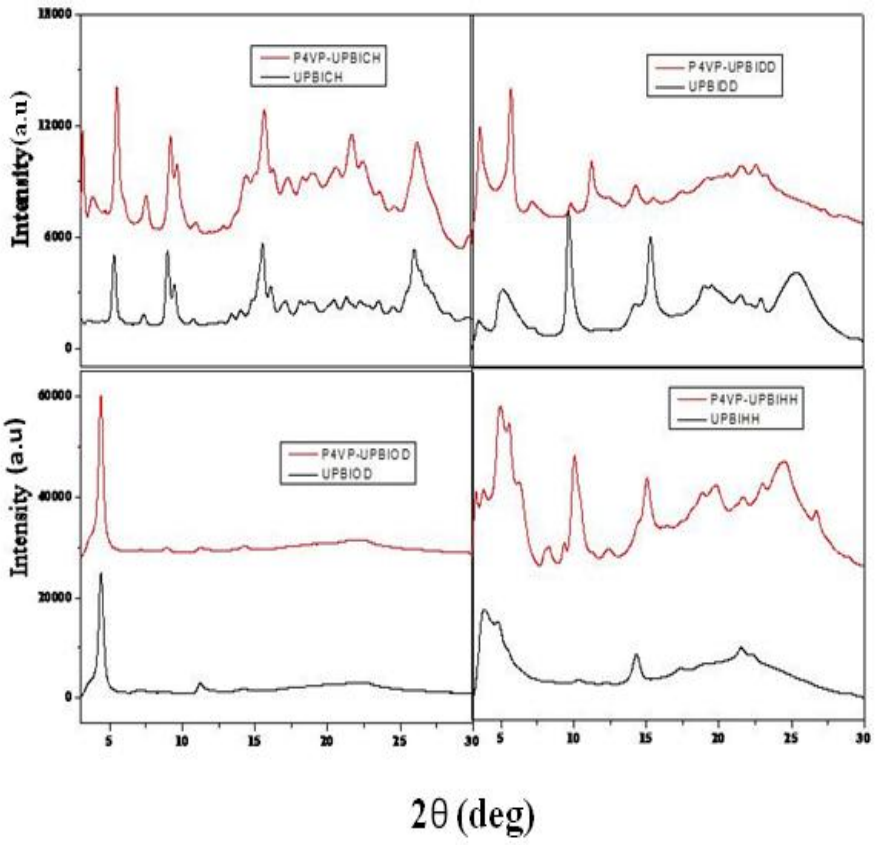

Figure 8: Room temperature XRD pattern of Pristine **UPBIs** and **P4VP-UPBI** complexes.

To get further insights to the morphology of the supramolecular complexes, the TEM analysis of the complexes were done. The samples were prepared in dry DMF with a concentration of 2mg/ ml and drop casted on Cu grid and stained with I_2 vapours. The pristine UPBIs and the homopolymer P4VP dis not exhibit any characteristic morphology, whereas all the four complexes showed nice lameller morphology with a length scale of 5 nm (figure 9). From the XRD analysis it is clear that except UPBIOD

all the three complexes possessed lamellar arrangement. P4VP-UPBIOD also showed lamellar arrangement in the TEM analysis. Hydrogen bonding assisted self assembly helps to arrange these molecules in a particular manner.

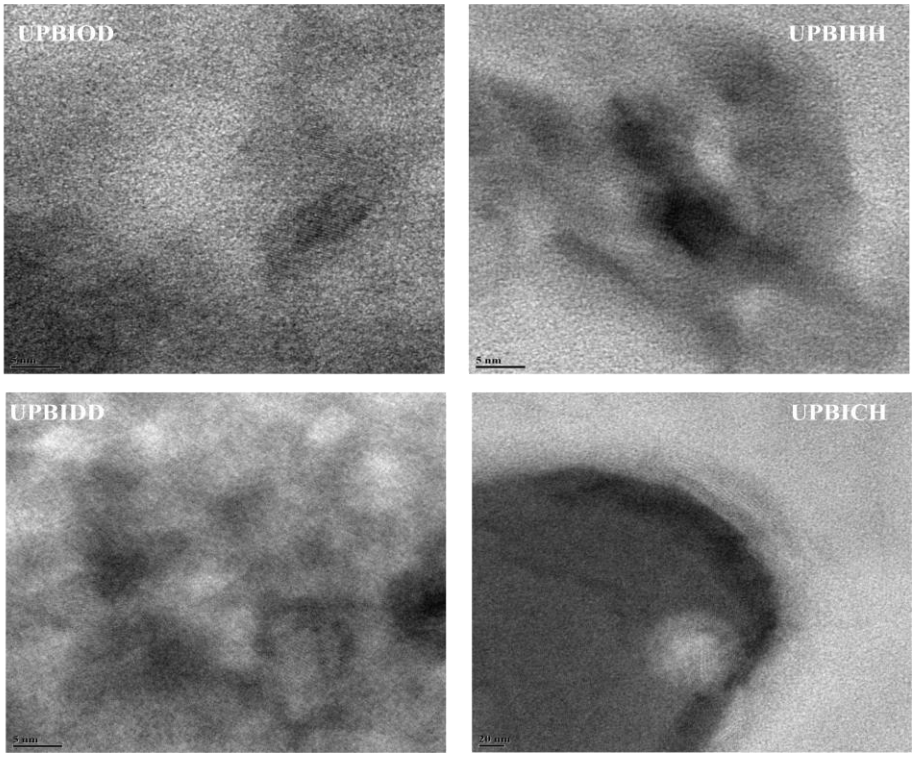

Figure 9: TEM analysis of **P4VP–UPBI** complexes in dry DMF (2mg/ml)

4.4.5 SCLC measurements:

The SCLC mobility measurements of annealed UPBI and P4VP-UPBI complexes were measured and is summarised in table 2. The device architecture was similar to that in chapter 2. For both the pristine UPBIs and complexes the active layers were drop casted from DMF and annealed up to 100 ^{o}C . Among the UPBIs, UPBIDD showed the highest mobility in the order of 10^{-4} cm^2 V^{-1} s^{-1}. Other UPBIs showed the mobilties in the order of 10^{-5}. After complexation the mobility value of P4VP-UPBICH complex improved by one orderwhile for the others it was retained. Table 2 lists the average mobility values for the pristine systems and corresponding complexes. Even though the mobility values were not so high, it is promising that after complexing with P4VP the mobility values of UPBIs

were preserverd since the complexation afforded improved processability which was not available with the pristine molecules.[18]

	SCLC mobility ($cm^2 V^{-1} s^{-1}$) After Annealing	
	Pristine	**Complexes**
UPBIHH	**1.04×10^{-5}**	**5.13×10^{-5}**
UPBIOD	**5.68×10^{-6}**	**4.30×10^{-5}**
UPBIDD	**3.15×10^{-4}**	**1.13×10^{-4}**
UPBICH	**5.86×10^{-6}**	**1.68×10^{-5}**

Table 2: SCLC mobility measurement values of **UPBIs** and **P4VP-UPBI** complexes.

4.6 Conclusion:

In this chapter we have studied the influence of side chain variation in unsymmetrical perylenebisimides and their supramolecular comb copolymer formation with P4VP. Four novel PDP substituted unsymmetrical perylenebisimides were synthesized and characterized. All the UPBIs studied here exhibited room temperature columnar liquid crystalline phase. The **UPBIOD** with octyl dodecyl substitution formed columnar hexagonal phase where as the **UPBIHH** and **UPBIDD** formed columnar rectangular phase. The **UPBICH** with cyclohexyl branching showed columnar lamellar phase. The supramolecular comb copolymers of these UPBIs with P4VP were studied using XRD and TEM. The supramolecular comb copolymers formed nice lamellar morphology in the TEM analysis. The SCLC mobily measurements showed improvement in the mobility values after complexing with P4VP. This could be attributed to the improved ordering of the UPBIs brought about by the P4VP template.

4.7. References:

1. F. Würthner, *Chem. Commun.***2004,** 1564.
2. M. Sommer, S. M.Lindner, M. Thelakkat, *Adv. Funct. Mater*.**2007,** *17*, 1493.
3. G. Horowitz , F. Kouki , P. Spearman , D. Fichou , C. Nogues , X. Pan , F. Garnier , *Adv. Mater*. **1996**, 8, 242
4. Chen, Z.; Stepanenko, V.; Dehm, V.; Prins, P.; Siebbeles, L. D. A.; Seibt, J.; Marquetand, P.; Engel, V.; Würthner, F. *Chem. Eur. J.* **2007**, 13, 436
5. A. Facchetti, M.-H. Yoon, T. J. Marks, *Adv. Mater*.**2005,** *17*, 1705**.**
6. M. Muccini, *Nat. Mater*.**2006,** *5*, 605.
7. a) Singh, R.; Aluicio-Sarduy, E.; Kan, Z.; Ye, T; MacKenzie, R. C.I.; eivanidis, E. *J. Mater. Chem . A*, 2014, 2, 14348 .b) Zhang, X.; Zhan, C.; Yao, C*hem.Mater*..**2015**, 27, 166
8. M. Sommer, A. S. Lang, M.Thelakkat, *Angew. Chem. Int. Ed.* **2008,** *47*, 7901.
9. J. Ruokolainen, R. Mäkinen, M. Torkkeli, R. Serimaa, T. Mäkelä, G. Ten Brinke, O. Ikkala, *Science* **1998,** *280*, 557.
10. J. Ruokolainen, G. Ten Brinke, O. Ikkala, *Adv. Mater.* **1999,** *11*, 777.
11. K. de Moel, A. G. O.R. van Ekenstein, H. Nijland, E. Polushkin, G. Ten Brinke, *Chem. Mater.* **2001,** *13*, 4580.
12. O. Ikkala, G. Ten Brinke, *Science* **2002,** *295*, 2407.
13. O. Ikkala, G. Ten Brinke, *Chem. Commun.* **2004,** 2131.
14. W. Van Zoelen, T. Asumaa, J. Ruokolainen, O. Ikkala, G. Ten Brinke, *Macromolecules* **2008,** *41*, 3199.
15. J. Ruokolainen, G. Ten Brinke, O. Ikkala, *Macromolecules* **1996,** *29*, 3409.
16. G. Ten Brinke, O. Ikkala, *Macromol. Symp.* **2003,** *203*, 103.
17. Rancatore, B. J.; Mauldin, C. E.; Tung, S-H.; Wang, C.; Hexemer, A.; Strzalka, J.; Fréchet, J. M. J.; Xu, T. *ACS Nano*, **2010**, 4, 2721.
18. Narayan, R.; Kumar, P.; Narayan, K. S.; Asha, S. K. *Adv. Funct. Mater.* **2013**, 23, 2033.
19. Saibal, B.; Ashar, A. Z.; Devi, R. N.; Narayan, K. S.; Asha, S. K. *ACS Appl. Mater. Interfaces* 2014, 6, 19434−19448.

20. Narayan, R.; Kumar, P.; Narayan, K. S.; Asha, S. K.*J. Mater. Chem. C* , **2014** 2, 6511.
21. Narayan, R.; Kumar, P.; Narayan, K. S.; Asha, S. K. *Adv. Funct. Mater.* **2013**, 23, 2033–2043.
22. Wicklein, A.; Lang, A.; Muth, M.; Thelakkat, M. *J. Am. Chem. Soc*.**2009**, *131*, 14442-14453.
23. A. Arulkashmir, B. Jain, J. C. John, K. Roy,K. Krishnamoorthy, *Chem. Commun.*, **2014**, 50, 326.
24. G. A. Bhavsar and S. K. Asha,Chem.–Eur. J., 2011, 17, 12646.
25. Prajitha, K. P.; Chithiravel, S.; Krishnamoorthy, K.; Asha, S. K, *J. Mater. Chem. C*, **2014**, 2, 9882.
26. C. W. Struijk, A. B. Sieval, J. E. J. Dakhorst, M. van Dijk,P. Kimkes, R. B. M. Koehorst, H. Donker, T. J. Schaafsma,S. J. Picken, A. M. van de Craats, J. M. Warman, H. Zuilhof , E. J. R. Sudh¨olter,J. Am. Chem. Soc., 2000, 122, 11057.
27.

Chapter 5

PS-P4VP Block Copolymer Assisted Supra Molecular Comb Coil Self Assembly of Unsymmetrical Perylenebisimide.

5.1 Abstract:

The Supra molecular comb coil copolymer formation of **PS-b-P4VP** with n type semiconducting perylenebisimide (**UPBIHH**) was studied by varying the molar ratio of the latter from 0.25 to 1. The self assembly was well studied with the help of FT-IR, NMR, XRD and TEM. Upon varying the molar ratio of **UPBIHH** a change in the morphology was observed as confirmed from TEM imaging. Supra molecular complexes of PS-b-P4VP block co polymers with unsymmetrical perylenebisimide were formed through the hydrogen bond interaction between the pyridine units on P4VP and the phenolic –OH on the perylenebisimide. The supra molecular complexes showed worm like morphology in the TEM at 100 nm scale. In addition, lamellar morphology at a length scale of 5 nm could also be observed in the TEM images. This confirmed the assembly-within-assembly of comb co polymer formation inside the larger block co polymer organization.

5.2 Introduction:

The previous chapter described the supra molecular comb copolymer formation of perylenebisimides with P4VP homopolymer. This chapter is focussed on the supramolecular comb coil copolymer formation of perylenebisimide with PS-b-P4VP block copolymer. Self assembly of block copolymers have received wide attention in the area of nano science due to its ability to form wide range of nanostructures depending upon the number of copolymer blocks, their volume fraction, miscibility of each blocks etc.[1-3] Further varieties of architectures can be obtained if the comb architecture is introduced in to a diblock copolymer by selectively complexing one of the block with low molecular weight surfactant. The resultant supra molecular comb coil block copolymer can display two kinds of morphology 1) large length scale (> 100 nm) morphology driven by the microphase separation between the comb and coil block 2) smaller length scale (< 20 nm) morphology due to the segregation between the polymer backbone and the surfactants in the comb block. And this kind of morphology is called as "Structure – within- Structure." or "assembly–within-assembly". Lamella–within–Lamella, Lamella-within-Cylinder, Lamella-within-Sphere etc are some of the most commonly observed morphologies in supra molecular comb coil block copolymeric systems.[4-6]

The supramolecular comb coil copolymer was poineered and widely studied by Ikkala and co-workers. The non covalent hydrogen bonding between PS-b-P4VP and pentadecyl phenol molecule are well explored by them.[7, 8] By varying the relative block lengths of the P4VP-*b*-PS selectively all the classical morphologies could be obtained with a series of structure-within-structure morphologies. This concept of attaching small molecules to block copolymer based supramolecules was applied by the group of Ting Xu and Frèchet *et al.* to a p-type organic semiconductor like quaterthiophene named '4T' which was hydrogen bonded to PS-*b*-P4VP resulting in solution processable nanostructured semiconductor composites with charge carrier mobilities in the order of 10^{-4} cm^2 V^{-1} s^{-1}, which was comparable to the existing semiconductors already used in OPV devices.[9] Chen *et al.* developed a series of rod-coil diblock copolymers poly[2,7-(9,9-dihexylfluorene)]-*b*-poly(4-vinylpyridine (PF-*b*-P4VP) and the P4VP coil blocks were hydrogen bonded with PDP which enabled different morphology transitions from lamellar to cylindrical or from cylindrical to spherical due to the increase of volume fraction of

P4VP(PDP) comb blocks.[10] Mezzenga *et al.* studied blends of regio regular P3HT-*b*-P4VP rod-coil block copolymers with the fullerene derivative PCBM which was the first attempt of studying the self assembly of a n-type semiconducting material in a comb coil copolymeric systems.[11] TEM imaging and spectroscopic results showed thermally stable nanostructured thin films self-assembled from ordered P3HT domains and PCBM-enriched P4VP domains. They also studied the device properties of this supramolecular donor-acceptor diblock copolymer as active layer in photovoltaic cells which showed energy conversion efficiencies higher than those containing conventional block copolymers.

As discussed earlier, perylenebisimides are one of the most widely studied n type semiconductors for optoelectronics applications owing to their unique combination of high electron mobility, large molar absorption coefficients, excellent self-assembling ability, versatile structural modification as well as good thermal and photochemical stabilities.[12- 16]There are no reports of non covalent self assembly of PBI molecules with a block copolymers. In this chapter we have attempted to study the coil comb self assembly of perylenebisimide with PS-b-P4VP. The block copolymer $(PS)_{20500}$ - $(P4VP)_{36000}$ with a PDI 1.08 was purchased commercially. The unsymmetrical PBI, UPBIHH (as discussed in chapter 4) was synthesized and different supramolecular complexes were made with PS-b-P4VP by varying four different molar ratios of UPBI (0.25 to 1). Among the UPBIs discussed in the previous chapter the UPBIHH was selected because of its low melting temperature and high solubility in common organic solvents like chloroform, DCM etc. These comb coil systems were well characterised with the help of FT-IR, NMR, XRD and TEM analysis.

5.3. Experimental Section

5.3.1. Materials: $(PS)_{20500}$ - $(P4VP)_{36000}$ was purchased from Polymer inc. Ltd. It was dried in vacuum oven at 60 °C for 3 days prior to use. PTCDA, Pentadecyl phenol, Zinc acetate were purchased from Aldrich. Hexyl heptyl amine was synthesised as per procedure.[17] Sodium nitrite, imidazole, potassium hydroxide and potassium carbonate were purchased from Merck Chemicals Ltd and used as such. Dimethyl Acetamide (DMF), Acetic acid (AcOH), tertiary butanol (tBuOH) and ethanol were purchased from Merck Chemicals Ltd and were purified using standard procedures.

5.3.2. Instrumentation techniques: Infrared spectra were obtained using Bruker α-T spectrophotometer in the range of 4000-400 cm^{-1}. ^{1}H and ^{13}C NMR spectra were recorded in $CDCl_3$ using Bruker AVENS 400 MHz spectrophotometer. Chemical shifts (δ) are reported in ppm at 298 K, with trace amount of tetramethylsilane (TMS) as internal standard. MALDI-TOF analysis was carried out on a Voyager-De-STRMALDI-TOF (Applied Biosystems, Framingham, MA, USA) instrument equipped with 337 nm pulsed nitrogen laser used for desorption and ionization. The operation was in a reflector mode with an accelerating voltage of 25 kV. Micromolar solutions of the compounds in THF were mixed with DHB matrix and spotted on stainless steel MALDI plate and dried well. Wide Angle X-ray Diffractogram (WXRD) were obtained using a Philips analytical diffractometer with CuKα emission. All the samples were recorded in the (2θ) range of 3–50 degrees using a PANalytical X'pert Pro dual goniometer diffractometer and analyzed using X'pert software. An X'celerator solid-state detector was employed in wide-angle experiments. The radiation used was CuKα (1.54 Å) with a Ni filter, and the data collection was carried out using a flat holder in Bragg–Brentano geometry. Small angle X-ray scattering (SAXS) was employed to investigate the phase behaviour of the complexes. The scattering experiments were conducted on a three pinhole collimated Bruker Nanostar machine equipped with rotating copper anode, operating at 45 kV and 100 mA providing characteristic Kα radiation of 1.54 Å. The measurements were carried out in the normal resolution mode having a q range of 0.011 – 0.2 Å. The bulk sample was sandwiched between two kapton films inside the sample holder. The scattered data was collected using a 2D Histar detector and later converted from 2D to 1D by azimuthal averaging using Bruker software. 1D data presented after background subtraction is plotted as I v/s q, where $q = (4\pi/\lambda)\ Sin\theta$, λ is the wavelength of the incident X-rays and 2θ is the scattering angle. Transmission Electron microscopy (TEM) was done using an FEI-Tecnai^{TM}-F20 electron microscope operating at 200 kV.

5.3.3. Synthesis of Unsymmetrical Perylenebisimide UPBIHH

UPBIHH was synthesised following the same procedure as given in chapter 4. Yield: 68%. M.P.: 235 °C.^{1}H NMR (400 MHz, $CDCl_3$, δ ppm) : 8.69-8.51 (m, 8H, perylene), 6.86–7.09 (m, 3H; Ar**H**-PDP), 5.18 (m, 1H, imide-N-C**H**), 2.41 (t, ^{3}J= 2.8 Hz, 4H; Ar-C**H**$_2$), 2.00 (m, 1H, imide-N-CH_2-C**H**), 0.98-0.86 (m, 9H, end CH_3 of hexyl heptyl group + terminal C**H**$_3$ of C-15 alkyl chain). ^{13}C NMR (100 MHz, $CDCl_3$, δ ppm): 166.3, 163.6, 161.9, 158.9, 155.8, 143.1, 136.7, 130.3, 129.8, 126.2, 124.9, 123.1, 122.6, 113.3, 106.2, 55.6, 32.7, 31.9, 29.9, 26.9, 22.8, 14.3. FT-IR (KBr, cm^{-1}): 3367, 2957, 2921, 2854, 1698,

1655, 1591, 1505, 1463, 1441, 1402, 1348, 1299, 1249, 1177, 1092, 967, 856, 806, 749, 632. MALDI-TOF (DHB matrix): m/z calculated for $C_{60}H_{74}N_2O_5$: 860.51; found 861.51[M^+1], Elemental analysis calculated (%): C 79.78, H 8.26, N 3.10; found: C 79.29, H 8.32, N 3.81.

5.3.4. Supra molecular complex preparation: PS-b-P4VP as well as the unsymmetrical perylenebisimide (**UPBI**) was dried in vacuum oven at 60 °C for 3 days. **PS-P4VP-UPBI** complexes were prepared from dry chloroform solutions by varying the molar ratio of UPBI from 0.25 to 1. In a typical procedure the block copolymer was first dissolved in chloroform to which desired amount of **UPBI** was added and the solution was stirred for 24 hours. Concentration of the solutions was kept at 1wt%. Subsequently the solvent was evaporated slowly on a hot plate at 40 °C and further dried in vacuum oven at 65 °C for 3 days, slowly cooled to room temperature and stored in desiccator thereafter.[18]

5.4. Results and Discussion

5.4.1. Supramolecular Comb Coil copolymer with PS-b-P4VP

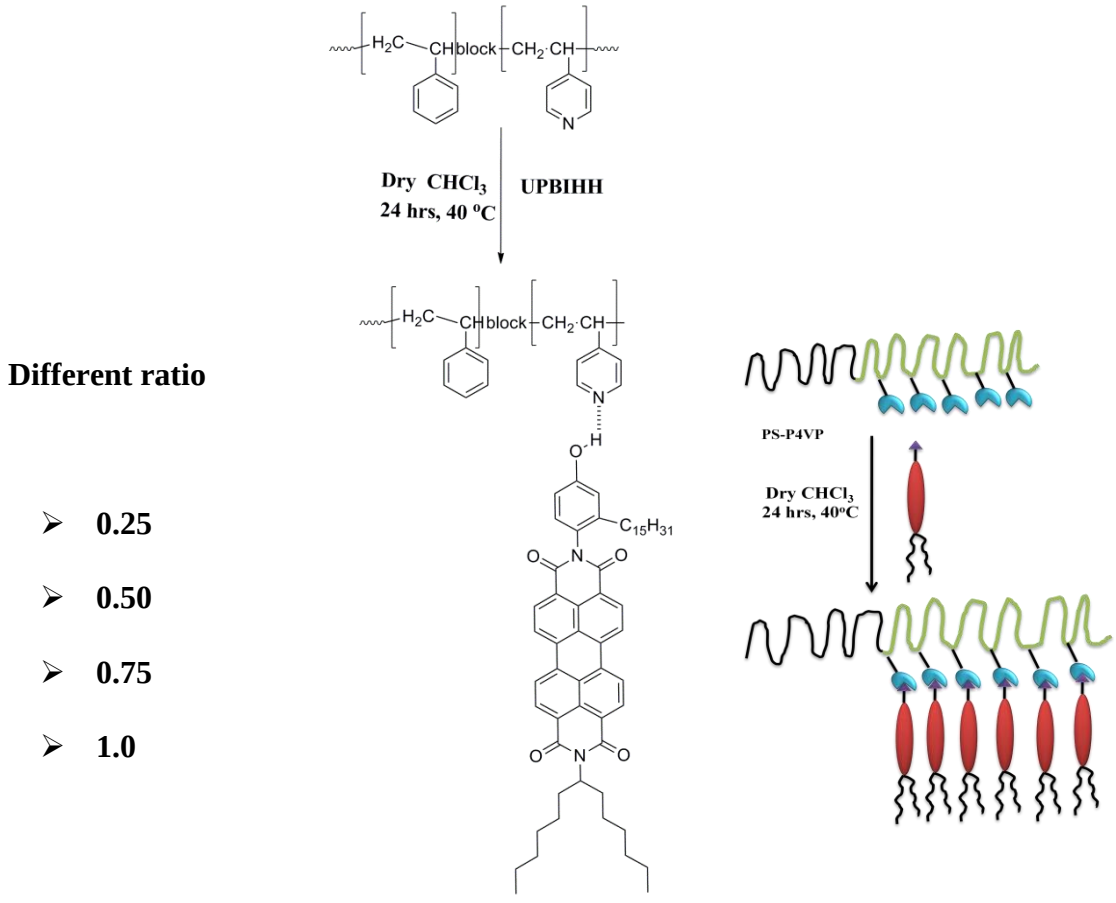

Scheme1. Structure and schematic diagram of the **PS-b-P4VP-UPBIHH** polymeric supramolecular complex formed by varying different molar ratios of **UPBIHH** with **PS-b- P4VP** polymer.

The hydrogen bonded complexes were prepared by varying four different molar ratio of UPBIHH (0.25, 0.50, 0.75, 1) with PS-b-P4VP in dry chloroform as solvent, stirring at ambient conditions for 24 hours, followed by removal of solvent by heating. The complexes were named **PS-P4VP(UPBIHH)$_{0.25}$, PS-P4VP(UPBIHH)$_{0.50}$, PS-P4VP(UPBIHH)$_{0.75}$, PS-P4VP(UPBIHH)$_{1}$** according to the molar ratio of UPBIHH used for complex formation. The schematic drawing along with the chemical structure of the hydrogen bonded polymeric **PS-P4VP-UPBI** complexes is given in Scheme-1.

5.4.2. Confirmation of hydrogen bonding - FT-IR and ^{1}H-NMR studies.

The supramolecular complex formation was traced by FT-IR spectroscopy as given in the previous chapter. As in the case of P4VP, PS-b-P4VP also shows a symmetric ring stretching mode at 993 cm^{-1} which gets shifted to 1003 cm^{-1} after complete complexation. The carbon-nitrogen stretching band at 1597 cm^{-1} for free pyridine groups was difficult to trace in the **PS-P4VP- UPBIHH** complexes since pentadecylphenol unit attached to the perylene core also had absorption band in the same region. Another characteristic absorption band of pure P4VP around 1413 cm^{-1} was devoid of any overlapping absorptions from pristine **UPBIHH** and its shift to higher wavelength upon complexation was traced. The FT-IR spectrum of different PS-P4VP(UPBIHH) complexes are given in figure 1. A gradual shift in the peak position was observed as the degree of complexation increased from n= 0.25 to 1.00.

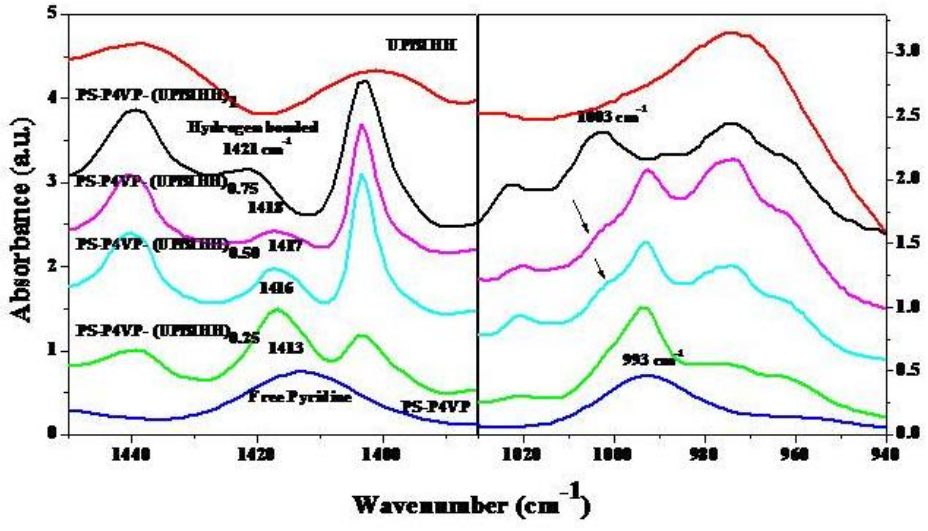

Figure 1: FTIR plots comparing the (a) 1413 cm^{-1} and (b) 993 cm^{-1} region of **PS-P4VP(UPBIHH)$_n$** with pure **PS-P4VP** and **UPBIHH** (n = 0.25, 0.50, 0.75, 1.00).

This could be clearly understood from the FT-IR plots of **PS-P4VP-UPBIHH** complexes with n = 0.25, 0.50, 0.75 and 1.00. When the degree of complexation was 0.25 the peak shift was relatively small and on going from 0.25 to 0.75, it increased further and achieved a maximum shift of +10 for 993 cm^{-1} and +8 for 1413 cm^{-1} in the 1:1 complexes. This observation was similar as in the case of P4VP (UPBIHH) complexes also. The supra molecular complexation of PS-P4VP with UPBIHH was traced with the help of ^1H NMR spectroscopy in $CDCl_3$ also. Figure 2 shows the expanded aromatic region for PS-b-P4VP, UPBIHH and PS-P4VP-(UPBI)n complexes. **UPBIHH,** had sharp signals corresponding to the 8 aromatic protons in the region 8.74-8.56 ppm, and signals corresponding to the 3 aromatic protons of pentadecyl phenol (PDP) unit at 7.2 (d, 1H), 6.86 (s, 1H) and 6.76 (d, 1H) ppm respectively. On the other hand, PS-b-P4VP had three sets of broad signals corresponding to four aromatic pyridine protons with intensity distribution corresponding to two protons each at 8.32 (d, 2H,) and 6.36 ppm (d, 2H,) and the styrene protons at 7.06 (d, 2H) and 6.55 (d, 2H) which merged with pyridine protons. After complexation with PS-b-P4VP an overall broadening of the spectrum wais observed confirming the polymeric nature of supramolecular complexes. A clear down field shift was observed for the pentadecyl phenol protons which was involved in the H bonding with P4VP. In UPBIHH the d protons of PDP appeared at δ 6.74 ppm which got shifted to 6.83 ppm (0.09 ppm shift) and the c protons got shifted from 6.86 ppm to 6.91 ppm in PS-P4VP-$(UPBIHH)_{0.25}$ complexes. For PS-P4VP$(UPBIHH)_{0.5,}$ the c protons were observed at 6.89 ppm and d protons at 6.80 ppm and in the case of PS-P4VP-$(UPBIHH)_{0.75}$ the c protons were observed at 6.88 ppm and d protons at 6.79 ppm. For the 1: 1 complex (PS-P4VP-UPBIHH) also same δ values was observed as in the case of PS-P4VP-$(UPBIHH)_{0.75}$ for c and d protons were observed. The maximum shift was observed for PS-P4VP-$(UPBIHH)_{0.25}$ complexes, that is for d protons a chemical shift if 0.09 ppm (and c protons 0.05 ppm). Upfield shift was observed upon increasing molar ratio of UPBIHH which got saturated at the 1:1 complexes. While comparing the 1:1 complexes with the pristine UPBIHH a down field shift of 0.05 ppm is observed for the d protons and 0.02 ppm for c protons respectively. The clear downfield shift in the 0.25 molar complex is due to the effect of hydrogen bonding with P4VP which reduces the electron density among these protons.

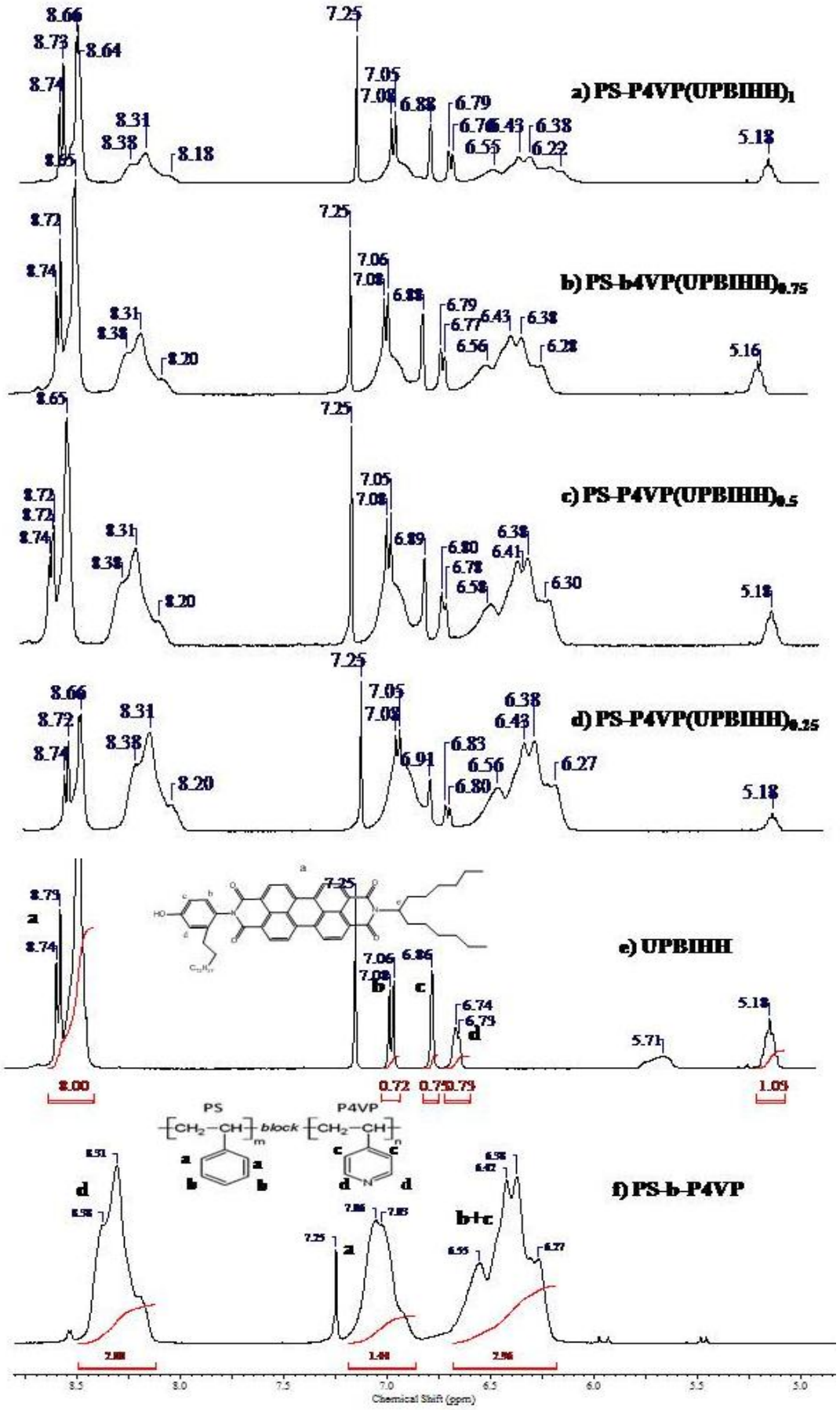
a) PS-P4VP(UPBIHH)1
b) PS-b4VP(UPBIHH)0.75
c) PS-P4VP(UPBIHH)0.5
d) PS-P4VP(UPBIHH)0.25
e) UPBIHH
f) PS-b-P4VP
PS
P4VP
block
Chemical Shift (ppm)

Figure 2: ^{1}H NMR spectrum of **PS-b-P4VP**, **UPBIHH**, **PS-b-P4VP-(UPBIHH)$_n$** (n= 0.25 to 1) in CDCl3 (10 mg/ml).

Upon increasing the UPBIHH concentration, the chances for PBI core aggregation also increased which can increase the electron density around these protons. So upon higher molar ratio both the aggregation effect and hydrogen bonding plays an important role which can be a reason for the upfield shift while going from 0.25 to 1 molar ratio. But over all a downfield shift was observed which clearly indicated the formation of the supra molecular complexes.

5.4.3. Bulk structure analysis of Supra molecular coil comb polymer:

The SAXS profile of block copolymer used in this study along with its supra molecular complexes are given in figure 3. The samples in chloroform were drop casted over kapton film and the SAXS data was recorded. Block copolymers are well known to form nanostructures. The PS-b-P4VP block copolymer showed 4 peaks in the SAXS region having q values 0.15, 0.16, 0.18, 0.19 corresponding to d values of 41.86, 39.25, 34.88, 33.05 nm. After complexing with UPBIHH no noticeable shift in the scattering pattern was observed confirming that after compexation also the block copolymer structure was preserved.

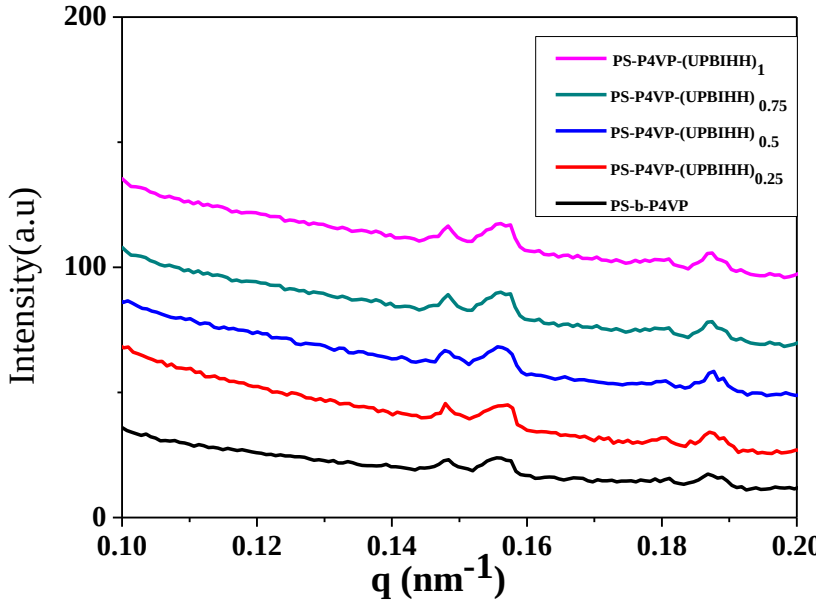

Figure 3: Room temperature SAXS profile of **PS-b-P4VP** and **PS-P4VP (UPBIHH)$_n$** (n = 0.25 to 1)

The room temperature XRD data of supra molecular complexes along with pristine UPBIHH is given in figure 4. The block copolymer PS-P4VP gave a broad diffraction pattern in this region. As discussed in the previous chapter the UPBIHH had a columnar rectangular arrangement in the room temperature. After complexation with the block copolymer even though the amorphous nature got increased some of the peak in the pristine molecule got preserved. The pi –pi stacking peak was present at $2\theta = 21.7^{o}$ in both the supramolecular complexes and UPBIHH. No characteristic peak shift was observed among the supramolecular complexes while increasing the molar ratio from 0.25 to 1.

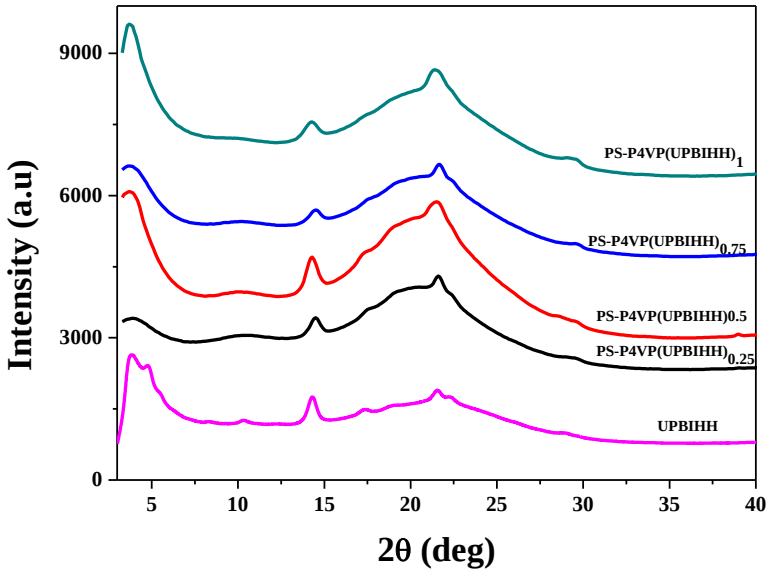

Figure 4: Room temperature XRD pattern of **UPBIHH** and **PS-P4VP (UPBIHH)$_n$** (n= 0.25 – 1).

5.4.4. Morphology studies of Supra molecular comb coil polymer:

.

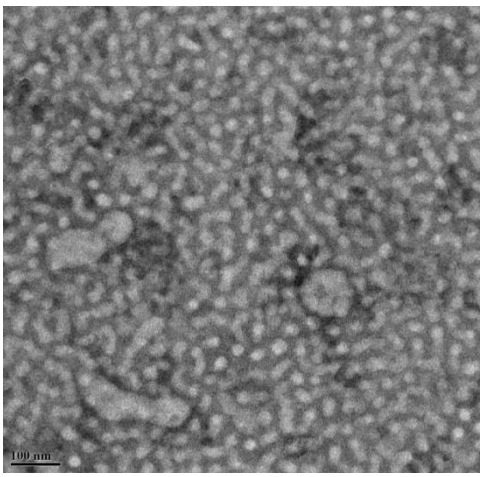

Figure 5 : TEM analysis of **PS-b-P4VP** in Dry DMF (2mg/ ml).

TEM analysis helps to give the insights in to the morphology of the comb coil structure of these systems. The samples are drop casted on Cu grid from dry DMF (2mg / ml) followed by I_2 staining. The TEM morphology of the commercial block copolymer used for this study is given in figure 5. It showed typical block copolymer morphology at a length scale 100 nm scale.[4-7] We could not trace any other kind of organization in this system in lower scale. The TEM analysis of supramolecular complexes are given figure 6. There was a clear change in morphology while increasing the molar ratio of UPBI from 0.25 to 1. At lower molar ratio of UPBI the TEM images resembled the block copolymer TEM image as given in figure 5. When n = 0.75 the worm like morphology was observed for the supramolecular complexes, which got changed in to cylindrical morphology for n =1.

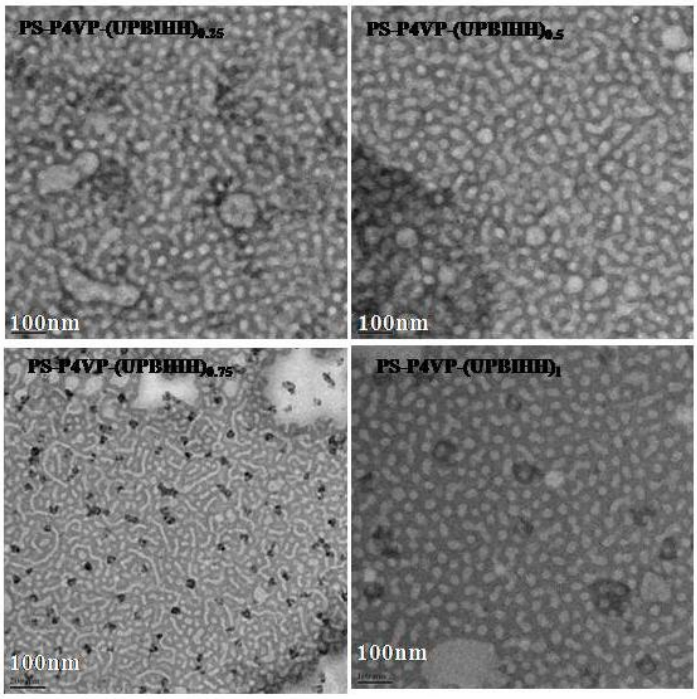

Figure 6: TEM images of **PS-P4VP (UPBIHH)n** (n = 0.25 to 1) in Dry DMF (2mg/ ml).

At lower length scale a clear lamella structure was observed in all the systems as given in figure 7, confirming the comb coil morphology of these systems. At higher length scale

(100 nm) the coil comb morphology of the block co polymeric system was present where as at lower length scale (5nm) the comb morphology (lamella) formed by the hydrogen bonding interaction between the P4VP and UPBIHH was present. From this it is clear that the morphology present in this system served as an example of "assembly-within-assembly."

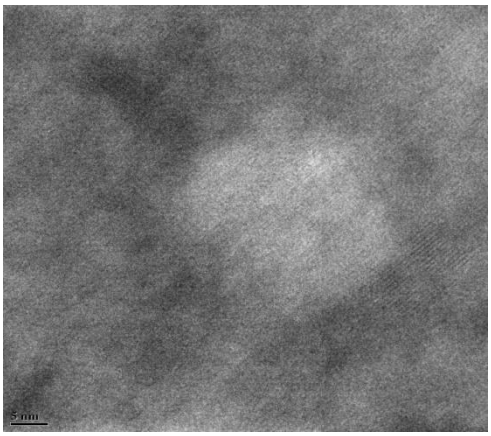

Figure 7: The Zoomed TEM image of PS-P4VP-UPBIHH at lower length scale.

5.5 Conclusions:

The supra molecular comb coil copolymer formation of PS-P4VP with n type semiconducting perylenebisimides was studied by varying the molar ratio of PBI from 0.25 to 1. The self assembly was well studied with the help of FT-IR, NMR, XRD and TEM. Upon varying the molar ratio a change in the morphology was observed through TEM imaging. At higher length scale this supra molecular complexes showed typical block copolymer morphology where as at lower length scale lamellar morphology of comb copolymer was present. This confirmed the "Assembly –within-Assembly" morphology of the comb coil copolymers. As discussed in the introduction this is a novel approach in literature where the comb coil copolymer formation of perylenebisimide was studied. These studies are preliminary and more insight to SAXS analysis should be under taken in order to study the structure-property relationship in depth.

5.6 References:

1. J. Ruokolainen, R. Mäkinen, M. Torkkeli, R. Serimaa, T. Mäkelä, G. Ten Brinke, O. Ikkala, *Science* **1998,** *280*, 557.
2. J. Ruokolainen, G. Ten Brinke, O. Ikkala, *Adv. Mater.* **1999,** *11*, 777.
3. K. de Moel, A. G. O.R. van Ekenstein, H. Nijland, E. Polushkin, G. Ten Brinke, *Chem. Mater.* **2001,** *13*, 4580.
4. O. Ikkala, G. Ten Brinke, *Science* **2002,** *295*, 2407.
5. O. Ikkala, G. Ten Brinke, *Chem. Commun.* **2004,** 2131.
6. W. Van Zoelen, T. Asumaa, J. Ruokolainen, O. Ikkala, G. Ten Brinke, *Macromolecules* **2008,** *41*, 3199.
7. J. Ruokolainen, G. Ten Brinke, O. Ikkala, *Macromolecules* **1996,** *29*, 3409.
8. G. Ten Brinke, O. Ikkala, *Macromol. Symp.* **2003,** *203*, 103.
9. Rancatore, B. J.; Mauldin, C. E.; Tung, S-H.; Wang, C.; Hexemer, A.; Strzalka, J.; Fréchet, J. M. J.; Xu, T. *ACS Nano*, **2010**, 4, 2721.
10. H.-S. Sun, C.-H. Lee, C.-S. Lai, H.-L. Chen, S.-H. Tung, W.-C. Chen, *Soft Matter* **2011,** *7*, 4198.
11. N. Sary, F. Richard, C. Brochon, N. Leclerc, P. Lévêque, J.-N. Audinot, S. Berson, T. Heiser, G. Hadziioannou, R. Mezzenga, *Adv. Mater*. **2010,** *22*, 763.
12. Narayan, R.; Kumar, P.; Narayan, K. S.; Asha, S. K. *Adv. Funct. Mater.* **2013**, 23, 2033.
13. F. Würthner, *Chem. Commun.***2004,** 1564.
14. M. Sommer, S. M.Lindner, M. Thelakkat, *Adv. Funct. Mater.***2007,** *17*, 1493.
15. M. Sommer, A. S. Lang, M.Thelakkat, *Angew. Chem. Int. Ed.***2008,** *47*, 7901.
16. Chen, Z.; Stepanenko, V.; Dehm, V.; Prins, P.; Siebbeles, L. D. A.; Seibt, J.; Marquetand, P.; Engel, V.; Würthner, F. *Chem. Eur. J.* **2007**, 13, 436
17. Wicklein, A.; Lang, A.; Muth, M.; Thelakkat, M. *J. Am. Chem. Soc.*,**2009**, *131*, 14442-14453.
18. B. Nandan, M. K. Vyas, M. Böhme, M. Stamm, *Macromolecules* ,**2010**, *43*, 2463.

Chapter 6

Conclusions and Summary

Perylenebisimides has been widely explored as an n type semiconducting material for optoelectronics applications owing to their unique combination of high electron mobility, large molar absorption coefficients, excellent self-assembling ability, versatile structural modification as well as good thermal and photochemical stabilities. The self assembly of PBI and its derivatives play a crucial role in improving the charge transport and overall device efficiency. So there is huge demand to focus on the self assembling behaviour of PBI based systems to improve the device performance. In this context the thesis entitled "**Pentadecyl Phenol Functionalized Perylenebisimide Building Blocks for Optoelectronic Applications**" describes the synthesis and liquid crystalline self assembly of an amphiphilic pentadecyl phenol substituted novel perylenebisimides and its derivatives. The symmetrical and unsymmerical perylenebisimides were synthezied and characterized well. The liquid crystalline properties were well studied with DSC, PLM and WXRD. The charge transporting properties of these systems were studied by SCLC (Space Charge Limited Current) method which clearly indicated the importance of self assembly in charge transport.

The introduction chapter of this thesis gave a clear overview of the literature reports on perylene based small molecules and polymeric systems. From this review we understood that the device performance of PBI based molecule were lagging behind the fullerene based system and research should take forward with new design and synthetic stratergies for novel PBI based systems to get good device performance. The entire thesis is mainly focussed on the liquid crystalline self assembly of the PBI. Liquid crystalline materials have several advantages over organic single crystalline materials including easy processing, ability to form thin films, long range self assembly, less number of grain boundaries etc which are the key factors for efficient charge transporting. There for they find applications in optoelectronic materials such as organic field effect transistors (OFET), organic light emitting diodes (OLED), organic photovoltaic cells (OPV) etc. In the columnar liquid crystals, the disc like mesogens are stacked one on top of another surrounded by the flexible alkyl chain resulting in mesophase formation. Upon thermal annealing, these molecules can form single large domain with less number of grain boundaries as a result of their inherent self healing property due to their partial liquid-like behavior. But the main challenge in this area is the attainment of mesogenicity in a temperature range that is adaptable on a device substrate. The clearing temperatures

should be low and ideally the liquid crystalline phase should be retained at room temperature. However, the design of a suitable LC material for a desired application requires a basic understanding of the structure-property relationship. The spacer chain length plays an important role on the entire packing and bulk confirmation of the liquid crystalline molecules. So far there are no similar studies reported on perylene based systems; our study is expected to give more information regarding the influence of spacer length on the packing, which could prove beneficial in designing systems with appropriate odd or even numbered spacers Since the perylenebisimides are a highly explored family of chromophores for potential optoelectronic application.

The entire thesis is mainly focussed on the self assembly of pentadecyl phenolbased PBI.The second chapter of the thesis discussed the structure- property relationship in the charge transporting behaviour of PBI esters. Here, a homologous series of pentadecyl phenol functionalized perylenebisimide (PBI) terminated with trialkoxy gallate esters were synthesized, where the terminal alkyl chain length was varied from n = 4 to 12 (**PBI-En**). The thermotropic liquid crystalline (LC) characteristics of the molecules were analyzed using differential scanning calorimetry (DSC), polarized light microscopy (PLM) combined with variable temperature wide angle X-ray diffraction (WXRD) techniques. A clear odd-even oscillation was observed in the melting as well as isotropization enthalpies as a function of alkyl spacer length in the terminal gallate unit with the even spacers exhibiting higher values. The higher members of the series with n > 8 exhibited thermotropic liquid crystalline textures in the PLM which remained stable until room temperature. The nature of the LC phase was identified to be columnar rectangular and columnar hexagonal based on detailed analysis of the WXRD pattern recorded in the LC phases. The SCLC mobility values columnar hexagonal phase exhibited a mobility value one order (10^{-3} $cm^2V^{-1}s^{-1}$) higher than that of crystalline (10^{-4} $cm^2V^{-1}s^{-1}$) and two orders higher than that of columnar rectangular phase (10^{-5} $cm^2V^{-1}s^{-1}$) indicating a strong dependence of packing on bulk mobility.

The third chapter studied the odd even effect and liquid crystalline properties of twin liquid crystalline perylenebisimides. A series of twin Perylenebisimide (PBI) molecules were synthesized and characterized having the structure PBI-(methylene spacer)n-PBI where the length of the central poly methylene spacer segment was varied from n = 1 to 12. The PBI unit was imidized with ethyl hexyl branched alkyl segment at the terminal and pentadecyl phenol at the other end which was linked up through the poly methylene

spacer to form the twin molecules. The differential packing afforded by the odd and even spaced central methylene segments resulted in an odd-even oscillation of the clearing transitions as well as their enthalpies with higher values observed for the even twins. The odd-even oscillation was quite prominent for the spacers till n<7 after which it tapered off. The differential packing afforded by the odd and even spaced central methylene segments resulted in an odd-even oscillation of the clearing transitions as well as their enthalpies with higher values observed for the even twins. Except for the two odd lower members **PBI-T1** and **PBI-T3**, all other samples exhibited nematic liquid crystalline phases. **PBI-T1** and **PBI-T3** exhibited smetic phase which was retained till room temperature upon cooling. **PBI-T2** and **PBI-T4** showed a higher temperature nematic LC phase which was short lived and crystallized out immediately while cooling, whereas **PBI-T5** and **PBI-T6** formed room temperature nematic phase. The higher spacered twins n > 7 also showed nematic LC phase.

.The last two chapters of this thesis work explore the hydrogen bonding induce supramolecular comb and comb-coil assembly of unsymmetrical perylenebisimides with poly 4 vinyl pyridine (**P4VP**) and poly styrene block poly 4 vinyl pyridine (**PS-b-P4VP**) respectively.The fourth chapter of the thesis highlights the supramolecular comb copolymer formation of unsymmetrical perylenebisimides (UPBIs) with P4VP. Here, The self assembly of unsymmetrical perylenebisimides (**UPBIs**) having pentadecyl phenol at one end and different alkyl groups like cyclo hexyl (**UPBICH**), octyl dodecyl (**UPBIOD**), hexyl heptyl (**UPBIHH**), dodecyl (**UPBIDD**) on the other termini were studied. All the UPBIs exhibited room temperature columnar liquid crystalline phases. **UPBIOD** organised in to columnar hexagonal phase, UPBICH formed columnar lamellar phase while both **UPBIDD** and **UPBIHH** columnar rectangular phase. The supramolecular comb copolymer of these **UPBIs** with **P4VP** homo polymers (**P4VP-UPBI**) were synthesised by dissolving 1:1 molar ratio of **UPBI** with **P4VP** in solvent followed by the removal of solvent. All the **P4VP-UPBI** comb copolymers showed lamellar morphology in TEM analysis. The SCLC mobility measurements of the **P4VP–UPBI** comb copolymers showed comparable mobility values with respect to the pristine **UPBI** molecules.

In the last working chapter the supramolecular comb coil formation of unsymmetrical **PBI** with **PS- b-P4VP** was carried out. The supramolecular comb coil copolymer formation of **PS-P4VP** with n type semiconducting perylenebisimide (**UPBIHH**) was

studied by varying the molar ratio of the later from 0.25 to 1. The self assembly was well studied with help of FT-IR, NMR, XRD and TEM. Upon varying the molar ratio of **UPBIHH** a change in the morphology was observed as confirmed from TEM imaging. Supra molecular complexes of **PS-b-P4VP** block co polymers with unsymmetrical perylenebisimide were formed through the hydrogen bond interaction between the pyridine units on **P4VP** and the phenolic –OH on the perylenebisimide. The supra molecular complexes showed worm like morphology in the TEM at 100 nm scale. In addition, lamellar morphology at a length scale of 5 nm could also be observed in the TEM images. This confirmed the assembly-within-assembly of comb co polymer formation inside the larger block co polymer organization.

This thesis work systematically studied how the self assembling behaviour of perylenebisimides and their tuning by various strategies – variation of substituents or self assembly with template polymers. A library of new molecules have been developed with their entire structural details were presented. It is expected that this study would contribute more to the understanding of structure-property relationship in perylenebisimide literature.

List of Publications in International Journals:

1. Prajitha, K. P.; Chithiravel, S.; Krishnamoorthy, K.; Asha, S. K, Structure-Property Relationship in Charge transporting behavior of Liquid crystllaine perylenebisimides. *J. Mater. Chem. C*, **2014**, 2, 9882.

2. Prajitha, K. P and Asha, S. K, Synthesis and Structural Characterization of Twin Liquid Crystalline Perylenebisimides *New j. Chem.*, **2016**, 40, 8471.

3. Prajitha, K. P.; Chithiravel, S.; Krishnamoorthy, K.; Asha, S. K, Hydrogen Bond Assisted Nano Self Assembly Of Unsymmetrical Perylenebisimides with Poly 4 Vinyl Pyridine (P4VP) for better Charge Transport (Manuscript under preparation).

4. Prajitha, K. P and Asha, S. K, Supramolecular comb coil selfassembly of PS-b-P4VP Block copolymer with unsymmetrical Perylenebisimide (Manuscript under preparation).

Papers Presented in Conferences:

1. Prajitha.K.P. and Asha. S. K. "Twin Liquid crystalline Perylenebisimedes: Synthesis and structural characterizations." **National Science Day**, CSIR-NCL, Pune, **2013.**

2. Prajitha. K. P. and Asha. S. K. "Pentadecyl phenol substituted liquid crystalline perylenebisimides for opto electronics applications." **MACRO+FAPS 2013 - International Conference on Frontiers of Polymers and Advanced Materials**, Indian Institute of Science, Bangalore,**2013**.

3. Prajitha. K. P.; Chithiravel, S.; Krishnamoorthy, K.; Asha, S. K, Structure-Property Relationship in Charge transporting behavior of Liquid crystllaine perylenebisimides." **8th Asian Photochemistry Conference**, CSIR-NIIST, Thrivananthapuram, Kerala, **2014**.

4. Prajitha. K. P and Asha, S. K, Synthesis and Structural Characterization of Twin Liquid Crystalline Perylenebisimides. **Macro 2015 – International Symposium on Science and Technology**,Indian Association for the Cultivation of Science, West Bengal, Kolkata, **2015**.